

Electrochemical determination of gallic acid in food matrices using novel materials.

CHIKERE, C.O.

2020

The author of this thesis retains the right to be identified as such on any occasion in which content from this thesis is referenced or re-used. The licence under which this thesis is distributed applies to the text and any original images only – re-use of any third-party content must still be cleared with the original copyright holder.

ELECTROCHEMICAL DETERMINATION OF
GALLIC ACID IN FOOD MATRICES USING
NOVEL MATERIALS

CHRYS. O. CHIKERE

BSc (Hons), MSc. (Instrumental Analytical Science)

PhD

2020

**ELECTROCHEMICAL DETERMINATION OF
GALLIC ACID IN FOOD MATRICES USING
NOVEL MATERIALS**



by

Chrysantus Onyinye CHIKERE,

BSc (Hons), MSc. (Instrumental Analytical Science)

A thesis submitted in partial fulfilment of the requirements of the Robert Gordon University for the degree of Doctor of Philosophy

May 2020

DECLARATION

I, Chrysantus Onyinye Chikere, hereby declare that the thesis entitled "Electrochemical determination of Gallic acid in food matrices using novel materials" is my own original research. I confirm that this thesis has not been submitted at this university or any other institution to claim any other qualification. I have acknowledged and properly cited, with a list of references any sources from journal articles, books, or any other unpublished articles.

Chrysantus O. Chikere

ABSTRACT

Gallic acid (GA) as an endogenous polyphenol, has shown many different important properties, that have influenced their use in the food and pharmaceutical industry. These properties include their antioxidant capacity, anticancer, antitumor, anti-HIV and anti-ulcerogenic activities. The most commonly used GA determination techniques have been the spectrophotometric and chromatographic techniques. However, these techniques have shown some drawbacks, like being expensive, labour intensive, time-consuming, and not being suitable for *in-situ* measurements. Electrochemical methods using cyclic voltammetry (CV) and differential pulse voltammetry (DPV) at inert glassy carbon electrode (GCE) or carbon paste electrodes (CPE) have also been used in the determination of GA. However, despite their easy application and fast result generation, their sensitivity and selectivity have been relatively inadequate, for the analysis of GA found in beverages and pharmaceutical products. Hence, the aim of this study to investigate and develop novel nanomaterials based electrochemical sensors for fast, sensitive, cost-effective, and selective determination and analysis of GA.

In this study the detection of GA was achieved in red and white wines, using CV by the development of graphene oxide nanoparticles and other metal oxide nanoparticles modified carbon-based working electrodes. The synthesised metal oxide nanoparticles were characterised using, scanning electron microscopy (SEM), energy-dispersive x-ray spectroscopy, Fourier transform infrared spectroscopy and Zetasizer for particle size analysis. Meanwhile, the characterisation of the developed electrodes was carried out by using CV, DPV and electrochemical impedance spectroscopy, the electrochemical effects of the electrodes were analysed.

The results in this thesis are presented of a novel graphene oxide nanocolloids-SiO₂ nanoparticles combination used for the electrochemical determination of GA. The results show enhanced peak currents, with high sensitivity and selectivity. The anodic peak current was enhanced from 241 μA for the bare GCE to 411 μA for the modified GCE; with an LOD of 2.09 x 10⁻⁶ mol L⁻¹ within a range of 6.25 x 10⁻⁶ to 1.0 x 10⁻³ mol L⁻¹. A synergistic effect between SiO₂ nanoparticles and graphene oxide nanocolloids in the determination of GA was proposed.

Synthesised amorphous zirconium oxide nanoparticles were used for the modification of carbon paste electrode and used for the determination of GA. The electrode modification enhanced the electrochemical activity of GA, with increased sensitivity and selectivity. The modified electrode produced an enhanced anodic peak from 260 μA for the bare electrode to 451 μA . With an LOD of 1.24×10^{-7} mol L^{-1} within a range of 1×10^{-6} to $1.0 \times 1 \times 10^{-3}$ mol L^{-1} . A novel proposal for the interaction and effect of the amorphous zirconia nanoparticles on the graphite in the CPE was made.

Zinc oxide nanoparticles and cobalt oxide nanoparticles were also used individually for the modification of carbon paste electrodes. The modified electrodes showed an enhanced effect on GA oxidation. This enhanced effect was an increase in anodic peak current from 261 μA to 414 μA when the CPE was modified. The LOD produced by the ZnO nanoparticles-modified CPE was 1.86×10^{-7} mol L^{-1} within a concentration range of 1×10^{-3} to 5×10^{-2} mmol L^{-1} . Meanwhile, the effect of scan rate and the effect of pH shows that the electrodes were more effective in acidic pH and the GA/electrode interaction were an adsorption-controlled process.

Cobalt oxide nanoparticles were also synthesised, characterised, and used for the modification of CPE. The modified electrode produced an enhanced anodic peak current from 302 μA for the bare CPE to 404 μA for the modified electrode. The limit of detection of the modified electrode was studied and found to be 1.52×10^{-6} mol L^{-1} at a concentration range of 1×10^{-4} to 1×10^{-3} mol L^{-1} .

The modified electrodes were successfully used for the determination of GA in real samples of red and white wine. Based on the electrochemical activities of the different electrodes made, the Zirconium dioxide nanoparticles modified carbon paste electrode, seem to have produced the best results. The zirconium dioxide modified CPE showed increased sensitivity and better limit of detection for GA.

KEYWORDS

Gallic acid, antioxidants, electrochemistry, cyclic voltammetry, differential pulse voltammetry, glassy carbon electrode, carbon paste electrode, metal oxide nanoparticles, nanomaterials, nanoparticles.

DEDICATION

*This Thesis is Richly Dedicated
In Honour and Memory of my late mother
Lolo Felicia Chikere Emekwatah.
May your humble soul continue to rest in the Lord.
Amen.*

ACKNOWLEDGEMENTS

I would want to start by thanking the Almighty God for his guidance and protection through this trying journey of a PhD research. May his name be glorified. Amen

Further thanks go to my supervisory team, Dr Carlos Fernandez, Prof Paul Kong, and Dr Nadimul Faisal, who has been a constant source of support, supervision, encouragement, and advice, in the course of this arduous journey in Robert Gordon University. Carlos as my principal supervisor has been a source of inspiration and a dependable gentleman. I would say I am deeply indebted to you, for your guidance, understanding and patience.

I would also want to thank my lovely wife Dr Adanma Chrys-Chikere, who has been on my side through thick and thin, in the course of this sometimes-lonely journey of PhD research. Without you and my wonderful children, Eliana and Elnathan, I do not think I would have been able to get to this point. I appreciate all your sacrifices and most importantly the times I have not been there for you guys because of this work. I am so grateful for all you have done to make this a reality. I am also very grateful for the support and encouragement from my dad Nze Akaraka Christopher Chikere Emekwatah, my kid brothers Pius, Charles, Gilles, Paschal and Rev. Angelbert.

A special thanks go to all my colleagues in the N540 research hub of the School of Pharmacy and Life Science, who in their different ways have been part of this journey. You guys have been wonderful, and I will miss the time I spent with you all in the research hub and the laboratories.

Last but not the least, I would want to thank all the staff of Lab N601, N604 of the School of Pharmacy and Life Sciences and Lab N512 of the School of Engineering of the Robert Gordon University Aberdeen. Special thanks also go to Dr Kyari Yates, Dr Stuart Waddell and Dr Colin Thompson for your advice, support, and encouragement in the course of this research. I would always be indebted to you guys.

PUBLICATIONS AND PRESENTATIONS

The following papers, conference publications and conference presentation have emanated from this thesis and the work in general.

Published Journal Articles:

- **CHIKERE, C. et al.**, 2020. Electroanalytical determination of gallic acid in wine samples using Cobalt oxide nanoparticles-modified carbon paste electrodes. *Journal of Materials Research and Technology* (In REVIEW).
- **CHIKERE, C. et al.**, 2020. Interaction between amorphous zirconia nanoparticles and graphite: Electrochemical applications for gallic acid-sensing using carbon paste electrodes in wine. *Nanomaterials*, 10(3), p. 537
- **CHIKERE, C. et al.**, 2019. Zinc oxide nanoparticles modified carbon paste electrode used for the electrochemical determination of Gallic acid. *Journal of Physics: Conference Series*, 1310, p. 012008.
- **CHIKERE, C.O. et al.**, 2019. The synergistic effect between graphene oxide nanocolloids and silicon dioxide nanoparticles for gallic acid sensing. *Journal of Solid State Electrochemistry*, 23(6), pp. 1795–1809.

Other publications:

- ALZHRANI, H., BENTLEY, C., BOHN, P.W., **CHIKERE, C.**, COMMANDEUR, D., CROOKS, R.M., EHI-EROMOSELE, C., EWING, A., GALEYEVA, A. and HERBACH, T., 2018. Energy conversion at nanointerfaces: general discussion. *Faraday discussions*, **210**, pp. 333-351.
- ALZHRANI, H., ANTOINE, C., BAKER, L., BALME, S., BHATTACHARYA, G., BOHN, P.W., CAI, Q., **CHIKERE, C.**, CROOKS, R.M. and DAS, N., 2018. Processes at nanopores and bio-nanointerfaces: general discussion. *Faraday discussions*, **210**, pp. 145-171.
- ALZHRANI, H., BENTLEY, C., BURROWS, R., CAO, C., CAI, Q., **CHIKERE, C.**, CROOKS, R.M., DUNEVALL, J., EDWARDS, M. and EWING, A., 2018. Dynamics of nanointerfaces: general discussion. *Faraday discussions*, **210**, pp. 451-479.

Conference presentations:

- Oral Presentation: "New electrode materials for electrochemical biosensing and the analysis of environmentally toxic chemicals", 8th Scottish Symposium on Environmental Analytical Chemistry, Glasgow, UK, December 2015.
- Oral Presentation: "Non-enzymatic voltammetric determination of glucose by CuO nanobelt graphene composite modified glassy carbon electrode", Nanostruc 2016, Aberdeen, UK, September 2016.
- Oral Presentation: "New electrode materials for energy storage devices (Battery Applications) and electrochemical sensors", IWMP 2019, Bucharest, Romania, May 2019
- Poster Presentation: "Novel graphene-based electrode materials for selective electrochemical determination of antioxidants", Glasgow, UK, June 2016
- Poster Presentation: "Graphene oxide nanocolloids and SiO₂ nanoparticles modified glassy carbon electrode for electrochemical determination of Gallic acid", Electrochemistry at Nano-interfaces Faraday Discussion 2018, Bath, UK, June 2018
- Poster Presentation: "Zinc oxide nanoparticles modified carbon paste electrode used for the electrochemical determination of Gallic acid" ANNIC 2018, Berlin, Germany, October 2018

TABLE OF CONTENT

DECLARATION	I
ABSTRACT	II
KEYWORDS	III
DEDICATION	IV
ACKNOWLEDGEMENTS	V
PUBLICATIONS AND PRESENTATIONS	VI
TABLE OF CONTENT	VIII
List of Tables	XVII
List of Figures	XVIII
Terms and Abbreviations	XXV
Thesis Overview	XXIX
CHAPTER ONE	1
1.0 GENERAL INTRODUCTION AND LITERATURE REVIEW	1
1.1 Overview.....	1
1.2 Electrochemical analytical methods.....	3
1.2.1 Electrochemical sensors.....	5
1.3 Voltammetric Analysis.....	7
1.3.1 Voltammetric Cell	8
1.4 Cyclic Voltammetry	11
1.4.1 Reversible System	13
1.4.2 Irreversible System.....	15
1.4.3 Quasi-reversible	16
1.5 Differential Pulse Voltammetry.....	17
1.5.1 The Electrical Double Layer.....	20
1.5.2 Mass Transport	21
1.6 Antioxidants.....	24

1.6.1 Natural Antioxidants	27
1.7 Gallic acid.....	28
1.7.1 Gallic acid structure and its antioxidant activity.....	28
1.7.2 Importance of Gallic Acid	30
1.7.3 Gallic acid in wine	31
1.8 Review of electrochemical determination of Gallic acid: Graphene Oxide and Metal Oxide Nanoparticles	31
1.8.1 Chemically Modified Electrodes	34
1.8.2 Modified electrodes for Gallic acid determination.....	36
1.8.3 Metal oxide nanoparticles modified electrodes.....	37
1.8.4 Graphene oxide nanoparticles modified electrodes.....	42
1.9 Research Aims and Objectives.....	45
CHAPTER TWO	47
2.0 EXPERIMENTAL MATERIALS AND METHODS	47
2.1 Introduction.....	47
2.2 Reagents.....	47
2.3 Analytes.....	48
2.3.1 Phosphate Buffers.....	48
2.3.2 Preparation of potassium ferricyanide solution	49
2.3.3 Preparation of Antioxidant solutions.....	49
2.3.4 Preparation of real sample (orange juice and wines) solutions	49
2.4 Synthesis of metal oxide nanoparticles.....	50
2.4.1 Synthesis of ZnO nanoparticles.....	50
2.4.2 Synthesis of Silicon oxide nanoparticles	50
2.4.3 Synthesis of Zirconium nanoparticles.....	51
2.4.4 Synthesis of Cobalt oxide nanoparticles	51
2.4.5 Graphene oxide nanocolloids	52

2.5 Instrumentation, Software, and Ancillary Equipment.....	52
2.5.1 Electrochemical Cell Set-Up	53
2.5.2 Scanning Electron Microscopy	53
2.5.3 Energy dispersive X-ray analysis (EDXA)	54
2.5.4 Fourier Transform Infrared Spectroscopy (FTIR)	54
2.5.5 X-ray Powder Diffraction (XRD).....	55
2.5.6 Dynamic Light Scattering (DLS) Analysis	56
2.6 Electrodes.....	56
2.6.1 Working Electrodes	56
2.6.2 Reference Electrodes	58
2.6.3 Counter Electrodes	59
2.7 Experimental Methods.....	60
2.7.1 Electrochemical Methods	60
2.7.2 Electroactive surface area of the electrodes	61
2.8 Electrochemical Studies	61
2.8.1 Electrochemical impedance spectroscopy.....	62
2.8.2 Effect of scan rate	63
2.8.3 Effect of the quantity of modifier	63
2.8.4 Effect of adsorption time	63
2.8.5 Effect of pH on the analyte	64
2.8.6 Reproducibility and repeatability of the method	64
2.8.7 Stability of electrode.....	64
2.8.8 Sensitivity	64
2.8.9 Limit of detection.....	65
2.8.10 Interference study.....	65
2.9 Chromatographic Measurements.....	66
2.9.1 Measurement and Analysis of Gallic acid	67

2.10 Spectrophotometric Measurements.....	68
2.10.1 2,2-Diphenyl-1-picrylhydrazyl (DPPH) Assay.....	68
2.10.2 Ferric Reducing Antioxidant Power (FRAP) Assay.....	69
CHAPTER THREE	71
3.0 MODIFICATION OF CARBON PASTE ELECTRODE FOR GALLIC ACID SENSING USING AMORPHOUS ZIRCONIA NANOPARTICLES	71
3.1 Introduction.....	71
3.2 Experimental.....	72
3.2.1 Materials and Reagents	72
3.2.2 Synthesis of amorphous Zirconium dioxide nanoparticles.....	73
3.2.3 Preparation of amorphous zirconia nanoparticles-CPE.....	73
3.2.4 Electrochemical measurements using amorphous zirconia nanoparticles modified carbon paste electrode	73
3.4 Results and Discussion	74
3.4.1 Characterisation of the prepared amorphous ZrO ₂ nanoparticles-modified Carbon Paste Electrode.....	74
3.4.2 X-ray Powder Diffraction analysis.....	76
3.4.3 Fourier Transform Infrared Spectroscopy Analysis.....	77
3.4.4 Effect of pH on the Gallic acid oxidation on the amorphous zirconia nanoparticles modified carbon paste electrode	78
3.4.5 Electrochemical behaviour of Gallic acid at the zirconium dioxide nanoparticles modified CPE	79
3.4.6 Electrochemical Impedance Spectroscopy Analysis	82
3.4.7 Determination of the modified electrode surface area.....	84
3.4.8 Interaction between the amorphous zirconia nanoparticles and graphite.....	85
3.4.9 Effect of scan rate on the determination of Gallic acid	87
3.4.10 Effect of ZrO ₂ nanoparticles concentration on CPE	89
3.4.11 Effect of time on the adsorption of GA on the modified CPE.....	90

3.4.12 Effect of the modified electrode on the concentration of GA (Determination of linear detection range and LOD).....	91
3.4.13 The amorphous Zirconia nanoparticles modified CPE as compared to other work in the literature	93
3.4.14 The reproducibility and repeatability of using the modified electrode CPE for GA determination	93
3.4.15 Stability of the modified electrode	94
3.4.16 Interference studies on GA determination	95
3.4.17 Analytical application of the modified CPE.....	96
3.5 Conclusion	99
CHAPTER FOUR	101
4.0 GRAPHENE OXIDE NANOCOLLOIDS AND SiO ₂ NANOPARTICLES MODIFIED GLASSY CARBON ELECTRODE FOR ELECTROCHEMICAL DETERMINATION OF GALLIC ACID.....	101
4.1 Introduction	101
4.2 Experimental.....	102
4.2.1 Materials and Reagents	102
4.2.2 Silicon oxide nanoparticles synthesis.....	102
4.2.3 Characterisation of nano-GO-SiO ₂ -nanoparticles	103
4.3. Electrochemical Measurements	103
4.3.1 Determination of adsorption time.....	104
4.3.2 Selectivity of the modified electrode.....	104
4.4 Results and Discussion	104
4.4.1 Characterisation of nano-GO-SiO ₂ -nanoparticles modified glassy carbon electrode.....	104
4.4.2 Determination of the active surface area of the electrode	106
4.4.3 Fourier Transform Infrared Spectroscopy (FTIR)	110
4.4.4 Electrochemical Impedance Spectroscopy (EIS)	113
4.4.5 Effect of scan rate on GA determination	114
4.4.6 Oxidation of Gallic acid at bare GCE and nano-GO-SiO ₂ -nanoparticles modified GCE	115

4.4.7 Electrochemical behaviour of Gallic acid at the nano-GO-SiO ₂ nanoparticles-GCE.....	117
4.4.8 Effect of nano-GO and SiO ₂ nanoparticles concentrations in the modifying mixture	119
4.4.9 Effect of volume of nano-GO-SiO ₂ nanoparticles on GCE	120
4.4.10 Effect of adsorption time	121
4.4.11 Effect of pH on Gallic Acid Oxidation	122
4.4.12 The Mechanism of the Interaction between nano-GO-SiO ₂ -nanoparticles-GCE and Gallic Acid solutions.....	125
4.4.13 Linear detection range	127
4.4.14 Reproducibility and repeatability test	129
4.4.15 Stability of the electrode.....	129
4.4.16 Selectivity test.....	130
4.4.17 Interference study.....	132
4.4.18 Analytical application of modified electrode to determine the concentrations of Red/White Wine and Orange juice by using the standard addition method	134
4.5 Conclusion	136
CHAPTER FIVE.....	137
5.0 THE EFFECT OF ZINC OXIDE NANOPARTICLES ON THE ELECTROCHEMICAL DETERMINATION OF GALLIC ACID USING CARBON PASTE ELECTRODE.....	137
5.1 Introduction.....	137
5.2 Experimental.....	138
5.2.1 Materials and Reagents	138
5.2.2 Synthesis of ZnO nanoparticles.....	138
5.2.3 Characterisation of the ZnO nanoparticles	138
5.3 Results and Discussion	138
5.3.1 Characterisation of ZnO nanoparticles	138
5.3.2 Fourier Transform Infrared Spectroscopic analysis	140
5.3.3 Electrochemical characterisation of the ZnO nanoparticles modified carbon paste electrode	140

5.3.4 Electroactive surface area of ZnO nanoparticles-CPE.....	143
5.3.5 Electrochemical Impedance Spectroscopy (EIS)	145
5.3.5 Effect of pH on GA determination	146
5.3.6 Effect of scan rate on GA determination	147
5.3.7 Effect of concentration and limit of detection for GA determination	148
5.3.8 Reproducibility and repeatability of the method	149
5.3.9 Stability of method.....	150
5.3.10 Interference study.....	150
5.3.11 Analytical application of the method.....	151
5.4 Conclusion	153
CHAPTER SIX	155
6.0 COBALT OXIDE NANOPARTICLES MODIFIED CARBON PASTE ELECTRODE FOR THE ELECTROCHEMICAL DETERMINATION OF GALLIC ACID	155
6.1 Introduction	155
6.2 Experimental.....	155
6.2.1 Materials and Reagents	155
6.2.2 Synthesis of Cobalt oxide nanoparticles	156
6.3 Results and discussion.....	156
6.3.1 Characterisation of the prepared Cobalt Oxide nanoparticles-modified CPE	156
6.3.2 Dynamic Light Scattering (DLS) Analysis	157
6.3.3 Thermogravimetric analysis (TGA).....	157
6.3.4 Fourier Transform Infrared Spectroscopy (FTIR)	158
6.3.5 Electrochemical behaviour of Gallic acid at the modified carbon paste electrode.....	159
6.3.6 Effect of pH on Gallic acid oxidation	161
6.3.7 Effect on the scan rate	163
6.3.8 Effect of concentration changes of Cobalt oxide nanoparticles	164
6.3.9 Effect of time on adsorption of GA	165

6.3.10 Effect of the modified electrode on GA concentration	166
6.3.11 Reproducibility and repeatability of the method	168
6.3.12 Stability of the method	169
6.3.13 Interference study.....	170
6.3.14 Analytical Application of the modified electrode for the determination of GA in Red/White Wine.....	171
6.4 Conclusion	175
CHAPTER SEVEN	176
7.0 GENERAL CONCLUSIONS AND FUTURE PERSPECTIVE	176
7.1 Conclusions.....	176
7.2 Future Perspective	180
REFERENCES	183
APPENDIX I.....	213
8.1. PUBLICATION PAGES	213
APPENDIX II	219
8.2 General Calculations	219
8.2.1 Electrochemical Calculations	219
8.2.2 Statistical analysis	219
APPENDIX III.....	220
8.3 DPPH Assay	220
8.4 FRAP Assay.....	222
APPENDIX IV	225
8.5 HPLC Confirmatory Test	225
APPENDIX V	228
8.6 Electrochemical Optimisation with Gallic Acid in Methanol.....	228
8.6.1 Effect of electrolyte in the Methanol solvent.....	228
8.6.2 Determination of Gallic acid in Methanolic KCl.....	229

8.6.3 Effect of pH Value	230
8.6.4 Effect of Scan Rate	235
8.6.5 Effect of Concentration	240

List of Tables

TABLE 1. 1. DIFFERENT ELECTROCHEMICAL DETERMINATION OF PHENOLIC ACIDS (GALLIC ACID) USING CYCLIC VOLTAMMETRY	33
TABLE 1. 2. METAL OXIDE NANOPARTICLES IN DIFFERENT ELECTROCHEMICAL SENSOR SYSTEMS FOR THE DETERMINATION OF DIFFERENT ORGANIC COMPOUNDS	39
TABLE 1. 3. METAL OXIDE NANOPARTICLES AND METAL NANOPARTICLES COMPOSITES IN DIFFERENT ELECTROCHEMICAL SENSOR SYSTEMS FOR THE DETERMINATION OF GALLIC ACID.....	41
TABLE 2. 1. LIST OF CHEMICALS USED.....	47
TABLE 2. 2. PHOSPHATE BUFFER SOLUTIONS BETWEEN THE PH 5.8 – 8.0 AT 25 °C (ADAPTED FROM SIGMA-ALDRICH, UK)	49
TABLE 3. 1. EFFECTS OF VARIOUS SUBSTANCES ON THE DETERMINATION OF 5×10^{-4} MOL L ⁻¹ GALLIC ACID.....	96
TABLE 3. 2. RESULTS OF THE ANALYSIS OF GA IN SPIKED RED AND WHITE WINE	99
TABLE 4. 1. THE DIFFERENT ELECTRODES AND THEIR CALCULATED ELECTROACTIVE SURFACE AREA.	110
TABLE 4. 2. THE PEAK POTENTIAL AND PEAK CURRENT VALUES OF THE DIFFERENT ELECTRODES AND THE CORRESPONDING ELECTROLYTE ANALYSED	117
TABLE 4. 3. EFFECTS OF VARIOUS SUBSTANCES ON THE DETERMINATION OF 1×10^{-3} MOL L ⁻¹ GALLIC ACID.....	133
TABLE 4. 4 RESULTS OF THE ANALYSIS OF GA IN SPIKED RED WINE, WHITE WINE AND ORANGE JUICE	135
TABLE 5. 1. THE PARTICLE SIZE DISTRIBUTION AND AVERAGE SIZE OF THE SYNTHESISED ZNO NANOPARTICLES	139
TABLE 5. 2. THE DIFFERENT MODIFIED ELECTRODES AND THE PEAK CURRENTS ATTAINED.....	142
TABLE 5. 3. EFFECTS OF VARIOUS SUBSTANCES ON THE DETERMINATION OF 1×10^{-3} MOL L ⁻¹ GALLIC ACID.....	151
TABLE 5. 4. RESULTS OF THE ANALYSIS OF GA IN SPIKED RED WINE AND WHITE WINE.....	153
TABLE 6. 1. THE PEAK CURRENTS (I_p) AND PEAK POTENTIALS (E_p) PRODUCED BY THE DIFFERENT ELECTRODES USED FOR THE DETERMINATION OF 1×10^{-2} MOL L ⁻¹ GA IN 0.1 MOL L ⁻¹ PHOSPHATE BUFFER AT PH 2.0 AND SCAN RATE 100 MVS ⁻¹	161
TABLE 6. 2. PEAK CURRENTS AND PEAK POTENTIALS PRODUCED BY 1×10^{-3} MOL L ⁻¹ GA MEASURED BY CV USING COO-NANO-CPE AT DIFFERENT PH AND SCAN RATE 100 MVS ⁻¹	163
TABLE 6. 3. RESULTS OF THE ANALYSIS OF GA IN SPIKED RED WINE, WHITE WINE, AND ORANGE JUICE	174
TABLE 7. 1. METAL OXIDE NANOPARTICLES AND METAL NANOPARTICLES COMPOSITES IN DIFFERENT ELECTROCHEMICAL SENSOR SYSTEMS FOR THE DETERMINATION OF GALLIC ACID AND OUR ELECTRODES.....	180
APPENDIX TABLE 8. 1 THE ANTIOXIDANT SCAVENGING ACTIVITY OF GA, TR, AA AND VA ANALYSED USING DPPH ASSAY.....	222

List of Figures

FIGURE 1. 1. CHEMICAL STRUCTURE OF GALLIC ACID, GA (3,4,5-TRIHYDROXYBENZOIC ACID).....	1
FIGURE 1. 2. A VOLTAMMETRIC CELL THAT CONSISTS OF TWO ELECTRODES, WITH A POTENTIAL PROFILE OF THE CELL, SHOWING THE POTENTIAL DROP AT THE ANODE, IR LOSS, POTENTIAL DROP AT THE CATHODE.....	8
FIGURE 1. 3. AN OPERATIONAL AMPLIFIER POTENTIOSTAT. THE THREE ELECTRODES CONSIST OF THE WORKING ELECTRODE (WE), REFERENCE ELECTRODE (RE), AND A COUNTER ELECTRODE (CE)	10
FIGURE 1. 4. THE PLOT OF POTENTIAL VS. TIME IN A CYCLIC VOLTAMMETRY	11
FIGURE 1. 5. A TYPICAL VOLTAMMOGRAM OF A REDOX SPECIES (FERRICYANIDE) SHOWING THE PLOT OF CURRENT VS. POTENTIAL OBTAINED THROUGH CV, WITH PARAMETERS LIKE ANODIC PEAK POTENTIAL (EA), CATHODIC PEAK POTENTIAL (EC), ANODIC PEAK CURRENT (IA) AND CATHODIC PEAK CURRENT (IC)	12
FIGURE 1. 6. VOLTAMMOGRAMS OF AN ELECTROCHEMICALLY IRREVERSIBLE SYSTEM, WITH THE OXIDATION PEAK CURRENT (IP OX) AND THE PEAK POTENTIAL (EP OX), WITH THE INITIAL SCAN PRODUCING OXIDATION.....	15
FIGURE 1. 7. DIFFERENTIAL PULSE VOLTAMMETRY, SHOWING POTENTIAL-TIME WAVEFORM. AS A SCHEMATIC WAVEFORM OF PULSES SUPERIMPOSED ON A STAIRCASE.....	18
FIGURE 1. 8. AN EXAMPLE OF A COMPLETE DIFFERENTIAL PULSE VOLTAMMOGRAM SHOWING $N(E-EP)$ AGAINST THE PEAK CURRENT IP.....	19
FIGURE 1. 9. SCHEMATIC DIAGRAM OF THE ELECTRICAL DOUBLE LAYER, SHOWING THE INNER AND OUTER HELMHOLTZ PLANE (IHP AND OHP).....	21
FIGURE 1. 10. CHEMICAL STRUCTURES OF PHENOLIC ACIDS.....	26
FIGURE 1. 11. THE DIFFERENT ALLOTROPIC FORMS OF CARBON, SHOWING THE BASIC SIX-MEMBERED AROMATIC RINGS AS SEEN IN THE GRAPHITE, DIAMOND AND FULLERENE (CULLED FROM 'CHEMISTRY GLOSSARY' 2018)	32
FIGURE 1. 12. SCHEMATIC REPRESENTATION OF GRAPHENE WHICH IS THE FUNDAMENTAL STARTING MATERIAL FOR FULLERENE MATERIALS, CARBON NANOTUBES (CNT) AND GRAPHITE. REPRODUCED FROM (BROWNSON AND BANKS 2014) WITH PERMISSION FROM SPRINGER NATURE.....	42
FIGURE 2. 1. AN EXPERIMENTAL SET-UP THAT WAS USED IN THE ELECTROCHEMICAL MEASUREMENTS.....	53
FIGURE 2. 2. SCHEMATIC DIAGRAM OF ESSENTIAL FEATURES OF FOURIER TRANSFORM INFRARED (FTIR) SPECTROMETER, WHERE THE IR SOURCE CREATES RADIATIONS THAT TRAVELS THROUGH THE SAMPLE.....	55
FIGURE 2. 3. (A) SCHEMATIC DIAGRAM OF A WORKING ELECTRODE, SHOWING THE NON-CONDUCTING POLYMER (TEFLON), THE CONNECTING WIRE AND THE REACTIVE CARBON DISK (B) GLASSY CARBON AND GOLD ELECTRODE (ADAPTED FROM ALVATEK).....	57
FIGURE 2. 4. SCHEMATIC IMAGE OF SATURATED CALOMEL ELECTRODE AND AG/AGCL REFERENCE ELECTRODES.....	59
FIGURE 2. 5. SCHEMATIC IMAGE (A) OF PLATINUM COUNTER ELECTRODES AND PICTURES OF COUNTER ELECTRODES (B), SHOWING THE COIL-SHAPED AND STRAIGHT ELECTRODES (ADAPTED FROM BASI INC.)	60
FIGURE 2. 6. SCHEMATICS SHOWING THE EQUIVALENT CIRCUIT USED FOR THE IMPEDANCE MEASUREMENT OF THE MODIFIED ELECTRODES AT THE ELECTRODE/POTASSIUM FERRICYANIDE INTERFACE. (A)THIS IS THE CIRCUIT USED FOR THE MEASUREMENT OF AN IDEAL RESISTOR (B) MEASUREMENT OF IMPEDANCE.....	62
FIGURE 2. 7. A SCHEMATIC DIAGRAM OF HIGH-PERFORMANCE LIQUID CHROMATOGRAPHY SHOWING THE MOVEMENT OF THE MOBILE PHASE AND THE SAMPLES TO THE SEPARATING COLUMN HOUSING THE STATIONARY PHASE, THEN TO THE UV-VIS DETECTOR AND THE COMPUTER MONITOR.	67
FIGURE 2. 8. (A) THE PICTURE SHOWS COLOUR CHANGE ATTRIBUTED TO THE CHEMICAL REACTION OF DPPH AND THE ANTIOXIDANTS, WITH THE CHEMICAL STRUCTURAL CHANGE OF DPPH. (B) THE 96 WELLS PLATE SHOWING THE EXACT COLOUR CHANGE AFTER THE REACTION.....	69
FIGURE 2. 9. PICTURE OF THE 96 WELLS PLATE SHOWING THE COLOUR CHANGE WITH THE FRAP REAGENTS WITH THE TROLOX STANDARD, THE ANTIOXIDANTS AND THE BLANK. THE STRENGTH OF THE ANTIOXIDANT INVOLVED IS SHOWN BY THE DEEP BLUE COLOUR CHANGE.	70

FIGURE 3. 1 PARTICLE SIZE DISTRIBUTION OF SYNTHESIZED AMORPHOUS ZRO ₂ NANOPARTICLES.....	74
FIGURE 3. 2. (A) THE SEM IMAGE ZRO ₂ NANOPARTICLES SHOWING THE MORPHOLOGY OF THE NANOPARTICLES (B) ONE OF THE SPECTRUMS OF THE ZRO ₂ NANOPARTICLES	75
FIGURE 3. 3. XRD OF ZRO ₂ NANOPARTICLES, SHOWING THE BROAD PEAKS CORRESPONDING TO TETRAGONAL ZRO ₂ AND MONOCLINIC ZRO ₂ STRUCTURE.....	76
FIGURE 3. 4. FTIR IMAGE SHOWING THE SPECTRA OF ZRO ₂ NANOPARTICLES.....	77
FIGURE 3. 5. CYCLIC VOLTAMMOGRAMS SHOWING THE EFFECT OF PH ON THE ELECTROCHEMICAL BEHAVIOUR OF 1 X 10 ⁻² MOL L ⁻¹ GALLIC ACID AT PH RANGE OF 2.0-8.0 (INSET). THE PLOT OF THE PEAK CURRENT (I _p) AGAINST DIFFERENT PH VALUES, SHOWING THE EFFECT OF PH ON THE ELECTROCHEMICAL BEHAVIOUR OF 1 X 10 ⁻² MOL L ⁻¹ GALLIC ACID USING ZRO ₂ NANOPARTICLES MODIFIED CPE AT A SCAN RATE OF 100 MVS ⁻¹	78
FIGURE 3. 6. THE PLOT OF THE PEAK POTENTIAL (E _p) AGAINST THE DIFFERENT PH VALUES OF THE BUFFER SOLUTION, SHOWING THE LINEAR RELATIONSHIP	79
FIGURE 3. 7. CYCLIC VOLTAMMOGRAMS OF 1 X 10 ⁻² MOL L ⁻¹ GA AT ZRO ₂ NANOPARTICLES-MODIFIED CPE, BARE CPE AND BARE GLASSY CARBON ELECTRODE (GCE) IN 0.1 MOL L ⁻¹ PHOSPHATE BUFFER OF PH 2.0 AT A SCAN RATE OF 100 MVS ⁻¹	80
FIGURE 3. 8. NYQUIST PLOT REPRESENTING THE EIS MEASUREMENT OF 5 MMOL L ⁻¹ USING THE BARE CPE AND ZRO ₂ NANOPARTICLES (INSET) THE EQUIVALENT CIRCUIT SHOWING RESISTORS AND CAPACITOR.....	83
FIGURE 3. 9. THE CYCLIC VOLTAMMOGRAMS OF 1.0 X 10 ⁻³ MOL L ⁻¹ [FE(CN) ₆] ^{3-/4+} REDOX SOLUTION, USING BARE CPE AND ZRO ₂ NANOPARTICLES-MODIFIED CPE.	84
FIGURE 3. 10(A). CYCLIC VOLTAMMOGRAMS OF 1 MMOL L ⁻¹ [FE(CN) ₆] ^{3-/4+} MEASURED USING THE ZRO ₂ NANOPARTICLES MODIFIED CPE AT INCREASING SCAN RATES FROM 25 - 250 MVS ⁻¹ (B). PLOTS OF I _p VS N ^{1/2} , WHICH WOULD BE USED TO CALCULATE THE TRUE SURFACE AREA.....	85
FIGURE 3. 11. PROPOSED INTERACTION BETWEEN ZRO ₂ NANOPARTICLES (MONOCLINIC ZIRCONIA) AND GRAPHITE, SHOWING A WEAK IONIC BOND BETWEEN SOME OF THE OXYGEN AND THE POSITIVE GRAPHITE SHEET; TOWARDS THE ELECTROCHEMICAL DETERMINATION OF GALLIC ACID.....	87
FIGURE 3. 12(A) CYCLIC VOLTAMMOGRAMS OF 5.0 X 10 ⁻⁴ MOL L ⁻¹ GALLIC ACID IN PHOSPHATE BUFFER OF PH 2.0 DETERMINED WITH A ZRO ₂ NANOPARTICLES-MODIFIED CPE AT DIFFERENT SCAN RATES FROM 10 TO 1000 MVS ⁻¹ . (B) THE PLOT OF THE SCAN RATE VS THE PEAK CURRENT. (C) THE PLOTS OF LOG I _p VS LOG N SHOWING STRAIGHT LINES	88
FIGURE 3. 13. DIFFERENTIAL VOLTAMMOGRAMS SHOWING THE EFFECT OF THE AMOUNT OF ZRO ₂ NANOPARTICLES IN THE CARBON PASTE ELECTRODES.	89
FIGURE 3. 14. (A)DPV VOLTAMMOGRAMS SHOWING THE EFFECT OF ADSORPTION TIME IN THE DETERMINATION OF 1 X 10 ⁻³ MOL L ⁻¹ GA IN A 0.1 MOL L ⁻¹ PHOSPHATE BUFFER OF PH 2.0 AT A SCAN RATE OF 100 MVS ⁻¹ (B) THE PLOTS SHOWING THE SAME EFFECT OF ADSORPTION TIME	90
FIGURE 3. 15. DIFFERENTIAL VOLTAMMOGRAMS OF VARIOUS CONCENTRATIONS OF GA AT ZRO ₂ NANOPARTICLES MODIFIED CPE IN A 0.1 MOL L ⁻¹ PHOSPHATE BUFFER AT 2.0 AT SCAN RATE OF 100 MVS ⁻¹ , WITH VOLTAMMOGRAMS (A-J) THAT CORRESPONDS TO THE FOLLOWING CONCENTRATIONS A) BLANK PBS, B) 0.01 MMOL L ⁻¹ , C) 0.025 MMOL L ⁻¹ , D) 0.05 MMOL L ⁻¹ , E) 0.075 MMOL L ⁻¹ , F) 0.1 MMOL L ⁻¹ , G) 0.25 MMOL L ⁻¹ , H) 0.5 MMOL L ⁻¹ , I) 0.075 MMOL L ⁻¹ J) 1 MMOL L ⁻¹	92
FIGURE 3. 16. THE CALIBRATION CURVE SHOWING THE LINEAR DETECTION RANGE OF 1 X 10 ⁻⁵ TO 1.0 X 10 ⁻³ MOL L ⁻¹ AND A LINEAR REGRESSION EQUATION OF I _p = 1125.4 C + 2.1113 (I _p : μA, C: MMOL L ⁻¹ AND R ² = 0.9945)	93
FIGURE 3. 17. DPV VOLTAMMOGRAM OF 1 X 10 ⁻³ MOL L ⁻¹ GALLIC ACID USING ZRO ₂ NANOPARTICLES MODIFIED-CPE TO DEMONSTRATE REPRODUCIBILITY.....	94
FIGURE 3. 18. CYCLIC VOLTAMMOGRAMS SHOWING THE DETERMINATION OF 1 X 10 ⁻² MOL L ⁻¹ GA IN 1 X 10 ⁻² PHOSPHATE BUFFER AT PH 2.0 AND SCAN RATE OF 100 MVS ⁻¹ ON A DAY ONE AND DAY THIRTY.....	95
FIGURE 3. 19. DPV VOLTAMMOGRAMS OF 5 X 10 ⁻⁴ MOL L ⁻¹ GALLIC ACID WITH DIFFERENT CONCENTRATIONS OF SOME KNOWN INTERFERING COMPOUNDS IN 0.1 MOL L ⁻¹ PHOSPHATE BUFFER AT PH 2.0 AND A SCAN RATE OF 100 MVS ⁻¹	96

FIGURE 3. 20. DPV VOLTAMMOGRAMS SHOW THE DETERMINATION OF GALLIC ACID IN A REAL SAMPLE OF RED WINES (INSET) CALIBRATION GRAPH CREATED USING THE ANALYSIS OF THE REAL SAMPLE.	97
FIGURE 3. 21. DPV VOLTAMMOGRAMS SHOWING THE DETERMINATION OF GALLIC ACID IN A REAL SAMPLE OF WHITE WINE.	98
FIGURE 3. 22. CALIBRATION PLOT CREATED USING DATA FROM THE DPV VOLTAMMOGRAMS OF ANALYSING WHITE WINE.	99
FIGURE 4. 1. (A) THE SEM IMAGE SiO_2 NANOPARTICLES SHOWING THE MORPHOLOGY OF THE NANOSPHERES AND THE DIFFERENT SPECTRUMS USED FOR THE EDX, WITH (B) SHOWING THE MORPHOLOGY OF THE NANO-GO- SiO_2 NANOCOMPOSITE. (C) THE EDX ANALYSIS OF THE SiO_2 NANOPARTICLES AND THAT OF THE NANO-GO- SiO_2 NANOCOMPOSITE.	106
FIGURE 4. 2. CV VOLTAMMOGRAMS OF $1.0 \times 10^{-3} \text{ mol L}^{-1} [\text{Fe}(\text{CN})_6]^{3-}$ AT BARE GCE, SiO_2 -NANOPARTICLES-GCE, NANO-GO-GCE AND NANO-GO- SiO_2 -NANOPARTICLES; SCAN RATE 100 mVs^{-1}	107
FIGURE 4. 3. CV VOLTAMMOGRAMS OF $1.0 \times 10^{-3} \text{ mol L}^{-1} [\text{Fe}(\text{CN})_6]^{3-}$ AT (A) NANO-GO- SiO_2 -NANOPARTICLES (B) NANO-GO-GCE (C) SiO_2 NANOPARTICLES-GCE AND (D) BARE GCE; AT DIFFERENT SCAN RATES OF 10, 25, 50, 100, 150, 200, 250 AND 300 mVs^{-1} . (INSET) THE PLOT OF PEAK CURRENTS AGAINST THE SQUARE ROOT OF THE SCAN RATES USED TO DEDUCE THE ELECTROACTIVE SURFACE AREA OF THE NANO-GO- SiO_2 -NANOPARTICLES GCE USING THE RANDLES-ŠEVČIK EQUATION.	109
FIGURE 4. 4. FTIR IMAGES SHOWING THE SPECTRA OF (A) GO-NANOCOLLOIDS (B) SiO_2 NANOPARTICLES AND (C) A COMBINATION OF THE GO-NANOCOLLOIDS AND SiO_2 NANOPARTICLES	112
FIGURE 4. 5. ELECTROCHEMICAL IMPEDANCE SPECTROSCOPY AT THE MODIFIED ELECTRODES SHOWING THE IMPEDANCE OF (A) NANO-GO- SiO_2 -NANOPARTICLES (B) NANO-GO (C) SiO_2 -GCE AND (D) BARE-GCE IN A $5 \text{ mmol L}^{-1} [\text{Fe}(\text{CN})_6]^{3-/4+}$ REDOX SOLUTION AT A FREQUENCY RANGE OF 100 kHz - 0.01 Hz AND A POTENTIAL OF 0.3 V (INSET) EQUIVALENT CIRCUIT OF THE MEASUREMENT	114
FIGURE 4. 6. CYCLIC VOLTAMMOGRAMS OF $5.0 \times 10^{-4} \text{ mol L}^{-1}$ GALLIC ACID IN PHOSPHATE BUFFER OF PH 2.0 DETERMINED WITH A NANO-GO- SiO_2 -NANOPARTICLES MODIFIED GLASSY CARBON ELECTRODE AT DIFFERENT SCAN RATES FROM 10 TO 1300 mVs^{-1} . (INSET) THE PLOT OF $\log I_p$ VS $\log \nu$ SHOWING A STRAIGHT LINE.....	115
FIGURE 4. 7. CYCLIC VOLTAMMOGRAMS OF $1 \times 10^{-2} \text{ mol L}^{-1}$ GA AT NANO-GO- SiO_2 NANOPARTICLES-MODIFIED GCE, SiO_2 NANOPARTICLES-MODIFIED GCE, NANO-GO-MODIFIED GCE AND A BARE GCE IN 0.1 mol L^{-1} PHOSPHATE BUFFER OF PH 2.0 AT A SCAN RATE OF 100 mVs^{-1} ($S/N=3$)	116
FIGURE 4. 8. THE PLOT OF CATHODIC PEAK POTENTIAL VS LOG OF SCAN RATE, WITH A REGRESSION EQUATION OF $Y = 0.1635X + 0.1368$, WITH R^2 VALUE OF 0.9975.....	119
FIGURE 4. 9. VOLTAMMOGRAMS SHOWING CHANGES IN THE CONSTITUTION OF THE NANO-GO- SiO_2 -NANOPARTICLES USED TO DETERMINE $1 \times 10^{-2} \text{ mol L}^{-1}$ GA IN 0.1 mol L^{-1} PHOSPHATE BUFFER AT PH 2.0 USING CV AT A SCAN RATE OF 100 mVs^{-1}	120
FIGURE 4. 10. VOLTAMMOGRAMS SHOWING THE EFFECT OF CHANGING VOLUMES OF NANO-GO- SiO_2 -NANOPARTICLES IN THE DETERMINATION OF $1 \times 10^{-2} \text{ mol L}^{-1}$ GA IN A $1 \times 10^{-1} \text{ mol L}^{-1}$ PHOSPHATE BUFFER AT PH 2.0 USING CV AT A SCAN RATE OF 100 mVs^{-1}	121
FIGURE 4. 11. (A) DPV VOLTAMMOGRAMS SHOWING THE EFFECT OF ADSORPTION TIME IN THE DETERMINATION OF $1 \times 10^{-3} \text{ mol L}^{-1}$ GA IN A 0.1 mol L^{-1} PHOSPHATE BUFFER OF PH 2.0 AT A SCAN RATE OF 100 mVs^{-1} (B) AND THE PLOTS SHOWING THE SAME EFFECT OF ADSORPTION TIME.....	122
FIGURE 4. 12. CYCLIC VOLTAMMOGRAMS SHOWING THE EFFECT OF PH ON THE ELECTROCHEMICAL BEHAVIOUR OF $1 \times 10^{-4} \text{ mol L}^{-1}$ GALLIC ACID. (INSET). THE PLOT OF THE PEAK CURRENT (I_p) AGAINST DIFFERENT PH VALUES, SHOWING THE EFFECT OF PH ON THE ELECTROCHEMICAL BEHAVIOUR OF $1 \times 10^{-4} \text{ mol L}^{-1}$ GALLIC ACID USING BARE GLASSY CARBON ELECTRODE AT A SCAN RATE OF 100 mVs^{-1}	123
FIGURE 4. 13. THE PLOT OF PH ON THE PEAK POTENTIAL E_p ON DETECTION OF $1 \times 10^{-4} \text{ mol L}^{-1}$ GALLIC ACID USING NANO-GO- SiO_2 -GCE AT A SCAN RATE OF 100 mVs^{-1}	124

FIGURE 4. 14. DIFFERENTIAL PULSE VOLTAMMOGRAMS OF VARIOUS CONCENTRATION OF GA AT NANO-GO-SIO ₂ -NANOPARTICLES IN A 0.1 MOL L ⁻¹ PHOSPHATE BUFFER AT PH 2.0 AT A SCAN RATE OF 100 MVS ⁻¹ , WITH VOLTAMMOGRAMS (A-K) THAT CORRESPOND TO THE FOLLOWING CONCENTRATIONS A) 0.0, B) 0.00625 MMOL L ⁻¹ , C) 0.0125 MMOL L ⁻¹ , D) 0.025 MMOL L ⁻¹ , E) 0.05 MMOL L ⁻¹ , F) 0.075 MMOL L ⁻¹ , G) 0.1 MMOL L ⁻¹ , H) 0.25 MMOL L ⁻¹ , I) 0.5 MMOL L ⁻¹ , J) 0.75 MMOL L ⁻¹ , K) 1 MMOL L ⁻¹	128
FIGURE 4. 15. THE CALIBRATION CURVE FOR THE DETERMINATION OF GALLIC ACID.....	128
FIGURE 4. 16. DIFFERENTIAL PULSE VOLTAMMOGRAMS DEPICTING THE STABILITY OF THE MODIFIED ELECTRODE AFTER 30 DAYS	130
FIGURE 4. 17. CYCLIC VOLTAMMOGRAMS SHOWING THE 0.36 MMOL L ⁻¹ URIC ACID CONCENTRATION, 0.48 MMOL L ⁻¹ GA AND A MIXTURE OF THE TWO CONCENTRATIONS OF GA AND UA IN A 0.1 MOL L ⁻¹ PHOSPHATE BUFFER SOLUTION AT A PH 2.0 AT SCAN RATE 100 MVS ⁻¹	131
FIGURE 4. 18. CYCLIC VOLTAMMOGRAMS SHOWING THE CONSTANT 0.36 MMOL L ⁻¹ UA CONCENTRATION AND INCREASING GA CONCENTRATION FROM 0.1 TO 0.48 MMOL L ⁻¹ (A TO E) IN A 0.1 MOL L ⁻¹ PHOSPHATE BUFFER AT PH 2.0 AT A SCAN RATE OF 100 MVS ⁻¹ . (INSET) A GRAPH SHOWING THE INCREASING CONCENTRATION OF GA AGAINST THE INCREASING PEAK CURRENT IN A CONSTANT UA CONCENTRATION OF 3.6 X 10 ⁻⁴ MOL L ⁻¹	132
FIGURE 4. 19. DPV VOLTAMMOGRAMS OF 1 X 10 ⁻³ MOL L ⁻¹ GALLIC ACID WITH DIFFERENT CONCENTRATIONS OF SOME KNOWN INTERFERING COMPOUNDS IN 0.1 MOL L ⁻¹ PHOSPHATE BUFFER AT PH 2.0 AND A SCAN RATE OF 100 MVS ⁻¹	133
FIGURE 4. 20. VOLTAMMOGRAMS OF ALIQUOTS OF 1 X 10 ⁻² MOL L ⁻¹ OF GA ADDED INTO RED WINE USING A STANDARD ADDITION METHOD.....	135
FIGURE 5. 1. (A) SEM IMAGE OF ZNO NANOPARTICLES (B) SEM IMAGE OF ZNO-NANOPARTICLES HOMOGENIZED IN THE CARBON PASTE ELECTRODE (C) THE EDXA ANALYSIS OF THE SYNTHESISED COMPOUND SHOWING ITS COMPOSITION OF ZINC AND OXYGEN.....	139
FIGURE 5. 2. FT-IR SPECTRA OF ZNO NANOPARTICLES.....	140
FIGURE 5. 3. VOLTAMMOGRAMS OF 1 X 10 ⁻² MOL L ⁻¹ GALLIC ACID IN A 1 X 10 ⁻¹ MOL L ⁻¹ PBS BUFFER AT PH 2.0, DETERMINED USING A CARBON PASTE ELECTRODE, ZNO CARBON NANOTUBE-CPE AND ZNO NANOPARTICLES MODIFIED CARBON PASTE ELECTRODE USING CYCLIC VOLTAMMETRY, AT A SCAN RATE OF 100 MVS ⁻¹ AT ROOM TEMPERATURE.....	141
FIGURE 5. 4. CYCLIC VOLTAMMOGRAMS OF THE DIFFERENT CPE MODIFICATIONS USED TO DETERMINE 1 X 10 ⁻² MOL L ⁻¹ GA IN 1 X 10 ⁻¹ MOL L ⁻¹ PHOSPHATE BUFFER AT PH 2.0 WITH A SCAN RATE OF 100 MVS ⁻¹ . (A) ZNO-CPE MODIFICATION (B) ZNO-CNT-CPE MODIFICATION, (C) CNT-CPE MODIFICATION AND (D) THE DIFFERENT ELECTRODES PUT TOGETHER.	143
FIGURE 5. 5. (A) VOLTAMMOGRAMS OF NANO-ZNO-CPE AND BARE CPE (B) VOLTAMMOGRAMS OF 5 MMOL L ⁻¹ OF K ₃ FE[(CN) ₆] ³⁻ / ⁴⁺ AT DIFFERENT SCAN RATES USED FOR THE CALCULATION OF THE REACTIVE SURFACE AREA OF THE MODIFIED CPE.(C) THE PLOT OF PEAK CURRENT VS SQUARE ROOT OF SCAN RATE.....	144
FIGURE 5. 6. ELECTROCHEMICAL IMPEDANCE SPECTROSCOPY (EIS) AT CPE SHOWING THE BARE CPE AND THE NANO-ZNO-CPE IN A 5 MMOL L ⁻¹ K ₃ FE[(CN) ₆] – K ₄ FE [(CN) ₆ . FREQUENCY RANGE FROM 0.01-100KHZ.....	145
FIGURE 5. 7. (A). CYCLIC VOLTAMMOGRAMS SHOWING THE EFFECT OF PH ON THE ELECTROCHEMICAL BEHAVIOUR OF 1 X 10 ⁻⁴ MOL L ⁻¹ GALLIC ACID. (B). THE PLOT OF THE PEAK POTENTIAL (EP) AGAINST DIFFERENT PH VALUES, SHOWING THE EFFECT OF PH ON THE ELECTROCHEMICAL BEHAVIOUR OF 1 X 10 ⁻³ MOL L ⁻¹ GALLIC ACID USING A ZNO-NANOPARTICLES-CPE AT A SCAN RATE OF 100 MVS ⁻¹	147
FIGURE 5. 8. (A) CYCLIC VOLTAMMOGRAMS OF NANO-ZNO-CPE IN A 1 X 10 ⁻¹ MOL L ⁻¹ PBS (PH 2.0) WITH A 1 X 10 ⁻² MOL L ⁻¹ GA AT A SCAN RATE OF 25 TO 1100 MVS ⁻¹ (B) THE LINEAR RELATIONSHIP BETWEEN THE I _p AND THE SCAN RATE AND (C) THE LINEAR RELATIONSHIP BETWEEN THE I _p VS SQUARE ROOT OF THE SCAN RATE.	148
FIGURE 5. 9. (A) DIFFERENTIAL PULSE VOLTAMMOGRAMS OF VARIOUS CONCENTRATION OF GA AT ZNO-NANOPARTICLES-CPE IN A 0.1 MOL L ⁻¹ PHOSPHATE BUFFER AT PH 2.0 AT A SCAN RATE OF 100 MVS ⁻¹ WITH VOLTAMMOGRAMS (A-J) THAT CORRESPONDS TO THE FOLLOWING CONCENTRATIONS A) 0.0, B) 0.001 MMOL L ⁻¹ , C) 0.0025 MMOL L ⁻¹ , D) 0.005 MMOL L ⁻¹ , E) 0.0075 MMOL L ⁻¹ , F) 0.01 MMOL L ⁻¹ , G) 0.025 MMOL L ⁻¹ , H) 0.05 MMOL L ⁻¹ , I) 0.5 MMOL L ⁻¹ . (B) THE CALIBRATION CURVE FOR THE DETERMINATION OF GA.....	149

FIGURE 5. 10. VOLTAMMOGRAMS OF 1×10^{-3} MOL L ⁻¹ GALLIC ACID IN A 1×10^{-1} MOL L ⁻¹ PBS BUFFER AT PH 2.0 MEASURED USING NANO-ZNO-CPE TO MEASURE (A) REPEATABILITY AND (B) STABILITY USING CYCLIC VOLTAMMETRY, AT A SCAN RATE OF 100 MVS ⁻¹ AT ROOM TEMPERATURE.....	150
FIGURE 5. 11. (A) DIFFERENTIAL PULSE VOLTAMMOGRAMS OF ALIQUOTS OF 1×10^{-2} MOL L ⁻¹ OF GA ADDED INTO RED WINE USING A STANDARD ADDITION METHOD. (B) CALIBRATION CURVE CREATED USING DATA FROM THE DPV VOLTAMMOGRAMS OF ANALYSING RED WINE.....	152
FIGURE 5. 12. (A) DIFFERENTIAL PULSE VOLTAMMOGRAMS OF ALIQUOTS OF 1×10^{-2} MOL L ⁻¹ OF GA ADDED INTO RED WINE USING A STANDARD ADDITION METHOD. (B) CALIBRATION CURVE CREATED USING DATA FROM THE DPV VOLTAMMOGRAMS OF ANALYSING RED WINE.....	153
FIGURE 6. 1. (A) THE SEM IMAGE OF COBALT OXIDE NANOPARTICLES SHOWING THE MORPHOLOGY OF THE NANOPARTICLES WITH (INSET) CO ₃ O ₄ IN 100 NM (B)SEM IMAGE OF COO-NANO-CPE, WITH THE PARAFFIN HOLDING THE COBALT OXIDE NANOPARTICLES AND GRAPHITE TOGETHER.	156
FIGURE 6. 2. FT-IR IMAGE SHOWING THE SPECTRA OF CO ₃ O ₄ NANOPARTICLES.....	159
FIGURE 6. 3. CYCLIC VOLTAMMOGRAMS OF 1×10^{-2} MOL L ⁻¹ GA AT CO ₃ O ₄ NANOPARTICLES-MODIFIED CPE, BULK CO ₃ O ₄ NANOPARTICLES-MODIFIED CPE, BARE CPE AND BARE GLASSY CARBON ELECTRODE (GCE) IN 0.1 MOL L ⁻¹ PHOSPHATE BUFFER OF PH 2.0 AT A SCAN RATE OF 100 MVS ⁻¹	160
FIGURE 6. 4. (A) THE CYCLIC VOLTAMMOGRAMS OF 1×10^{-3} MOL L ⁻¹ GA IN THE DIFFERENT PH RANGE OF 2.0 TO 10.0 AT A SCAN RATE 100 MVS ⁻¹ (B) ZOOMED IMAGE OF THE VOLTAMMOGRAMS (C) A GRAPH OF PH AGAINST THE PEAK CURRENTS.....	162
FIGURE 6. 5. (A) CV VOLTAMMOGRAMS OF 1×10^{-3} MOL L ⁻¹ GA IN 1×10^{-1} MOL L ⁻¹ PHOSPHATE BUFFER SOLUTION AT PH 2.0, SHOWING DIFFERENT SCAN RATES RANGING FROM 50 -1400 MVS ⁻¹ (B) PLOT OF THE SCAN RATES FROM 50-400 MVS ⁻¹ AGAINST THE PEAK CURRENT.....	164
FIGURE 6. 6. VOLTAMMOGRAMS SHOWING CHANGES IN THE CONSTITUTION OF THE CARBON PASTE ELECTRODE USING 5%, 10%, 15% AND 20% COBALT OXIDE NANOPARTICLES CONSTITUTED IN THE MODIFIED CPE. THIS WAS USED TO DETERMINE 1×10^{-2} MOL L ⁻¹ GA IN 1×10^{-1} MOL L ⁻¹ PHOSPHATE BUFFER AT PH 2.0 USING CV AT A SCAN RATE OF 100 MVS ⁻¹	165
FIGURE 6. 7. (A) DPV VOLTAMMOGRAMS SHOWING THE EFFECT OF TIME ON THE ADSORPTION OF GA ON THE SURFACE OF COO-NANO-CPE IN THE DETERMINATION OF 1×10^{-3} MOL L ⁻¹ GA IN A 1×10^{-1} MOL L ⁻¹ PHOSPHATE BUFFER OF PH 2.0 AT A SCAN RATE OF 100 MVS ⁻¹ (B) THE PLOTS SHOWING THE SAME EFFECT OF TIME ON ADSORPTION	166
FIGURE 6. 8. DIFFERENTIAL VOLTAMMOGRAMS OF VARIOUS CONCENTRATIONS OF GA AT COO-NANO-CPE IN A 0.1 MOL L ⁻¹ PHOSPHATE BUFFER AT 2.0 AT SCAN RATE OF 100 MVS ⁻¹ , WITH VOLTAMMOGRAMS (A-J) THAT CORRESPONDS TO THE FOLLOWING CONCENTRATIONS A) BLANK PBS, B) 1×10^{-4} MMOL L ⁻¹ , C) 2.5×10^{-4} MMOL L ⁻¹ , D) 5×10^{-4} MMOL L ⁻¹ , E) 7.5×10^{-4} MMOL L ⁻¹ , F) 1×10^{-3} MMOL L ⁻¹ , G) 2.5×10^{-3} MMOL L ⁻¹ , H) 5×10^{-3} MMOL L ⁻¹ , I) 7.5×10^{-3} MMOL L ⁻¹ , J) 1×10^{-2} MMOL L ⁻¹ (INSET) PLOT OF CONCENTRATION OF GA AGAINST PEAK CURRENTS.....	167
FIGURE 6. 9. THE PLOT OF THE PEAK CURRENT (I _p) AGAINST THE CONCENTRATION OF GA, SHOWING THE EFFECT OF CONCENTRATION ON THE ELECTROCHEMICAL BEHAVIOUR OF INCREASING GA CONCENTRATION, USING COO-NANO-CPE AT A SCAN RATE OF 100 MVS ⁻¹	168
FIGURE 6. 10 DPV VOLTAMMOGRAMS OF 5×10^{-4} MOL L ⁻¹ GALLIC ACID SHOWING (A) REPRODUCIBILITY OF THE COO NANOPARTICLES MODIFIED CPE (B) REPEATABILITY OF THE COO NANOPARTICLES MODIFIED CPE.....	169
FIGURE 6. 11. DPV VOLTAMMOGRAMS OF 5×10^{-4} MOL L ⁻¹ GALLIC ACID, SHOWING VOLTAMMOGRAMS MEASURED BY THE SAME ELECTRODES AFTER 0 DAYS, 15 DAYS AND 30 DAYS: SHOWING STABILITY.	169
FIGURE 6. 12. DPV VOLTAMMOGRAMS OF 5×10^{-4} MOL L ⁻¹ GALLIC ACID WITH DIFFERENT CONCENTRATIONS OF SOME KNOWN INTERFERING COMPOUNDS IN 0.1 MOL L ⁻¹ PHOSPHATE BUFFER AT PH 2.0 AND A SCAN RATE OF 100 MVS ⁻¹	170
FIGURE 6. 13. (A) VOLTAMMOGRAMS OF ALIQUOTS OF 1×10^{-2} MOL L ⁻¹ OF GA ADDED INTO RED WINE USING A STANDARD ADDITION METHOD (B) CALIBRATION CURVE OF THE STANDARD ADDITION OF GALLIC ACID.	172
FIGURE 6. 14. (A) VOLTAMMOGRAMS OF ALIQUOTS OF 1×10^{-2} MOL L ⁻¹ OF GA ADDED INTO WHITE WINE USING A STANDARD ADDITION METHOD (B) CALIBRATION CURVE OF THE STANDARD ADDITION OF GALLIC ACID.	173

FIGURE 6. 15. (A) VOLTAMMOGRAMS OF ALIQUOTS OF 1×10^{-2} MOL L⁻¹ OF GA ADDED INTO ORANGE JUICE USING A STANDARD ADDITION METHOD (B) CALIBRATION CURVE OF THE STANDARD ADDITION OF GALLIC ACID. 174

APPENDIX FIGURE 8. 1. (A) GRAPH SHOWING THE IC₅₀ OF GALLIC ACID, WHICH IS THE AMOUNT GALLIC ACID NEEDED TO SCAVENGE 50% OF THE FREE RADICAL, WHICH IN THIS CASE IS DPPH. (B) THE LINEAR PLOT USED TO DEDUCE THE IC₅₀..... 221

APPENDIX FIGURE 8. 2 (A) GRAPH SHOWING THE IC₅₀ OF VANILLIN, WHICH IS THE AMOUNT OF VANILLIN NEEDED TO SCAVENGE 50% OF THE FREE RADICAL, WHICH IN THIS CASE IS DPPH. (B) THE LINEAR PLOT USED TO DEDUCE THE IC₅₀..... 221

APPENDIX FIGURE 8. 3 THE PLOT OF THE ANTIOXIDANT ACTIVITY OF GALLIC ACID USING FRAP 223

APPENDIX FIGURE 8. 4 THE PLOT OF THE ANTIOXIDANT ACTIVITY OF VANILLIN DETERMINED USING FRAP 223

APPENDIX FIGURE 8. 5 THE PLOT OF THE ANTIOXIDANT ACTIVITY OF ASCORBIC ACID DETERMINED USING FRAP 224

APPENDIX FIGURE 8. 6. CHROMATOGRAM OF GALLIC ACID STANDARD AT RETENTION TIME 3.13 MINS. GIVING THE TIME GALLIC ACID WOULD BE EXPECTED IN A RED OR WHITE WINE. 225

APPENDIX FIGURE 8. 7. CHROMATOGRAM OF RED WINE SHOWING THE GALLIC ACID PEAK AT RETENTION 3.16 MIN. 225

APPENDIX FIGURE 8. 8. CHROMATOGRAM OF WHITE WINE SHOWING THE GALLIC ACID PEAK AT THE RETENTION TIME 3.12 MIN 226

APPENDIX FIGURE 8. 9. CALIBRATION GRAPH OF THE GALLIC ACID STANDARD, FROM THE HPLC CHROMATOGRAMS..... 227

APPENDIX FIGURE 8. 10. VOLTAMMOGRAMS OF 1×10^{-2} MOL L⁻¹ GALLIC ACID IN DIFFERENT BUFFERS MEASURED AT A SCAN RATE OF 100 MVS⁻¹ (A) 1×10^{-1} PHOSPHATE BUFFER, (B) 0.33 MOL L⁻¹ METHANOLIC KCL (C) ETHANOLIC KNO₃ (D) COMBINATION OF THE VOLTAMMOGRAMS OF 1×10^{-2} MOL L⁻¹ GALLIC ACID IN METHANOLIC KCL AND THAT OF ETHANOLIC KNO₃..... 229

APPENDIX FIGURE 8. 11. VOLTAMMOGRAMS OF 1×10^{-3} MOL L⁻¹ GA IN DIFFERENT SOLVENTS AND ELECTROLYTES USING CYCLIC VOLTAMMETRY AT A SCAN RATE OF 100 MVS⁻¹ AT ROOM TEMPERATURE..... 230

APPENDIX FIGURE 8. 12. CYCLIC VOLTAMMOGRAMS SHOWING THE EFFECT OF THE PH OF THE METHANOLIC KCL ELECTROLYTE ON THE DETECTION OF 1 MMOL L⁻¹ GALLIC ACID AT A SCAN RATE OF 100 MVS⁻¹ ROOM TEMPERATURE 231

APPENDIX FIGURE 8. 13. (A) VOLTAMMOGRAMS OF 1×10^{-3} MOL L⁻¹ VA IN 0.1 MOL L⁻¹ PHOSPHATE BUFFER USING GLASSY CARBON ELECTRODE AT A SCAN RATE OF 100 MVS⁻¹ AT ROOM TEMPERATURE SHOWING THE EFFECT OF DIFFERENT PH (B) PLOT OF PH VS THE PEAK CURRENTS (C) PLOT OF THE EFFECT OF PH VS THE PEAK POTENTIAL..... 232

APPENDIX FIGURE 8. 14. (A) VOLTAMMOGRAMS OF 1×10^{-3} MOL L⁻¹ AA IN 0.1 MOL L⁻¹ PHOSPHATE BUFFER USING GLASSY CARBON ELECTRODE AT A SCAN RATE OF 100 MVS⁻¹ AT ROOM TEMPERATURE SHOWING THE EFFECT OF DIFFERENT PH (B) PLOT OF PH VS THE PEAK CURRENTS (C) PLOT OF THE EFFECT OF PH VS THE PEAK POTENTIAL..... 233

APPENDIX FIGURE 8. 15. (A) VOLTAMMOGRAMS OF 1×10^{-3} MOL L⁻¹ GA IN 0.1 MOL L⁻¹ PHOSPHATE BUFFER USING GLASSY CARBON ELECTRODE AT A SCAN RATE OF 100 MVS⁻¹ AT ROOM TEMPERATURE SHOWING THE EFFECT OF DIFFERENT PH (B) PLOT OF PH VS THE PEAK CURRENTS (C) PLOT OF THE EFFECT OF PH VS THE PEAK POTENTIAL..... 234

APPENDIX FIGURE 8. 16. (A) VOLTAMMOGRAMS OF 1×10^{-2} MOL L⁻¹ VANILLIN IN METHANOLIC KCL AT DIFFERENT SCAN RATES SHOWING CHANGES IN PEAK CURRENT AS SCAN RATE INCREASES (B) PLOT OF THE PEAK CURRENT AGAINST THE SCAN RATE FROM 20 MVS⁻¹ TO 100 MVS⁻¹ (C) PLOT OF THE PEAK CURRENT AGAINST THE SQUARE ROOT OF SCAN RATE (D) PLOT OF THE PEAK POTENTIAL AGAINST THE LOG OF THE SCAN RATE..... 237

APPENDIX FIGURE 8. 17. (A) VOLTAMMOGRAMS OF 1×10^{-2} MOL L⁻¹ ASCORBIC ACID IN METHANOLIC KCL AT DIFFERENT SCAN RATES OF RANGE 20 MVS⁻¹ TO 140 MVS⁻¹, SHOWING CHANGES IN PEAK CURRENT AS SCAN RATE INCREASES (B) PLOT OF THE PEAK CURRENT AGAINST THE SQUARE ROOT OF SCAN RATE (C) PLOT OF THE PEAK POTENTIAL AGAINST THE LOG OF THE SCAN RATE..... 239

APPENDIX FIGURE 8. 18. (A) VOLTAMMOGRAMS OF 1×10^{-2} MOL L⁻¹ GALLIC ACID IN METHANOLIC KCL AT DIFFERENT SCAN RATES SHOWING CHANGES IN PEAK CURRENT AS SCAN RATE INCREASES (B) PLOT OF THE PEAK CURRENT AGAINST THE SCAN RATE FROM 20 MVS⁻¹ TO 140 MVS⁻¹ (C) PLOT OF THE PEAK CURRENT AGAINST THE SQUARE ROOT OF SCAN RATE (D) PLOT OF THE PEAK POTENTIAL AGAINST THE LOG OF THE SCAN RATE..... 240

APPENDIX FIGURE 8. 19. (A) VOLTAMMOGRAMS OF INCREASING CONCENTRATION OF VANILLIN IN METHANOLIC KCL BUFFER, AT A SCAN RATE OF 100MV/S (B) LINEAR PLOT OF CURRENT AGAINST POTENTIAL; DEPICTING THE LINEAR RELATIONSHIP BETWEEN INCREASE CONCENTRATION OF THE VANILLIN AND THE PEAK CURRENT; WITH LINEAR REGRESSION EQUATION OF $I_p = 39.871 \text{ CONC. (MMOL L}^{-1}) + 9.9519$ AND $R^2 = 0.9922$ 241

APPENDIX FIGURE 8. 20. (A) VOLTAMMOGRAMS OF INCREASING CONCENTRATION OF GALLIC ACID IN METHANOLIC KCL BUFFER, AT A SCAN RATE OF 100MV/S (B) LINEAR PLOT OF CURRENT AGAINST CONCENTRATION; DEPICTING THE LINEAR RELATIONSHIP BETWEEN INCREASE CONCENTRATION OF GALLIC ACID AND THE PEAK CURRENT.242

Terms and Abbreviations

A	Ampere or electrode area
AA	Ascorbic acid
AFM	Atomic force microscopy
Ag/AgCl	Silver and silver chloride electrode
AmZr	Amorphous zirconia
BDE	Bond dissociation enthalpy
BDD	Boron doped diamond electrode
C	Concentration
CA	Chronoamperometry
CAT	Catalase
CCE	Carbon ceramic electrode
CNT	Carbon nanotubes
CPE	Carbon paste electrode
Cs	Chitosan
CV	Cyclic voltammetry
CWES	Coated wire electrodes
D	Diffusion coefficient
DA	Dopamine
DFT	Density functional theory calculations
DLS	Dynamic light scattering
DOSs	Density of states
DPPH	1,1-diphenyl-2-picrylhydrazyl
DPV	Differential pulse voltammetry
DVLO	Derjaguin-Landau-Verwey-Overbeek
E	Potential
EDX	Energy dispersive X-ray spectroscopy
EDXA	Energy dispersive X-ray analysis
EIS	Electrochemical impedance spectroscopy
E_{pa}	Anodic peak potential
E_{pc}	Cathodic peak potential
Eq.	Equation
ERGO	Electrochemically reduced graphene oxide
F	Faraday constant
FC	Folin-Ciocalteu

FETS	Field effect transistors
FRAP	Ferric reducing ability of plasma
FTIR	Fourier-Transform Infrared Spectroscopy
GA	Gallic acid
GCE	Glassy carbon electrode
GO	Graphene oxide
GPX	Glutathione peroxidase
GR	Graphene
GSH	Glutathione
HAT	Hydrogen atom transfer
HPLC	High performance liquid chromatograph
Hz	Hertz
I	Current
IES	Ion selective electrode
IHP	Inner Helmholtz Plane
I_o	Current density
IP	Ionisation potential
I_{pa}	Anodic peak current
I_{pc}	Cathodic peak current
K_m	Michaelis constant
K_s	Heterogeneous electron transfer rate
LOD	Limit of Detection
LOQ	Limit of Quantification
MO	Metal oxides
MO NPs	Metal oxide nanoparticles
MWCNT	Multi-walled carbon nanotubes
n	Number of electrons transferred
Nano-GO	Graphene oxide nanocolloids
NPs	Nanoparticles
OHP	Outer Helmholtz Plane
PBs	Phosphate buffer solution
R	Molar gas constant
R_{ct}	Electron transfer resistant
RE	Reference electrode
rGO	Reduced graphene oxide

RNS	Reactive nitrogen species
ROS	Reactive oxygen species
R_s	Resistance of electrolyte
RSD	Relative standard deviation
Q	Charge
QCM-D	Quartz Crystal Microbalance with dissipation monitoring
SCE	Saturated calomel electrode
SdPLET	Sequential double proton loss electron transfer
SEM	Scanning electron microscope
SET	Single electron transfer
SOD	Superoxide dismutase
Std. dev.	Standard deviation
SPEs	Screen printed electrode
SPLET	Sequential proton loss electron transfer
SWCNT	Single-Walled Carbon Nanotube
SWV	Square wave voltammetry
T	Temperature
t	Time
TEAC	Trolox equivalent antioxidant capacity
TNrGO	Titanium nitride-reduced graphene oxide
TPC	Total phenolic content
t_R	Retention time
Trolox	6-hydroxy-2,5,7,8-tetramethylchroman-2-carboxylic acid
UA	Uric acid
μA	Micro-Ampere
UV	Ultraviolet
v	Scan rate
V	Volts
VA	Vanillin
VASP	Vienna ab initio simulation package
v/v	Volume per volume
WE	Working electrode
WCrGO	Wolfram carbide reduced graphene oxide
XPS	X-ray photoelectron spectroscopy
XRD	X-ray power diffraction

Z	Impedance
Z^1	Real complex plane impedance
Z^2	Imaginary complex plane impedance
Z_w	Warburg impedance

Thesis Overview

The thesis describes the development of electrodes using new materials for the electrochemical determination of GA and it is structured into seven different chapters.

Chapter 1 describes the different electrochemical methods used and the theories behind the use of these methods. This chapter also looks at the main analyte GA, its importance in everyday life and a review of the various different electrodes that have been used for its electrochemical determination.

Chapter 2 of this thesis is basically the materials and methods chapter of the thesis. It describes in detail the different techniques used for the determination of GA and the methods used for the fabrication of the different working electrodes. The procedures that were followed for the preparation of the buffer solutions and other solutions used in the course of the studies. This chapter also describes in detail, the instruments used and the reason why they were used.

In **Chapter 3** the electrochemical oxidation of GA at a metal oxide nanoparticle modified carbon paste electrode (CPE) was investigated. The main aim of the work here was to develop a carbon paste electrode modified with ZrO₂ nanoparticles for the sensitive and selective determination of GA. The carbon paste electrode was modified with amorphous zirconia nanoparticles and the corresponding voltammetric results of the ZrO₂-modified-CPE showed efficient electrochemical oxidation of GA, with a significantly enhanced peak current from 261 $\mu\text{A} \pm 3$ for the bare carbon paste electrode to about 451 $\mu\text{A} \pm 1$ for the ZrO₂ nanoparticles modified CPE.

Chapter 4 describes the development of an electrochemical sensor based on the synergistic effect of graphene oxide nanocolloids and SiO₂ nanoparticles on the determination of GA. The developed electrochemical sensor produced voltammetric results that showed, the graphene oxide nanocolloids and SiO₂-nanoparticles exhibited efficient electrochemical oxidation of GA. The oxidation of GA showed a significant enhancement of the response signal, from 241 $\pm 3.8 \mu\text{A}$ for the bare GCE to about 411 $\pm 0.9 \mu\text{A}$ for the modified GCE. The selectivity of the modified electrode was studied with the simultaneous determination of gallic

acid (GA) and uric acid (UA) and their selectivity were demonstrated with distinct peaks at potentials of 0.51 V and 0.68 V respectively.

Chapter 5 further details the electrochemical behaviour of GA on the surface of a zinc oxide nanoparticles-modified carbon paste electrode. The zinc oxide nanoparticles were used to modify carbon paste electrode for a fast and sensitive electrochemical determination of GA. Using CV and DPV techniques the nano-ZnO-modified electrode exhibited an efficient and sensitive GA oxidation, that showed a significant enhancement of the peak current from $250 \pm 1.3 \mu\text{A}$ for CPE to about $410 \pm 2.0 \mu\text{A}$ for the ZnO nanoparticles modified CPE.

In Chapter 6 another metal oxide nanoparticle was used for the modification of carbon paste electrode for the electrochemical determination of GA. Cobalt oxide nanoparticles were synthesised, characterised and then used for modification of carbon paste electrode, for GA determination. The electrochemical behaviour of GA on the Cobalt oxide nanoparticle modified CPE (CoO-nano-CPE) was studied using CV, by measuring $1 \times 10^{-2} \text{ mol L}^{-1}$ of GA in a $1 \times 10^{-1} \text{ mol L}^{-1}$ phosphate buffer, pH 2.0 at a scan rate of 100 mVs^{-1} . The modified electrode produced a peak current of $404 \pm 1.8 \mu\text{A}$ at a peak potential of 0.61 V as compared to the bare CPE with a peak current of 302 ± 3.8 .

Chapter 7 the final chapter of this thesis gives us a general conclusion of the work done and a look at the future. This chapter looks at the importance of some of the findings in the area of electrochemical determination of GA. It also looks at the individual electrodes and some of their drawbacks; in a view to recommending the most effective. Meanwhile, looking forward, the chapter also proposed some experiments which I could have done and their importance in future works.

CHAPTER ONE

1.0 GENERAL INTRODUCTION AND LITERATURE REVIEW

1.1 Overview

Gallic acid (GA) ($C_6H_2(OH)_3COOH$) is known chemically as 3,4,5-trihydroxybenzoic acid (Figure 1.1) and it is a naturally occurring phenolic compound found in grapes, banana, blueberries, tea and several medicinal plants (Yilmaz, Kekillioglu and Mert 2013). GA has also been used in the pharmaceutical industry for products like Dermatol, AiroI and bismuth salts of GA (Becerra-Herrera *et al.* 2015). A number of studies have shown GA to have anti-carcinogenic (Chia *et al.* 2010), anti-tumour (Liang *et al.* 2012), anti-mutagenic (Jeng Dong *et al.* 2011), anti-HIV (Kratz *et al.* 2008) and antioxidant capacities. This has led to its recommended use as an antioxidant in the human diet because it can reduce the risk of the development of disease; by slowing down or preventing molecular oxidation in the body, known as oxidative stress (Pinchuk *et al.* 2012). Furthermore, human diseases like Alzheimer's disease, cardiovascular diseases, Parkinson's disease, diabetes and cancer have been linked to oxidative stress (Prieto-Simón *et al.* 2008; Pisoschi, Cimpeanu and Predoi 2015).

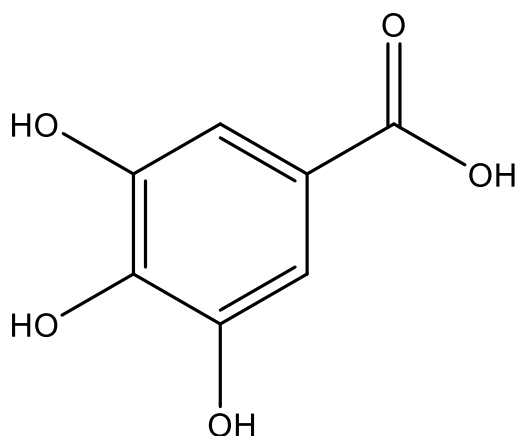


Figure 1. 1. Chemical structure of Gallic acid, GA (3,4,5-trihydroxybenzoic acid)

The importance of GA and other natural antioxidants (vitamins, carotenoids, flavonoids, or phenolic compounds) in our diets and health; in oxidative stress control or reduction, has led to the development of several *in-vitro* chemically based assays. These assays have been used to determine the antioxidant capacities and properties of these antioxidants. The analytical methods include

spectrophotometric methods (Chen, Bertin and Froidi 2013; Tasioula-Margari and Tsabolatidou 2015), chromatographic (Saraji and Mousavi 2010; Porgali and Büyüktuncel 2012), flow injection-chemiluminescence (Parveen *et al.* 2013) and electrochemical methods (Kariuki, Ervin and Olafson 2015; Tashkhourian and Nami-Ana 2015; Ghaani *et al.* 2016). However, there have been some drawbacks in using the chromatographic and spectrophotometric methods, because of the cost and size of the equipment, sample pre-treatment/preparation time and the use of expensive and toxic reagents. Hence, there is still the need for a simple, low-cost, portable, and sensitive analytical method, which fits well with the electrochemical method being studied.

Electrochemical analytical methods have progressively been developed for the determination of antioxidant capacity and the concentration of total polyphenols in food and plasma. They have also been developed for specific determination and quantification of GA as an antioxidant. These electrochemical techniques together with the sensors, have the advantage of being fast, sensitive, inexpensive and with little or no sample pre-treatment. They can also be produced in miniatures and do not have a problem of colour discrimination (Sochor *et al.* 2013; Kariuki, Ervin and Olafson 2015). Their high sensitivity, selectivity, low cost, speed and relative portability have influenced their use in research for the development of analytical sensors for antioxidants like GA and other organic compounds (Rassaei *et al.* 2011; Chang *et al.* 2014; Liang *et al.* 2016). Electrochemical sensors and biosensors have been mainly developed by using voltammetric techniques such as cyclic voltammetry (CV) and differential pulse voltammetry (DPV). The voltammetric techniques used in the development of these sensors are made up of voltammetric cells. A voltammetric cell is a three-electrode cell, with working, reference and auxiliary(counter) electrodes. The main electrode that is developed into an electrochemical sensor is the working electrode (WE). The working electrode could be a glassy carbon electrode (GCE), gold electrode, silver electrode, platinum electrode, boron-doped electrode, and many other modified electrodes.

Glassy carbon electrodes are often used for the electrochemical determination of antioxidants. However, the surface area of the electrode has been shown to be a limiting factor with regards to sensitivity and capacity to determine the antioxidant capacity or polyphenol content in analytes such as wine. This has been because of the complex nature of the carbon/solution interface, caused by the variability

in surface history (McCreery 2017). Thus, glassy carbon electrodes have been modified to improve the sensitivity and their capacity to determine antioxidants like GA. The use of graphene, graphite and metal oxides nanoparticles have been found to be useful in this regard, because of the increased surface area they provide, their stability and nano-size (Eremia *et al.* 2013; Shang, Zhao and Zeng 2014; George, Antony and Mathew 2018).

Graphene nanoparticles and metal oxide nanoparticles modified carbon paste electrode have shown good promise towards the determination of individual antioxidants like GA as recorded in other studies (Tashkhourian and Nami-Ana 2015). This has been as a result of their size, stability, and very high surface area. The strong affinity of metal oxide nanoparticles towards the surfaces of the electrodes can be easily achieved through physical adsorption, electrodeposition, covalent bonding and electro-polymerisation (Wang and Hu 2009).

1.2 Electrochemical analytical methods

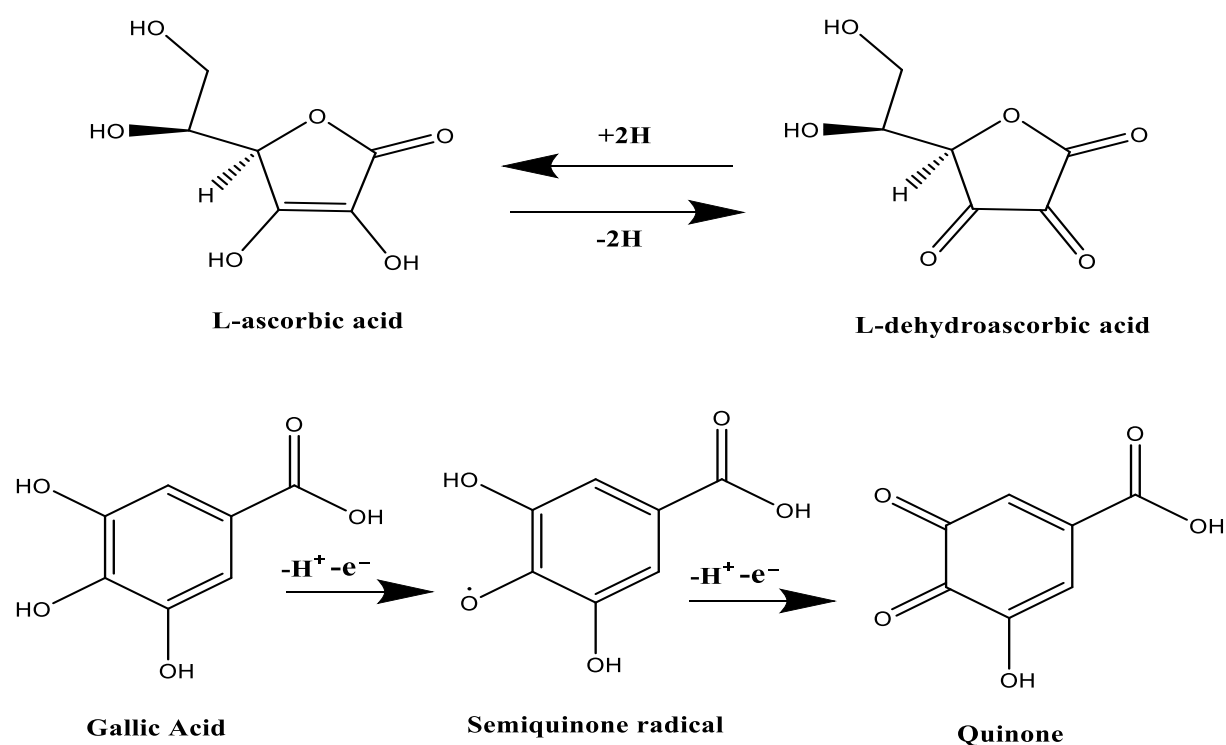
Electrochemical analytical methods have progressively been developed for the determination of antioxidant capacity and total polyphenols in food and plasma. This has been because of the reasons listed in section 1.1 and some specific advantages they have over spectrophotometric methods. These include the possibility of measuring analytes in the presence of interference or measurement of coloured samples. This can be seen in the masking of ascorbic acid (AA) by other organic compounds found in fruit juice (Hoyos-Arbeláez, Vázquez and Contreras-Calderón 2017). Furthermore, the presence of highly water-soluble pigment anthocyanins in wine and fruit juices hinders direct spectrophotometric measurements (Lino *et al.* 2014). Other advantages favouring electrochemical methods include (i) the ability of electrochemical methods to measure a broad concentration range of different types of analytes and solvents. (ii) They can work in a wide range of temperatures, (iii) the possibility of simultaneous determination of analytes (Pisoschi, Cimpeanu and Predoi 2015).

With regards to antioxidant determination, another advantage of using electrochemical methods over the widely used spectrophotometric methods is the electro-activity of the antioxidants. This is the ability of an antioxidant to function as electron donors and proton receptors (Scheme 1.1, page: 5). These different measurements are mainly to determine the total reducing power of the antioxidant and develop a suitable electrochemical method to make such determinations

(Piljac-Žegarac et al. 2010; Yilmaz, Kekillioglu and Mert 2013; Ghaani et al. 2016; Pisoschi et al. 2016). Different electrochemical parameters can be used for the determination of different aspects of the analyte, including antioxidants. Examples of such parameters are voltammetric charge, peak current and peak potential.

A voltammetric charge is a charge induced on the surface of the electrode or sensor as a result of the applied potential (Burke and Murphy 1979).

The peak potential is the potential at which the analyte is oxidised or reduced in the course of an applied potential scan, in an electrochemically induced redox reaction (Bard and Faulkner 2001). Meanwhile, the peak current is the maximum current attained by an oxidation or reduction peak (voltammogram) in the course of an applied potential scan; which is used to determine the antioxidant capacity of antioxidants (Holze 2016).



Scheme 1.1. Showing electroactivity of Ascorbic acid and Gallic acid. Here the L-ascorbic acid goes through a redox reaction to L-dehydroascorbic acid and Gallic acid is oxidised to semiquinone and quinone.

1.2.1 Electrochemical sensors

Chemical sensors are solid-state devices that provide data and general information about their immediate environment. The sensor helps in the transformation of signals that are generated by mostly chemical interactions of the interested analyte and the device, into usable quantitative or qualitative information. The quantitative and qualitative signals are then converted into an analytical signal. The sensor signals are typically electronic in nature, like current, voltage or conductance change usually generated by the analyte. Chemical sensors and most importantly electrochemical sensors are made up of a physical transducer and a chemically sensitive layer or recognition layer. The transducer transforms the response from the chemically sensitive or recognition layer, into a detectable signal seen on a modern instrument/software.

Electrochemical sensors are thus defined as devices whose signals from the analyte could be transformed into current, voltage, impedance/conductance, or resistance. There are three main categories of electrochemical sensors, which include amperometric, conductometric and potentiometric sensors. When compared to other types of sensors like optical, mass, and thermal sensors; electrochemical sensors are more sensitive, simple, and low cost. They can be used to analyse solid, liquid, or gaseous analytes, with the liquid and gases being the most common analytes.

The potentiometric sensors were among the earliest sensors, as they had widespread practical applications. For example, they were developed into pH electrodes, for H⁺ proton measurement. Potentiometric sensors are generally divided into three categories which include coated wire electrode (CWES), ion-selective electrodes (ISE), and field-effect transistors (FETS) (Stradiotto, Yamanaka and Zanoni 2003). Potentiometric sensors work by measuring the potential difference between the sensor and the analyte. The changes in the concentration of ions in the analyte solution generate a potential difference, that is recorded and analysed. A potentiometric measurement provides an equilibrium condition between the electrode and the electroactive species in the solution. This is in contrast with amperometric measurements that demonstrate a diffusion-limited condition. Thus, they lead to a logarithmic relationship between the voltage and the concentration of the analyte, unlike the linear relationship in amperometric measurements. Using a potentiometric chemical sensor, the

relationship between the ionic concentration of the analyte in solution and the potential is demonstrated by the Nernst equation thus:

$$E = E^0 - \frac{0.0592 \text{ V}}{n} \log_{10} \frac{A_{Red}}{A_{Ox}} \quad \text{Equation 1.1}$$

Where E and E^0 are the cell potential and the standard cell potential respectively, while n , in this case, is the number of electrons transferred in the cell reaction, and A_{Red} and A_{Ox} are the reduced and oxidised species (concentration/ion).

Conductimetric sensors measure mainly the electrical resistance change (resistivity) which occurs between the analyte and the conductive layer of the sensor. The conductimetric sensors are generally not selective, however with the development of modified surfaces they have been improved.

Amperometric sensors work by measuring the current that is generated by the electrochemical oxidation or reduction of the electroactive species that is the analyte. The process between the signal and the transduction is achieved by the control of the potential of the working electrode at a fixed potential value. This is normally relative to the reference electrode, and the current is being monitored as a function of time. In the working of amperometric sensors, the applied potential generates the electron transfer reaction of the electroactive analyte being measured (Wang 2006). The current generated is directly proportional to the electron transfer reaction rate and concentration of the electroactive analytes in the solution. This relationship is demonstrated in the equation 1.2 below.

$$N = Q/nF \quad \text{Equation 1.2}$$

Where N is the number of moles of the electroactive species, F is the Faraday's constant (96487 C mol^{-1}), Q is the amount of current produced and n is the number of electrons transferred per mole. Most of the electrodes and sensors used for the electrochemical determination of GA are amperometric sensors. Examples of such sensors are seen in the work of Tashkhourian *et al.* (2013). The sensors that would be developed in this research would be mainly amperometric sensors.

1.2.1.1 Conductivity of an electrode

The conductivity of an electrode can be described as the measure of the ease at which an electric charge or heat can go through a material (electrode). Hence a conductor is often defined as a material which presents minimal resistance to the flow of an electric current or thermal energy. Thus, there is the classification of materials as metals, semiconductors, and insulators, based on their conductive capability. Metals are the most conductive, while insulators like ceramics, wood and organic polymers are the least conductive.

1.2.1.2 Resistivity of an electrode

The resistivity of an electrode or an electrode material is the resistance to the flow of an electric current. This is a measure of how strongly a material opposes the flow of electric current.

1.3 Voltammetric Analysis

Voltammetry is made up mainly of a group of electroanalytical techniques, where information about the analyte is generated by measurement of the current as a function of an applied potential. This can also be defined as the measurement of a flow of current in an electrochemical cell as an applied and varying potential is being passed through the system (Henze 2001). Electrochemical changes occur within an analyte in reaction to the applied potential at the electrode analyte interface, depicting the concentration of a specific species. Voltammetry provides very good sensitivity, good concentration range for inorganic and organic analytes, very fast analysis time, wide temperature range, determination of the electrode/analyte kinetics, works in many different solvents and electrolytes, with the ability to determine different analytes simultaneously.

Sensitivity in voltammetry can be defined as the slope of the calibration curve, produced when the peak current is plotted against the concentration of the analyte. This is mostly seen in the limit of detection (LOD) where voltammetry has shown limits of detections as low as $1 \times 10^{-9} \text{ mol L}^{-1}$ as compared to HPLC with LODs of $10^{-5} \text{ mol L}^{-1}$. Voltammetric analysis of samples are carried out in broad concentration ranges from $10^{-9} - 10^{-4} \text{ mol L}^{-1}$ (Xiong et al. 2017; Shahamirifard et al. 2018). Meanwhile the analysis of compounds using voltammetry could take place in wide temperature ranges from $25 \text{ }^{\circ}\text{C} - 40 \text{ }^{\circ}\text{C}$, with scan times of about

35 seconds (Xiong et al. 2012), as compared to the room temperature analysis of DPPH assay or HPLC, with very long analysis times ranging from 30 mins to 1 hrs.

1.3.1 Voltammetric Cell

The voltammetric cell is an electrochemical cell made up of two or three electrodes (Figure 1.2), that are immersed into a solution which contains the analyte; as well as an excess of an unreactive electrolyte (supporting electrolyte).

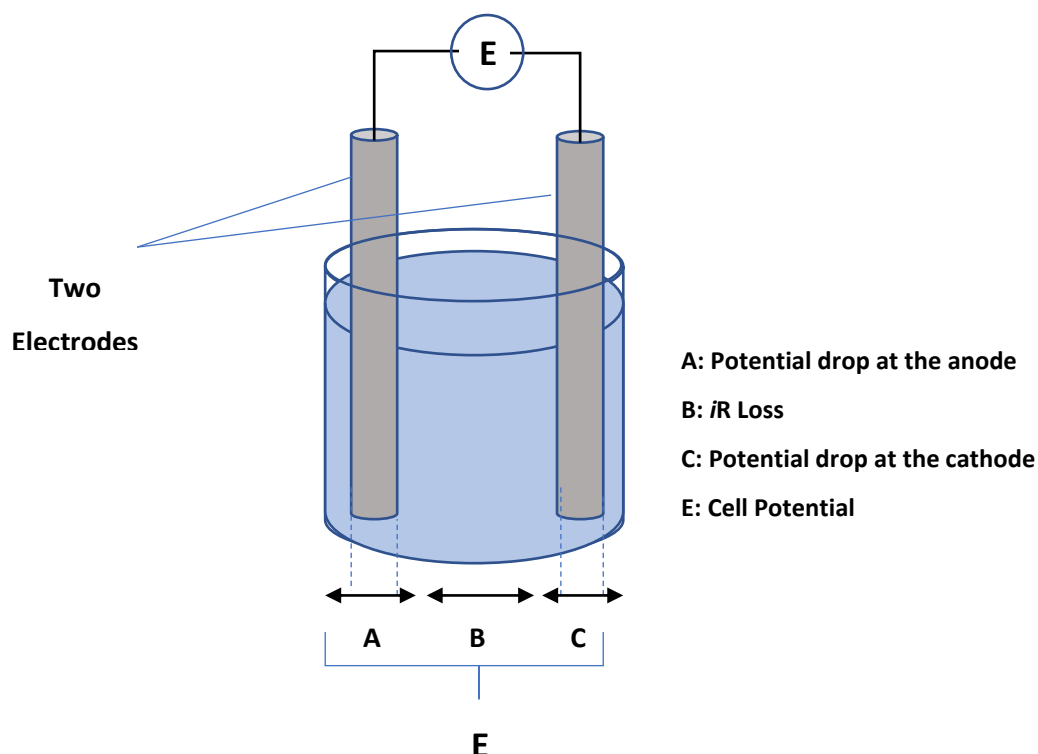


Figure 1. 2. A voltammetric cell that consists of two electrodes, with a potential profile of the cell, showing the potential drop at the anode, iR Loss, potential drop at the cathode.

In a two-electrode voltammetric cell, a working electrode and a counter electrode are employed. The role of the counter electrode is to maintain an electro-neutrality in the solution; hence, producing a counter to the reaction happening at the working electrode (Climent and Feliu 2015). Meanwhile, the potential difference between these two electrodes is the cell potential, which is the sum of different potentials (potential drop at the cathode, potential drop at the anode and the iR loss/drop) within the cell. The ohmic drop or the iR drop (ΔE_{ohm}) is the resistance of the analyte or solution being analysed, during the flow of electrical through the cell. This is also known as ohmic polarization which is related to the rate of ion flow between electrodes and can be defined by the magnitude of current,

electrolyte conductivity and the distance between the two electrodes (Bard and Faulkner 2001).

The ohmic/ iR drop affects the cell potential when current flows through the system. This is as a result of reduced conductivity or resistivity of the electrolyte solution, caused by the ionic strength and dielectric constant of the solvent. It is when the ohmic iR drop is negligible in a two-electrode cell, that the cell potential is equal to the potential difference of the two electrodes (Bard and Faulkner 2001). Although the two-electrode cell can be used in galvanic cells, the setup is not enough for the control of the potential of the working electrode in an electrochemical cell. This is because, the reference electrode also works as the counter electrode, hence the current flow causes momentary changes in potential through the electrode. This then causes an unstable potential within the electrode. This is a problem when fast voltammetric analytical methods are being used in organic solvents or in large scale electrolysis. The ohmic drop in the cause of analysing organic compounds must be minimized to have a stable potential, which is difficult with a two-electrode cell. However, the problems are solved using three-electrode set-up cells (Zoski 2007). The three electrodes are the reference electrode (RE), the counter electrode (CE) and the working electrode (WE). In a three-electrode cell, there is an applied voltage between the reference and the working electrode, where an operational amplifier prevents the flow of current between the two electrodes. Thus, the electric current would only flow between the counter electrode and the working electrode; such that the external voltage required is achieved. Without any flow of electric current through the reference electrode (non-polarisable), the potential would remain constant.

The working electrode whose potential varies with time is the electrode where the electrochemical reaction of interest occurs. The dimension of the working electrode is mainly very small, to enhance the tendency of its being polarized. The reference electrode which is commonly silver-silver chloride electrode (Ag/AgCl) or saturated calomel operates with a constant potential throughout the experiment.

The auxiliary electrode or counter electrode (platinum wire), works by conducting electricity from the source in the analyte to the working electrode. The material often used for counter electrodes are materials that would not affect the functioning of the working electrode, platinum, or graphite. The placement of the counter electrode in the cell is done in such a way that, products from reactions

around it, do not affect the reactions around the working electrode. However, in practice, because of the slow diffusion of the solution, the products do not affect the functioning of the working electrode. On the other hand, the reference electrode must be placed close to the working electrode, to avoid ohmic problems. This can be easily achieved by the use of what is known as a Luggin capillary. In a Luggin capillary set up, the Ag/AgCl reference electrode in this case, is placed in a glass capillary that has a narrow tip called the Luggin capillary. The capillary is then filled with the analyte, with the reference electrode in it and placed close to the working electrode. The capillary tip, being close to the working electrode at a very small distance, reduces the ohmic drop between the two electrodes (Zoski 2007). The ideal distance between the working electrode and the tip of the Luggin capillary is investigated and kept constant through the course of the experiments. Furthermore, the surface area of the counter electrode needs to be larger than that of the working electrode. This is to prevent the reactions that happen around the electrode from being the current determining reactions of the cell. Meanwhile, the signal source works as a linear scan-voltage generator as seen in Figure 1.3.

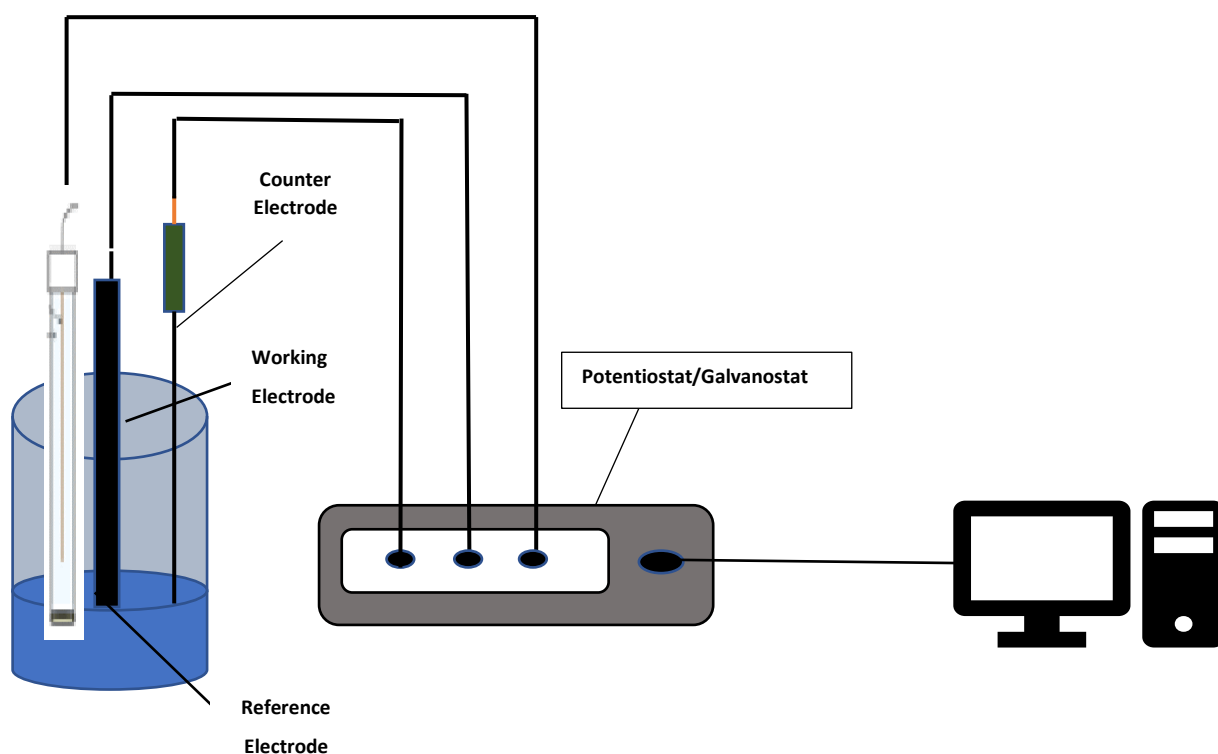


Figure 1. 3. An operational amplifier potentiostat. The three electrodes consist of the working electrode (WE), reference electrode (RE), and a counter electrode (CE)

1.4 Cyclic Voltammetry

Cyclic voltammetry is one of the most extensively used electrochemical technique for the determination of different properties of antioxidants. The technique provides information about the diffusive or adsorptive nature of the electrode process, the thermodynamics of reduction/oxidation (redox) processes, and the kinetics of heterogeneous electron-transfer reactions. Thus, cyclic voltammetry is mostly used for analysing electroactive species and for determining reaction mechanisms and rate constants. The technique typically scans the potential of a stationary working electrode linearly, which is being used in an unstirred solution, and express them in peak potentials and peak currents through the voltammograms. Thus, the results are shown in voltammogram plots of current against the applied potential. The method is carried out by a controlled potential scan, as the current is measured during the oxidation or reduction of the analyte (Holze 2016). This controlled potential is applied linearly with time as can be seen in Figure 1.5 and this is done as usual in a system composed of three electrodes, a working electrode, a counter electrode and a reference electrode. (Figure 1.3, page: 11).

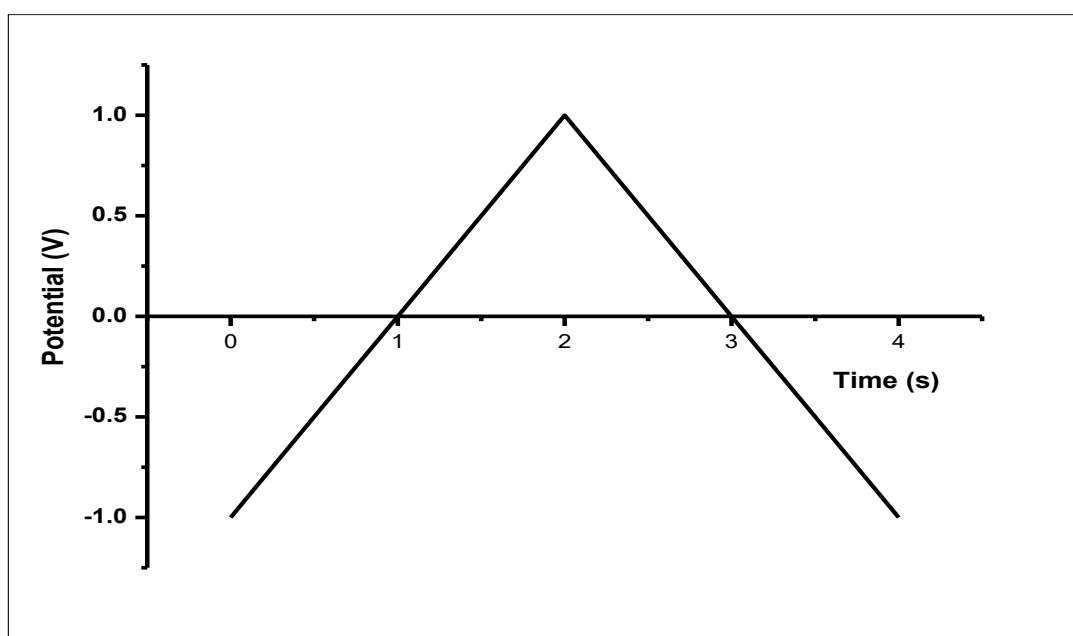


Figure 1. 4. The plot of potential vs. time in a cyclic voltammetry

On the other hand, the current vs. potential plot is what is referred to as the voltammograms (Figure 1.5). Voltammograms provide very important data like E_a (anodic potential), E_c (cathodic potential), I_a (anodic peak current) and I_c (cathodic peak current). Using the Randles-Ševc'ik equation for a reversible reaction, other parameters like reactive surface area (A) of the electrode used and the number of electrons (n) involved in the reaction can be determined.

The Randles-Ševc'ik equation 1.3 is thus: -

$$I_p = (2.69 \times 10^5) n^{3/2} A D^{1/2} \nu^{1/2} C \quad \text{Equation 1.3}$$

Where I_p is the peak current measured in Amperes, n is the electron stoichiometry measured per mole, A is the area of electrode in cm^2 , D is the diffusion coefficient measured in cm^2 per second (s), ν is the scan rate in volts per second (V s^{-1}) and C is the concentration in mole per cm^3 (mol cm^{-3}).

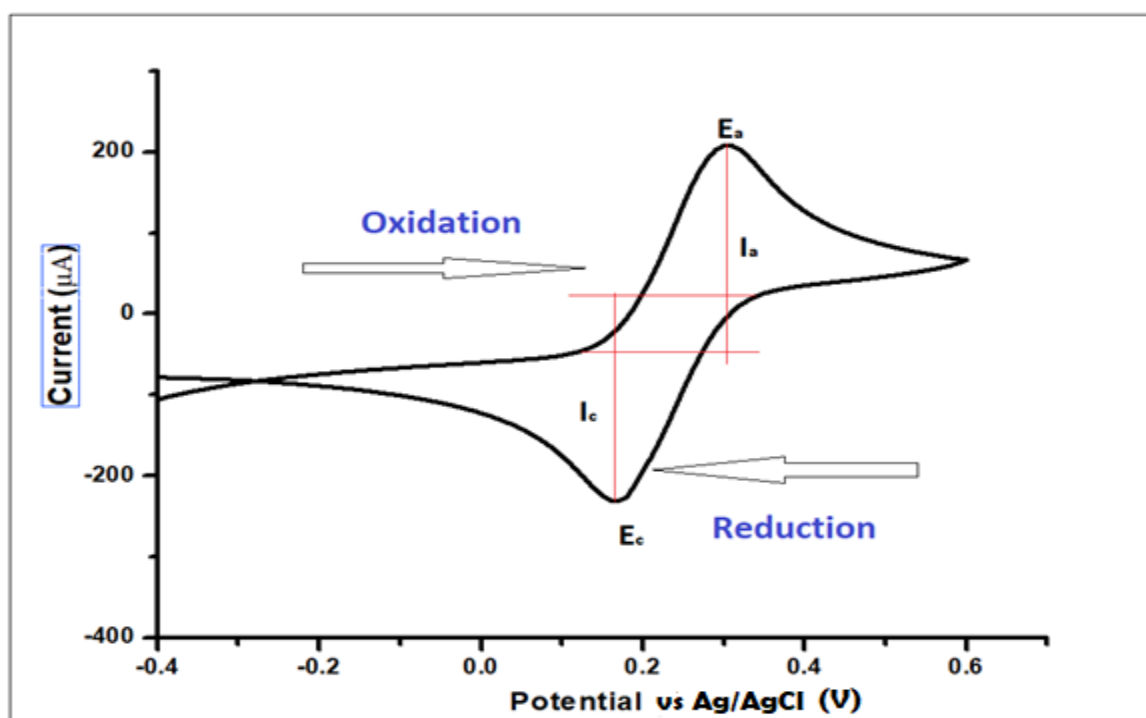


Figure 1. 5. A typical voltammogram of a redox species (Ferricyanide) showing the plot of current vs. potential obtained through CV, with parameters like anodic peak potential (E_a), cathodic peak potential (E_c), anodic peak current (I_a) and cathodic peak current (I_c)

Meanwhile using cyclic voltammetry to measure a single electron transfer redox species, where there are oxidation and a reduction (reversible redox reaction); an equilibrium gets established on the electrode surface. The Nernst equation that

describes the relationship between the electrode potential and the concentration of the analyte at the electrode surface is as follows in equation 1.4: -

$$E = E^o - \frac{RT}{nF} \ln \frac{[Red]}{[Ox]} \quad \text{Equation 1.4}$$

Where $[Red]$ and $[Ox]$ are the concentrations of the reduced and oxidised forms of the analyte at the electrode surface, R is the universal gas constant in $J K^{-1} mol^{-1}$, T is the temperature in Kelvin (K), F is the Faraday constant in $C mol^{-1}$, n is the number of electrons transferred at the reaction on the electrode surface and E^o is the standard cell potential of the reaction.

This formal potential or standard potential can also be estimated by using the midway potential whilst using cyclic voltammetry, which can be described by equation 1.5: -

$$E_{mid} = (E_a + E_c)/2 \quad \text{Equation 1.5}$$

Where E_a is the anodic potential and E_c is the cathodic potential.

There is evidence of a linear relationship between the concentration of some antioxidants during CV measurement, with the area under the anodic peak or the peak current (I_p) of the anodic scan (Chevion, Roberts and Chevion 2000). Amongst the different voltammetric methods used in the measurement of GA and other phenolic compounds in the characterisation of food samples, cyclic voltammetry has been shown to be very informative. The technique provides information on the thermodynamics involved in the redox processes happening in the sample, the kinetics of the electron transfer reaction processes and the chemical as well as adsorption process that occurs, which is mainly expressed in peak potential and peak current in voltammograms.

Cyclic voltammograms can be categorised into three main types based on the electrochemical reaction that takes place at the surface of the electrode. The three categories are reversible, irreversible, and quasi-reversible.

1.4.1 Reversible System

In cyclic voltammetry, the reversible system is described as a system with fast electrode kinetics, while the mass transport conditions are slow. Hence the electrode kinetics are faster than the rate of diffusion (which is the mass transport condition). The voltammograms (current-potential plot) that develop in a reversible system, two peaks of oxidation and reduction would normally show up

at the formal potential of the redox species. A reversible electrochemical process (Figure 1.5) obeys the Nernst equation as shown in Equation 1.1 and 1.4, which shows that a half cell potential will change by 59 mV/n per 10-fold change in concentration of an analyte that is undergoing one-electron oxidation or reduction. This gives us a peak to peak separation ($E_p^{ox} - E_p^{red}$) ~ 59 mV. Thus, in the reversible limit, the peak to peak separation ~ 59 mV (at 298 K) is independent of scan rate. Meanwhile, in both limits reversible or irreversible, the peak current is scan rate dependent (Holze 2016).

The ratio of the cathodic peak current (I_{pc}) and the anodic peak current (I_{pa}) which is I_{pc}/I_{pa} , is mostly used for the estimation of the degree of reversibility of the redox reaction. If the ratio is close or equal to one, it shows a more reversible reaction, while the difference between the cathodic and anodic peak potential is also used for the determination of the reversibility of a system. Where the difference δE_p is or close to 59 mV/n (25 °C) and n is the number of electrons transferred at the electrode surface, the system is fully reversible. However, when the value of δE_p is above 59 mV/n the system can be considered as quasi-reversible with a slow charge transfer (Holze 2016).

Rewriting the Nernst equation whilst using log10 at a standard temperature of $T=298$ K would give us the following equations 1.6 and 1.7.

$$E = E^0 - \frac{2.303RT}{nF} \log \frac{[ox]}{[red]} \quad \text{Equation 1.6}$$

When the Temperature is $T = 298$ K, $R = 8.314$ VCK⁻¹mol⁻¹ and $F = 96500$ Cmol⁻¹, then RT/F would be equal to 25.7 mV; thus Equation 1.6 would change to: -

$$E = E^0 - \frac{0.059}{n} \log \frac{[ox]}{[red]} \quad \text{Equation 1.7}$$

In a situation where the peak is too broad, and the potential difficult to get in a reversible system; the peak potential can then be analysed using the half peak potential $E_{1/2}$ which corresponds to the half peak current. This would be calculated thus, with a normal peak potential giving us the following equations 1.8 and 1.9

$$E_p = E^0 - 1.109 \frac{RT}{nF} \quad \text{Equation 1.8}$$

Then the $E_{p/2}$ would be as follows:-

$$E_{1/2} = E^0 + 1.109 \frac{RT}{nF} \quad \text{Equation 1.9}$$

Using the absolute values of the peak potential and that of the half peak potential in a reversible system, we would produce equation 1.10:-

$$\left| E_p - E_{1/2} \right| = 2.218 \frac{RT}{nF} \quad \text{Equation 1.10}$$

Which hence shows us that, the peak potential (E_p) is independent of the scan rate (v), while the peak current would be proportional to the square root of the scan rate.

1.4.2 Irreversible System

For an irreversible electrochemical system, the electrode kinetics are slower than the mass transportation process of diffusion. Hence, in this case, the electrode kinetics is said to be slower than the rate of diffusion. In such an irreversible system, cyclic voltammetry and a linear sweep would generate the same voltammograms as there are no peaks in the reverse scan (Figure 1.6).

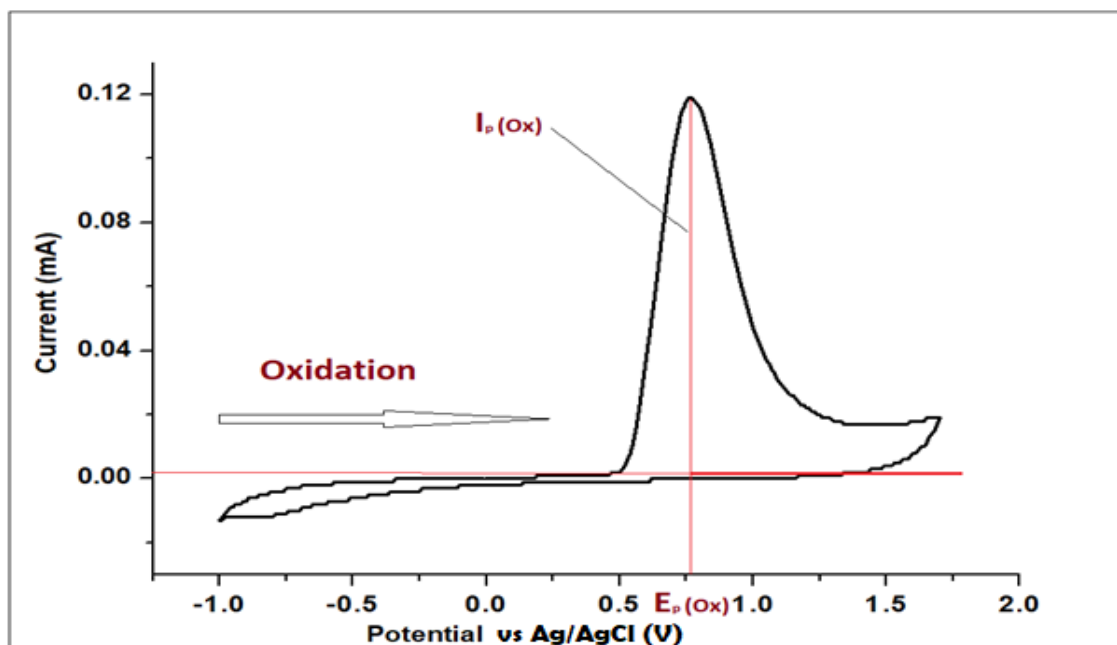


Figure 1. 6. Voltammograms of an electrochemically irreversible system, with the Oxidation peak current (I_p ox) and the peak potential (E_p ox), with the initial scan producing oxidation.

Using the waveshape of the forward peak, which is characterised by the difference in potential between the potential, E_p that corresponds to the peak current, and the $E_{1/2}$ (half peak potential) that corresponds to half of the peak current. Hence, at an irreversible reduction or irreversible oxidation, the Nernst equation would be presented thus: -

$$\left| E_p - E_{1/2} \right| = 1.857 \frac{RT}{\alpha F} \quad \text{Equation 1.11}$$

With the oxidation peak current being proportional to the square root of the scan rate, the peak potential tends to shift by $30/\alpha F$ for each decade change in scan rate. Furthermore, the difference in the peak and the half-wave potentials should adhere to the equation 1.11 above.

1.4.3 Quasi-reversible

The quasi-reversible systems are electrochemical systems that are found to be intermediate between reversible and irreversible systems. In this type of reaction systems as described by Matsuda and Ayabe (1955), the reaction undergoes electron transfer kinetic limitations. In a one-step and one electron reaction as can be seen in equation 1.12.



The forward and the backward reactions contribute significantly to the currents measured in the over potential range where mass transfer effects are not important. The current is thus given by the following equation 1.13

$$i = FAD_0^{\frac{1}{2}}C_0f^{\frac{1}{2}}v^{\frac{1}{2}}\psi(E) \quad \text{Equation 1.13}$$

Where, $f = F/RT$, $\psi(E)$ is a function of the quasi-reversible system, A is the area of the electrode in cm^2 , D_0 is the diffusion coefficient in cm^2s^{-1} , C_0 is the concentration in mol cm^{-3} of the analyte and v is the scan rate in Vs^{-1} .

Meanwhile Λ is defined in equation 1.14., which is the dimensionless parameter (Nicholson parameter) developed from the theory of Matsuda and Ayabe, and Nicholson and Shain, who used equation 1.14 to describe the relation between the

standard rate constant K^0 and the mass transport (diffusion). From this equation one can estimate the transition between reversible and irreversible electrochemical reactions (also known as quasi-reversible).

$$\Lambda = K^0 / [D_0^{1/2} (F/RT)^{1/2} v^{1/2}] \quad \text{Equation 1.14}$$

Where Λ in equation 1.14 is greater than 10, the behaviour of the system would approach that of a reversible system. The values of the peak current (i_p), the peak potential (E_p) and half peak potential ($E_{p/2}$) in this system depends on the Λ and α , where Λ is the Nicholson parameter and α is the transfer coefficient. The peak is given by $i_p = i_p(\text{rev})K(\Lambda, \alpha)$, where $i_p(\text{rev})$ is the reversible i_p value and the function $K(\Lambda, \alpha)$ shown as a function with the Nicholson parameter and the transfer coefficient. In this system, the peak currents increase with the square root of the scan rate but are not always proportional to the square root of the scan rate.

1.5 Differential Pulse Voltammetry

Differential pulse voltammetry is a type of voltammetry that uses a waveform that consists of a pulse produced at a constant amplitude, superimposed on a staircase-like waveform (Figure 1.7). In DPV potential, pulses of fixed, small amplitudes are superimposed on a changing base potential. This was a technique that was first proposed by Barker and Gardner in 1958 (Sholz 2010), for the electrochemical detection of compounds at lower detection and quantification limits.

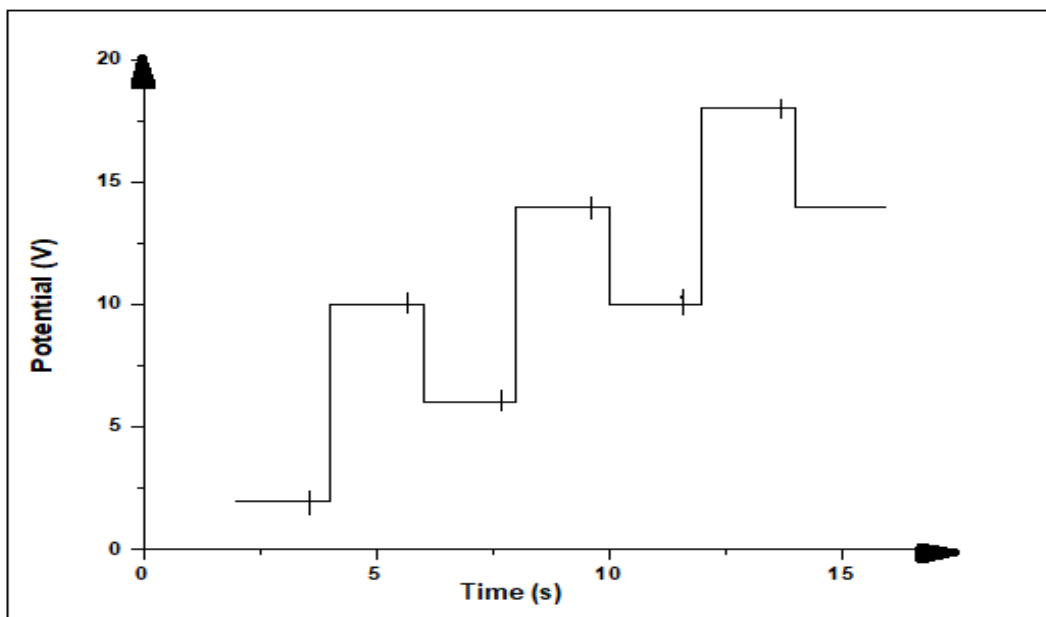


Figure 1. 7. Differential pulse voltammetry, showing potential-time waveform. As a schematic waveform of pulses superimposed on a staircase.

The technique is regarded to be one of the most sensitive voltammetric techniques, as there is hardly any charging current as opposed to the Faradaic current. The high sensitivity is attributed to the relatively large ratio of the faradaic current to the charging current. The reduction of the charging current is as a result of the current sampling that occurs twice; this is before the pulse application and at the end of the pulse application. Thus, the differential pulse voltammogram is attained by the subtraction of the sampled current before the pulse application from the pulse end current. Then the difference (ΔI), is plotted against the staircase potential. This is normally a measurement of the change in current with respect to the applied potential. The effect of having the voltammograms represented as ΔI against potential, is the fact that DPV is peak-shaped, with the peak height being proportional to the analyte concentration (Figure 1.8).

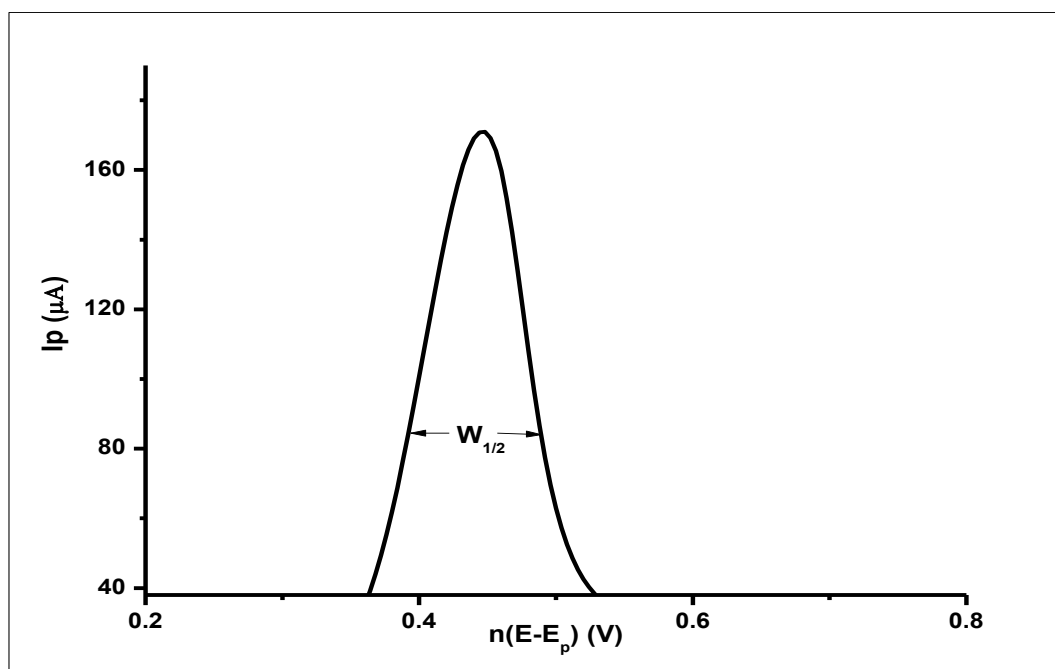


Figure 1. 8. An example of a complete differential pulse voltammogram showing $n(E-E_p)$ against the peak current I_p .

Hence the peak potential E_p can be related to $E_{1/2}$ for the determination of the reversibility or irreversibility of a system while being studied with DPV. This relationship is demonstrated thus: -

$$E_p = E_{1/2} - \frac{\Delta E}{2} \quad \text{Equation 1.15}$$

Where E_p is the peak potential, $E_{1/2}$ is the half peak potential and ΔE is the pulse amplitude. Equation 1.15 however, is being used for oxidation reactions, while equation 1.16 would be used for a reduction reaction.

$$E_p = E_{1/2} + \frac{\Delta E}{2} \quad \text{Equation 1.16}$$

From equations 1.15 and 1.16, it is seen that for oxidation processes with an increase in pulse amplitude, the peak shifts to the negative direction. Meanwhile, for reducing pulse amplitude, the peak shifts to the positive direction. Like earlier

discussed the peak current is directly proportional to the concentration of the electroactive analyte, which is represented by equation 1.17: -

$$I_p = \frac{nFAD^{1/2}C}{\sqrt{\pi t_m}} \left(\frac{1-\sigma}{1+\sigma} \right) \quad \text{Equation 1.17}$$

Where $\sigma = \exp(nF\Delta E_p/2RT)$, and ΔE is the pulse amplitude. Generally, as ΔE increases, the quotient $\left(\frac{1-\sigma}{1+\sigma} \right)$ increases and gets to one, but at this point, the resolution may become relatively low.

1.5.1 The Electrical Double Layer

The electrical double layer is described in electrochemistry as that specific interfacial region that is formed when an electrode is immersed in an electrolyte solution (Bard and Faulkner 2001). The electrical properties of these layers are very important in electrochemical measurements because the double layer is seen as a capacitor. For the working electrode to obtain the required potential, the double-layer capacitor would first be appropriately charged. Thus, a capacitive current that has nothing to do with the oxidation or reduction of the electrolyte, would have to flow through the electrical circuit. This capacitive current with its information and structure of the double layer, generally interferes with the electrochemical investigations. The double-layer structure (Figure 1.9) and its capacitance are dependent on parameters such as the electrode materials which include metals and different types of carbon. It is also dependent on the presence of polymeric film layers or oxide layers, the type of supporting electrolyte and solvent, temperature, and the extent to which the ions or molecules are being adsorbed. With these different parameters and the composition of the double layer, the electron transfer rate at the electrode/liquid interface is being influenced. This is either positively or negatively charged, that some ions are adsorbed on the electrode surface and enhance electron transfer (heterogeneous catalysis), while others decrease electron transfer rate as inhibitors. There are also conditions where some surface-active compounds would strongly adsorb onto the electrode surface and insulate it, thus decreasing the voltammetric peaks. A classic simplified model of the double layer formed on the surface of a working electrode can be seen in Figure 1.9. The outer Helmholtz plane (OHP) and the

inner Helmholtz plane are shown here. The IHP normally passes through the centres of the adsorbed ions known as the compact layer, while the OHP passes through the centres of the hydrated ions in contact with the metal electrode. Carbon electrodes also show a double layer, like metal electrodes, however, their physical properties and differences in electrochemical activity influence the electron transfer process much better than metal electrodes. This is because carbon electrodes in the form of graphite have a high electron density around its structure available for transfer, thus highly conductive.

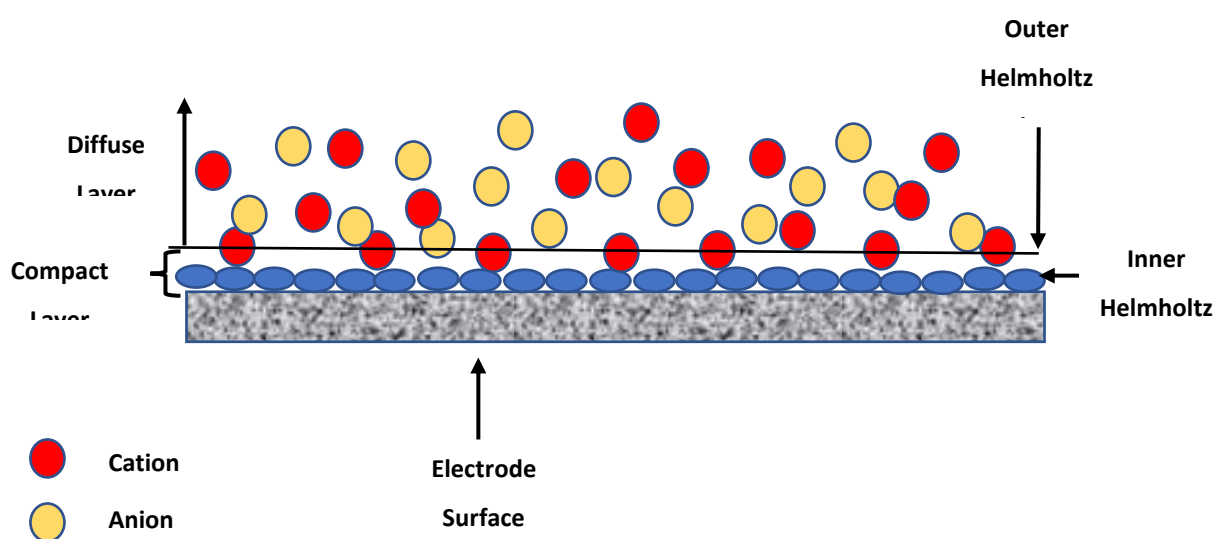


Figure 1. 9. Schematic diagram of the electrical double layer, showing the Inner and Outer Helmholtz Plane (IHP and OHP)

1.5.2 Mass Transport

Mass transfer can be described as the movement of materials, electrons, analytes, or reactants from one location in a solution to the other. This movement can be caused by differences in electrical or chemical potential or from the movement of different volumes of the elements that make up the solution (Bard Faulkner 2001). The electron transfer process at the double layer influences the rate of reaction at the electrode-liquid interface, which is being activated by the potential difference of cell. However, the rate at which the molecules and electrons are being transported to the electrode surface might have a larger influence on the reaction rate. The electrode processes that involve all the changes in and around the

electrode consist of the electrode reaction and the mass transport. At the electrode-analyte interface, there are three possible mass transport processes that can take place. This includes diffusion, convection, and migration.

1.5.2.1 Diffusion

Diffusion is the movement of different species in a solution, being influenced by a concentration gradient of the different molecules in the solution. Diffusion happens mainly because of an inhomogeneous solution seeking to maximized entropy. This is mimicked by the Brownian motion of solute particles that enrich regions of low local concentration from neighbouring regions of large concentration. Charged and uncharged species are equally affected by diffusion, thus both ions and molecules diffuse. In the electrochemical determination of antioxidants (GA), diffusion plays a very significant role in that, as the reaction takes place at the electrode, there is a reduction of the reactants around the electrode than further in the solution. Meanwhile, the concentration of the product increases around the electrode causing reactants to diffuse from the bulk towards the electrode.

The rate at which the solutes move by diffusion was proposed mathematically by Adolf Fick, hence producing the first (equation 1.18) and second (equation 1.19) laws of diffusion (Scholz 2010).

$$\text{Fick's first law:} \quad J = \frac{dm}{dtA} = -D \frac{\delta C}{\delta x} \quad \text{Equation 1.18}$$

Where J (mol/m² s) is the flux, dm (mol) is the change in the amount of matter in small time dt (seconds), A (m²) is the area, D (m²/s) is the diffusion coefficient, C (mol/m³) is the concentration of the particles, and x (m) is the position parameter. It should be noted that the negative sign, just shows that diffusion occurs in the opposite direction of increasing concentration (movement from high to low).

However, Fick's first law of diffusion can only be applied to steady-state conditions, where the composition of the solution does not change with time. Hence the need for the Fick's second law of diffusion, where any possible changes in the solute composition profile with time could be measured.

$$\text{Fick's second law:} \quad \frac{\delta C_0}{\delta t} = D_0 \left(\frac{\delta^2 C_0}{\delta x^2} \right) \quad \text{Equation 1.19}$$

Here the equation considers a normal diffusion on an electrode surface at x direction, where the C_0 is the rate of change of the concentration as a function of the time t . In most electrochemical processes, diffusion is found to be the most significant transport process.

1.5.2.2 Convection

Convection is a mass transport process where the entire species is being transferred from one point of the solution or fluid to another by the movement of the solution itself (Oldham and Zoski 1986). In this mass transport process, solutes leave or reach the area surrounding the electrodes by being in the moving solution. The movement of the solutes in the solution can be due to stirring, vibrating, pumping, or flowing of the solution. Two kinds of convection mass transport have been identified, they are, forced convection and natural convection. Forced convection occurs because of some induced motion, which could be done by stirring the solution, electrode rotation, bubbling gases into the solution and pumping the solution across the electrode. Meanwhile, natural convection is the sort of mass transport where the movement is caused by temperature changes or density differences at the electrode surface (Holze 2016). As much as the natural convection can be very important, the effect of the forced convection is far larger. Natural convection hardly has any effect on electrochemical reactions because these reactions are very fast and occur within 10 to 20 secs.

1.5.2.3 Migration

Migration as a mass transport process involves the movement of charged particles or ions along the field lines of an electric field (Batchelor-Mcauley *et al.* 2015). The movement or force experienced by the ion is proportional to the charge on the ion and the electrical potential gradient. When potentials are applied in electrochemical systems, the electrode creates a charged interface, which either attracts or repels the charged ions around it by an electrostatic force.

Migration affects only charged particles or ions, while the neutral species in the solution do not migrate. Electrochemical systems or voltammetric cells and measurements tend to simplify the transport of oxidative or reductive species with inert background electrolytes which are normally in high concentrations. Such electrolytes could be salts like KCl, that does not undergo electrolysis but tend to

migrate with the electric field. The migration with the electric field protects the reactants or analytes from the migratory effect of the electric field.

1.6 Antioxidants

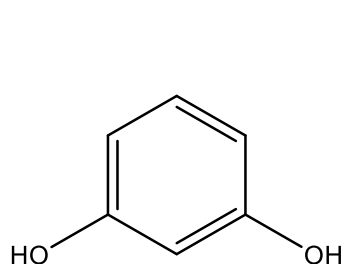
Antioxidants are organic compounds or molecules found naturally in plants and animals, where they can function as inhibitors to the oxidation of substrates or can significantly delay the oxidation. They also have the ability to scavenge radicals and form new more stable radicals (Halliwell and Gutteridge 1995) and are sometimes referred to as phenolic compounds. The antioxidant system of the body consists of compounds like catalase (CAT), superoxide dismutase (SOD) and glutathione peroxidase (GPX), that are mainly enzymes. Meanwhile, β -carotene, ascorbic acid (Vitamin C), and α -tocopherol (Vitamin E) are the non-enzymatic ROS scavengers that help in building-up defences. These enzymes and non-enzymatic compounds, play the essential balancing role in the system for the efficiency and health of the organism (Gülçin 2012).

Phenolic compounds have been found to be the most abundant antioxidant molecules in diets (López-Cobo *et al.* 2015). Their chemical structures have made them the most effective antioxidant molecules, and this is due to the presence of hydroxyl groups bonded to an aromatic ring. The arrangement of the phenolic groups on the aromatic ring has a very large influence on the antioxidant activity of the phenolic acids. Several other factors like the number and position of the hydroxyl group, other functional groups and their positions with respect to the hydroxyl group influence the antioxidant and antiradical activities (Badhani, Sharma and Kakkar 2015). GA as a phenolic acid has three hydroxyl groups bonded to the aromatic ring in an *ortho* position with respect to each other. This presents the order that determines the strong antioxidant capacity of the GA. As the number of the hydroxyl group on the aromatic ring increases so does the antioxidant capacity, with GA showing a high antioxidant capacity amongst other polyphenols (Hugo *et al.* 2012). GA as a compound processes four acid protons with different pKa values 4.0 (-COOH group), 8.7, 11.4 and > 13 (-OH groups)(Ji, Zhang and Shen 2006). This makes the three hydroxyl groups attached to the aromatic ring prone to oxidation, that results to the formation of hydrogen peroxide, quinones and semiquinones (Eslami *et al.* 2010).

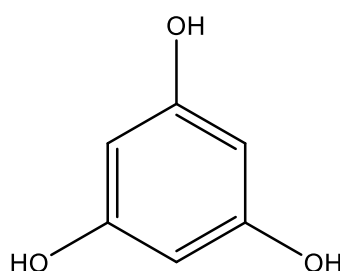
Phenolic compounds have different classifications based on the number of carbons in the molecules. Swain and Bate-Smith (1962) classified them as common and

less common phenolic compounds, while Ribereau-Gayon (1972) grouped them according to where they are found; like in plants, less widely distributed and presence in polymers. Using Harborne and Simmonds classification, phenolic compounds would be simple phenolics (C_6) (Figure 1.10(A)), phenolic acids (C_6-C_1) (Figure 1.10(B)), acetophenones and phenylacetic acids (C_6-C_2) (Figure 1.10(C)), cinnamic acids, cinnamyl aldehydes and alcohols (C_6-C_3) (Figure 1.10(D)), chalcones, aurones, flavones, flavonols, anthocyanins (C_{15}), betacyanins (C_{18}), biflavonyls (C_{30}), benzophenones, xanthonenes, stilbenes ($C_6-C_1-C_6$, $C_6-C_2-C_6$), quinones etc. (C_6 , C_{10} , C_{14}). Due to the roles of these phenolic compounds in plants, they have been found in foods of plant origin and have also been part of daily meals.

(a) Simple Phenolics

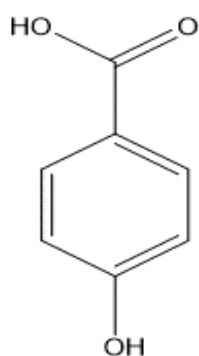


Resorcinol
(1,3-dihydroxybenzene)

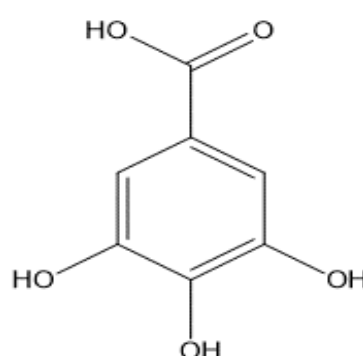


Phloroglucinol
(1,3,5-trihydroxybenzene)

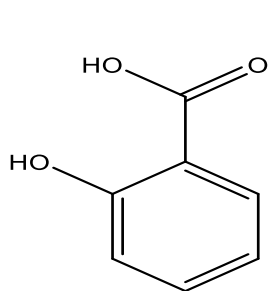
(b) Phenolic acids and aldehydes



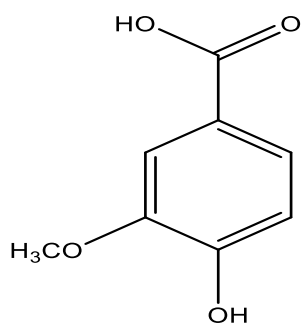
p-hydroxybenzoic Acid



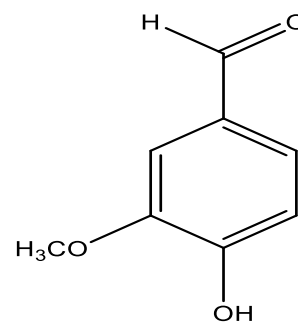
Gallic Acid



Salicylic Acid

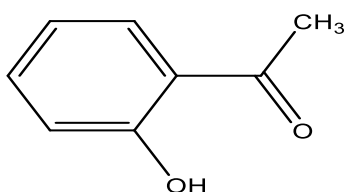


Vanillic Acid

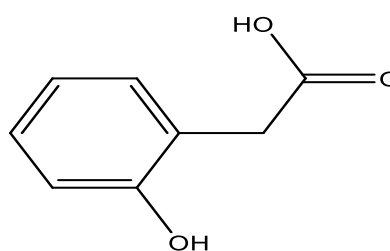


Vanillin

(c) Acetophenones and Phenylacetic acids

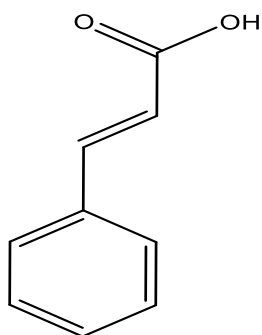


2-Hydroxyacetophenone

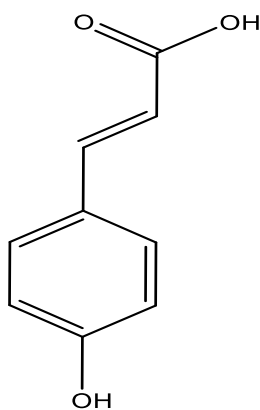


2-Hydroxyphenyl acetic acid

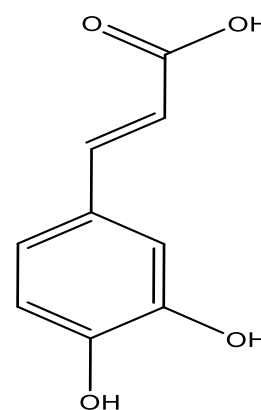
(d) Cinnamic acids



Cinnamic Acid



p-Coumaric Acid



Caffeic Acid

Figure 1. 10. Chemical Structures of Phenolic acids

1.6.1 Natural Antioxidants

Natural antioxidants are organic compounds produced naturally by plants and animals to prevent or remove oxidative damage to targeted molecules. They function as endogenous defences that maintain the free radical and oxidative stress balance. These include the work they do inhibiting free radical oxidation reaction, chain-breaking antioxidants propagating the interruption of autooxidation chain reactions. They also prevent oxidants in inhibiting free lipid radicals formation (Heim, Tagliaferro and Bobilya 2002; Kancheva 2009). Furthermore, they have also worked as singlet oxygen quenchers in synergy with other antioxidants (Darmanyán *et al.* 1998; Min and Boff 2002); in the conversion of hydroperoxides to stable compounds. They have also worked as reducing agents and metal chelators. Antioxidants have converted metal pro-oxidants like iron and copper derivatives into stable products and inhibitors of lipoxygenases which are pro-oxidative enzymes (Pokorný 2007; Carocho and Ferreira 2013).

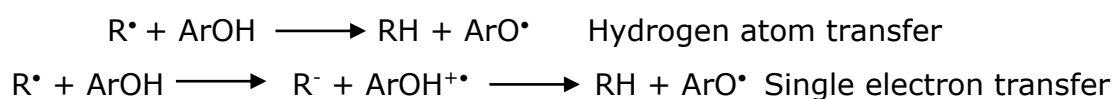
The focus of the work would be on the phenolic acids; these compounds compose of hydroxycinnamic and hydroxybenzoic acids. Phenolic acids are found to be everywhere in plants and are sometimes found as esters and glycosides; their antioxidant activity includes their action as chelators and free radical scavenging on hydroxyl and peroxy radicals, superoxide anions and peroxy nitrates (Terpinic *et al.* 2011). Meanwhile, one of the most studied compound in the hydroxybenzoic group of antioxidants is GA which is a precursor for tannins (Krimmel *et al.* 2010). The chelating ability of GA and tannic acid has affected the bioavailability of certain minerals (iron, zinc, and calcium) by forming insoluble complexes. The formation of these complexes with a mineral like iron, can cause iron deficiency (Tako *et al.* 2014). However, there is evidence that, the accumulation of iron in the pre-frontal cortex and changes in ferritin distribution enhances ROS production. This then enables oxidative stress that might cause degenerative diseases like Alzheimer's and Parkinson's disease. Thus, using the chelating potential of the hydroxyl groups, GA can inhibit the ferrous catalysed DNA damage, by either binding to Fe(II) or stabilizing the Fe(III)-polyphenol complex formed by autooxidation from oxygen (Perron *et al.* 2010).

1.7 Gallic acid

GA ($C_6H_2(OH)_3COOH$) also known as 3,4,5-trihydroxybenzoic acid (Figure 1.1 and 1.11) is a colourless or slightly yellow crystalline organic acid, obtained from gallnuts, sumac, witch hazel, tea leaves, oak bark and other plants; with a molecular weight of $170.12 \text{ g mol}^{-1}$ (NCBI 2018). It has a melting point of $260 \text{ }^\circ\text{C}$ and could be decomposed at temperatures between $235 \text{ }^\circ\text{C}$ and $240 \text{ }^\circ\text{C}$ producing CO_2 and CO . They are soluble in water, alcohol, glycerol, and ether, but insoluble in other organic compounds like benzene and chloroform (National Institute of Health (NIH), 2015). The compound is an endogenous plant polyphenol, found in abundance in tea, grapes, berries and many other fruits as well as in wine (López-Vélez, Martínez-Martínez and Valle-Ribes 2003). It can exist free and as part of tannins. Structurally as is the case with other phenolic acids, GA has three hydroxyl group attached to the benzene ring positions 3, 4 and 5 of the rings. The number of hydroxyl groups attached to the benzene ring has had a massive influence on the antioxidant activity of GA. As the electrochemical oxidation of GA occurs at the hydroxyl groups attached to the benzene ring.

1.7.1 Gallic acid structure and its antioxidant activity

The antioxidant capacity of GA has been mainly attributed to the phenol groups attached to the benzene ring. The antioxidant action of GA as a phenolic acid, occurs either by the donation of hydrogen atom, known as hydrogen atom transfer (HAT) or by the donation of electrons also known as single electron transfer (SET)(Badhani, Sharma and Kakkar 2015).



Where R^\bullet is a free radical, $ArOH$ is the phenolic acid, RH substrate molecule and ArO^\bullet is the GA free radical (Phenolic acid radical).

The bond dissociation enthalpy (BDE) for the O-H bond and ionization potential (IP) are the two specific molecular properties responsible for which of the above mechanism would be most favoured in the course of gallic acid action as an antioxidant. This is because, the weaker the OH bond, the faster will be the reaction with free radicals. Although, it has been found that, the both mechanisms

occur in parallel; but at different rates, with the HAT mechanism being prevalent (Wright, Johnson and DiLabio 2001). Furthermore, the action of GA can also be dependent on the nature of the reacting free radical and the polarity of the environment. In aqueous medium, sequential proton loss electron transfer (SPLET) and sequential double proton loss electron transfer (SdPLET) prevails for the GA radical scavenging reactions of these HO• and HOO• radicals, respectively. Meanwhile in non-polar mediums, HAT mechanism occurs for HOO• radicals, while both HAT and radical adduct formation (RAF) occurs for HO• radicals.

In spite of all the stated mechanism, there is evidence that suggests the electron donating capacity of the carboxylate group lowers the BDE value of GA, as it converts to carboxylate. This results to a greater antioxidant efficiency of GA as compared to its other derivatives. This means the radicalization of GA creates a radical whose unpaired electron spin density is delocalised all around the GA molecule, with the largest amount found around the carbon atoms bonded to the -OH group (Šolc et al. 2014). Thus, two radicals, 3-OH (5-OH) and 4-OH can possibly be gotten from the abstraction of hydrogen atom from the corresponding meta or para -OH groups. The para O-H being the weakest because of its low binding energy. On the hand, there is a believe that the presence of an electron withdrawing group like the carboxylic group (-COOH), with an electron donating hydroxyl group (-OH) at the ortho position stabilises the free radical by resonance. The presence of this relatively stable GA free radical known as a semiquinone (ArO•), reacts slowly with the substrate, while also reacting rapidly with the ROS, which would have oxidised the substrate.

The antioxidant action of the GA can be demonstrated in these four simple steps below, demonstrating its chain-breaking antioxidant ability during lipid peroxidation.

1. $\text{RH} \longrightarrow \text{R}^\bullet$ (Initiation reaction)
2. $\text{R}^\bullet + \text{O}_2 \longrightarrow \text{RO}_2^\bullet$ (Addition of O_2)
3. $\text{RO}_2^\bullet + \text{RH} \longrightarrow \text{ROOH} + \text{R}^\bullet$ (H-atom exchange)
4. $\text{RO}_2^\bullet + \text{ArOH} \longrightarrow \text{ROOH} + \text{ArO}^\bullet$

1.7.2 Importance of Gallic Acid

GA was first identified by scientist Carl Wilhelm Scheele in 1786, as reported by Fernandes and Salgado (2016); and has since attracted so much research because of its antioxidant capacity (Kim 2007). GA has been used therapeutically, pharmacologically and as a food additive. GA was shown in 1942 by Golumbic and Mattil to be a powerful antioxidant for lard and vegetable oils (Golumbic and Mattill 1942). Their antioxidant activity was further compared to Trolox and ascorbic acid; and they were found to be as effective as both of these compounds (Yen, Duh and Tsai 2002). Meanwhile, Bajpai and Patil (2008) confirmed the use of GA as a preservative in the food and beverage industry, where its antioxidant capacity was used for free radical scavenging.

In addition to its antioxidant capacity, the pharmacological activities of GA include its anticancer activity described by Chia *et al.* (2010) in the study of the anti-neoplastic effect of GA. Meanwhile, Liang *et al.* (2012) studied the antitumor effect of GA on osteosarcoma and found it to be effective.

The compound has also shown anti-HIV activities as described by Kratz *et al.* (2008), where GA and pentyl gallate were found to show an inhibitory effect on Herpes Simplex Virus type 1 (HSV 1) and Human Immunodeficiency Virus (HIV 1). GA and its derivative dodecyl (lauryl) gallate have been found to also show antimicrobial activities (Kubo *et al.* 2003). They also demonstrated antifungal activities with the octyl gallate derivative of GA (Kubo *et al.* 2001).

Jung *et al.* (2013) studied the antiulcerogenic capacity of GA, where 100 mg/kg of GA showed 40.6% inhibition of gastric lesion of rats. While Couto *et al.* (2013) demonstrated the anti-inflammatory effect of GA when they used sprayed dried leaves of *Phyllanthus niruri* on carrageenan-induced inflammation on mouse paw. Recent research on the pharmacological uses of GA has also brought about knowing the effect of GA as an inhibitor for insulin amyloid fibril formation. The latter attribute has potential application to some neurodegenerative diseases, such as Alzheimer's, Parkinson's and Huntingdon's diseases (Liu *et al.* 2013, 2014; Jayamani and Shanmugam 2014).

Other important areas where GA had been used was in the leather industry where it acts as a chelating agent (Costa *et al.* 2013). Meanwhile, GA has been used in the development of photographs as recorded by Beniwal *et al.* (2013). With so much use and importance of GA in the pharmaceutical and food industry, there is the need for very good analytical methods for its determination in solution.

1.7.3 Gallic acid in wine

In addition to all the therapeutic, pharmacological and food additive uses, gallic acid is the main hydroxybenzoic acid found in red wine, formed mainly by the hydrolysis of the flavonoid gallate esters (Gris et al. 2013). Though they are a minor component in newly brewed wine, gallic acid can be found in older wine samples, as they are produced from the hydrolysis of gallate esters of hydrolysable tannins and condensed tannin. The wine hydrolysable tannins come from oak and might be in concentrations of close to 100 mg L⁻¹ for white wines in barrels for about 6 months, while red wines would have up to 250 mg L⁻¹ in barrels for two or more years. Gallic acid appears to be stable in wine during ageing. It is one of the phenolic compounds that are easily seen during the chromatographic separation of wine. Gallic acid is found in quantities of about 70 mg L⁻¹ in red wine and about 10 mg L⁻¹ in white wine samples (Waterhouse 2002).

As the hydroxybenzoic acids are being extracted from the oak barrels and also being produced from the breakdown of larger phenolics as the wine ages, the flavour of the wine is being enhanced. The total antioxidant capacity of wines are being enhanced as the wine gets older and produces more gallic acid from the hydrolysis of the flavonoid esters and the oak barrels (Minussi et al. 2003).

1.8 Review of electrochemical determination of Gallic acid: Graphene Oxide and Metal Oxide Nanoparticles

Over the years, there have been different types of carbon-based materials that have been used in modification of electrodes, for the electrochemical determination of GA. These include graphene, graphene oxide, carbon nanotubes, graphite and metal oxide nanoparticles modified electrodes.

Carbon-based electrodes have been continuously used for the detection of GA, because of their low cost, biocompatibility, and rapid electron transfer. The carbon-based materials include glassy carbon, carbon nanotubes used sometimes as modifiers, graphene, graphene oxide and carbon paste (graphite). The commonly known carbon electrodes are homogenous and heterogenous in their structural composition. The homogenous carbon electrodes are glassy carbon electrodes, carbon nanotubes, vitreous carbon, fullerenes, screen printed, graphite and diamond. On the other hand, carbon paste and the modified carbon pastes are the heterogeneous carbon electrodes. Although all carbon-based

electrode materials have the structural six-membered aromatic rings (Figure 1.11) with sp^2 and sp^3 bonding, they show some specific differences from each other. This is by the differences in the relative density of the basal and the edge plane, that have an influence on adsorption and electron transfer of the electrodes. The high degree of electron delocalization and the weak van der Waals, leads to the very good electrical conductivity in the different allotropes (Ghadimi *et al.* 2017).

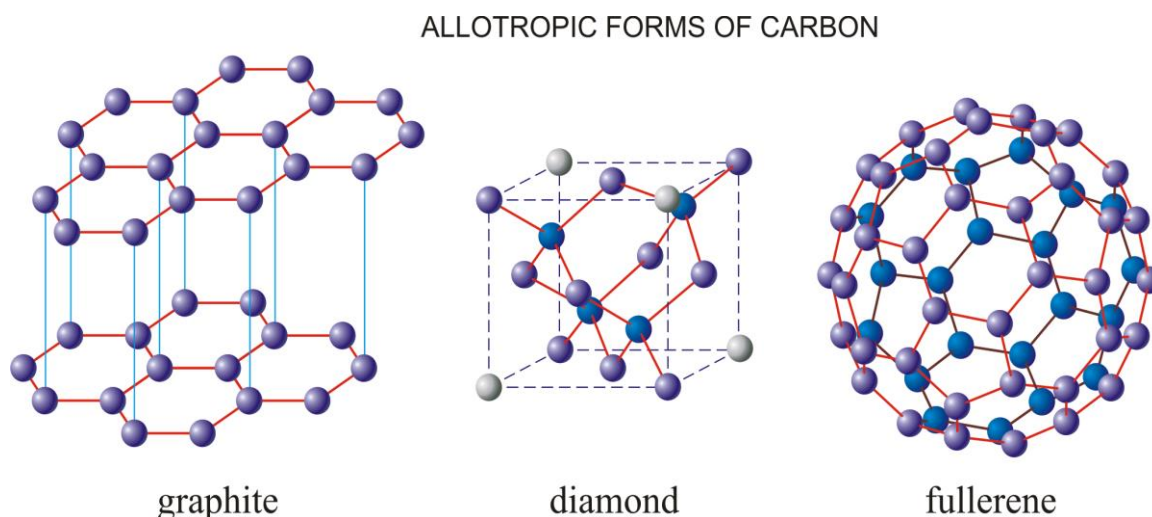


Figure 1. 11. The different allotropic forms of carbon, showing the basic six-membered aromatic rings as seen in the graphite, diamond and fullerene (Culled from 'Chemistry Glossary' 2018)

One of the early uses of carbon-based material for the electrochemical determination of GA was the work of Gunckel *et al.* (1998). They studied the electron-donating power of gallates, using the electrochemical characteristics of the gallates and the physicochemical properties of glassy carbon electrode. Using CV in neutral and acidic solutions, on a bare glassy carbon electrode; they found out that, electrochemical oxidation occurs through two electrons transfer steps. They also found out that, the intensity of the gallate derivatives were in the following sequence $GA \geq i\text{-propylgallate} > \text{propylgallate} > i\text{-butylgallate} > \text{butylgallate} > i\text{-pentylgallate} > \text{pentylgallate}$. The well-studied physicochemical properties of the glassy carbon electrode include the increasing oxides on the surface of the electrode. The homogenous structural arrangement of the aromatic rings and the pristine surface that can be generated by heat or abrasive polishing. The result of which, lower background current and increased electron transfer is attained; GA and many other phenolic acids have been electrochemically

determined, using CV and DPV (Gunckel *et al.* 1998; Kilmartin, Zou and Waterhouse 2001, 2002; Kilmartin and Hsu 2003; Yakovleva *et al.* 2007; Makhotkina and Kilmartin 2009, 2010, 2012, 2013; Piljac-Žegarac *et al.* 2010) (Table 1.1).

Table 1. 1. Different electrochemical determination of phenolic acids (Gallic acid) using Cyclic Voltammetry

	Type of electrochemical Technique	Electrode Used	Medium Analysed	Antioxidants (Phenolic acids)	Reference
1	Cyclic Voltammetry Differential Pulse Voltammetry Hydrodynamic Voltammetry	Glassy Carbon Electrode	Standards of Gallic acid and Gallates	Gallic acid, Propyl Gallate, Butyl Gallate, Pentyl Gallate	Gunckel <i>et al.</i> 1998
2	Cyclic Voltammetry	Glassy Carbon Electrode	White Wine Red Wine	Catechin Gallic acid	Kilmartin, Zou and Waterhouse 2001
3	Cyclic Voltammetry	Glassy Carbon Electrode	White Wine Red Wine	Catechin	Kilmartin, Zou and Waterhouse 2002
4	Cyclic Voltammetry	Glassy Carbon Electrode	Green Tea Oolong Tea Black Tea and Coffee	Catechin Gallic acid	Kilmartin and Hsu 2003
5	Cyclic Voltammetry	Glassy Carbon Electrode	Standards	Quercetin, Gallic acid, Caffeic acid, Vanillic acid	Yakovleva <i>et al.</i> 2007
6.	Cyclic Voltammetry	Glassy Carbon electrode	Tea solutions	Gallic acid	Piljac-Žegarac <i>et al.</i> 2010
7	Cyclic Voltammetry	Glassy Carbon Electrode	Red Wine White Wine	Catechin, Gallic acid, Coumaric acid, Rutin and Quercetin	Makhotkina and Kilmartin 2010

Using the glassy carbon electrode and mainly CV, the antioxidant capacity of red wine, white wine, green tea, black tea, and tea solutions were being determined. Most of the results showed a comparable result to the spectrophotometric analytical methods. Although, glassy carbon electrodes, were able to determine the antioxidant capacity of these beverages, there was still the drawback of electrode fouling, sensitivity, and antioxidant selectivity.

These drawbacks have led to the in depth work of Yakovleva *et al.* (2007), where they determined the mechanism for the oxidation of phenolics. They found out that, the oxidation of the phenolic acids was a two electrons reaction, with a suggestion that, the first oxidation step of phenolics might be at the 4-

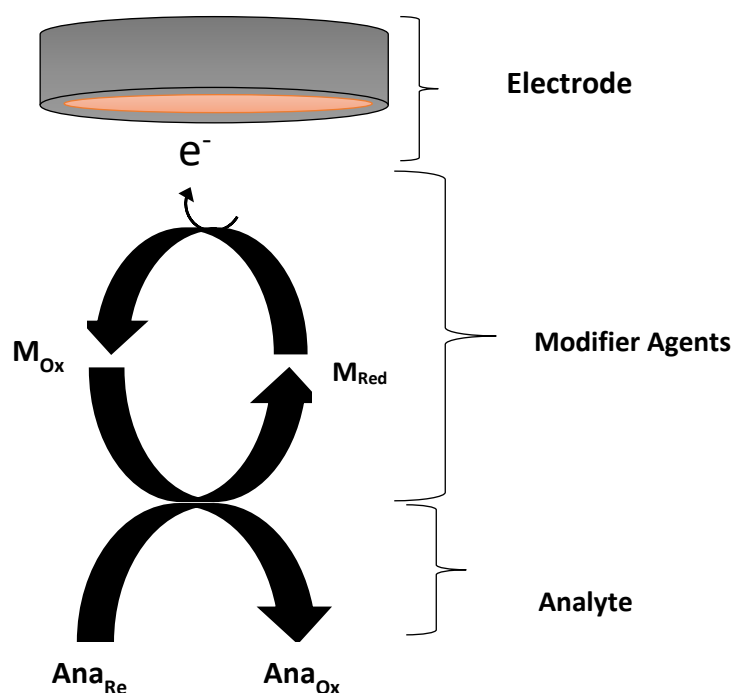
hydroxybenzoic acid structure (possibly the para or ortho structure). This then laid a foundation for Piljac-Žegarac *et al.* (2010), who proposed that, the major contributors of the antioxidant capacity of tea were oxidised at a potential of 440 mV. They attributed the oxidation at the peak potential of 440 mV to ortho-dihydroxy-phenol and gallate groups (GA).

Understanding the drawbacks of glassy carbon electrodes towards the sensitivity and selectivity, Panizza and Cerisola (2009) used a different type of carbon-based electrode, boron-doped diamond electrode (BDD), for the electrochemical degradation of GA. Using this electrode, they characterised the electrochemical behaviour of GA, where the kinetic of GA degradation was studied using CV. They found out that, at low potentials, when the electrolytes are stable, the formation of the GA film on the anode surface results in the deactivation of BDD. Their work was very important as it suggested the saturation of GA molecules on the electrode surface as they form a GA film.

With the advancement of the different electrochemical techniques for the determination of GA; and the need for more specific analysis, so was the need for the electrodes to be more specific. Hence, the need for further modification of the carbon-based electrodes. This continued with the modification of these carbon-based electrodes to attain the analytical needs of researchers.

1.8.1 Chemically Modified Electrodes

The immobilization of chemical compounds or even nanomaterials onto electrode surfaces have been developing progressively in the last 50 years as the study of electrochemistry progresses (Cheemalapati 2018). Electrochemists have become so interested in the deliberate modification of electrodes by adsorbing, coating, or attaching specific molecules to the surface of electrochemical electrodes. Chemically modified electrodes (CME) are electrodes that are deliberately modified by the immobilization of a modifier agent on the electrode surface. The modifier agent can be immobilised on the electrode surface by irreversible adsorption, chemisorption, self-assembled layers, covalent bonding, chemical reactions, and polymer layers (Scheme 1.2).



Scheme 1.2 A general representation of an electrochemically induced redox reaction by a chemically modified electrode. Showing the redox interaction at the modifier and the electron transfer on the electrode surface.

As compared to conventional electrodes (glassy carbon or carbon paste electrodes), there is greater control of the electrode characteristics and reactivity. This is by using the physicochemical properties of the modifier agents, like increased electroactivity, catalytic properties, ionic activity or even particle sizes of the modifier. The chemically modified electrodes have unique features, like a thin film on the electrode surface; that is sometimes coated by drop-casting. The modified surfaces tend to produce the following outcomes:-

- They transfer/upgrade the known physicochemical properties of the modifier to the electrode surface
- They tend to be selective towards the specific analytes
- They enhance the electroactivity of the electrode, when materials with large surface areas are used as modifiers (nanomaterials).
- Some materials would enhance the diffusion kinetics as well as the electron transfer
- They also extract and accumulate analytes on the electrode surface.

Glassy carbon and their derivative electrodes are amongst the most commonly used substrates for modification. They provide a very wide potential window, with a low-background current and very strong chemical stability (Sajid *et al.* 2016).

Chemically modified electrodes used for the determination of GA would help in selectivity, sensitivity, and reproducibility in the presence of interferences. This is by helping in the reduction of ohmic resistance, commonly seen in wide potential window electrode materials. However, there are some drawbacks, that may affect the response of chemically modified electrodes. These may include the nature of the coating material, the way the materials were synthesised, the nature of analyte and the mechanism of the electrode coating.

1.8.2 Modified electrodes for Gallic acid determination

Chemically modified electrodes have been used over the years for the electrochemical determination of GA (Er-raki *et al.* 1998; Luo *et al.* 2013a; Sangeetha and Narayanan 2014; Gao *et al.* 2016; Puangjan and Chaiyasith 2016; Raja *et al.* 2017; Stanković *et al.* 2017; Xiong *et al.* 2017; Węgiel, Burnat and Skrzypek 2018). Different types of modifications have been used including nanomaterials-based modifications. The modification of electrodes using nanoparticles as compared to the bulk compounds (macroelectrodes) for electrochemical analysis, have these four main advantages – They provide:-

- High effective surface area
- Increased mass transport
- Catalysis
- And relative control over the microenvironment.

Recent studies have shown considerable interest in the use of metal nanoparticles as electroactive sensing materials in the modification of chemically modified electrodes. Noble metal nanoparticles like gold, platinum, and silver, have been commonly used because of their unique size-dependent electrical, optical, magnetic, and chemical properties. These have also shown good electron transfer kinetics (Wang and Hu 2009; Campbell and Compton 2010; Medina-Plaza *et al.* 2015). On the other hand, carbon nanomaterials also have advanced greatly in the chemical modification of electrodes. Graphene and carbon nanotubes (CNT) (multi-walled carbon nanotubes (MWCNT) and single-walled carbon nanotubes (SWCNT)), have been so popular in electrode modification. This is because of their high surface area to volume ratio, biocompatibility, high electrical conductivity, mechanical and chemical strength (Agüí, Yáñez-Sedeño and Pingarrón 2008; Goyal, Chatterjee and Rana 2010; Lee *et al.* 2010; Eguílaz *et al.* 2016). With the increase interest in the metal and carbon-based nanomaterials, there was also the

need to further improve their functionality in the electrochemical determination of organic compounds. Hence, further research into their oxides (metal oxide nanoparticles and graphene oxide nanoparticles).

Graphene oxide nanoparticles (GON) and metal oxide nanoparticles are employed in the modification of electrodes, that are used for electrochemical sensing of antioxidants (GA). The oxygenated groups in GON can influence the electrochemical, electronic and mechanical properties of the compound, hence the reason for the difference between pristine graphene and graphene oxide (Gómez-Navarro *et al.* 2010). Due to the polar oxygen groups found in GO, the compound is highly dispersible in solvents like water (Stankovich *et al.* 2006). The dispersed GO can be deposited easily on various substrates by drop-casting, dip-coating, spraying or spin coating (Kim *et al.* 2010) and be used as good electrode materials.

Furthermore, just like GON, metal oxide nanoparticles with different morphologies have exhibited different types of electrical, electrochemical, and photochemical properties due to their sizes, stability, and very high surface area. These compounds mainly function in electroanalysis, by toughening the conductive sensing interface, catalysis and electrical contact to redox centres (Katz, Willner and Wang 2004). When used as electrodes or electrode-modifiers in electrochemical analysis, they transfer electrons between the analyte and the transducer like electronic wires or electro-catalysts (George, Antony and Mathew 2018). Hence, their use as electrodes for electrochemical determinations.

1.8.3 Metal oxide nanoparticles modified electrodes

Many highly sensitive and novel electroanalytical devices or electrodes have been made using nanostructured metal oxide compounds. This is because, they are cost-effective and show great sensitivity and selectivity, when coupled with other biorecognition molecules (Wei *et al.* 2007; Batchelor-McAuley *et al.* 2008; Tashkhourian *et al.* 2014; Fayemi and Adekunle 2015; Medina-Plaza *et al.* 2015; Tashkhourian and Nami-Ana 2015). Metal oxide nanoparticles (MO NPs) have been made using different synthetic methods, which gives the nanoparticles different physical morphologies. The MO NPs exhibit various types of electrical properties because of their sizes, increased surface area and stability, which tend to toughen the conductive sensing interface, express catalytic properties, and speedy electron transfer. The affinity of metal oxide nanoparticles on the surface of electrodes

when used for modification can be achieved by chemical covalent bonding, physical adsorption, electro-polymerization or electrodeposition (Wang and Hu 2009).

Some of the major transition MO NPs that have been used in electrochemical studies include, tungsten, iron, gold, cobalt, silver, vanadium, copper, zinc, nickel, zirconium, manganese, and titanium. However, gold and silver have been the main metals, used in developing metal oxide nanoparticles modified electrochemical sensors (Daniel and Astruc 2004; Campbell and Compton 2010; Li, Schluesener and Xu 2010; George, Antony and Mathew 2018); with a limited number of work done using them in the determination of GA.

Metal oxide nanoparticles like Fe_2O_3 , Fe_3O_4 (Iron oxide nanoparticles), MnO , MnO_2 , Mn_3O_4 (Manganese oxide nanoparticles), TiO_2 (Titanium dioxide nanoparticles), CuO , Cu_2O (Copper oxide nanoparticles), ZnO (Zinc oxide nanoparticles), ZrO_2 (Zirconia nanoparticles) and some of their composites have been used as modified electrodes for electrochemical analysis. All these have been in the determination of different organic compounds like glucose, quercetin, uric acid, caffeine, dopamine, hydrazine, phenol, catechol, ascorbic acid, ferulic acid and in some cases heavy metals. The Table. 1.2, is a table of the different metal oxide nanoparticles modified electrodes that have been used in the determination of other organic compounds apart from GA. Though the metal oxide nanoparticles have been used in the determination of other organic compounds, there are still some drawbacks in using them. Some of the drawbacks are sometimes poor ion transport kinetics, wide band gap, which sometimes make the MO NPs function as semiconductors or insulators and the pulverisation of electrode film by the metals. The pulverisation of the electrode film is mainly because of the reasonable volume expansion and contraction, during the process of charging and discharging. To overcome some of these drawbacks and profit from the enormous capabilities of MO NPs, they are hybridized with different carbonaceous materials, forming alloys with other metals or with polymers. Hence, the frequent modification of carbon paste electrodes with metal oxide nanoparticles and carbon nanotubes.

Table 1. 2. Metal Oxide Nanoparticles in different electrochemical sensor systems for the determination of different organic compounds

	Metal oxide nanoparticles-Electrode	Electrochemical technique	Medium Analysed	Analytes	Limit of Detection $\mu\text{mol L}^{-1}$	Linear Response $\mu\text{mol L}^{-1}$	Ref.
1	Fe ₂ O ₄ @CNT/GCE	SWV	-	Ascorbic acid	0.24	5 -235	(Fernandes <i>et al.</i> 2014)
2	Fe ₃ O ₄ /MB-CPE	DPV	Water samples	Hydrazine and Phenol	0.018 24.3	0.1-12 100-470	(Benvidi <i>et al.</i> 2016)
3	Mn ₃ O ₄ -NPs/N-GR/CPE	Amperometry	Urine	Glucose	1.0	2.5 -529.5	(Yang <i>et al.</i> 2015)
4	MnO ₂ /f-MWCNT/GCE	SWV	Serum	Ferulic acid	0.01	0.082 -220	(Vilian and Chen 2015)
5	CuO-Gr/CPE	DPV	Serum, Urine	Acetaminophen and Caffeine	0.008 0.01	0.025-5.3 0.025-0.3	(Khoshhesab 2015)
6	Porous Cu ₂ O nanospheres-rGO/GCE	DPV	-	Uric acid and Dopamine	0.112 0.015	1.0 - 138 0.05 -109	(Mei <i>et al.</i> 2016)
7	TiO ₂ -Graphene/GCE	DPV	Denatured DNA	Adenine and Guanine	0.1 0.15	0.5 - 200 0.5 - 200	(Fan <i>et al.</i> 2011)
8	TiO ₂ /PtP/GCE	Amperometry	Tea and Apple Juice	Quercetin	0.0008 mg/L	0.002-50 mg/L	(Tian <i>et al.</i> 2014)
9	ZnCo ₂ O/GCE	CA	-	Glucose and Dopamine	36.9 15.4	10 - 290 5 - 100	(Naik and Rout 2015)
10	MnCo ₂ O ₄ /GCE	DPASV	Water	Cadmium	0.72 $\mu\text{g/L}$ -		(Velmurugan and Chen 2017)

There have been a lot of metal nanoparticles (MNPs) and limited number of metal oxide nanoparticles modified electrodes developed for the electrochemical determination of phenolic acids and most importantly GA (see Table 1.3 below). This is because of the importance of GA with its strong antimutagenic, anticarcinogenic and antioxidant properties (Peyrat-Maillard, Bonnely and Berset 2000; Dalla Pellegrina *et al.* 2005).

One of the early uses of metal oxide nanoparticles for the determination of GA was done by Tashkhourian *et al.* (2013), where they used TiO₂ nanoparticles for the modification of the carbon paste electrode. Titanium dioxide nanoparticles were used because of their versatility, having high surface area, relatively good conductivity, good optical transparency, and good biocompatibility. Using the properties inherent in this metal oxide nanoparticle, they found that, the electrochemical behaviour of GA was improved significantly at the modified electrode relative to the bare electrode. Under optimized conditions and using DPV, GA was determined at a limit of detection (LOD) of $9.4 \times 10^{-7} \text{ mol L}^{-1}$ and the modified electrodes were used to detect GA in tap water, black and green tea. In their further work, Tashkhourian and Nami-Ana (2015) synthesised SiO₂ nanoparticles and used it in the modification of carbon paste electrode. Silica nanoparticles regarded as another metal oxide nanoparticle, are robust inorganic

solids that show high specific surface area, and a three-dimensional structure, made up of highly open spaces interconnected to each other. With the physical and structural capabilities of SiO₂ nanoparticles; Tashkhourian and Nami-Ana, compared the outcome of the modification with multiwalled carbon nanotubes (MWCNTs) as opposed to graphite and found that, the silica functioned better in graphite than in MWCNT. With an LOD of 2.5×10^{-7} mol L⁻¹, they concluded that, SiO₂ nanoparticles-CPE exhibited remarkable electrochemical effect towards GA determination.

On the other hand, Andrei *et al.* (2016), reported the development of an electrochemical sensor made of cerium oxide nanoparticles (CeO₂ NPs) for the detection of GA in wine samples. In this case, further, insight was acquired towards using metal oxide nanoparticles for the electrochemical determination of GA. Cerium oxide nanoparticles have a unique catalytic and free scavenging property, which was harnessed by Andrei *et al.* in this case. They developed and characterised a disposable single-use electrochemical sensor based on the oxidase-like activity of CeO₂ NPs (nanoceria), where phenolic compounds with the dihydroxybenzene functionality were oxidised to their corresponding quinones on a screen-printed carbon electrode (SPE). The sensor and the electrochemical reaction conditions were optimised, and they used CV with the modified electrode for the determination of GA, caffeic acid (CA), quercetin (QC), epicatechin and ascorbic acid (AA). They concluded with a demonstration of the feasibility of nanoceria particles as oxidase mimetics for the detection of antioxidants found in wine.

Most recently Shahamirifard *et al.* (2018) developed a carbon paste electrode modified by a nanocomposite containing ZrO₂ nanoparticles (zirconia) (ZrO₂NPs), choline chloride (ChCl) and gold nanoparticles (AuNPs) creating a composite of ZrO₂-ChCl-AuNPs/CPE for the simultaneous electrochemical determination of GA and uric acid (UA). They used DPV for the simultaneous determination of GA and UA, at the optimum condition. This nanocomposite showed a linear response in the increasing ranges of 0.22-55 μmol L⁻¹ for GA and 0.12 -55 μmol L⁻¹ for UA, producing an LOD of 2.5×10^{-8} mol L⁻¹ and 1.5×10^{-8} mol L⁻¹ respectively. The applicability of the modified electrode was proven by using the electrode to detect GA in green tea and fruit juices, while the simultaneous detection of GA and UA was done in a human urine sample.

With the growing importance of these metal oxide nanoparticles in these different areas, there is also the increase need for their study in GA determination. However, most of the nanomaterials modified electrodes are mainly the bare metal nanoparticles of silver and gold. Except for titanium dioxide (TiO₂) and silicon dioxide (SiO₂), nanoparticles, there seem to be a massive gap in the use of only a metal oxide nanoparticle (not as composites with other compounds or metal oxides) as sensors in the electrochemical determination of GA and other antioxidants in general.

Table 1. 3. Metal Oxide Nanoparticles and Metal Nanoparticles composites in different electrochemical sensor systems for the determination of Gallic acid

	MO NPs and MNP Electrode	Electrochemical technique	Medium Analysed	Analytes	Limit of Detection (μmol L⁻¹)	Linear Response (μmol L⁻¹)	Ref.
1	Zn-Al-NO ₃ /LDHf/GCE	DPV	Green Tea samples	Gallic acid Caffeic acid	1.6 2.6	4.0 – 600 7.0 – 180	(Kahl and Golden 2014)
2	TH/NiHCF	DPV CA	Spiked Tea and Milk	Gallic acid H ₂ O ₂	1.66 0.557	4.99 – 1200 1.67 – 1110	(Sangeetha and Narayanan 2014)
3	S _{DOD} AuNP-LB	CV	Organic acid solutions	Caffeic acid Gallic acid	5.6	0.1 – 10	(Medina-Plaza <i>et al.</i> 2015)
4	CS-fFe ₂ O ₃ -ERGO/GCE	DPV	Red and White wine	Gallic acid	0.15	1 – 100	(Gao <i>et al.</i> 2015)
5	[Cu ₂ tpmc](ClO ₄) ₄ /CGCE or CGE	DPV	Wine	Gallic acid	0.15-CGE 4.6 – CGCE	0.25 – 100	(Petković <i>et al.</i> 2015)
6	AuMCs/SF-GR/GCE	DPV	Black Tea, Urine	Gallic acid Uric acid	10.9 nM 0.12μM	0.05 – 8.0 0.2 – 50.0	(Liang <i>et al.</i> 2016)
7	AgNP/Delph/GCE	Amperometry	Fruit Juice	Gallic acid	0.28	0.60 – 8.68	(Ghaani <i>et al.</i> 2016)
8	PDDA-GR-Pt/GCE	SWV	Jianmin Yanhou Tablet, Beverages	Galli acid	0.007	0.03- 1	(Gao <i>et al.</i> 2016)
9	ZrO ₂ /Co ₃ O ₄ /rGO/FTO	DPV	Tea, Rice, Grape	Gallic acid, Caffeic acid, Protocatec huic acid	-	-	(Puangjan and Chaiyasith 2016)
10	Bi ₂ MoO ₆ /Bi ₂ S ₃ Nanobelts	Photo electro-chemistry	Rose Oral Liquids	Gallic acid	-	-	(Wang <i>et al.</i> 2017)
11	ZrO ₂ -ChCl-AuNPs/CPE	DPV	Green Tea Fruit juices	Gallic acid and Uric acid	0.025 0.015	0.22 – 55 0.12 – 55	(Shahamirifard <i>et al.</i> 2018)

1.8.4 Graphene oxide nanoparticles modified electrodes

Graphene is a one-atom-thick sp^2 bonded carbon sheet, that is also described as a flat monolayer of carbon atoms which is tightly packed into a two-dimensional (2D) honeycomb lattice that also forms a building block for graphitic materials (Shao et al. 2010a) (Figure 1.12). Graphene can be structurally wrapped into various other dimensions 0D fullerenes, 1D nanotubes or stacked into 3D graphite (Geim and Novoselov 2007). The strictly two-dimensional structure shows an exceptionally high crystal and electronic quality, which has led to its high usage in electrochemical applications. Its extraordinary electronic transfer properties, high electrical conductivity, good mechanical, and high surface area has led to its use for electrochemical sensors. Hence, their capability to improve the electrocatalytic performance of electrodes when they are immobilized on electrode surfaces (Liang *et al.* 2016). This is because of their unique properties, which include wide potential windows, inertness when acting as a catalyst and good electro-catalytic activity. Thus, owing to these unique properties, graphene, graphene oxides and their derivatives have become very desirable materials for electrochemical sensors.

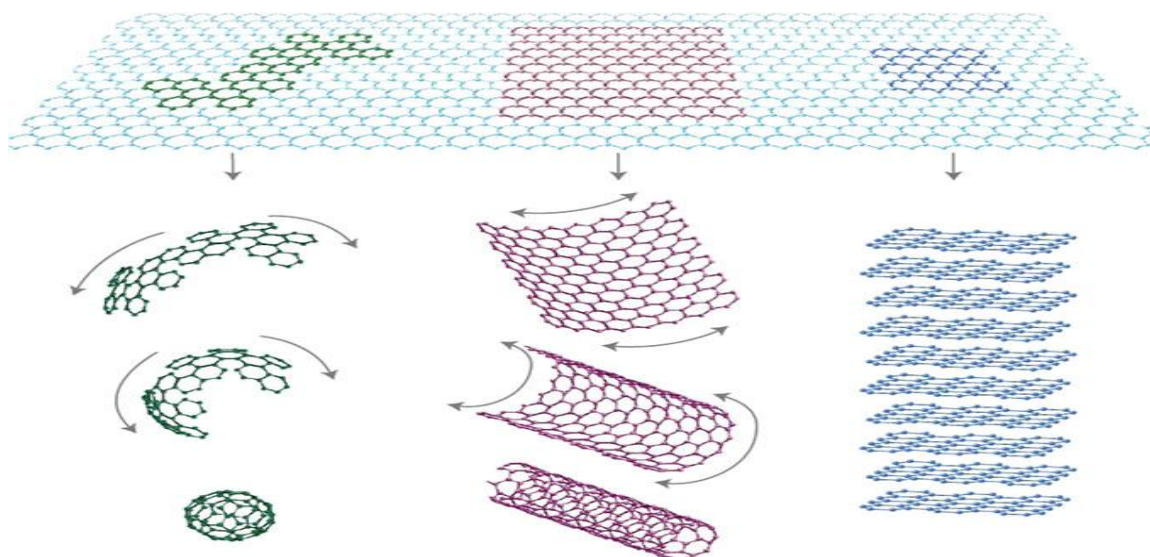


Figure 1. 12. Schematic representation of graphene which is the fundamental starting material for fullerene materials, carbon nanotubes (CNT) and graphite. Reproduced from (Brownson and Banks 2014) with permission from Springer Nature.

Graphene oxide (GO) is typically produced by the chemical exfoliation of graphite powder using very strong oxidants like potassium permanganate (KMnO_4) dissolved in concentrated sulphuric acid (conc. H_2SO_4) (Murali *et al.* 2010). GO exhibits various excellent properties, because of its specific 2D structure and various oxygenated functional groups. The oxygenated groups in GO strongly affect the electronic, mechanical, thermal, optical, and electrochemical properties. For the electrochemical properties, its favourable electron mobility and unique surface properties give it a high electrocatalytic power as it is used in sensors (Shao *et al.* 2010b). Graphene, graphene oxide and reduced graphene oxide (rGO), have been used consistently as described in the literature for the electrochemical determination of a great variety of organic compounds (Fan *et al.* 2011; Xie *et al.* 2013; Mei *et al.* 2016; Wang *et al.* 2016b; Stanković *et al.* 2017; Węgiel, Burnat and Skrzypek 2018). Most importantly these graphene electrodes and their modifications, have also been used for the determination of antioxidants (GA) (Ma *et al.* 2013; Gao *et al.* 2015; Puangjan and Chaiyasith 2016; Stanković *et al.* 2017; Węgiel, Burnat and Skrzypek 2018). However, there are hardly any graphene oxide nanoparticles electrochemical sensors, that have been used for the determination of GA.

One of the early usages of graphene oxide for GA determination, was the work of Ma *et al.* (2013). They developed a photoelectrochemical sensor, with polyaniline-reduced graphene oxide- TiO_2 composite for the selective sensing of GA. They made use of the two-dimensional π -conjugation structure of graphene, that makes it a good electron receptor and conductor in photocatalysis. Hence, their ability to accelerate electron transfer and effectively suppress charge recombination. With the inability of TiO_2 to absorb visible light due to its large band gap, the reduced graphene oxide and TiO_2 (rGO- TiO_2), helped increase the absorption of visible light with a narrower band gap. GA was then determined using the increase in photocurrent as there was an amplified electron transfer from GA to polyaniline in the course of analysis. Meanwhile, Gao *et al.* (2015), developed a sensitive electrochemical sensor for GA in wine, which was based on an electrochemically reduced graphene oxide (ERGO), with hybrids of chitosan (CS) and fishbone-shaped Fe_2O_3 (f Fe_2O_3) using DPV. They used the composite matrix to modify GCE. Their work was based on the single-atom-thick sheet, of hexagonally formed sp^2 -bonded carbon atoms of graphene oxide. Also, the large number of polar groups like hydroxyl, epoxide and carboxylate groups that makes the GO hydrophilic. This

helps in their use as dispersants in hydrophobic substances (Wang *et al.* 2014). However, they suggested that the oxidation on the electrode surface destroys the perfectly conjugated structure of the GO creating poor electron transport capacity. Hence the transformation of GO in the composite to rGO to stabilise the electron transport. This presented a superior electrochemical response when used for the determination of GA, as compared to having just a single component modified electrode like CS- fFe₂O₃/GCE without electrochemically reduced graphene oxide (ERGO). Using DPV as the electrochemical technique, the oxidation peak currents showed a good linear relationship, with the logarithmic values of the concentration of GA in a range of 1.0×10^{-6} mol L⁻¹ to 1.0×10^{-4} mol L⁻¹. The analytical estimation of the limit of detection was 1.5×10^{-7} mol L⁻¹. Furthermore, Puangjan and Chaiyasith (2016) developed a nanocomposite catalyst which was used to modify a fluorine-doped tin electrode. They produced a novel ZrO₂/Co₃O₄/reduced graphene oxide (rGO) nanocomposite by a reflux method, which was then used in the modification of an electrochemical sensor by having it cast on to the surface of a fluorine-doped tin oxide (FTO) electrode. They applied the structural importance of GO as a good platform for different metal oxide catalysts like Fe₂O₄ (Lian *et al.* 2010) and TiO₂ (Fan *et al.* 2011) in different applications. They harnessed this nano-composite catalyst with graphene support, to provide a multiphase nanocomposite characteristic and a multi-functionality of the metal oxide-organic framework. The ZrO₂/Co₃O₄/reduced graphene oxide (rGO) nanocomposite/FTO electrode showed synergistic catalytic effect towards the electrochemical determination of GA, caffeic acid and protocatechuic acid; showing a linear relationship between the oxidation peak currents and increasing concentrations in the range of 6.24 to 477.68 nmol L⁻¹ for GA and an LOD of 1.5 nmol L⁻¹.

With the continued interest in graphene, graphene oxide and their derivatives for the modification of GCE, for the sensitive and selective determination of GA; many other electrodes have been developed. Stanković *et al.* (2017) studied the electrochemical behaviour and properties of two modified GCE using titanium nitride doped rGO (TnrGO) and wolfram carbide doped rGO (WcrGO) for the quantification of GA in wine, using DPV. They used rGO which has a higher electrical conductivity than graphene, due to the high amounts of disrupted sp² bonds and created the composites of nanostructured titanium nitride and wolfram carbide. Their main aim was to use the nanostructured properties of titanium

nitride and wolfram carbide. Comparing both nanomaterials, at linear ranges of 4.5 – 76 $\mu\text{mol L}^{-1}$ for TnrGO and 10 – 100 $\mu\text{mol L}^{-1}$ for WcrGO, they determined GA with LODs of 1.1 $\mu\text{mol L}^{-1}$ and 3.1 $\mu\text{mol L}^{-1}$ respectively. Meanwhile recently, Węgiel, Burnat, and Skrzypek (2018) developed a carbon-ceramic electrode (CCE) modified with reduced graphene oxide for the voltammetric determination of GA. In this work, reduced graphene oxide was used as in the other cases to modify the CCE and GA was determined by square wave voltammetry.

With the increasing interest in graphene oxide, there is also the need for electrodes that could combine the electrochemical properties and nano-properties of GO for electrochemical sensors. Most of the work that used carbon-based nanomaterials for GA determination are those done using carbon nanotubes. Thus, there is a gap in the literature for the use of graphene oxide nanoparticles. The fact that, there are hundreds of different modifications of electrodes for the electrochemical determination of GA, this work would focus mainly on nanomaterials modified electrodes. Within these nanomaterials, specific emphasis would be made on graphene-oxide nanoparticles and metal oxide-based nanoparticles and their interactions.

1.9 Research Aims and Objectives

The aim of this work is to investigate and develop novel nanomaterials based electrochemical sensors for fast, sensitive, cost-effective, and selective determination and analysis of GA.

The aim of the research would be achieved by completing the following objectives:

1. To review modern nanomaterials (graphene oxide nanoparticles and metal oxide nanoparticles) used in the modification of electrodes as applied to the electrochemical determination and analysis of GA.
2. Study and identify the chemical and physical properties of GA that would influence its electrochemical detection and determination.
3. Investigate cyclic voltammetry and differential pulse voltammetry as reliable electroanalytical methods and the best way to enhance their analytical capability.
4. Synthesis some metal oxide nanoparticles for electrode modification
5. Modify a working electrode with graphene oxide nanoparticles and use it for the determination of GA in beverages.

6. Modify carbon paste electrodes with metal oxide nanoparticles and use them for the determination of GA in beverages.
7. Study the effect of the nanoparticles on GA oxidation
8. Characterise any modifications done on the electrode using SEM, EDXA, XRD and FTIR.
9. Develop electrodes made up of metal oxide nanoparticles and propose an interaction mechanism between the nanoparticles and graphite compounds.

CHAPTER TWO

2.0 EXPERIMENTAL MATERIALS AND METHODS

2.1 Introduction

In the course of this work, which included the development of modified electrodes for the determination of GA, different experimental reagents, techniques, and apparatus were used. An overview of the different procedures and the related theories are described in this chapter.

2.2 Reagents

Unless specifically stated, all chemicals were of the highest purity and used as received from the stated vendor with no further purification. All solutions used in the course of the studies, were freshly prepared solutions, protected from light by refrigeration at 4 °C when not in use. The stock solutions were also refrigerated and kept away from light. Aqueous solutions were prepared using doubly distilled water (18.2 Meg Ω -cm). Commercially available wine samples (Casillero Del Diablo Cabernet Sauvignon and Sauvignon Blanc) and orange juice (Innocent Smooth Orange Juice) were purchased from ASDA (Aberdeen, UK). All reagents used in the preparation of Britton-Robinson buffer (0.1 mol L⁻¹ acetic acid, 0.1 mol L⁻¹ boric acid, 0.1 mol L⁻¹ phosphoric acid), potassium hexacyanoferrate (III) (K₃Fe(CN)₆) were from Sigma Aldrich (London, UK). The other reagents used, are as reported in Table 2.1.

Table 2. 1. List of Chemicals used

	Reagents	CAS-No.	M. Wt.	Purity	Supplier
1	Gallic acid	149-91-7	170.12	-	Sigma Aldrich
2	Vanillin	121-33-5	152.15	99%	Sigma Aldrich
3	Ascorbic acid	50-81-7	176.12	≥99%	Sigma Aldrich
4	Quercetin	6151-25-3	302.24	≥95%	Sigma Aldrich
5	Trolox	53188-07-1	250.29	≥97%	Sigma Aldrich
6	Graphene oxide Nanocolloids	-	2 mg/mL dispersion in water	-	Sigma Aldrich
7	Zirconium (IV) oxide	1314-23-4	123.22	≥99%	Sigma Aldrich
8	Zirconium Hydroxide	14475-63-9	159.25	≥97%	Sigma Aldrich

8	Potassium Chloride	7447-40-7	74.55	≥99%	Sigma Aldrich
9	Zinc nitrate hexahydrate	10196-18-6	297.49	≥99%	Sigma Aldrich
10	Zinc oxide	1314-13-2	81.39	99.99%	Sigma Aldrich
11	Cobalt (II) nitrate hexahydrate	10026-22-9	182.94	≥98%	Sigma Aldrich
12	Cobalt (II,III) oxide	1308-06-1	240.80	≥99.99%	Sigma Aldrich
13	Sodium Hydroxide	1310-73-2	40	≥97%	Sigma Aldrich
14	Tetraethyl orthosilicate	78-10-4	208.33	≥99.99	Sigma Aldrich
15	Acetic acid	64-19-7	60.05	≥99%	Sigma Aldrich
16	Boric acid	10043-35-3	61.83	≥99.5%	Sigma Aldrich
17	Phosphoric acid	7664-38-2	98	-	Merck
18	Sodium dihydrogen phosphate dihydrate	10049-21-5	137.99	≥98%	Merck
19	Disodium hydrogen phosphate heptahydrate	7782-85-6	268.07	≥99.99	Merck
20	Sodium acetate trihydrate	6131-90-4	82.03	-	Merck
21	Methanol	67-56-1	32.04	≥99.9%	Merck
22	Potassium nitrate	7757-79-1	101.10	≥99%	Merck
23	Potassium Ferricyanide	13746-66-2	329.24	≥99%	Sigma Aldrich
24	2,2-Diphenyl-1-picrylhydrazyl (DPPH)	84077-81-6	618.74	-	Sigma Aldrich

2.3 Analytes

2.3.1 Phosphate Buffers

A solution of $1 \times 10^{-1} \text{ mol L}^{-1}$ phosphate buffer was used in this study. This was prepared by mixing known volumes of disodium hydrogen orthophosphate ($2 \times 10^{-1} \text{ mol L}^{-1} \text{ Na}_2\text{HPO}_4$) and sodium dihydrogen orthophosphate ($2 \times 10^{-1} \text{ mol L}^{-1} \text{ NaH}_2\text{PO}_4$) (table 2.1) to make up a 50 mL solution which was subsequently diluted to 100 mL with deionised water. The different mixtures of the two salts solutions produced phosphate buffer solutions of specific pH, as shown in table 2.2.

The pH of the buffer solution was adjusted with phosphoric acid ($1 \times 10^{-2} \text{ mol L}^{-1}$) and sodium hydroxide ($1 \times 10^{-1} \text{ mol L}^{-1}$) for low and high pH, respectively.

**Table 2. 2. Phosphate Buffer Solutions between the pH 5.8 – 8.0 at 25 °C
(Adapted from Sigma-Aldrich, UK)**

pH at 25 °C	X mL Na₂HPO₄ (2 x 10⁻¹ mol L⁻¹)	Y mL NaH₂PO₄ (2 x 10⁻¹ mol L⁻¹)
5.8	4.0	46.0
6.0	6.15	43.85
6.2	9.25	40.75
6.4	13.25	36.75
6.6	18.75	31.25
7.0	30.5	19.5
7.2	36.0	14.0
7.4	40.5	9.5
7.6	43.5	6.5
7.8	45.75	4.25
8.0	47.35	2.65

2.3.2 Preparation of potassium ferricyanide solution

A 100 mL of K₃Fe(CN)₆ (10 mmol L⁻¹) stock solution was prepared by dissolving K₃Fe(CN)₆ (3.2 g) and KCl (0.75 g) in a 100 mL water. The potassium ferricyanide stock solution was further used for lower concentration dilution. The solution was used for EIS measurements and for the determination of the electroactive surface area of the electrodes being studied.

2.3.3 Preparation of Antioxidant solutions

Newly prepared antioxidant solutions of GA, vanillin, ascorbic acid, and Trolox (1 x 10⁻² mol L⁻¹ respectively) were made up daily and used in the course of this work. The relevant amount of the specific antioxidant was weighed out and dissolved in the relevant quantity of phosphate buffer.

2.3.4 Preparation of real sample (orange juice and wines) solutions

The commercially available real samples of white wine, red wine and orange juice were analysed for the determination of GA using the standard addition method and differential pulse voltammetry. The orange juice, white and red wine (diluted in 10 mL electrochemical cell) as blanks were analysed in triplicate. The blank samples were diluted in phosphate buffer (1 x 10⁻¹ molL⁻¹, pH 2.0). Standard addition of GA aliquots (1 x 10⁻² mol L⁻¹) were then added to the electrochemical

cell and stirred vigorously for 2 mins, using a magnetic stirrer. After each GA aliquot addition, the voltammograms were recorded. All the wine samples for a set of experiments/measurements were from newly opened wine bottles and wine samples were never re-used after they were opened.

2.4 Synthesis of metal oxide nanoparticles

All metal oxide nanoparticles used in the modification of the different working electrodes, were all synthesised as previously described in the literature (Venkatathri 2007; Gusatti *et al.* 2009; Pei *et al.* 2013; Wadekar, Nemade K.R. and Waghuley S.A. 2017), unless otherwise stated.

2.4.1 Synthesis of ZnO nanoparticles

The synthesis of ZnO nanoparticles was adapted according to Gusatti *et al.* (2009). In brief Zn(NO₃)₂.6H₂O (14.87 g) was dissolved in deionized water (100 mL) to make 0.5 molL⁻¹ solution and the solution was stirred for 25 mins using a magnetic stirrer. Then the resulting solution was heated to 70 °C while stirring. In a separate beaker, a one molar (1 molL⁻¹) solution of NaOH (1.2 g) was prepared in deionized water (30 mL) and stirred for 10 mins. The latter was then added dropwise into the Zn(NO₃)₂.6H₂O solution with continuous stirring to form a suspension with the temperature kept at 70 °C for 2 hrs with stirring. Then the mixed solution was left to settle at room temperature for a few hours and the precipitate formed, was filtered using a Whatman filter paper. The solid sample was dried in an oven at 65 °C for 24 hrs.

The synthesised metal oxide nanoparticles were then characterised using SEM and EDXA while the particle sizes were analysed using a Zetasizer. FTIR was also used for the determination of the bonds formed between the elements.

2.4.2 Synthesis of Silicon oxide nanoparticles

The synthesis of SiO₂ nanoparticles was carried out using the sol-gel method previously described (Venkatathri 2007). Aqueous ammonia (3.14 mL) was added to a solution of ethanol (74 mL) and deionised water (10 mL). Then tetraethyl orthosilicate (TEOS) (6 mL) was added with vigorous stirring at room temperature (25 °C). The reaction mixture was left to stir for 1hr, to yield uniform silica spheres in a sol. The latter was centrifuged, and the residue was washed with distilled

water and ethanol three times followed by drying at room temperature to yield the SiO₂ nanoparticles. The dried powder was left in a desiccator to avoid the absorption of water. The morphology and elemental composition of the synthesised nanoparticles were studied using SEM and EDXA, while the particles sizes were analysed using Zetasizer. The bonding formed in the elements were analysed with FTIR.

2.4.3 Synthesis of Zirconium nanoparticles

Zirconium oxide nanoparticles were synthesised by an adaptation from the hydrothermal synthesis method described by Pei *et al.* (2013). Briefly, Zirconium hydroxide (Zr(OH)₄, 0.25 g) was dissolved in deionised water (60 mL) and the solution was placed in a 100 mL synthesis autoclave reactor. The temperature of the autoclave was maintained at 80°-180°C at different times; then the autoclave was subsequently cooled down. The temperature was increased from 80 °C to 180 °C for 2hrs for every cycle. This was continued for 12 hrs, which was equivalent to 6 cycles. The white precipitate formed, was filtered, washed with deionised water several times; then dried at 60 °C to yield a white powder.

The nanoparticle morphology and the elemental composition of the ZrO₂ was observed by scanning electron microscopy (SEM) and EDXA respectively. Particle size analysis and XRD were undertaken for physical characterisation.

2.4.4 Synthesis of Cobalt oxide nanoparticles

The synthesis of cobalt oxide (Co₃O₄) nanoparticles was carried out by a co-precipitation method described by Wadekar, Nemade K.R. and Waghuley S.A. (2017). In this procedure, Co(NO₃)₂.6H₂O and NaOH in a 1:2 M ratio were dissolved in distilled water (20 mL) with constant stirring. Co(NO₃)₂.6H₂O (5.85 g) was weighed into deionised water (20 mL) to make a 1 molar solution. Based on the molar ratio, NaOH solution (2.0 mol L⁻¹) was added to Co(NO₃)₂.6H₂O (1.0 mol L⁻¹) dropwise under constant stirring for 2 hr at room temperature (25 °C). The mixture was then left to settle down overnight at the same room temperature. The next day, the cobalt hydroxide was found to have settled at the bottom of the beaker, while the excess solution on top was carefully decanted. The precipitate was then separated using a centrifuge, at 15000 RPM for 15mins and the liquid at

the top decanted. The residue was then heated at 80 °C for 5 h and a black colour compound was formed.

Then cobalt oxide nanoparticles synthesised were then characterised using SEM, EDXA, FTIR and particle size analysis.

2.4.5 Graphene oxide nanocolloids

The graphene oxide nanocolloids (Sigma-Aldrich) used in this study, was a dispersion in water (2 mg/ mL). The safety data sheet (SDS) of the compound describes the appearance to be black in a liquid or suspension form.

2.5 Instrumentation, Software, and Ancillary Equipment

All electrochemical measurements in this study were carried out using an Ivium Vertex One potentiostat-galvanostat (Eindhoven, Netherland).

The electrochemical experiments were analysed using an Iviumsoft software for Window 7, 8 or 10 and all data could be exported to Microsoft Excel. The general analysis of all the data produced and the plotting of the voltammograms was done using Microsoft Excel 2016 and OriginLab OriginPro 8.

The electrochemical cell was made up of commercially available glassy carbon electrode with a diameter of $\varnothing = 0.5$ cm, a KCl saturated Ag/AgCl reference electrode and a platinum counter electrode, all from BASi (West Lafayette, USA). The SEM imaging and EDX analysis were done using a Carl Zeiss Ltd scanning electron microscope, model EVO LS10, coupled to an Oxford Instrument INCA suite version 5.05 software for Windows 7 for the EDX analysis.

All pH measurements were carried out using a Fisher Scientific (Loughborough, UK) Mettler Toledo Benchtop pH meter.

Particle size analysis of the synthesised nanoparticles was carried out with a Malvern Zetasizer Nano series (Nano Zs), with a Malvern Zetasizer software 7.02 produced Malvern Instruments Ltd (Malvern, UK). The Zetasizer software loaded on to Microsoft Window XP contains a Macromedia flash© player software by Macromedia Inc. The instrument can measure the particle size of samples that have been suspended in liquids (water, ethylene glycol) in a range of 1 nm to about 1000 nm, with sample concentration of 0.00001% to 40%, with a sensitivity for molecular weight as low as 25 Da.

2.5.1 Electrochemical Cell Set-Up

In the course of this study the set-up of the electrochemical cell, was a standard three-electrode electrochemical cell configuration (Figure 2.1). The set-up consists of a working electrode (WE), a reference electrode (RE) and a counter electrode (CE) also known as an auxiliary electrode. The WE, were glassy carbon and carbon paste electrodes in a Teflon[®] holder depending on the analysis they were being used to analyse. The RE was an Ag/AgCl reference electrode that comprises of a silver wire immersed in a saturated solution of KCl and AgCl. While the CE was a high surface area Pt wire. The cell was connected to the potentiostat, that was connected to a computer monitor with the analytical software.

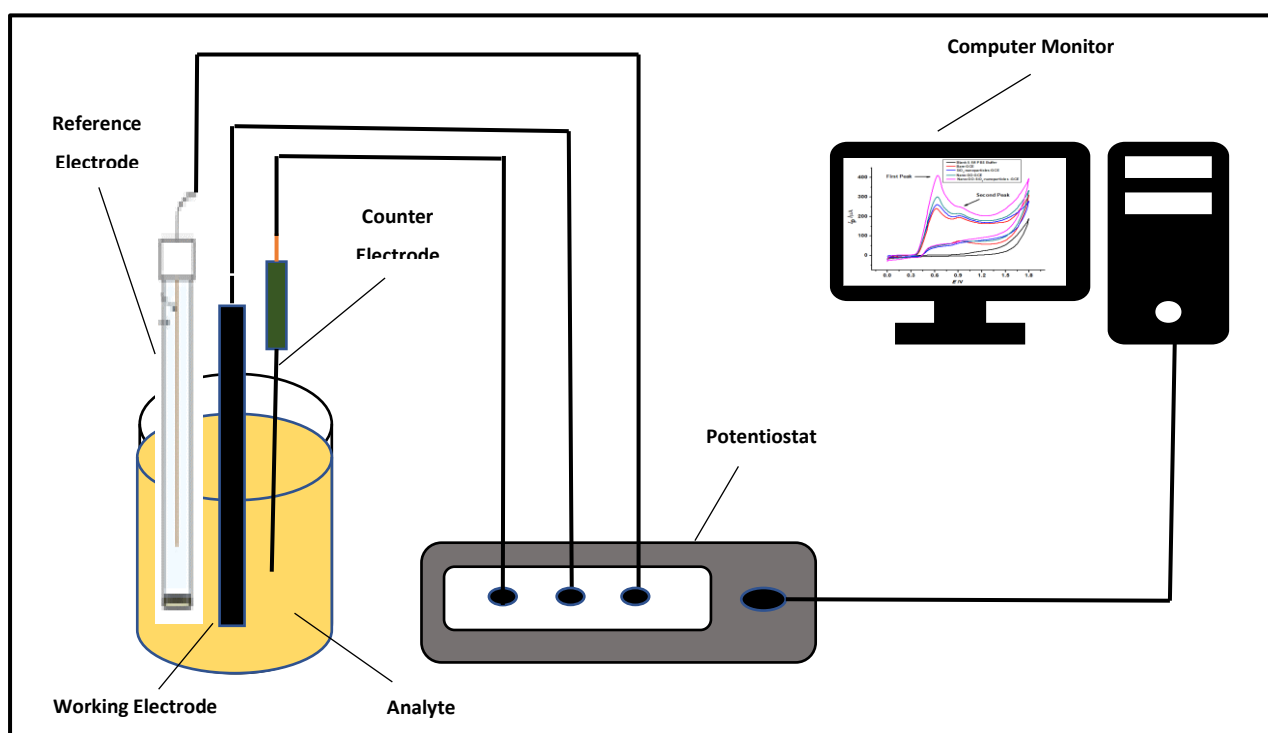


Figure 2. 1. An experimental set-up that was used in the electrochemical measurements.

2.5.2 Scanning Electron Microscopy

The SEM was carried out on a Carl Zeiss Ltd scanning electron microscope, model EVO LS10 (Oberkochen, Germany). About 0.1 mg of the nanoparticle samples were placed on the Zeiss screw mount, covered with double-sided carbon tape. The carbon tape is used because, it is more conductive than regular tape, as it helps in the transfer of electrons from the beam into the samples. Once the sample is placed on the mount, it is then put into the microscope for analysis.

The scanning electron microscope (SEM) is a microscope that uses electrons to create the image of the sample. The samples being analysed using SEM are sometimes required to be conductive, to enable the movement of the secondary electrons. Hence, a sputter coater is used to coat some samples with gold (Goldstein *et al.* 2017).

2.5.3 Energy dispersive X-ray analysis (EDXA)

The Energy dispersive X-ray analysis (EDXA) was also done using a Carl Zeiss Ltd (Oberkochen, Germany) scanning electron microscope, model EVO LS10, coupled to an Oxford Instrument INCA suite version 5.05 software for Windows 7 for the EDXA analysis. The nanoparticle samples were prepared the same as those used for SEM. EDXA mostly measures the X-rays that are emitted from the sample, when they are being bombarded by an electron beam. It should be noted that, the X-ray energy measured characterises the elemental composition of the sample, thus determining the amount of the different elements that make up the chemical composition (Scimeca *et al.* 2018).

2.5.4 Fourier Transform Infrared Spectroscopy (FTIR)

The FTIR analysis of all the nanoparticles used in the course of this work was done using the Thermo Scientific Nicolet iS50 FTIR Spectrometer (Loughborough, UK), equipped with a single bounce diamond crystal and deuterated triglycine sulfate detector. The nanoparticles samples being powders, were analysed using the attenuated total reflection (ATR) system. About 10 mg of the specific metal oxide nanoparticles powder to be analysed were made to make contact with the crystal at the top, such that, energy interaction occurs at the crystal and sample interface placed on the face of the crystal. Then the infrared beam was introduced, and the spectra recorded. The nanoparticles analysed were determined in the mid-infrared (MIR) range of 400 - 4000 cm^{-1} with a resolution of 4 cm^{-1} . Each of the spectra produced were collected from a total of 32 scans set in the absorbance mode.

Figure 2.2 shows a schematic diagram of the equipment and how the IR radiation moves through the sample, gets analysed and produces a spectrum. Some of the most important advantages of FTIR for analysis are their signal to noise ratio, high wavenumber accuracy ($\pm 0.01 \text{ cm}^{-1}$), very short scan time of approximately 10s, very high resolution of between 0.1 ~ 0.005 cm^{-1} (Gaffney, Marley and Jones 2002)

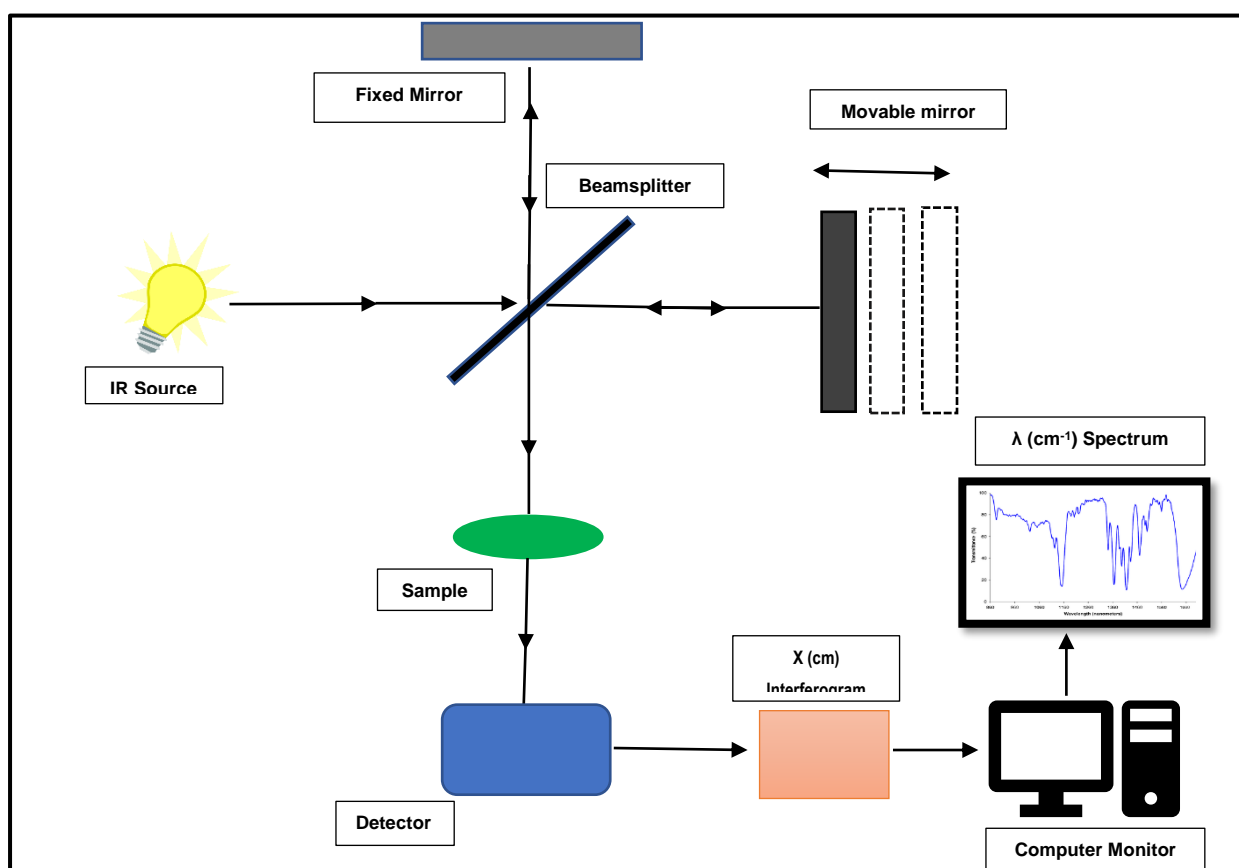


Figure 2. 2. Schematic diagram of essential features of Fourier Transform Infrared (FTIR) Spectrometer, where the IR Source creates radiations that travels through the sample.

2.5.5 X-ray Powder Diffraction (XRD)

The X-ray diffraction (XRD) patterns were collected at room temperature using a PANalytical Empyrean powder diffractometer (Malvern, UK) equipped with a Cu K α tube and a Johansson monochromator. Data were recorded on a low-background silicon sample holder in the range $5^\circ < 2\theta < 80^\circ$, with a step size of 0.013° . Data acquisition time was 50 minutes.

The XRD technique was used for the analysis of the crystalline structures of the synthesised metal nanoparticles that were used for the modification of the working electrodes.

2.5.6 Dynamic Light Scattering (DLS) Analysis

Dynamic light scattering (DLS), which is also known as Photon Correlation Spectroscopy or Quasi-Elastic Light Scattering is an analysis that illuminates a sample with a laser beam and the fluctuations of the scattered light are detected at a known scattering angle θ by a fast photon detector. DLS is important in that, it can measure particle sizes as low as 1 nm. The technique is widely used in the measurement of particle sizes in colloidal solutions (Yedurkar, Maurya and Mahanwar 2016).

The average particle sizes, size distribution and polydispersity index (PDI) of all the nanoparticles analysed by a 10-fold dilution of the samples in either deionised water or ethylene glycol as dispersants. The samples were transferred into cuvettes and the analysis carried out using the Malvern Zetasizer Nano series, with the sample temperature at 25 °C. The measurements of the particle sizes were dependent upon the particle size, surface structure, particle concentration and the ions in the mixture.

2.6 Electrodes

2.6.1 Working Electrodes

A working electrode in a voltammetric cell is the electrode that carries out the electrochemical event of interest in the cell. The electrochemical process occurs at the interface between the working electrode and the analyte. The potentiostat controls the applied potential of the working electrode as a function of the reference electrode potential.

Working electrodes used in voltammetry are made up from a variety of shapes and forms, where they are often small flat conducting disks press-fitted into an inert Teflon, Kel-F (poly-chlorotrifluoroethylene) or PEEK (poly-etheretherketone) rod. Then a wire is embedded in it for contact and connection (Figure 2.3).

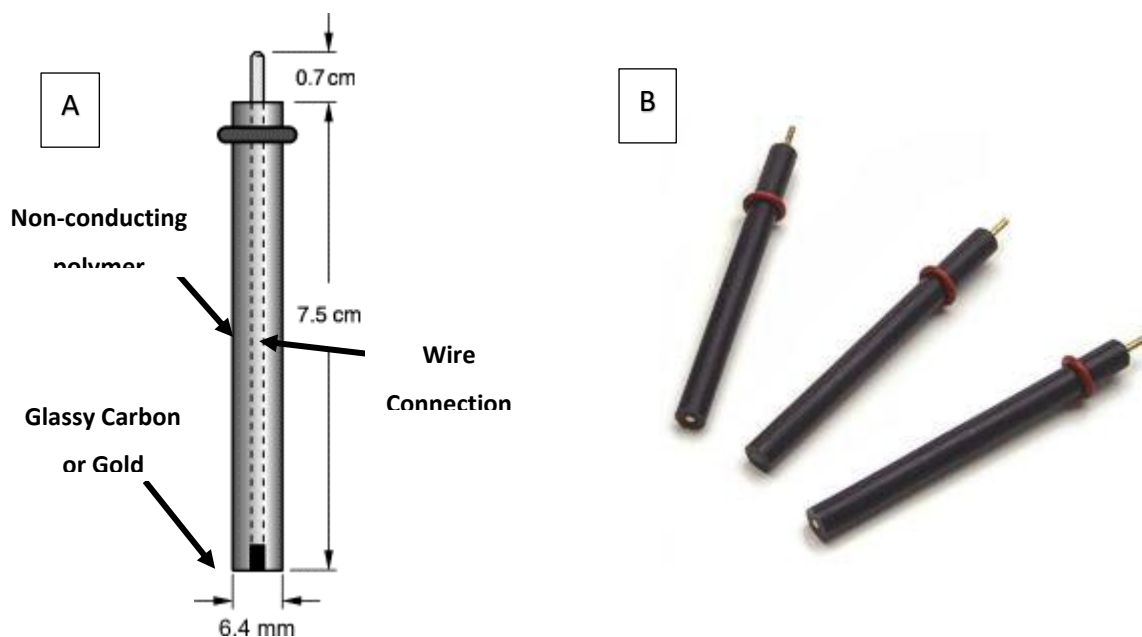


Figure 2. 3. (A) Schematic diagram of a working electrode, showing the non-conducting polymer (Teflon), the connecting wire and the reactive carbon disk (B) Glassy Carbon and Gold electrode (Adapted from Alvatek)

2.6.1.1 Preparation of GCE working electrodes

The appropriate amount of the synthesised SiO₂ nanoparticles were dispersed in a graphene oxide nanocolloids solution up to a concentration of 1 g L⁻¹. The concentration of 1 g L⁻¹ used for modification was the combination of the two nanomaterials that produced the best peak currents for GA when the analysis was carried out.

The mixture of SiO₂ nanoparticles and GO nanocolloids was then sonicated for 1 hr, to create a uniform dispersion of the two nanoparticles in the solution. The GCE was thoroughly polished with 0.1, 0.3, and 0.05 μm alumina paste on a felt lapping pad purchased from Alvatek (Tetbury, UK), to a shiny mirror finish. The polishing was done prior to every experiment, then the electrode was rinsed thoroughly with distilled water. The rinsed electrode was sonicated with water and ethanol respectively, to discard any alumina particles on the surface of the electrode. Ultrasonication of the polished electrode was done by using the Fisher Scientific ultrasonication bath from Fisher Scientific (Loughborough, UK).

After cleaning and drying the GCE, the nano-graphene oxide-SiO₂ nanoparticles mixture (graphene oxide nanocolloids 2 mg mL⁻¹ + SiO₂ nanoparticles 1 mg mL⁻¹) in deionised water was then drop cast on the surface of the GCE. The volume of

the drop cast was 5 μL of the mixture of graphene oxide (2 mg mL^{-1}) solution and SiO_2 nanoparticles (1 mg mL^{-1}) in deionised water and sonicated for 1 hour. The modified electrode was then left to dry at room temperature.

Other electrodes were also prepared using just SiO_2 nanoparticles solution and GO nanocolloids respectively to modify the surface of the GCE. The GCE- SiO_2 and GCE-GO prepared were left to dry at room temperature and later used for the determination of GA. The electrolytes and samples used for the experiment were thoroughly deoxygenated by aerating the samples with high purity nitrogen gas before every experiment.

2.6.1.2 Preparation of carbon paste electrode

The carbon paste electrode was prepared by hand mixing graphite powder with paraffin at a ratio of 70:30 (w/w) in an agate mortar, using the method described by Tashkhourian and Nami-Ana (2015). The CPE without any metal oxide nanoparticles were used as control CPE or referred to as bare CPE.

The amounts of metal oxide nanoparticles used for the modification was based on the quantity of the nanoparticles that produced the best electrochemical results. Hence, different concentrations of the specific metal oxide nanoparticles were studied, to arrive at an optimal concentration. The optimal concentration for all the metal oxide nanoparticles was found to be $\sim 10\%$ of the total electrode mixture. Furthermore, the metal oxide nanoparticles CPE were prepared with a mixture of graphite powder (0.6 g), metal oxide nanoparticles (0.1 g) and paraffin (0.3 g) in a ratio of 60:10:30 (w/w). Paraffin oil with a high density and viscosity, was weighed into the paste. The thoroughly mixed paste was then inserted into a Teflon tube of 2.87 mm internal radius and smoothed using a weighing paper. The electrical connection was made by connecting a copper wire into the tube. Fresh electrode surfaces of the electrode were renewed by polishing the electrode surface on Fisherbrand™ weighing paper by Fisher Scientific (Loughborough, UK)

2.6.2 Reference Electrodes

The reference electrode is used to measure the working electrode potential; hence the potential of the electrode remains constant so long as there is no current flow through it. This just means any potential changes in the cell are ascribed to the working electrode. The electrodes are not polarisable hence they are not sensitive

to the composition of the electrolyte or analyte in which they are immersed. With its well defined and equilibrium potential, the electrode is used as a reference point, against which other electrodes are measured (Elgrishi *et al.* 2018). The most commonly used reference electrodes are the saturated calomel electrode (SCE) and the silver/silver chloride electrodes (Ag/AgCl). (Figure 2.4).

In this work the Ag/AgCl reference electrode was used and it is comprised of a silver wire coated with AgCl and immersed in a saturated solution of potassium chloride (KCl) and AgCl; with a potential determined by the reaction $\text{AgCl(s)} + \text{e}^- = \text{Ag(s)} + \text{Cl}^-$.

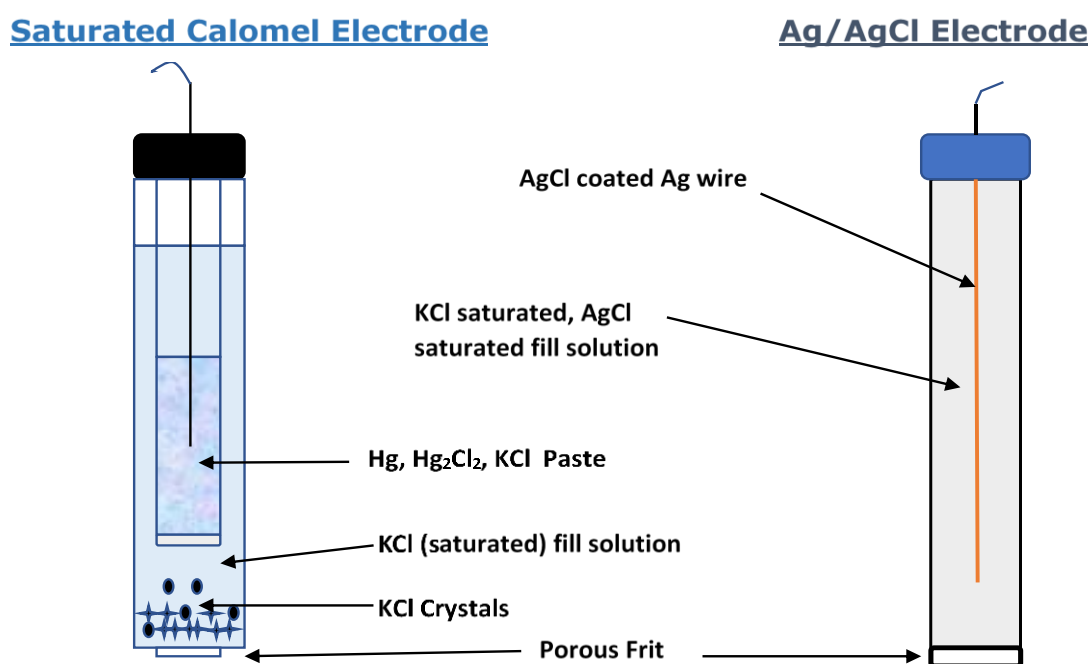


Figure 2. 4. Schematic image of saturated calomel electrode and Ag/AgCl reference electrodes

2.6.3 Counter Electrodes

The counter electrode (CE) also known as the auxiliary electrode (Figure 2.5) is the electrode that completes the electric circuit in an electrochemical cell. The current flow between the counter electrode and working electrode because the current in an electrochemical cell is recorded as electron flow between a CE and WE. The surface area of the counter electrode is always greater than that of the working electrode. This is to ensure that the kinetics of the reaction happening at the counter electrode does not inhibit those happening at the working electrode.

Hence in this electrode, platinum wires or discs are typically being used because of their inertness, though there are carbon-based counter electrodes (Zoski 2007).

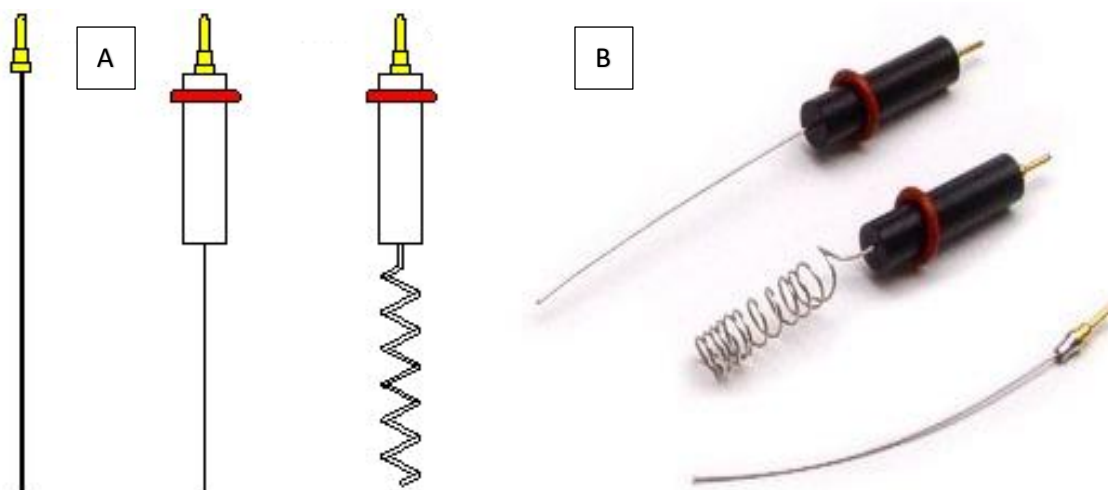


Figure 2. 5. (A) Schematic image of platinum counter electrodes and (B) pictures of counter electrodes, showing the coil-shaped and straight electrodes (Adapted from Basi Inc.)

2.7 Experimental Methods

2.7.1 Electrochemical Methods

The different electrochemical methods used in this work include, CV, DPV and EIS. CV is a dynamic electrochemical technique, where the applied potential is typically swept between two specific potential limits through a stationary working electrode, while the change of current generated is monitored; usually at a constant rate known as the scan rate.

Using an Ivium Vertex One potentiostat, the initial applied potential E_1 is swept to a potential E_v which is known as the vertex potential, then it is reversed and swept back to the final potential, E_f , which is normally at the initial potential.

Cyclic voltammetry was used in this study primarily for the study of the electrochemical behaviour of all the bare and modified electrodes used for the determination of GA and other antioxidants. Then it was also applied to investigate the active surface area of the electrode, the effect of scan rate and pH in the study of GA.

The main difference between CV and pulse voltammetry which includes normal, differential, and square wave voltammetry is the fact that, the double layer

capacitance is reduced to zero. The reduction of the double-layer capacitance to zero produces a current of mainly faradaic form. The ratio of the faradaic current to the charging current is relatively very large, hence the high sensitivity. The technique is regarded to be one of the most sensitive voltammetric techniques, as there is very little or no charging current as opposed to the faradaic current.

2.7.2 Electroactive surface area of the electrodes

Cyclic voltammetry was used to study $1 \times 10^{-3} \text{ mol L}^{-1}$ of Potassium ferrocyanide $[\text{Fe}(\text{CN})_6]^{3-}$ on the surface of the modified electrodes and swept over a potential range of -0.6 V to 0.6 V at various scan rates of 10, 25, 50, 100, 150, 200, 250 and 300 mVs^{-1} . Then the voltammograms recorded were used for the determination of the electroactive areas of the modified electrodes and that of the bare electrode. From the voltammograms, it was seen that, as the scan rates increased, so did the peak currents. Hence, all the peak currents were recorded relative to the scan rate and a linear regression equation created. The electroactive surface area of the modified electrode was calculated using the Randles-Ševčík equation (which represents the linear regression equation) for a reversible process, with a diffusion coefficient of $7.6 \times 10^{-6} \text{ cm}^2 \text{ s}^{-1}$ for $[\text{Fe}(\text{CN})_6]^{3-}$ and $n=1$. (Bard and Faulkner 2001)

$$I_{pa} = (2.69 \times 10^5) n^{2/3} A D^{1/2} \nu^{1/2} C_0 \quad \text{Equation 2.1}$$

Where n is the number of electrons transferred, A is the electroactive area of the electrode, D is the diffusion coefficient, ν is the scan rate and C the concentration of the redox probe used.

2.8 Electrochemical Studies

Electrochemical analysis of GA at the surface of the modified electrodes (GCE and CPE) was carried in a phosphate buffer solution ($1 \times 10^{-1} \text{ mol L}^{-1}$ pH 2.0), with the CV scanned at a potential range of 0.0 V to $+1.8 \text{ V}$ at a scan rate of 100 mVs^{-1} . Using DPV as described earlier in section 2.7.1, voltammograms were recorded in a potential range between 0.0 and $+1.2 \text{ V}$ with a pulse amplitude of 0.08 V and a pulse period of 0.2 s . All voltammograms were created using Origin Pro Software.

2.8.1 Electrochemical impedance spectroscopy

Electrochemical impedance spectroscopy was used as a technique to provide information on the impedance changes on the bare and modified electrodes (GCE and CPE) surfaces. This technique provides very good information regarding the properties of the modified electrode. These include how porous the electrode might be, its passivation properties, and information on the electrochemical mechanism of the surface of the electrode. The Nyquist plots were recorded and used for the determination of the electron transfer properties (electron transfer resistance) (R_{ct}) of the electrodes used.

When compared to an ideal resistor that has a circuit element limitation and no frequency consideration; impedance is a sort of resistance that works in conjunction with the capacitance of the materials being measured. Using Randles' equivalent circuit, when measuring the impedance of a modified electrode as compared to a resistor, there are the following differences. For a modified electrode surface the C_{DL} (double layer capacitance) is replaced by the constant phase element (CPE) (Figure 2.6). R_s is the polarisation resistance, R_{CT} is the charge transfer resistance and Z_w is the Warburg resistance.

The EIS measurement was carried out in the frequency range of 100 KHz – 0.01 Hz (50 points within the frequency range) in 0.1 mol L⁻¹ KCl containing 5 mmol L⁻¹ [Fe(CN)₆]^{3-/4-} redox solution.

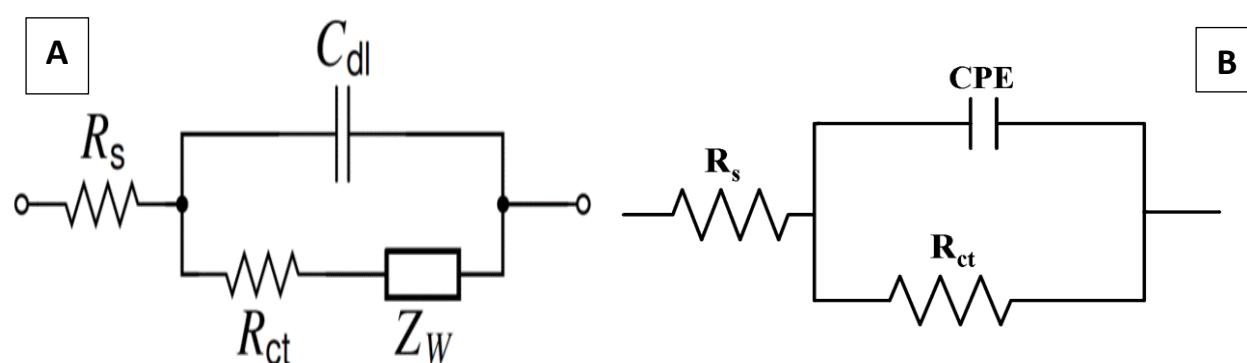


Figure 2. 6. Schematics showing the equivalent circuit used for the impedance measurement of the modified electrodes at the electrode/potassium ferricyanide interface. (A) This is the circuit used for the measurement of an ideal resistor (B) Measurement of impedance.

2.8.2 Effect of scan rate

The effect of the scan rate towards the electrochemical determination of GA was also investigated, by using CV to record the voltammograms of GA (0.5×10^{-3} mol L⁻¹) in a phosphate buffer (1×10^{-1} mol L⁻¹, pH 2.0) at increasing scan rates of 10, 25, 50, 75, 100, 150, 200, 300 mVs⁻¹ up to 1200 mVs⁻¹. From these data, plots of oxidation peak current vs. scan rate were done; the latter was used to determine whether the GA-electrode surface reaction was adsorption-controlled or not.

Furthermore, plots of the logarithm of oxidation peak current (Log I_p) against the logarithm of the scan rate (Log v) could be used to confirm if the reaction was an adsorption-controlled reaction. A positive shift of the peak potentials as the oxidation peak current increases with increase in scan rate could depict a kinetic limitation in the reaction (Raouf, Ojani and Kolbadinezhad 2009; Tashkhourian et al. 2013).

2.8.3 Effect of the quantity of modifier

Modifiers as used here, are referred to the compounds used for the modification of the working electrodes used in the course of this work.

The quantity of the modifiers used in the modification of the electrodes was studied. In the case of GCE, the modifiers were dropped on the surface of the electrode, while using the CPE the modifier was mixed with the paste.

The effect of the volume of the modifier on the surface of the GCE was studied using GA (1×10^{-2} mol L⁻¹) in a phosphate buffer (1×10^{-1} mol L⁻¹, pH 2.0) using CV at a scan rate of 100 mVs⁻¹. Volumes of 2 μL to 10 μL of the modifiers were studied, by dropping the modifier on the surface of the GCE and allowing it to dry at room temperature. The volume exhibiting the optimal oxidation peak current, was used subsequently.

2.8.4 Effect of adsorption time

The adsorption time of GA on to the modified electrode was studied by DPV measurement and the voltammograms for the determination of GA (1×10^{-3} mol L⁻¹) recorded every minute for up to six minutes. The peak currents recorded at different times were used for the determination of the adsorption time. This is the time at which, there is maximum adsorption at the surface of the electrode and any further voltammetric run does not produce any effect on the peak current.

2.8.5 Effect of pH on the analyte

The effect of pH on the GA solution towards its electrochemical activity and the activity of the modified electrode was studied. The voltammetric measurements of GA at different pH values (from 2.0 to 8.0) was used to determine the number of electrons and protons involved in GA oxidation. The electrochemical response from GA solution ($1 \times 10^{-4} \text{ mol L}^{-1}$) was studied at the different pHs using cyclic voltammetry with a scan rate of 100 mVs^{-1} , in phosphate buffer ($1 \times 10^{-1} \text{ mol L}^{-1}$). From the oxidation peak and the oxidation potentials of the GA solutions at different pH values, the best pH for the GA determination was deduced. The pH with the highest oxidation peak current was chosen for the subsequent electrochemical measurements.

2.8.6 Reproducibility and repeatability of the method

The reproducibility and repeatability of the method and the electrodes developed were tested by measuring eight replicates of GA (10 mL, $1 \times 10^{-3} \text{ mol L}^{-1}$) in phosphate buffer ($1 \times 10^{-1} \text{ mol L}^{-1}$, pH 2.0), while using three modified electrodes and the DPV voltammograms recorded. From the voltammograms, a relative standard deviation (RSD) was calculated and the latter was applied to study the repeatability and reproducibility of the method.

2.8.7 Stability of electrode

The stability of the modified electrodes was also studied. Three modified electrodes (GCE or CPE) were used to measure GA ($1 \times 10^{-3} \text{ mol L}^{-1}$) in phosphate buffer ($1 \times 10^{-2} \text{ mol L}^{-1}$) solutions after they were modified for day one. After 30 days the modified electrodes were used again to measure the same concentration of GA in a pH 2.0. The oxidation peak currents of the voltammograms on day one and those of day thirty, were used to calculate the corresponding RSD. RSDs with less than 10% error would be considered as relatively good stability of the electrodes.

2.8.8 Sensitivity

The sensitivity of the electrode is calculated as the equivalent to the linear portion of the plot of peak current (I_p) against the concentration of the analyte (GA) which is expressed as A/M (Ampere/Molarity). This can be described as the slope of the

regression equation of the calibration graph. For the specific electrode, the sensitivity can be measured by dividing the value of the slope of the calibration graph by the specific surface area of the electrode.

2.8.9 Limit of detection

The limit of detection (LOD) of the modified electrodes was studied. This is defined as the lowest concentration of the analyte likely to be reliably distinguished from the lowest limit of the blank, at which it is possible to detect the analyte (Armbruster and Pry 2008). DPV was used for the investigation of various concentrations of GA to the limit of detection with a scan rate of 100 mVs⁻¹ and pulse amplitude of 80 mV. Increasing concentration of GA (1×10^{-7} to 1×10^{-3} mol L⁻¹) were studied to give a calibration graph. The latter showed a linear relationship between the peak current and the increasing GA concentration. This produced a linear regression equation.

LOD was determined by measuring replicates (n=20) of the blank phosphate buffer (1×10^{-1} mol L⁻¹). The mean value and the standard deviation at a peak potential were determined. Using the linear regression equation or the equation of the calibration graph, the limit of detection was calculated thus, $(3 \times Std_{\text{Blank}})/m$, where Std_{Blank} is the standard deviation of the blank and m is the slope of the linear regression equation.

2.8.10 Interference study

The interference of foreign ions and other organic antioxidant compounds during the determination of GA was studied. This was carried out by the addition of different concentrations of foreign ions into a known concentration of the analyte. GA (5 mL, 1×10^{-3} mol L⁻¹) solution was added to a solution (5 mL, 1×10^{-1} mol L⁻¹) containing K⁺, Ca²⁺, Fe³⁺ and Na⁺ metals ions. For the organic antioxidant compounds, solution of ascorbic acid, caffeine, quercetin and caffeic acid (5 mL of a 1×10^{-3} mol L⁻¹) were respectively added to GA solutions (1×10^{-3} mol L⁻¹) with vigorous stirring (2 mins) followed by DPV recording. The tolerated limits of these metal ions for interference was defined as the highest concentration of foreign ions that would produce an error of no more than 5% in the determination of GA. With relative standard error values of less than 5%, these ions would be

considered not to interfere with the determination of GA at the first GA oxidation peak.

These metal ions used for the interference study were based on the complexation of these ions with GA (Fazary, Taha and Ju 2009; Hassanien *et al.* 2011) and the possibility of these organic compounds interfering with the electrochemical determination of GA.

2.9 Chromatographic Measurements

High-performance liquid chromatography (Figure 2.7) has been one of the most commonly used analytical techniques for the determination of antioxidants e.g. GA. The analytical technique is used to separate, identify, and quantify components mostly when they are found in a mixture like in wine or juice. This measurement was done using a method developed by Ragusa *et al.* (2019).

Here the chromatographic analysis was conducted using a Shimadzu HPLC system consisting of LC-20AD prominence liquid chromatography with an autosampler. The chromatograph was made up of a DGU 20A5 prominence degasser, a SIL 20A prominence autosampler and an SPD-M20A prominence diode array detector from Kyoto (Japan). The columns used, were C₁₈ ODS Hypersil-Keystone LC-18 (150 x 4.6 mm i.d., 3mm) in conjunction with a Supelguard LC-18 (2 cm x 2.1 mm i.d.) guard cartridge column. The HPLC analysis was done using a Shimadzu LC solution software (Kyoto, Japan)

The results of these chromatographic measurements are in the appendix section (pages 207 and 208) of this thesis, as the analyses were done as confirmatory tests only.

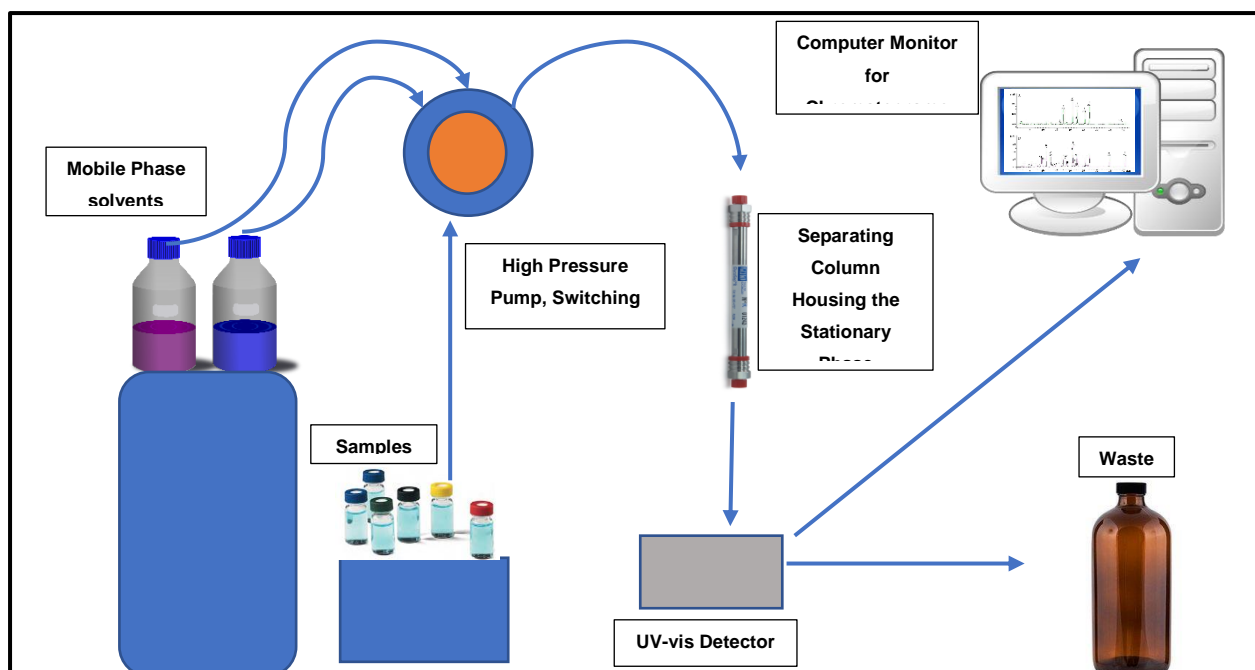


Figure 2. 7. A schematic diagram of high-performance liquid chromatography showing the movement of the mobile phase and the samples to the separating column housing the stationary phase, then to the UV-vis detector and the Computer Monitor.

2.9.1 Measurement and Analysis of Gallic acid

The standards used for this measurement were all dissolved in methanol and kept refrigerated at 4°C until further use. The wine samples were filtered through a 0.45 µm membrane and the filtrate transferred to vials. GA stock solution of 100 µg/mL was made up in methanol and lower concentrations were made up by further dilution.

The mobile phase consisted of solvent A and solvent B, which were 75:20:5, v/v/v of water/methanol/acetic acid for solvent A and 50:45:5, v/v/v for solvent B.

The gradient began with 0% of B at 0 min, 100% B at 40 min, 0% B at 50 min. Meanwhile, the system condition of flow was 1.0 mL/min at a column temperature of 25 °C, with a sample injection volume of 20 µL. The detection of GA was achieved at 280 nm.

Furthermore, the retention times for GA in this experiment was found to be at 3.13 min. The data produced from the increasing concentrations (0 µg/mL to 50 µg/mL) of the GA standard was then used to produce a calibration curve.

The concentration of GA in the analysed red and white wine were then calculated, by interpolating the corresponding peak areas.

2.10 Spectrophotometric Measurements

The two main spectrophotometric analytical methods used in the determination of the antioxidant capacity of the antioxidants used in the course of this work are the DPPH and the FRAP assay, which are common analytical assays used in the literature (Mudnic *et al.* 2010; Danilewicz 2015).

The results of these analyses would be seen in the appendix section (Page 203 to 206) of this thesis, as they were done as confirmatory experiments only.

2.10.1 2,2-Diphenyl-1-picrylhydrazyl (DPPH) Assay

For the measurement of the antioxidant capacity using DPPH, DPPH solution ($1 \times 10^{-2} \text{ mmol L}^{-1}$) was prepared using DPPH powder. Concentrations of stock antioxidant solution, GA (1 mg mL^{-1} stock) and vanillin (VA) (100 mg mL^{-1}) were prepared. All the solutions were kept refrigerated at $+4 \text{ }^\circ\text{C}$ and protected from light using aluminium foil.

The antioxidants were diluted serially and $50 \text{ }\mu\text{L}$ of each of the diluents, were pipetted into the corresponding wells of a 96 wells plate. DPPH solution ($100 \text{ }\mu\text{L}$, 0.01 mmol L^{-1}) was added to the appropriate wells, and incubated in the dark for 30 mins, at room temperature (Figure 2.8).

The absorbance was then later measured at 517 nm with a spectrophotometric plate reader. Figure 2.8 shows the chemical structures of reagents, colour, and structural changes, which takes place when DPPH reacts with the antioxidant. Figure 2.8 (B) from left to right, shows the reaction of the increasing concentrations of GA and vanillin in the 96 wells plate. The first two purple columns are the DPPH standards with $50 \text{ }\mu\text{L}$ methanol instead of GA or vanillin in them. The top three rows from the third column were used for Vanillin and the bottom three rows from the third column were used for GA.

From the visual analysis of the well plates, one could observe, a growing change in colour of the DPPH solution as the concentration of the antioxidant (either GA or vanillin) increased. There was also the observation of a better colour change with GA at comparable concentrations with the vanillin. This was attributed to GA being a better antioxidant than vanillin.

No change was observed in the wells that had just the methanol and DPPH, which suggested no reaction occurred.

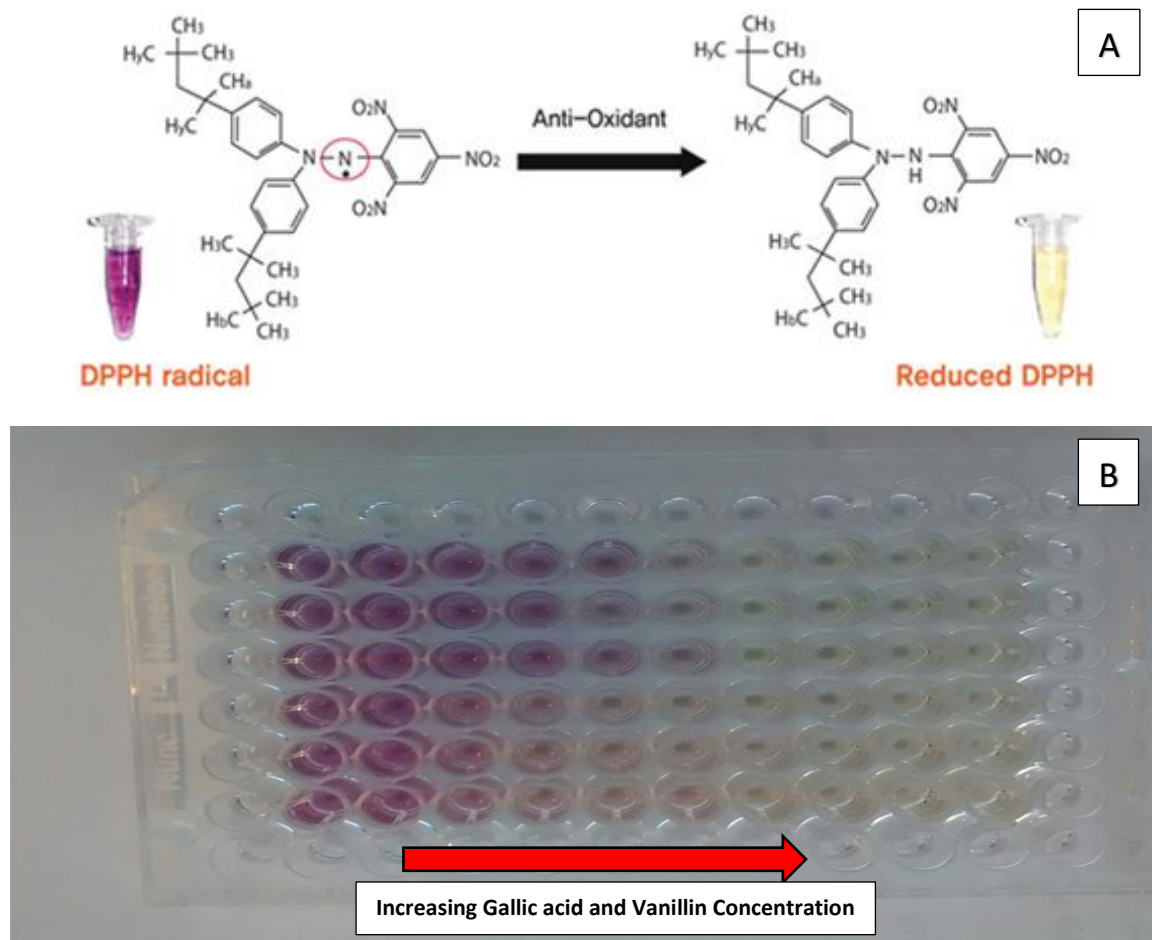


Figure 2. 8. (A) The picture shows colour change attributed to the chemical reaction of DPPH and the antioxidants, with the chemical structural change of DPPH. (B) The 96 wells plate showing the exact colour change after the reaction.

2.10.2 Ferric Reducing Antioxidant Power (FRAP) Assay

FRAP was also used to measure the antioxidant capacity. The method used was described by Thaipong *et al.* (2006), where freshly prepared FRAP reagents were prepared for every new FRAP experiment. The FRAP assay reagents included acetate buffer (25 mL, 300 mmol L⁻¹, pH 3.6); FeCl₃.6H₂O (2.5 mL, 20 mmol L⁻¹) and 2,4,6-Tris(2-pyridyl)-s-triazine (TPTZ) (2.5 mL, 10 mmol L⁻¹) and kept at 37°C.

Serially diluted concentrations of Trolox were prepared at ranges of 31.2 µg/mL to 312 µg/mL. The samples to be analysed were dissolved in a solvent of methanol/water (95/5 v/v). Just like the Trolox standard, the antioxidants were diluted further with the appropriate amount of water to the required concentration. The serially diluted antioxidant analytes (10 µL per diluent) were then added to 190 µL of the FRAP reagent, in the 96 wells plate. This was done just like the

Trolox and the blank. The mixture was then incubated in the dark for 30 mins. Measurement of the absorbance was done at 593 nm after the 30 mins incubation period.

Figure 2.9 shows a 96-wells plate set up for a FRAP assay. Just like the DPPH assay, the method was used to study two antioxidants (GA and vanillin). The first three columns from left to right are different concentrations of Trolox solution, while top three rows from the fourth column are vanillin samples and the bottom three rows from the fourth column are GA samples.

As the concentrations of the GA and vanillin samples increased from right to left, there is a deep blue colour changing depicting a reduction reaction attributed to the antioxidant capacity of the antioxidants.

The increasing concentration of Trolox from bottom to the top of the well plates show increasing antioxidant capacity as the colour changes to deep blue.

Meanwhile there was no colour change at the last two wells used as standards.

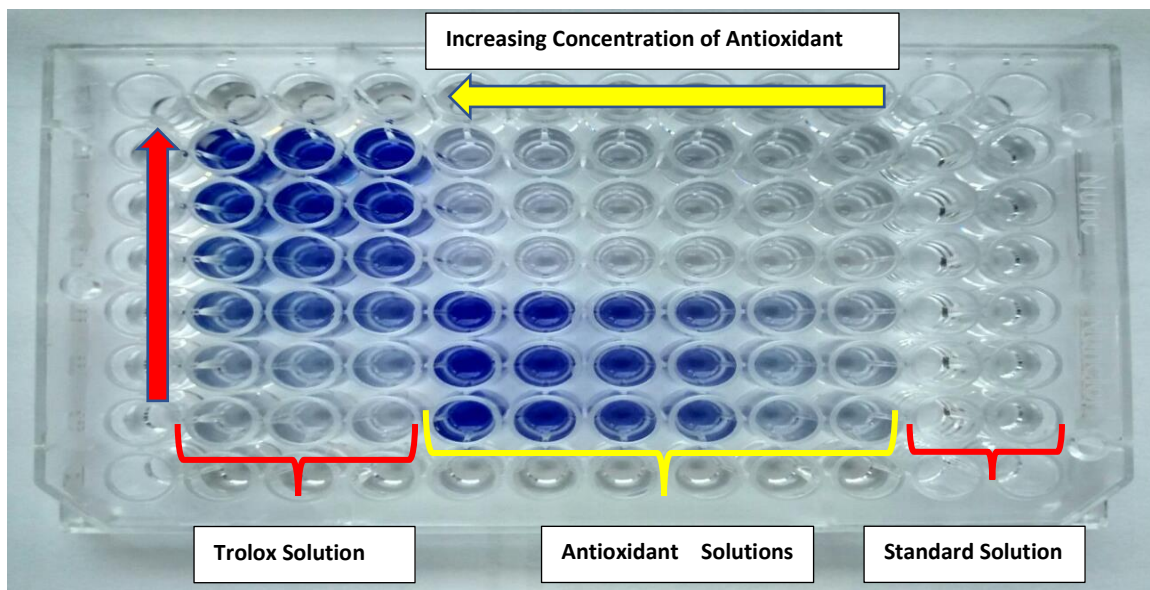


Figure 2. 9. Picture of the 96 wells plate showing the colour change with the FRAP Reagents with the Trolox standard, the antioxidants and the blank. The strength of the antioxidant involved is shown by the deep blue colour change.

CHAPTER THREE

3.0 MODIFICATION OF CARBON PASTE ELECTRODE FOR GALLIC ACID SENSING USING AMORPHOUS ZIRCONIA NANOPARTICLES

3.1 Introduction

In this Chapter, zirconium oxide nanoparticles are being used to modify a carbon paste electrode for the electrochemical determination of GA.

Nanoparticles and nanomaterials as earlier discussed in chapter 1, exhibit unique chemical, physical and electrochemical properties due to their very small sizes of usually between 1-100 nm, which are very different from the bulk of the same compounds (George, Antony and Mathew 2018). Based on these different properties, which includes their sizes, shapes, crystal structure, surface area, surface energy and chemical composition, nanomaterials have been broadly applied in different analytical methods (Penn, He and Natan 2003). These include the production of new and improved electrochemical sensors and biosensors for specific electrochemical determination of analytes (Luo *et al.* 2006; Zhu *et al.* 2015). There has been a wide use of chemically or physically modified electrodes with nanomaterials for sensitive and selective analytical determination of biologically important compounds like GA (Tashkhourian *et al.* 2013; Tashkhourian and Nami-Ana 2015). The application of carbon paste electrode being modified with nanostructured materials for the determination of biological compounds, have shown a reasonable improvement on the electrochemical behaviours of such compounds (Švancara *et al.* 2001; Li *et al.* 2011; Soltani *et al.* 2015).

Carbon paste electrodes have been widely applied in electrochemical studies due to their low cost, easy preparation, low background current relative to solid graphite or noble metal electrodes.

Zirconium oxide (ZrO_2) has attracted a considerable amount of attention being a versatile material that has been used for different practical applications. These include fuel cell technology (Park, Vohs and Gorte 2000), as catalyst or catalyst support (Li *et al.* 2001), oxygen sensor, protective coating for optical mirrors and filters (Zhang *et al.* 2000) and nano-electronic devices (Wright and Evans 1999). Zirconium oxide (ZrO_2) has been classified as a wide band semiconductor that tends to be more conductive at increased temperature (Ezhil Vilian, Rajkumar and Chen 2014). Hence the interest in the use of ZrO_2 nanoparticles as a modifier

because of the high surface area, good biocompatibility, chemical inertness, good conductivity and an affinity for oxygen-containing groups (George, Antony and Mathew 2018; Shahamirifard et al. 2018). There have been recent uses of zirconium dioxide nanoparticles for the modification of electrodes. Wang *et al.* (2015) proposed a simple and mild strategy for the development of a new electrochemical sensor made of zirconia and ordered macroporous polyaniline, for pesticide detection. Meanwhile Meng, Zheng and Li (2015), deposited zirconium dioxide nanoparticles on a carbon nanotubes modified gold electrode for the detection of nitrites. Furthermore, zirconium oxide nanoparticles were supported on graphene oxide, forming a nanocomposite for the electrochemical determination of dopamine and paracetamol in the presence of ascorbic acid (Ezhil Vilian, Rajkumar and Chen 2014). Then Teymourian et al. (2014) further used a composite of zirconium dioxide-reduced graphene oxide composite for the electrochemical sensing of ascorbic acid, uric acid and dopamine. While, TiO₂ (titanium dioxide) and ZrO₂ (zirconium dioxide) sol-gel modified carbon paste sensor was created for the detection of phenol by Lunsford *et al.* (2013). All these new zirconium oxide nanoparticles use, shows how important the compound and its composites has become in the development of sensors.

3.2 Experimental

3.2.1 Materials and Reagents

The materials and reagents used to carry out this study, have been discussed earlier (Chapter 2, Table 2.1, Pages 47-48). Specifically, the following reagents were used for the synthesis of zirconium dioxide nanoparticles and the preparation of the modified CPE.

Zirconium hydroxide (Zr(OH)₄) powder (M. wt. 159.25 g mol⁻¹), zirconium (IV) oxide (M. Wt. 123.22 g mol⁻¹; ≥ 99%), graphite powder, paraffin oil, analytical grade salts of potassium chloride and GA (anhydrous, M. Wt. 170.12 g mol⁻¹) were purchased from Sigma Aldrich (London, UK).

Analytical grade methanol, phosphoric acid (H₃PO₄) and sodium hydroxide were from Merck (Darmstadt, Germany). All the reagents were of the highest purity and no further purification was required. All the aqueous solutions used, were freshly made with 18.2 MΩ.cm resistance value doubly distilled water. All stock solutions prepared were refrigerated at 4 °C and protected from light.

3.2.2 Synthesis of amorphous Zirconium dioxide nanoparticles

The synthesis of the amorphous ZrO₂ nanoparticles has already been described in Chapter 2, Section 2.4.3 found on page 51 of this thesis.

3.2.3 Preparation of amorphous zirconia nanoparticles-CPE

The amorphous zirconia nanoparticles modified carbon paste electrode was prepared as earlier described. The amorphous zirconia nanoparticles-CPE was prepared using the same procedure described for all the metal oxide nanoparticles in this study (Chapter 2, section 2.6.1.2 on page 57).

3.2.4 Electrochemical measurements using amorphous zirconia nanoparticles modified carbon paste electrode

The electrochemical analysis of GA at the surface of the ZrO₂ nanoparticles modified CPE was carried out in phosphate buffer solution (1×10^{-1} mol L⁻¹, pH 2.0). The CV measurements were scanned within the range from 0.0 V to +1.8 V at a scan rate of 100 mVs⁻¹. Meanwhile, the DPV voltammograms were recorded at a potential range from 0.0 to +1.2 V with a pulse amplitude of 0.08 V and a pulse period of 0.2 s.

Electrochemical impedance spectroscopy was also applied as a technique that provides information on the impedance changes of the bare CPE and the ZrO₂ nanoparticles modified CPE surfaces with their Nyquist plots recorded. This EIS measurement was carried out in a frequency range of 100 KHz – 0.01 Hz (50 points within the frequency range) and a potential of 0.4 V in 0.1 mol L⁻¹ containing 5 mmol L⁻¹ [Fe(CN)₆]^{3-/4-} redox solution.

The accumulation time of GA on to the modified electrode was studied using DPV and the voltammograms for the determination of 1×10^{-3} mol L⁻¹ GA, were recorded every minute for 8 minutes (460 secs). This was the time needed for the GA to produce an optimal voltammogram on the surface of the modified electrode. The reproducibility and repeatability of the method while using ZrO₂ nanoparticles modified CPE was studied by measuring six replicates of GA (10 mL, 1×10^{-3} mol L⁻¹) in phosphate buffer solution (1×10^{-1} mol L⁻¹, pH 2.0) using three different modified electrodes and their respective differential pulse voltammograms recorded.

The interference of foreign ions in the determination of GA was investigated, by the addition of GA solution (5 mL, 1×10^{-3} mol L⁻¹) into solutions containing these metal ions Ca²⁺, Fe³⁺, K⁺ and Na⁺ (5 mL, 1×10^{-1} mol L⁻¹). On the other hand caffeine and ascorbic acid (5mL, 1×10^{-1} mol L⁻¹) respectively were added to GA solution (5mL, 1×10^{-3} mol L⁻¹) and stirred vigorously for 2 mins, then the voltammograms recorded using DPV.

3.4 Results and Discussion

3.4.1 Characterisation of the prepared amorphous ZrO₂ nanoparticles-modified Carbon Paste Electrode

The ZrO₂ nanoparticles modified CPE was characterised by studying the particle sizes using a Zetasizer. The Zetasizer uses the dynamic light scattering (DLS) technique, to measure the size of colloids, nanoparticles and molecules without requiring agitation. The resulting particle sizes of the ZrO₂ nanoparticles exhibit the size distribution starting from 30 to 270 nm (Figure 3.1). This shows an average particle size of 281.7 nm, which unfortunately was not clearly depicted on the SEM images of the particles. As the particles formed agglomerates of sizes between 10 to 100 μm.

Results

	Size (d.nm):	% Intensity:	St Dev (d.n...
Z-Average (d.nm): 281.7	Peak 1: 276.5	88.4	98.50
Pdl: 0.251	Peak 2: 3493	11.6	1163
Intercept: 0.914	Peak 3: 0.000	0.0	0.000
Result quality : Good			

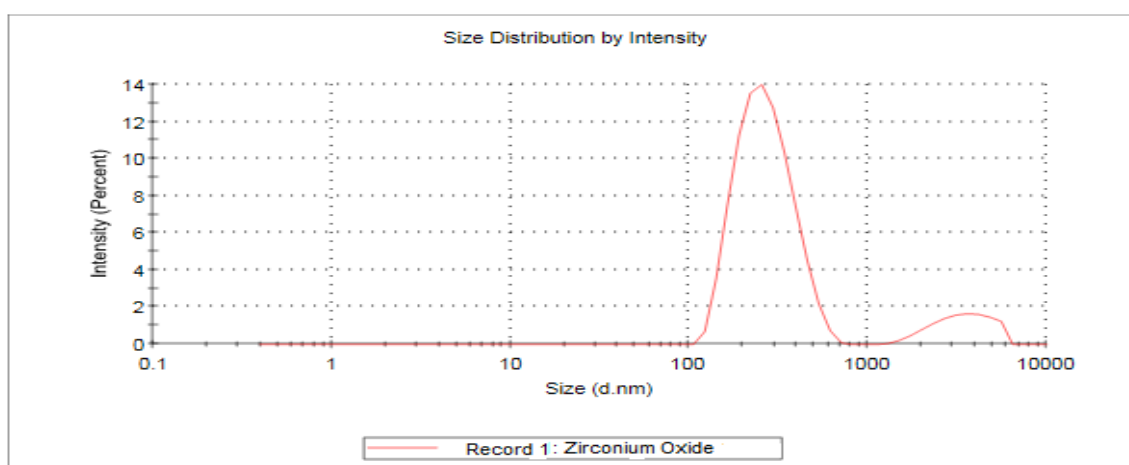


Figure 3. 1 Particle size distribution of synthesized amorphous ZrO₂ nanoparticles.

Meanwhile, SEM was used to reveal information about the external morphology, chemical composition and crystalline structure of the ZrO_2 nanoparticles. Results showed tetragonal-like structures of the ZrO_2 nanoparticles and the non-homogenous size distribution. This might have been because of the amorphous nature of the compound (Figure 3.2(A) and 3.2(B)). The particles did not appear as discrete particles, they formed small aggregations with average sizes ranging from 10 μm to about 100 μm .

The nanosized composition of the carbon paste electrode with the zirconium dioxide, as represented by the SEM images, enhances electron transfer and provides a better mass transport of the GA on the electroactive sites of the carbon paste electrode. (Figure 3.2(A) and 3.2(B)).

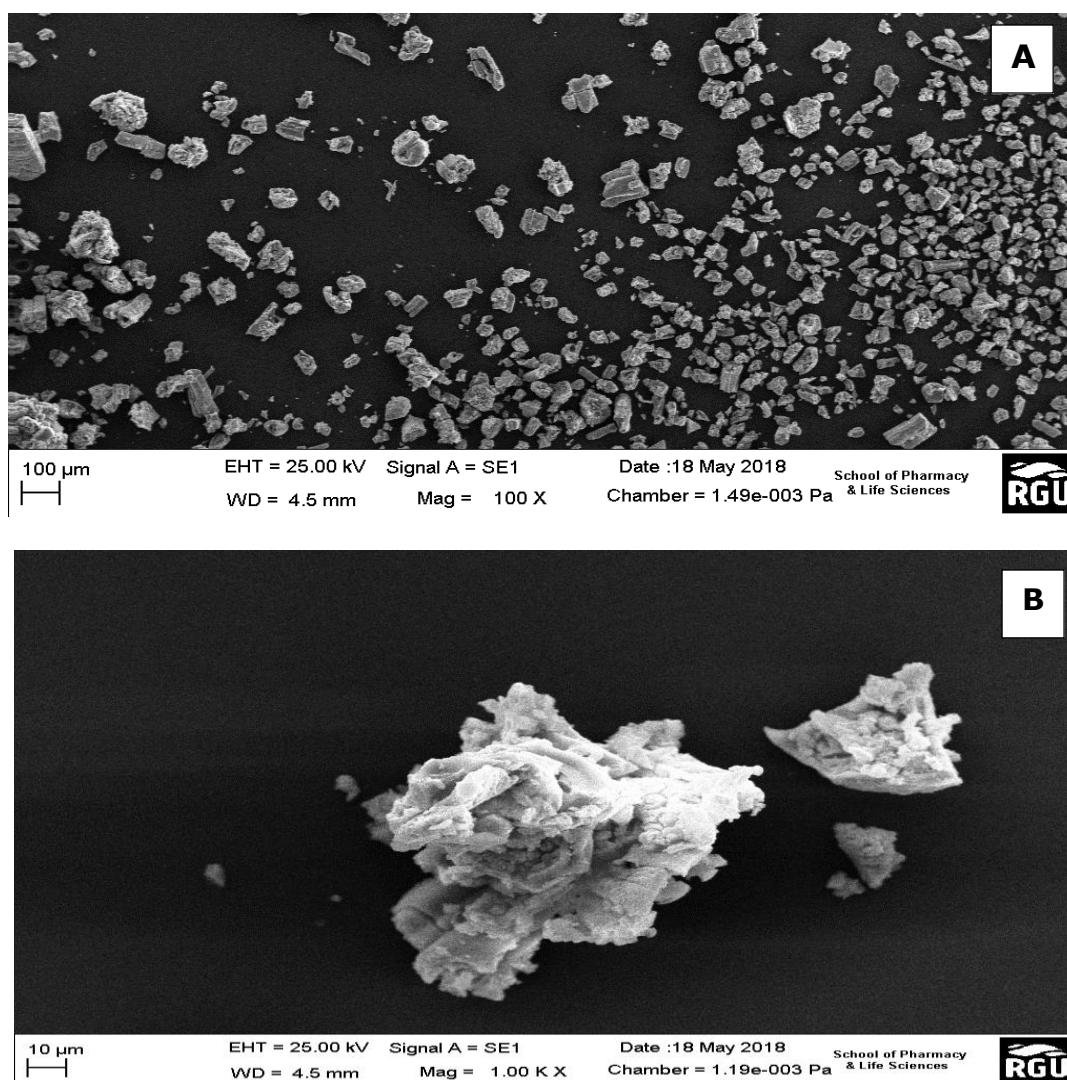


Figure 3. 2. (A) The SEM Image ZrO_2 nanoparticles showing the morphology of the nanoparticles (B) SEM image of one of the ZrO_2 nanoparticles agglomerated to sizes of about 10 μm

3.4.2 X-ray Powder Diffraction analysis

The XRD pattern of the prepared ZrO_2 nanoparticles (Figure 3.3), revealed a high structural disorder at long-range, which is compatible to XRD patterns of amorphous ZrO_2 (Silva Junior, Antonio and Longo 2018). The structures showed a broad peak corresponding to a reflection of tetragonal ZrO_2 and the close broader peaks corresponding to monoclinic ZrO_2 . The formation of the tetragonal shaped zirconia being the main phase of the nanoparticles, could be because of the presence of the hydroxide complex at the generation stage of the synthesis $[\text{Zr}(\text{OH})_4^{+2} \cdot \text{H}_2\text{O}]_4 + (\text{OH})^{-8}$ hydroxo-complex. This role played by the hydroxide complex in the formation of zirconia nanoparticles has previously been noted in the literature (KIM et al. 2009; Saad Al Farhan 2017). They suggested that, the predominant tetragonal phase is attributed to the presence of NaOH in the generation phase of the hydroxo-complex.

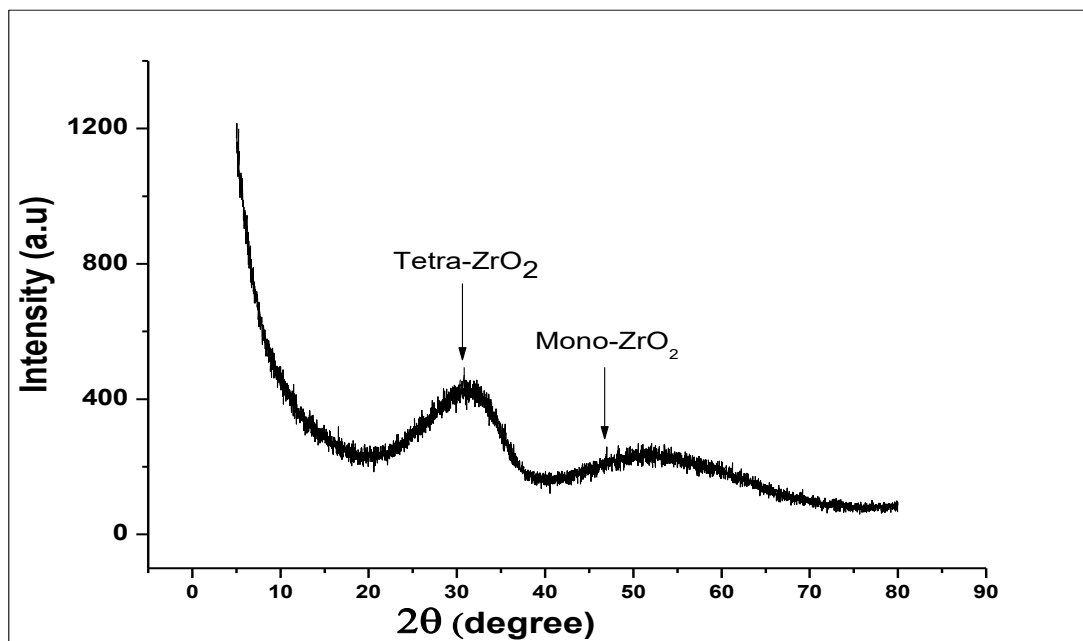


Figure 3. 3. XRD of ZrO_2 nanoparticles, showing the broad peaks corresponding to tetragonal ZrO_2 and monoclinic ZrO_2 structure

3.4.3 Fourier Transform Infrared Spectroscopy Analysis

Fourier Transform Infrared spectroscopy (FTIR) was also used for the characterisation of ZrO_2 nanoparticles and the spectrum of ZrO_2 spectrum was recorded from 400 to 4000cm^{-1} , to confirm the different bonds formed in the compound. The FTIR spectrum (Figure 3.4), shows a dominant absorption band between 500 - 600cm^{-1} , attributed to the deformation of $Zr-O-Zr$ bond. Meanwhile, the peak centred around 1000cm^{-1} and 1380cm^{-1} are assigned to the $Zr-O$ vibrational stretching. On the other hand, the bands around 1590cm^{-1} and 1650cm^{-1} is attributed to the bending vibrations of chemisorbed water molecules as described by Prakashbabu *et al.* (2014). Furthermore, the broad and strong peak at 3445cm^{-1} is ascribed to the adsorbed moisture on to the surface of the compound, showing the stretching of the $O-H$ group in the water. The FTIR produced by the synthesised ZrO_2 was compared to the FTIR analysis of a bulk ZrO_2 and the spectra were found to be about 98% sample match.

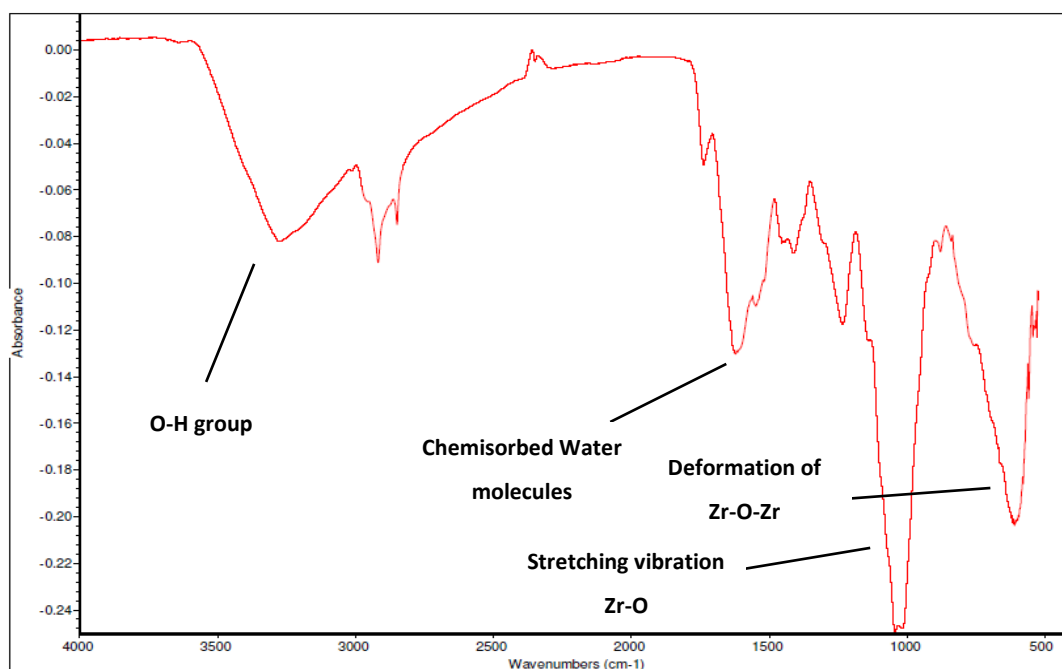


Figure 3. 4. FTIR image showing the spectra of ZrO_2 nanoparticles

3.4.4 Effect of pH on the Gallic acid oxidation on the amorphous zirconia nanoparticles modified carbon paste electrode

The pH of the buffer in which GA is dissolved affects the electro-oxidation activity of GA on the surface of the ZrO_2 nanoparticles modified CPE. This effect was studied using CV at ZrO_2 nanoparticles modified CPE. In Figure 3.5 the electrochemical behaviour of GA ($1 \times 10^{-2} \text{ mol L}^{-1}$) in phosphate buffer ($1 \times 10^{-1} \text{ mol L}^{-1}$) was investigated at a pH range of 2.0 to 8.0 with a 100 mVs^{-1} scan rate. Within that pH range, the anodic peak current of GA showed a reduction with increasing pH using CV and an increasing negative shift of the peak potential from 0.64 to 0.38 V (Figure 3.5). The voltammograms showed a well-defined and shaped oxidation peak at a pH of 2.0, with the highest peak current of $374.49 \mu\text{A}$, confirming a clear influence of the pH towards the electrochemical oxidation of GA at the ZrO_2 nanoparticles modified CPE surface. Thus, a phosphate buffer solution of pH 2.0 was used in the subsequent experiments.

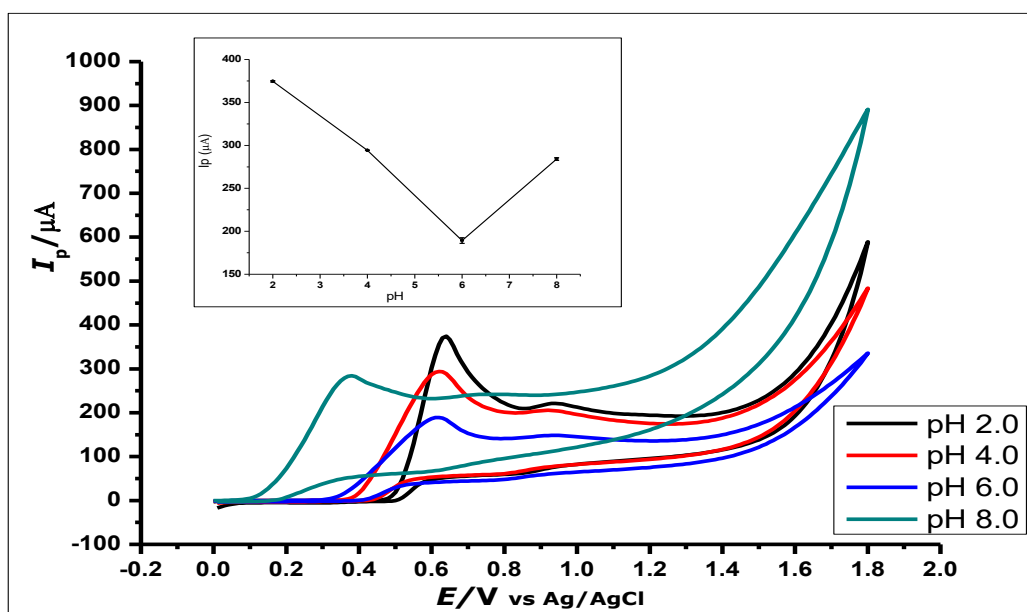


Figure 3. 5. Cyclic Voltammograms showing the effect of pH on the electrochemical behaviour of $1 \times 10^{-2} \text{ mol L}^{-1}$ Gallic Acid at pH range of 2.0-8.0 (Inset). The plot of the Peak Current (I_p) against different pH values, showing the effect of pH on the electrochemical behaviour of $1 \times 10^{-2} \text{ mol L}^{-1}$ Gallic acid using ZrO_2 nanoparticles modified CPE at a scan rate of 100 mVs^{-1}

Interestingly a further increase in the pH value of the solution showed no GA oxidation. The gradual negative shift of the peak potential as the pH increases showed a linear relationship between the anodic peak current and peak potentials

of the different pH values. The relationship between the pH and the peak potential E_p was studied and the graph showed a linear regression equation of $E_{pa} = -46.314 \text{ pH} + 471.24$ with $R^2 = 0.9941$, between pH 2.0 to pH 6.0 (Figure 3.6). The slope E_{pa}/pH of the regression line of 46 mV/pH that can be compared to the Nernstian value 59 mV/pH at 25 °C. This suggests that the number of electrons and protons involved in the oxidation of GA was equal (Novak, Šeruga and Komorsky-Lovrić 2009). As the pH increases, there is a decrease in the protonated degree of GA. Which means there is a decrease in the static attraction. However, at pH 8.0 the peak current increased, which is in line with other similar previous findings in a redox reaction with GA at pH 8.0 (Abdel-Hamid and Newair 2013).

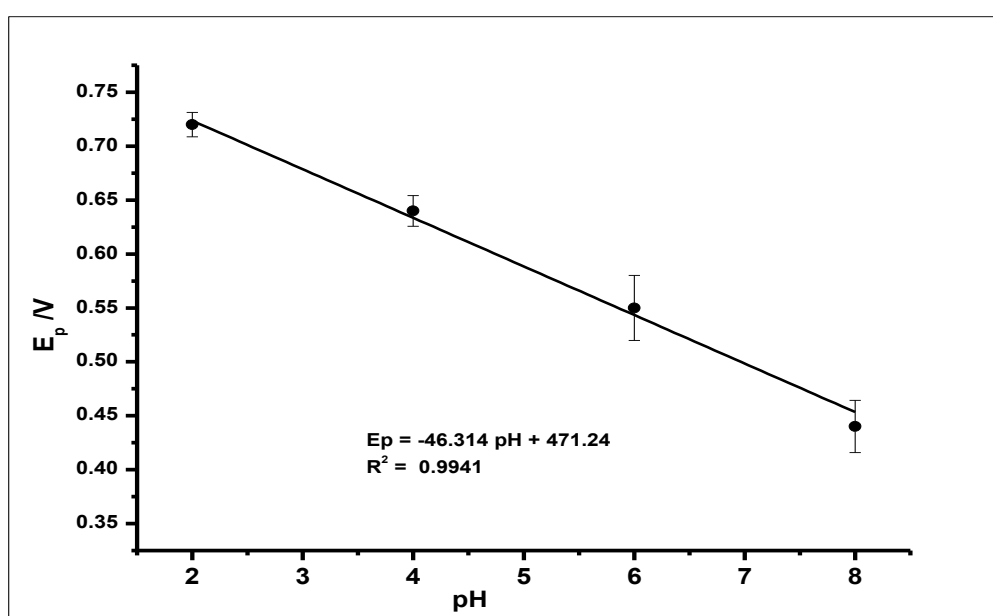


Figure 3. 6. The plot of the peak potential (E_p) against the different pH values of the buffer solution, showing the linear relationship in the determination of $1 \times 10^{-2} \text{ mol L}^{-1}$ Gallic acid

3.4.5 Electrochemical behaviour of Gallic acid at the zirconium dioxide nanoparticles modified CPE

Cyclic voltammetry (CV) and differential pulse voltammetry (DPV) was used to study the voltammetric behaviour of GA on the surface of the zirconia nanoparticles modified-CPE. The cyclic voltammograms of GA ($1 \times 10^{-2} \text{ mol L}^{-1}$), at bare CPE, amorphous zirconia nanoparticles modified CPE (AmZr nano-CPE), ZrO_2 and bare glassy carbon electrode, in phosphate buffer ($1 \times 10^{-1} \text{ mol L}^{-1}$, pH 2.0) at a scan rate of 100 mVs^{-1} (Figure 3.7) were recorded. The measurements

were done at applied potential range of 0.0 to 1.8 V at room temperature. The ZrO₂ nanoparticles modified CPE, produced peak currents of 451 ± 1.1 μA at a peak potential of 0.69 V. The bare CPE produced peak currents of 260 ± 3.2 μA at 0.64 V peak potential, while the bare glassy carbon electrode (GCE) produced 309 ± 0.65 μA peak current at a peak potential of 0.67 V. The peak potentials showed a positive shift, from the bare CPE to the ZrO₂ modified CPE. This shows there was no catalytic effect, attributable to the ZrO₂ nanoparticles modified CPE. However, there was peak current enhancement, which is attributed to the increased electroactive surface area by the amorphous ZrO₂ nanoparticles.

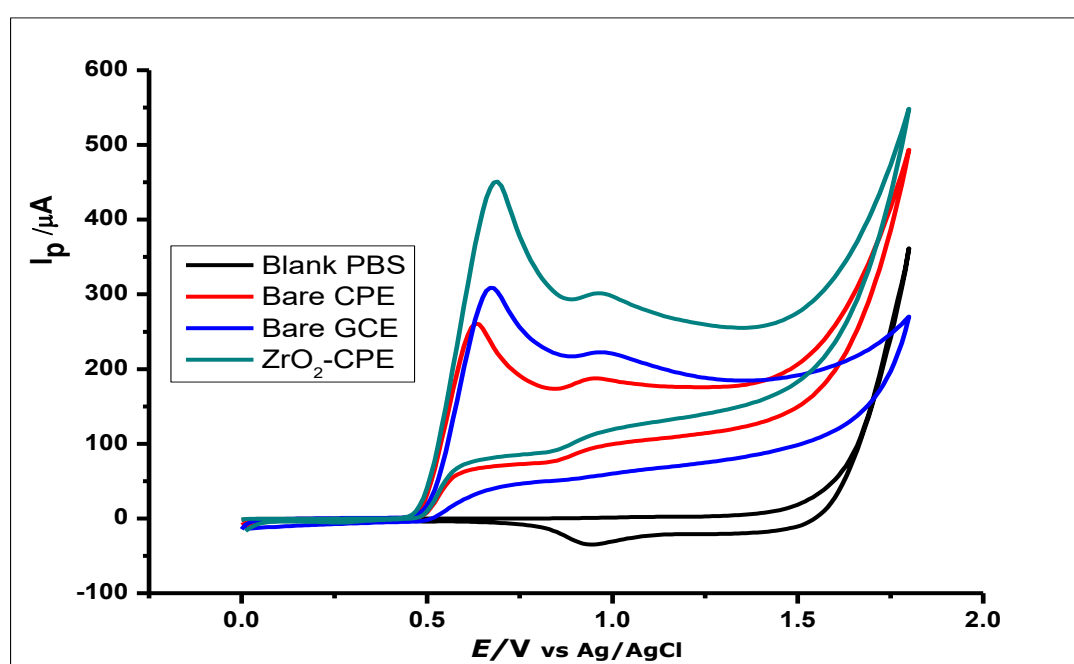


Figure 3. 7. Cyclic voltammograms of $1 \times 10^{-2} \text{ mol L}^{-1}$ GA at ZrO₂ nanoparticles-modified CPE, bare CPE and bare glassy carbon electrode (GCE) in 0.1 mol L^{-1} phosphate buffer of pH 2.0 at a scan rate of 100 mVs^{-1}

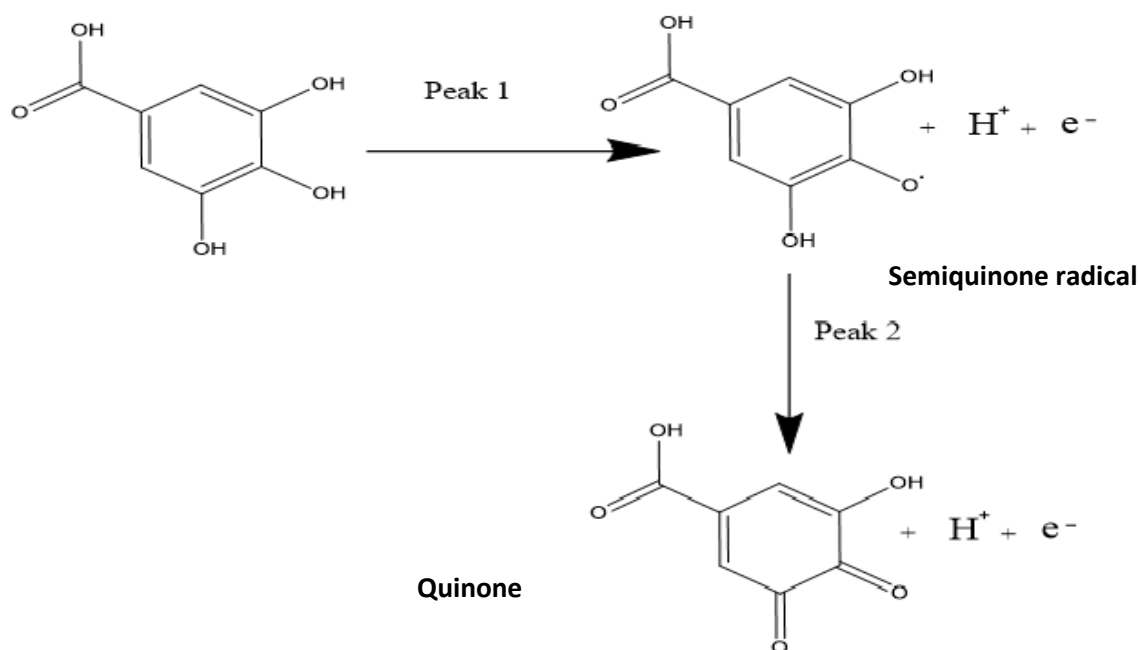
From the voltammograms shown in Figure 3.7, it was deduced that though the bare CPE or the bare GCE oxidised the GA, the modified CPE produced higher oxidation peak currents as compared to the bare electrodes.

The GA produced two oxidation peaks while using CV, in the course of the anodic sweep from 0.0 to 1.8 V. This is consistent with other cyclic voltammetric measurements of GA in the literature (Souza *et al.* 2011; Tashkhourian and Nami-Ana 2015; Oliveira-Neto *et al.* 2016). The voltammograms show two cathodic

peaks on the forward sweep, with the return sweep showing currents of very low intensity of about 90 μA and no reduction peak. This shows that, after the first oxidation, the GA peak undergoes another reaction that produces a second oxidation peak; and does not show any sign of reduction during the reverse sweep when using the modified CPE. Furthermore, in the absence of GA ($1 \times 10^{-1} \text{ mol L}^{-1}$ phosphate buffer), at the same potential range of 0.0 – 1.8 V and over the range where GA oxidation peak was observed, no oxidation peak was observed.

From the voltammograms, it can be affirmed that, ZrO_2 nanoparticles added to the carbon paste electrode, exhibited a significant effect in the electrochemical oxidation of GA. The electrochemical oxidation has also led to a significant enhancement of the peak current (I_p) from 261 μA to 451 μA .

The two peaks produced by the GA have been characterised in the literature as the formation of a semiquinone radical for the first peak, which then oxidises to a quinone in the second peak (Souza et al. 2011; Tashkhourian and Nami-Ana 2015). This oxidation at the first peak, has been shown to be that of the galloyl group as can be seen in scheme 3.1. This then leads to the second peak, developed from the third hydroxyl (-OH) group found in the galloyl moiety of the GA (Souza et al. 2011; Tashkhourian and Nami-Ana 2015). This is reinforced by the fact that, the carboxylic group (-COOH) gets electro-oxidised at 2.0 V and has a CO_2 bi-product (Novak, Šeruga and Komorsky-Lovrić 2009); while the oxidation peaks of the GA, in this case, occur at peak potentials of 0.69 V and 0.85 V when using cyclic voltammetry.



Scheme 3.1. The reaction mechanism of the oxidation of Gallic acid, showing the two peaks in CV and DPV

3.4.6 Electrochemical Impedance Spectroscopy Analysis

Electrochemical impedance spectroscopy (EIS) was used to probe the difference in the behaviour of the bare CPE and the ZrO_2 nanoparticles modified CPE. Using this electrochemical measurement, the bare carbon paste electrode and the zirconia nanoparticles modified CPE were used to measure $[\text{Fe}(\text{CN})_6]^{3-/4-}$ redox solution (5 mmol L^{-1}) (Nyquist plots, Figure 3.8). The Nyquist plots demonstrated the semicircle domain of the bare CPE and the modified CPE, indicating the charge transfer resistance attributed to the $[\text{Fe}(\text{CN})_6]^{3-/4-}$ redox reaction. The large semicircle portion exhibited by the bare CPE, corresponds to the high charge transfer resistance (R_{ct}), associated with the high capacitance. Meanwhile, the ZrO_2 nanoparticles modified CPE, with the ZrO_2 nanoparticles on the electrode surface reduces the barrier to interfacial electron transfer. Thus, this reduction results in a decrease of the semicircle radius, which indicates a facilitated electron transfer at the electrode interface. The response shown by the electrodes using EIS corresponds to the Randles equivalent circuit seen in Figure 3.8 (inset).

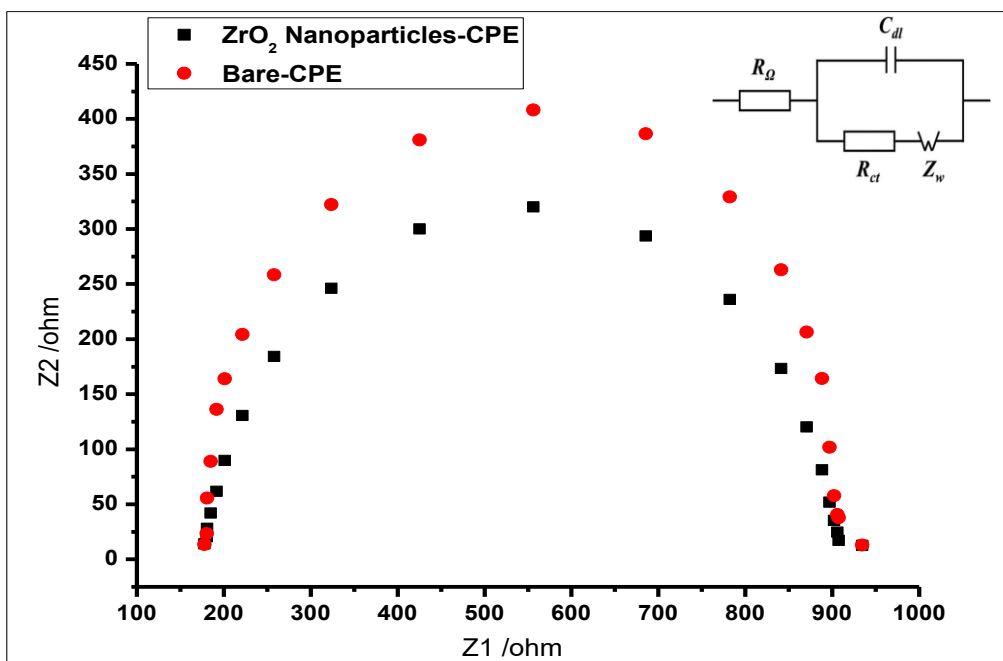


Figure 3. 8. Nyquist plot representing the EIS measurement of 5 mmol L⁻¹ using the bare CPE and ZrO₂ nanoparticles (inset) The equivalent circuit showing resistors and capacitor

Furthermore, the differences shown by the modification of CPE using ZrO₂ nanoparticles was demonstrated when the electrodes were applied to measure $1.0 \times 10^{-3} \text{ mol L}^{-1}$ [Fe(CN)₆]^{3-/4-} redox solution, with CV at a scan rate of 100 mVs⁻¹. Figure 3.9, showed an increase in the peak current, when CPE was modified as compared to the bare CPE, which is also confirmed in the EIS measurement. This shows that, the amorphous ZrO₂ nanoparticles modified electrode; even when used in a redox solution reduces the charge transfer resistance of the CPE.

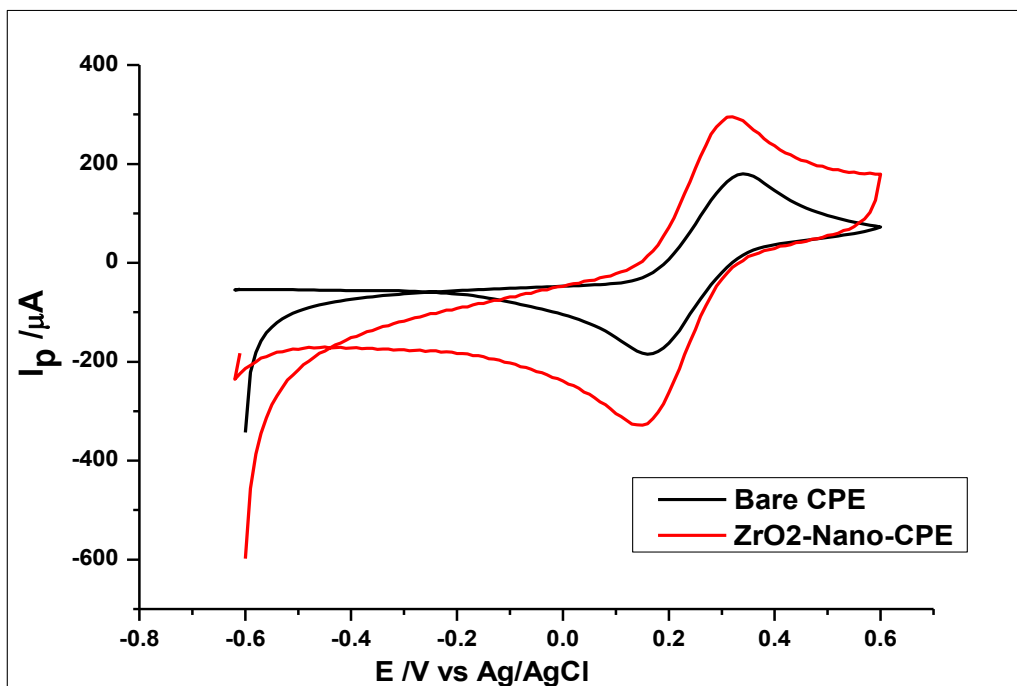


Figure 3. 9. The cyclic voltammograms of $1.0 \times 10^{-3} \text{ mol L}^{-1} [\text{Fe}(\text{CN})_6]^{3-/4+}$ redox solution, using bare CPE and ZrO_2 nanoparticles-modified CPE.

3.4.7 Determination of the modified electrode surface area

The surface area of the modified CPE was studied using $[\text{Fe}(\text{CN})_6]^{3-/4+}$ as the analyte. The topographical surface area of the zirconia nanoparticles modified CPE electrode that provided an increased surface, was used to measure Ferricyanide solution and the results are shown in Figure 3.10.

The values for the ratio of I_{pc}/I_{pa} from the $\text{K}_3[\text{Fe}(\text{CN})_6]^{3-/4+}$ (1.0 mmol L^{-1} dissolved in 100 mmol L^{-1} KCl) redox reaction were recorded as the scan rates were increased from 25 mVs^{-1} to 250 mVs^{-1} . From the voltammograms produced (Figure 3.9 and 3.10), the reaction was deduced to be a reversible system, hence the Randles-Sevcik equation (Equation 1.3) was employed to calculate the surface area of the electrode. The equation is as follows : $I_p = 2.69 \times 10^5 n^{3/2} A D^{1/2} v^{1/2} C_0$ where I_p is the anodic peak current for $[\text{Fe}(\text{CN})_6]^{3-/4+}$, A is the surface area of the electrode, n is the number electrons in the reaction ($n=1$), D is the diffusion coefficient which is $7.6 \times 10^{-6} \text{ cm}^2 \text{ s}^{-1}$, v is the scan rate and C is the concentration of $[\text{Fe}(\text{CN})_6]^{3-/4+}$

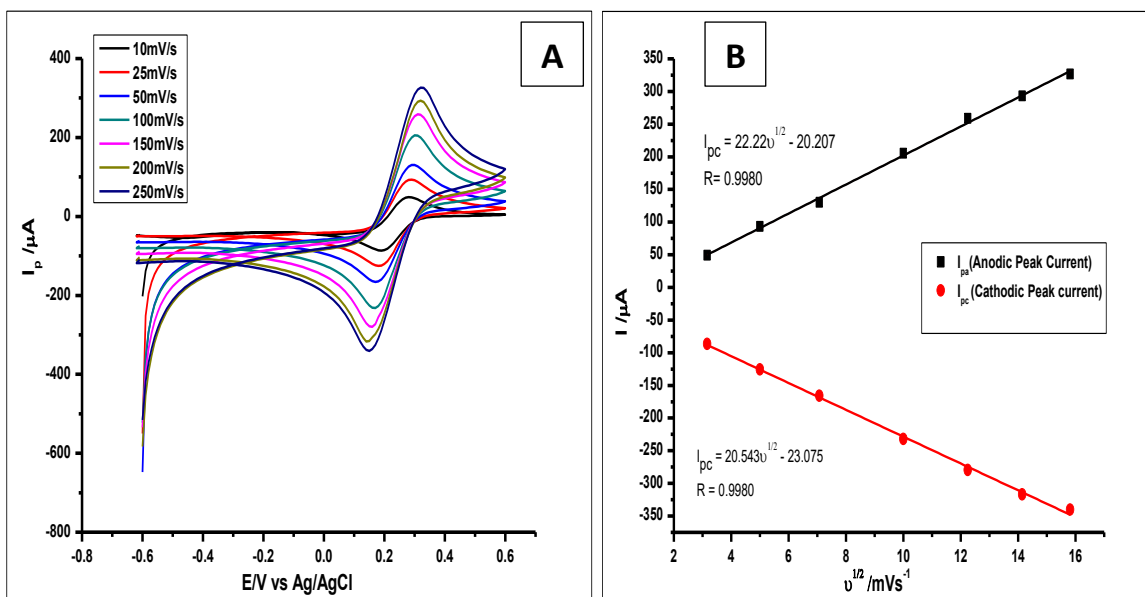


Figure 3. 10(A). Cyclic voltammograms of 1 mmol L⁻¹ [Fe(CN)₆]^{3-/4+} measured using the ZrO₂ nanoparticles modified CPE at increasing scan rates from 25 - 250 mVs⁻¹ (B). Plots of I_p vs v^{1/2}, which would be used to calculate the true surface area.

From the plot (Figure 3.10(B)) of the anodic peak current I_p against the square root of the scan rate (v^{1/2}), there was a linear relationship between the two parameters. Thus, the linear regression equations produced anodic peak currents were I_{pa} = 22.22 v^{1/2} - 20.207 with R² = 0.9980, while the cathodic peak current was I_{pc} = 20.543 v^{1/2} - 23.075 with R² = 0.9980. Hence the surface area calculated was 0.276 cm², which is higher than the surface area of the CPE of 0.0345 cm² and 0.0648 cm² for bare GCE. (Calculation was done as described in Appendix II, Section 8.2.1, Page 214). This shows that, the amorphous zirconia nanoparticles increased the surface area of the CPE. Hence, the increase in peak current when used in electrochemical measurements.

3.4.8 Interaction between the amorphous zirconia nanoparticles and graphite

Amorphous zirconia can be found in the monoclinic or tetragonal phase (Figure 3.3, page 74) as an oxide. It is typically laced with hydroxyl species like other metal oxides (Tsyganenko and Filimonov 1973), commonly used as catalysts and catalyst support materials. The tetragonal phase of zirconia does exist at low temperature, when they are synthesised from the initially formed amorphous

zirconia as shown previously in their XRD pattern (Molodetsky *et al.* 2000). The structure of Zirconium oxide provides a versatile surface because of its lack of a symmetrical lattice (Christensen and Carter 1998), with the possibilities of hydroxyls (Zr-OH), oxygen vacancies, coordinatively unsaturated Zr-O pairs and Lewis acid sites (Zr³⁺, Zr⁴⁺)(Kouva *et al.* 2015). Furthermore, Terki *et al.* (2006) proposed two different Zr-O bond distances and charge densities for the tetragonal Zirconia structure. They noticed that the Zr-O bond is covalent with some degree of ionic character. Hence the capability of electron transfer. It should also be noted that, dissociative adsorption of water on monoclinic zirconia is exothermic, thus happening at room temperature with hydroxylation at ambient temperatures (Radha *et al.* 2009).

On the other hand, Graphite being held together with van der Waal dispersion forces, show delocalized electrons moving around the sheet. This delocalization results in loosely bound π -electrons with very high mobility; hence the electrochemical properties of the graphite (Fachinger 2012). The mixing of the zirconia and graphite (Figure 3.11; page 84) produces an interaction that enhances the peak current of the oxidised GA. The physical mixing of the two electroactive compounds would have possibly produced weak ionic bonds, between the oxygen anions and the cations of the graphite sheet. With the adsorption of water on to the monoclinic zirconia and its inherently weak ionic character, with the delocalized electrons on the graphite sheets, the weak ionic bonds are formed as shown in Figure 3.8. Hence, the ZrO₂-Carbon paste mixture is structurally stable.

Furthermore, using data from the effect of the scan rate, the reaction of GA on the modified electrode is an adsorption-controlled reaction. This leads to a possibility of GA being adsorbed to the modified electrode by forming hydrogen bonds with ZrO₂ nanoparticles on the electrode. With the capability of electron transfer by the ZrO₂ and graphite (Figure 3.11), the oxidation of GA induced by the applied voltammetric potential, facilitates easy electron transfer. This is in line with our previous work, where we proposed a mechanism where, hydrogen bonding was formed between GA and SiO₂ nanoparticles with electrons being transferred. However, the GA detection capacity of the ZrO₂-CPE appears to be about 10-fold better than that of SiO₂ in graphene, because of the stability of the mild ionic interaction between ZrO₂ and the graphite.

In both cases, SiO₂-nanoparticles-graphene oxide nanocolloid-GCE and ZrO₂-CPE, we had proposed hydrogen bonding between GA and the modified electrodes. This is because the reactions were adsorption controlled reactions between GA and the both electrodes. Inasmuch as the two electrodes are oxide nanoparticles, SiO₂ nanoparticles have been described as insulators (Sainsbury and Fitzmaurice 2004), hence the possible difference in electroactivity.

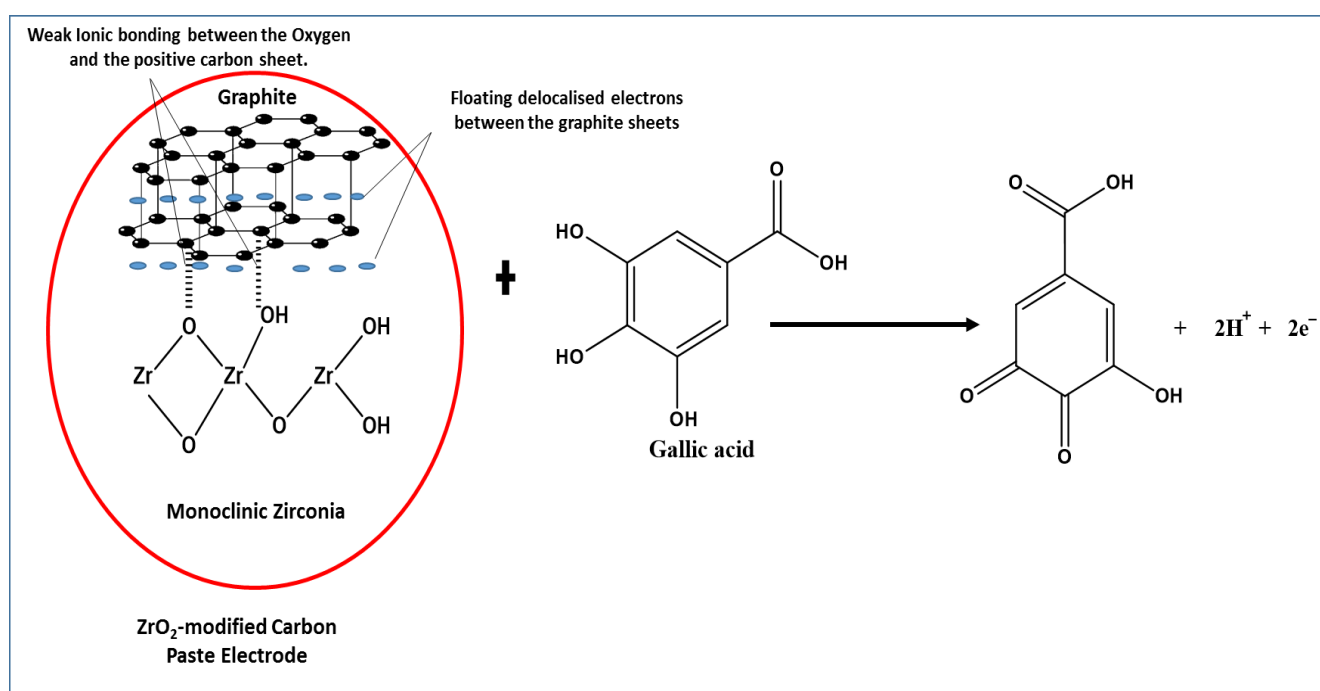


Figure 3. 11. Proposed interaction between ZrO₂ nanoparticles (Monoclinic zirconia) and graphite, showing a weak ionic bond between some of the oxygen and the positive graphite sheet; towards the electrochemical determination of Gallic acid

3.4.9 Effect of scan rate on the determination of Gallic acid

The effect of scan rate on the electrochemical behaviour of GA ($1 \times 10^{-3} \text{ mol L}^{-1}$) at the ZrO₂ nanoparticles CPE at different scan rates ranging from 25 – 1500 mVs⁻¹ was investigated using cyclic voltammetry. With increasing scan rate and the electro-oxidation of GA, there was a proportional increase in the peak current and a positive shift in peak potentials (Figure 3.12(A)). This increase, with a positive shift in the peak potential, suggests a kinetic limitation in the reaction (Raouf, Ojani and Kolbadezhad 2009). Plotting the peak current (I_p) against the scan

rate (v) in the scan rate range of 25 – 1000 mVs^{-1} produced a straight line (Figure 3.12(B)), suggesting the GA interaction with the ZrO_2 nanoparticles CPE was an adsorption-controlled process in this range. This led to a linear regression equation: $I_p (\mu\text{A}) = 0.0013 v(\text{mVs}^{-1}) + 0.2211$, $R^2 = 0.9956$

The plot of $\log I_p$ versus $\log v$ in the scan rate range of 25-1000 mVs^{-1} , also generated a straight line with a linear regression equation thus: $-\text{Log } I_p (\mu\text{A}) = 1.7884 \text{Log } v (\text{mV/s}) + 2.7607$ and $R^2 = 0.9902$; this is expected for a diffusion and an adsorption-controlled reaction in ideal reaction condition (Gao *et al.* 2016) as shown in Figure 3.12(C).

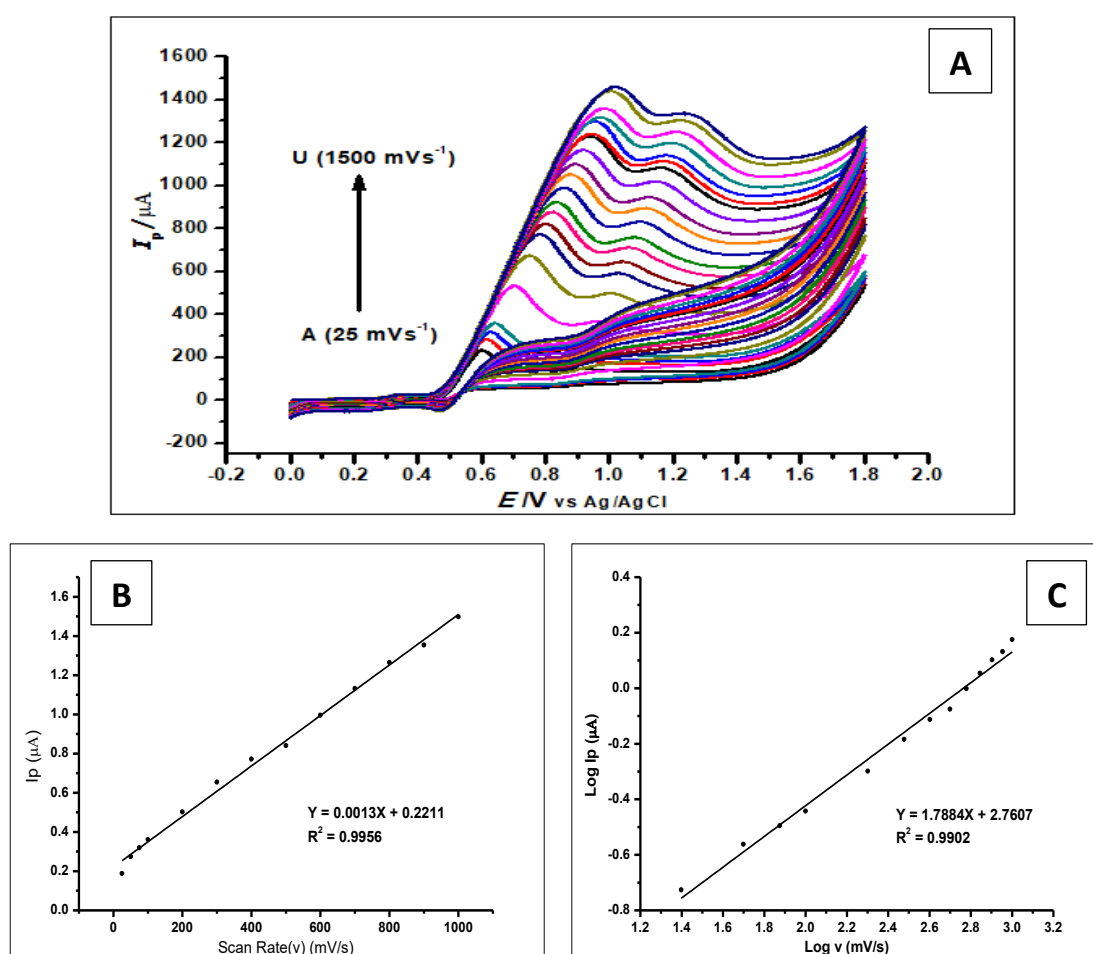


Figure 3. 12(A) Cyclic Voltammograms of $5.0 \times 10^{-4} \text{ mol L}^{-1}$ gallic acid in phosphate buffer of pH 2.0 determined with a ZrO_2 nanoparticles-modified CPE at different scan rates from 10 to 1000 mVs^{-1} . (B) The plot of the peak current vs scan rate. (C) the plots of $\log I_p$ vs $\log v$ showing straight lines

3.4.10 Effect of ZrO₂ nanoparticles concentration on CPE

The effect of the concentration of the ZrO₂ nanoparticles and the graphite in the carbon paste was studied (Figure 3.13). Different amounts of ZrO₂ nanoparticles powder were weighed into the graphite powder at quantities of 0.5 g, 1.0 g, 1.5 g and 2.0 g while adjusting the graphite powder appropriately (ratio 60:10:30, w/w/w, graphite:ZrO₂: paraffin). Then the modified carbon paste electrodes were used for the determination of GA (1×10^{-3} mol L⁻¹) in phosphate buffer (1×10^{-1} mol L⁻¹, pH 2.0), using DPV at a scan rate of 100 mVs⁻¹. The peak currents produced by the 0.1 g ZrO₂ nanoparticles mixtures were found to produce the best voltammograms, with the highest peak current. Hence, subsequently modified electrodes produced, used 0.1 g ZrO₂ nanoparticles. From Figure 3.13 it is observed that, as ZrO₂ nanoparticles concentration increased from 5% to 10%, the peak currents increased significantly. However, when the nanoparticles were further increased to 15% and 20%, the peak currents dropped drastically. Hence the 10% ratio was subsequently used for electrode preparation.

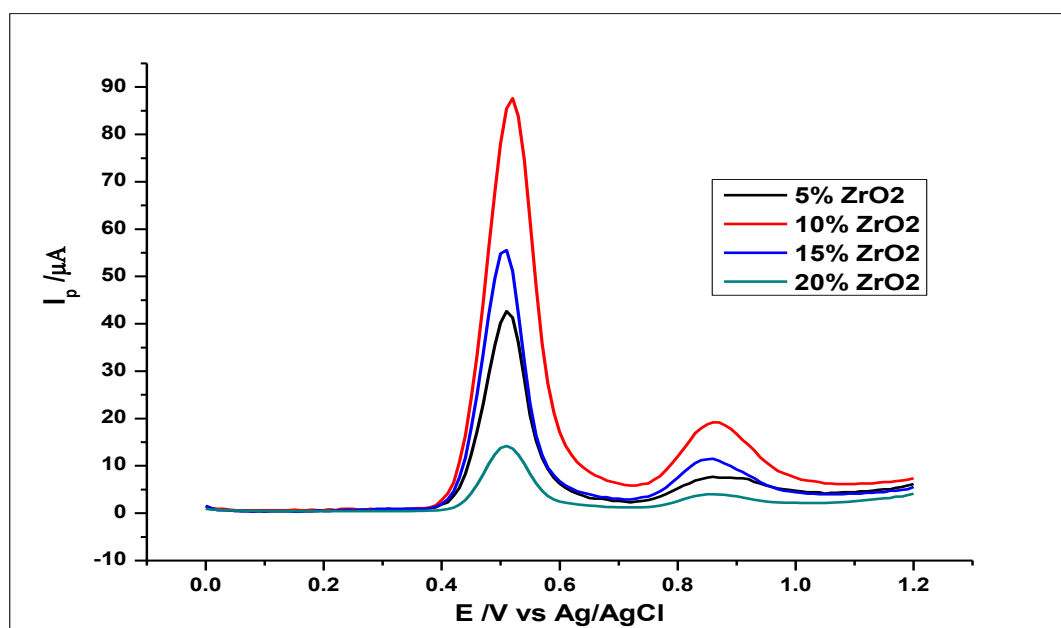


Figure 3. 13. Differential voltammograms showing the effect of the amount of ZrO₂ nanoparticles in the carbon paste electrodes.

3.4.11 Effect of time on the adsorption of GA on the modified CPE

The effect of time on the adsorption of GA on to the modified CPE was investigated by the detection of GA ($1 \times 10^{-3} \text{ mol L}^{-1}$) in phosphate buffer ($1 \times 10^{-1} \text{ mol L}^{-1}$, pH 2.0) at room temperature, at a scan rate of 100 mVs^{-1} using DPV. The measurement was done by recording the voltammograms produced by GA oxidation, every minute for six minutes. The peak currents recorded at different times were used for the analysis. Looking at the voltammograms produced (Figure 3.14(A)), the voltammograms show an increase in peak current as time increased. There was an increase in peak current after the first scan and subsequent scans after every minute to a maximum at the fifth minute. Further scans after the fifth minute showed a decrease in peak current. This phenomenon can be attributed to the adsorption-controlled reaction confirmed by the scan rate, where the GA reaches a saturation point on the surface of the electrode. Thus, any further scan did not produce an increase in peak current but a decrease. This is in agreement with the work done by Tashkhourian and Nami-Ana (2015) and our previous work.

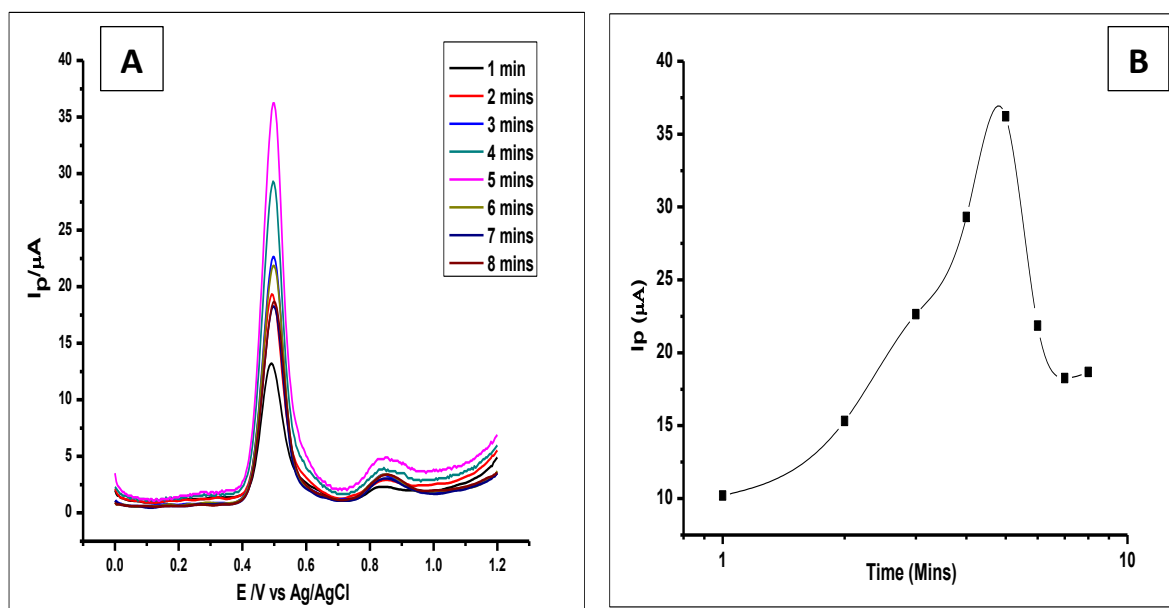


Figure 3. 14. (A)DPV voltammograms showing the effect of adsorption time in the determination of $1 \times 10^{-3} \text{ mol L}^{-1}$ GA in a 0.1 mol L^{-1} phosphate buffer of pH 2.0 at a scan rate of 100 mVs^{-1} (B) The plots showing the same effect of adsorption time.

3.4.12 Effect of the modified electrode on the concentration of GA (Determination of linear detection range and LOD)

Differential pulse voltammetry was used to investigate different concentrations of GA, to determine the effect of the amorphous ZrO₂ nanoparticles modified CPE on the increasing concentration of GA. The DPV results recorded at a potential range of 0 V to +1.2 V, the scan rate of 100 mVs⁻¹, pulse amplitude of 80 mV and pulse period of 0.2 s; were used for the determination of the limit of detection (LOD) of the modified electrode. The concentration increase of GA was studied in the range of 1 x 10⁻⁶ to 1 x 10⁻³ mol L⁻¹ and there was a correlated increase in the peak current (I_p), whilst the ZrO₂ nanoparticles modified electrode was being used. The measurements produced voltammograms as can be seen in Figure 3.15, where the peak currents increased in proportion with the increasing GA concentration. The DPV voltammograms produced two peaks at peak potentials of 0.51 V and 0.85 V as the different GA concentrations were being determined. These peaks have been characterised in the literature to be the formation of the semiquinone radical for the first peak, which oxidises to a quinone in the second peak. The peak potential in this case, shows a negative shift as compared to the peak potential in CV. This is attributed to the fact that DPV is more sensitive than CV, because of the immunity of DPV to residual current as compared to CV. With no charging current as opposed to the Faradaic current (Rebello *et al.* 2013; Vilas-Boas *et al.* 2019). Hence, a more reduced peak potential for the DPV peak current, than that of the CV.

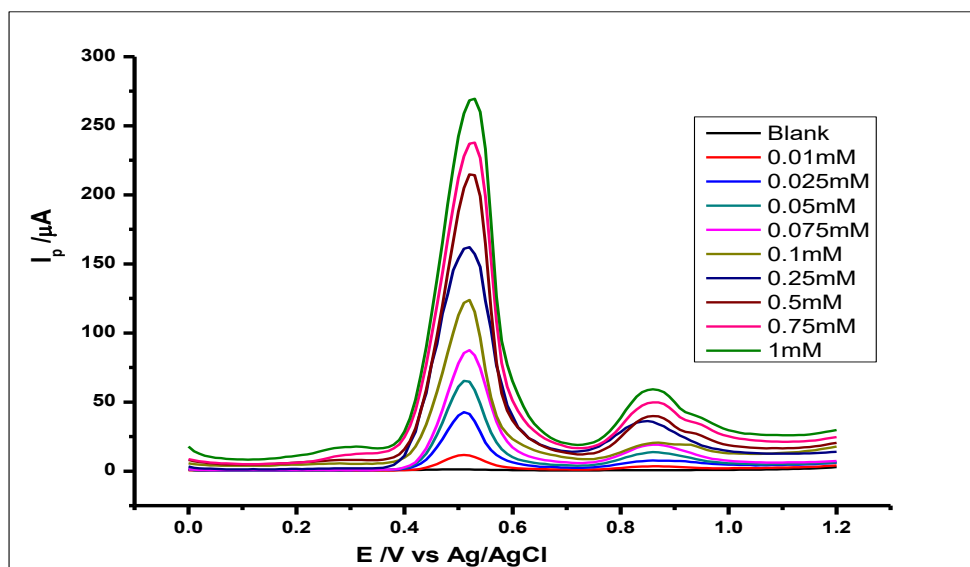


Figure 3. 15. Differential voltammograms of various concentrations of GA at ZrO₂ nanoparticles modified CPE in a 0.1 mol L⁻¹ phosphate buffer at 2.0 at scan rate of 100 mVs⁻¹, with voltammograms (a-j) that corresponds to the following concentrations a) Blank PBS, b) 0.01 mmol L⁻¹, c) 0.025 mmol L⁻¹, d) 0.05 mmol L⁻¹, e) 0.075 mmol L⁻¹, f) 0.1 mmol L⁻¹, g) 0.25 mmol L⁻¹, h) 0.5 mmol L⁻¹, i) 0.075 mmol L⁻¹ j) 1 mmol L⁻¹

The first and major peak of each of the voltammograms produced by the different concentrations was used to produce the analytical calibration graph as can be seen in Figure 3.16. This showed a linear relationship between the peak currents and the increasing concentration of GA. This linear relationship produced a linear regression equation of $I_p = 1125.4 C + 2.1113$ (I_p : μA , C : mmol L^{-1} and $R^2 = 0.9945$) within the range of 1×10^{-5} to 1×10^{-3} mol L⁻¹. Hence, the linear detection range which is the range at which the modified electrode's detection of GA is linear, was deduced to be 1×10^{-5} to 1.0×10^{-3} mol L⁻¹. The limit of detection (LOD) which was defined as $(3 \times \text{Std}_{\text{Blank}})/m$, where $\text{Std}_{\text{Blank}}$ is the standard deviation of the blank and m is the slope; was found to be 1.24×10^{-7} mol L⁻¹. With the limit of detection of 1.24×10^{-7} mol L⁻¹, the amorphous ZrO₂ nanoparticles modified CPE electrode is found to be comparable to other methods in literature based on the maximum permitted antioxidant levels in food within the EU and North America. The maximum permitted range for GA within the antioxidant level guidelines is 1.2×10^{-1} mol L⁻¹ to 6.0 mol L⁻¹. The recorded LOD being below these stipulated standard permitted level makes the modified electrode suitable for use in GA determination.

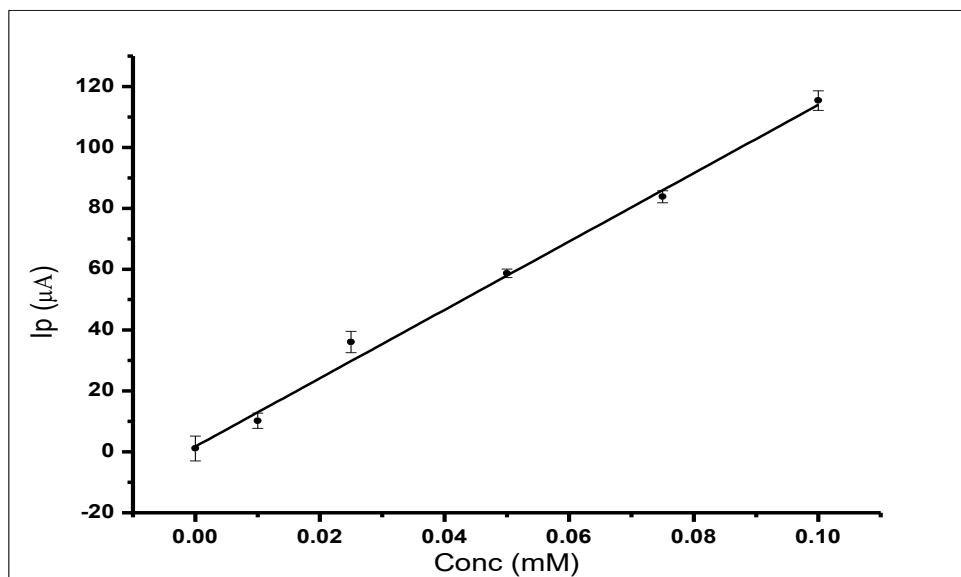


Figure 3. 16. The calibration curve showing the linear detection range of 1×10^{-5} to 1.0×10^{-3} mol L⁻¹ and a linear regression equation of $I_p = 1125.4 C + 2.1113$ (IP: μA , C: mmol L⁻¹ and $R^2 = 0.9945$)

3.4.13 The amorphous Zirconia nanoparticles modified CPE as compared to other work in the literature

As a metal oxide nanoparticle modified CPE electrode used for the determination of GA, the AmZr nanoparticle modified CPE demonstrated a comparable limit of detection with others in the literature. Tashkhourian *et al.* (2013) and Tashkhourian and Nami-Ana (2015) in their work modifying carbon paste electrodes with titanium oxide and silicon oxide nanoparticles respectively produced LODs of 9.4×10^{-7} mol L⁻¹ and 2.5×10^{-7} mol L⁻¹. These LODs are comparable to that seen in this work (1.24×10^{-7} mol L⁻¹) for the determination of GA and are also comparable to the work done by Souza *et al.* (2011) where he modified CPE with carbon nanotubes for the determination of GA.

3.4.14 The reproducibility and repeatability of using the modified electrode CPE for GA determination

The reproducibility of GA determination by the ZrO₂ nanoparticles modified carbon paste electrode was investigated, by using the modified electrode for the determination of 1×10^{-3} mol L⁻¹ GA using DPV. Eight independently produced electrodes were used to measure eight different samples of 1×10^{-3} mol L⁻¹ GA as can be seen in Figure 3.17. The oxidation current produced by the eight replicates

independently determined by the different electrodes gave a relative standard deviation (RSD) of 2.4%, which showed good reproducibility.

The repeatability of the method was also investigated by using the three modified electrodes to measure eight repeated $1 \times 10^{-3} \text{ mol L}^{-1}$ concentrations of GA. The relative standard deviation of the measured peak currents was found to be 3.02% showing good repeatability of the method.

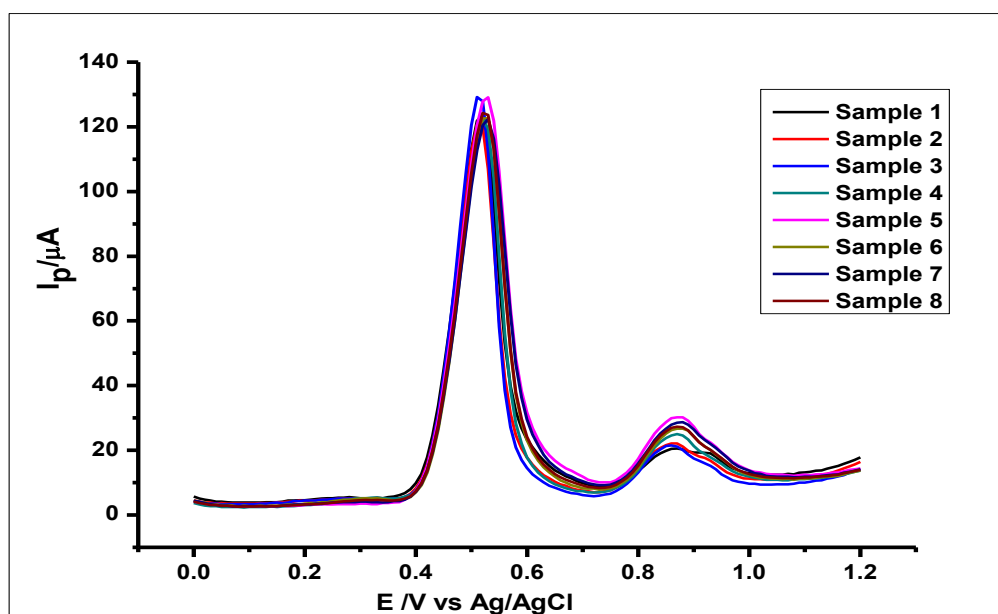


Figure 3. 17. DPV Voltammogram of $1 \times 10^{-3} \text{ mol L}^{-1}$ Gallic acid using ZrO_2 nanoparticles modified-CPE to demonstrate reproducibility

3.4.15 Stability of the modified electrode

The stability of the ZrO_2 nanoparticles modified CPE was investigated by using three freshly prepared modified CPE to determine GA ($1 \times 10^{-2} \text{ mol L}^{-1}$) using CV and the electrodes were then kept for 30 days. The electrodes were further applied to determine the concentration of GA ($1 \times 10^{-2} \text{ mol L}^{-1}$). The voltammograms generated on the 1st and 30th (Figure 3.18) demonstrated good stability with a relative standard deviation of 6.2%.

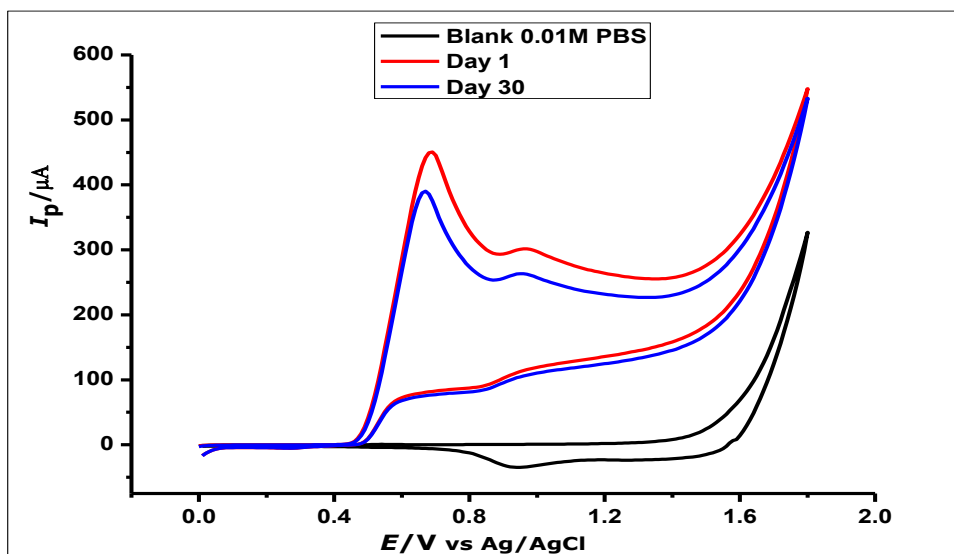


Figure 3. 18. Cyclic voltammograms showing the determination of $1 \times 10^{-2} \text{ mol L}^{-1}$ GA in 1×10^{-2} phosphate buffer at pH 2.0 and scan rate of 100 mVs^{-1} on a day one and day thirty.

3.4.16 Interference studies on GA determination

The modified electrode was used to study the effect of interference of various species towards the determination of GA ($5 \times 10^{-4} \text{ mol L}^{-1}$). This was carried out by the addition of different foreign ions to known quantities of the analyte. The ionic species used for this study, were Fe^{3+} , Ca^{2+} , Na^{+} and K^{+} ; while organic compounds included quercetin, caffeine, caffeic acid and ascorbic acid. The use of the different cations was due to their reported complexation with GA in the literature (Fazary, Taha and Ju 2009; Hassanien *et al.* 2011) and their possible capability of interfering with the electrochemical determination of GA. The tolerable interference limits of these ions are defined as the highest concentration or amount that would produce a relative standard deviation equals or less than 5%. From the results recorded (Figure 3.19 and Table 3.2), they showed relative standard deviations of less than 5%, hence, the ions did not interfere with the determination of GA. However, some slight positive shift of some of the peak potentials, were observed, that fell within the normal potential range of GA oxidation. Furthermore, the second GA oxidation peak showed some minor changes; with peak currents ranging from $40 \mu\text{A}$ to $60 \mu\text{A}$; but would not be considered as interference since only the first peak current is usually considered for electrochemical determination of GA.

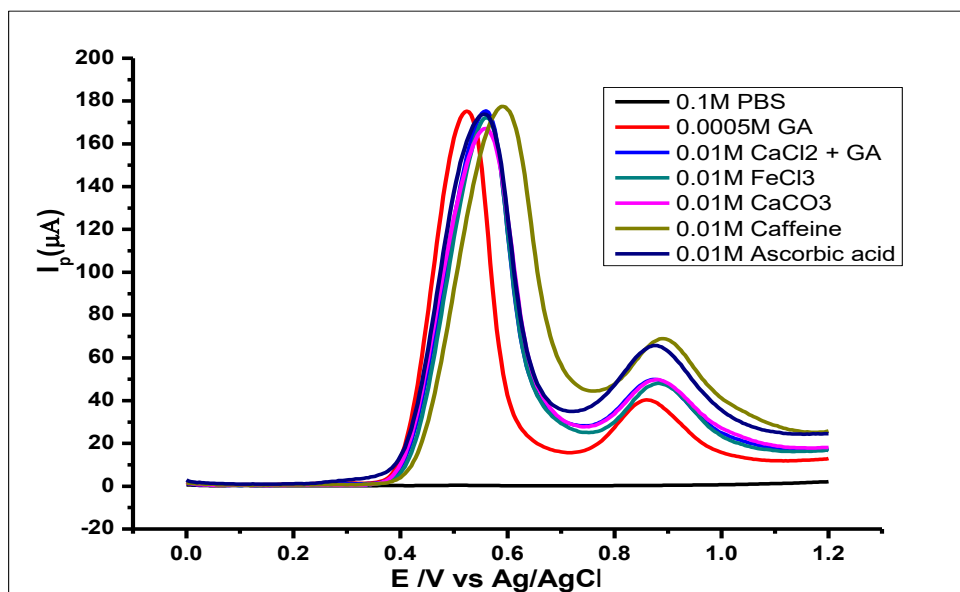


Figure 3. 19. DPV voltammograms of $5 \times 10^{-4} \text{ mol L}^{-1}$ Gallic acid with different concentrations of some known interfering compounds in 0.1 mol L^{-1} phosphate buffer at pH 2.0 and a scan rate of 100 mVs^{-1}

Table 3. 1. Effects of various substances on the determination of $5 \times 10^{-4} \text{ mol L}^{-1}$ Gallic acid

Interfering Species	Amount in Solution (mol L^{-1})	Relative Standard Deviation (%)
Ca^{2+}	1×10^{-2}	± 2.27
Na^{+}	1×10^{-2}	± 2.11
Fe^{3+}	1×10^{-2}	± 1.67
Cl^{-}	1×10^{-2}	± 2.42
CO_3^{2-}	1×10^{-2}	± 2.07
Ascorbic acid	1×10^{-2}	± 1.44
Caffeic acid	1×10^{-2}	± 3.32
Caffeine	1×10^{-2}	± 3.51
Quercetin	1×10^{-2}	± 3.06

3.4.17 Analytical application of the modified CPE

The ZrO_2 nanoparticles modified carbon paste electrode was used for the determination of spiked GA in red wine and white wine. The wines as samples were used because of work done in the literature that suggests the presence of GA in red wine and white wine (Souza *et al.* 2011; Węgiel, Burnat and Skrzypek 2018). In their work Souza *et al.* used carbon nanotube modified CPE for the determination of GA in wine samples. They attributed the anodic current peak to

o-dihydroxyphenol and gallate groups; concluding that these species are the major contributors to the antioxidant capacity in wine. Meanwhile, Wegiel, Burnat and Skrzypek used carbon ceramic electrode, modified with reduced graphene oxide and detected GA in red and white wine sample. This experiment was then carried out by the use of red and white wine samples respectively (10 fold dilution in 1×10^{-1} mol L⁻¹ phosphate buffer) as a blank.

Then there was standard addition of aliquots of known concentrations (0.9, 1.6, 2.3 and 2.9 mmol L⁻¹) of GA into the red/white wine samples and DPV was used to analyse the samples. The voltammograms were recorded (Figure 3.20 and Figure 3.21). From the voltammograms, one can see an oxidation peak from the blank. More oxidation peaks were produced with increasing GA concentrations in both the red and the white wine samples. Within the concentration range of 0 to 3.3×10^{-3} mol L⁻¹ of GA, the corresponding voltammograms are shown in Figures 3.20 and 3.21 and their analysis in Table 3.2. Increasing the concentration of GA produced a linear regression equation of $I_p = 10.9 \text{ Conc. (mM)} + 21.4$ and $R^2 = 0.9909$. (Figure 3.19 inset).

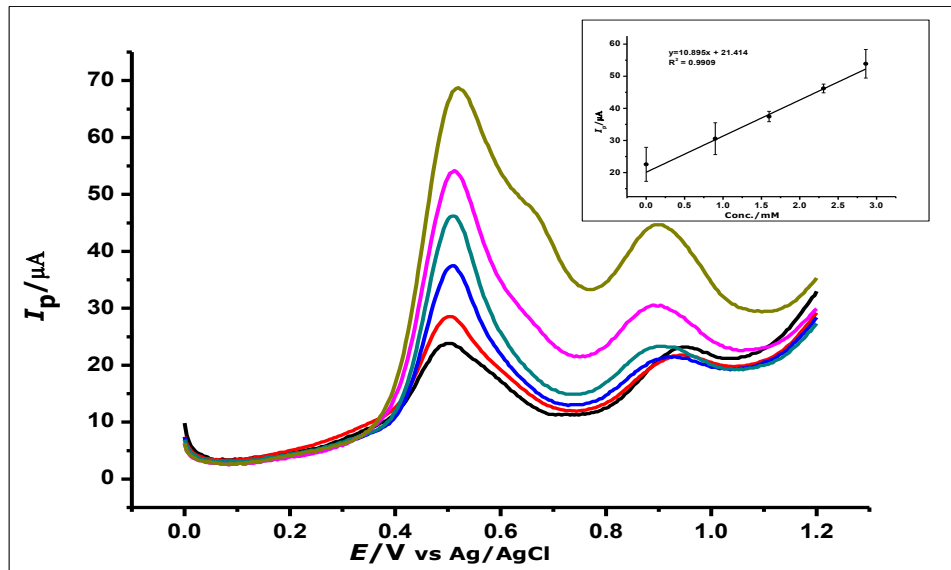


Figure 3. 20. DPV voltammograms show the determination of Gallic Acid in a real sample of red wines (Inset) Calibration graph created using the analysis of the real sample.

From the voltammograms of the white wine, the amorphous ZrO₂ nanoparticles modified CPE shows an oxidation peak between 0.4 V and 0.5 V. The oxidation peak current then increases when aliquots of GA were added to the solution. The

increasing peak current for the oxidation peak also falls between 0.4 V to 0.5 V. This acts as a confirmation of the presence of GA in the white wine, which can be seen in Figure 3.22.

Looking at Figure 3.22, there is a relationship between the increasing concentration of GA in the white wine solution and the increasing peak currents depicted by the voltammograms. This relationship is represented by the regression equation thus $I_p (\mu\text{A}) = 11.21 \text{ Conc (mmol L}^{-1}) + 21.735$ and $R^2 = 0.9956$ (Figure 3.22, Page 99).

Looking at Table 3.2 which shows the results of the analysis of GA in spiked Red and White Wine samples, one can observe an oxidation peak from the red and white wine samples without an gallic acid spike. The first peak can be attributed to the total antioxidant capacity of the wine samples, with the red wine showing $0.1030 \text{ mmol L}^{-1}$ and the white wine $0.049 \text{ mmol L}^{-1}$. However, when the spiking of the sample begins, one observes the presence of gallic acid at the peak potential where the wine sample showed an oxidation peak. This shows that, the modified electrode can detect gallic acid in the wine samples. However, the electrode shows relative errors of $< 10\%$, which is generally acceptable in this analysis. This is because there is no said gallic acid concentration standard in the wine industry, as their concentration is dependent production procedure (Lino et al. 2014) .

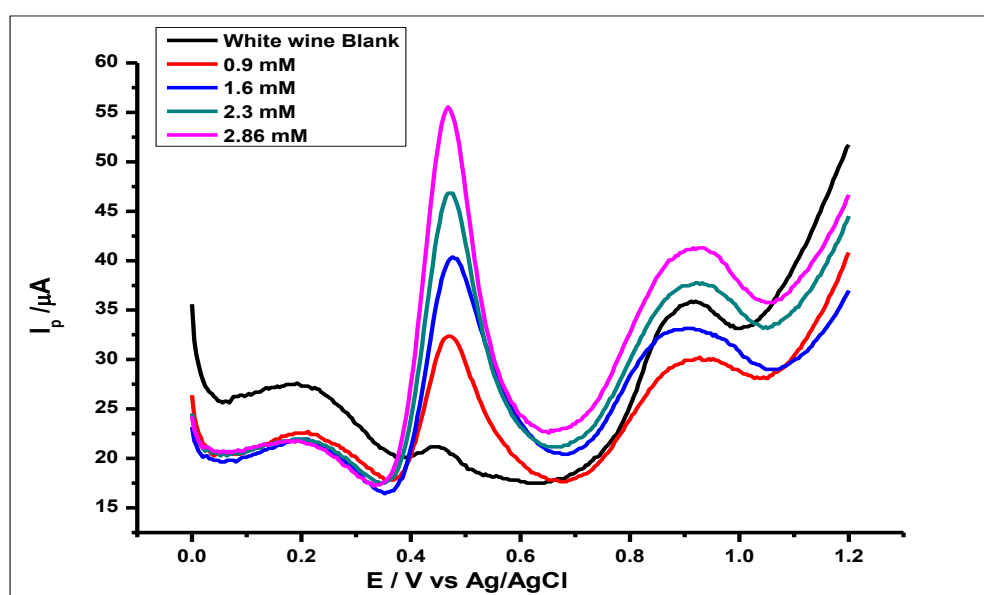


Figure 3. 21. DPV voltammograms showing the determination of Gallic Acid in a real sample of White wine.

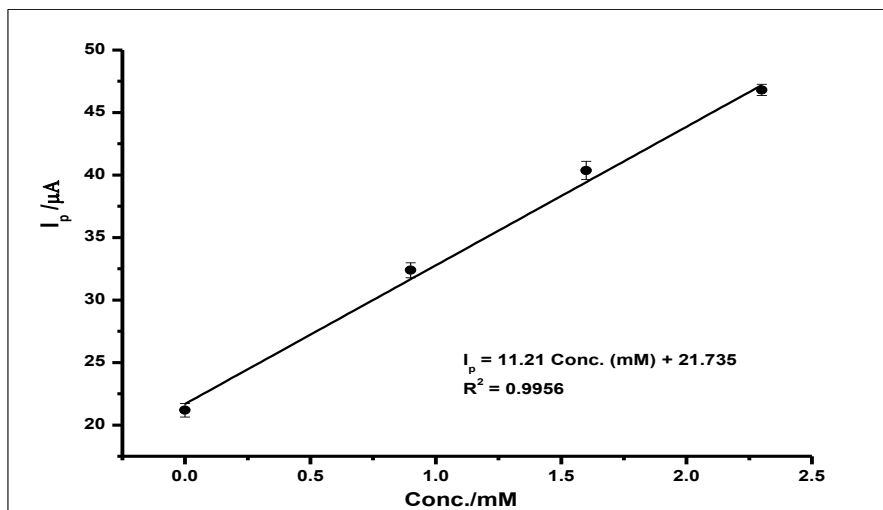


Figure 3. 22. Calibration plot created using data from the DPV voltammograms of analysing White Wine.

Table 3. 2. Results of the analysis of GA in spiked Red and White Wine

Samples	Added (mmol L ⁻¹)	Found (mmol L ⁻¹)	Recovery (%)	Relative Error
Red Wine	0	0.1030	-	-
	0.9	0.8360	92.8	±7.2
	1.6	1.469	91.8	±8.2
	2.3	2.273	98.7	±1.3
	2.86	2.98	104.2	±4.2
White Wine	0	0.049	-	-
	0.9	0.95	105.5	±5.5
	1.6	1.66	103.75	±3.75
	2.3	2.24	97.39	±2.61

3.5 Conclusion

Amorphous ZrO₂ nanoparticles were used for the first time to modify a carbon paste electrode. The electrode was used for the electrochemical determination of GA in a 1 x 10⁻¹ mol L⁻¹ phosphate buffer at pH 2.0. Cyclic and differential pulse voltammetry was used for the electrochemical determination, and it was found that, the amorphous ZrO₂ nanoparticles modified electrode enhanced the oxidation peak current when GA acid was analysed, as compared to the bare CPE. The electrode also showed an electrochemical oxidative effect towards the determination of GA within a concentration range of 1 x 10⁻⁵ to 1 x 10⁻³ mol L⁻¹. The modified electrode demonstrated selectivity towards the determination of GA

as it showed little or no interference from other flavonoids like Quercetin and other antioxidants.

The electrode was also found to be sensitive, fast, cost-effective, and simple for the determination of GA and it also showed good repeatability, reproducibility and good long-term stability. This is when compared to other composite electrodes, with more complex and expensive modifications in the literature; with limits of detection still in the range of 10^{-6} to 10^{-9} mol L⁻¹, as we demonstrated in our electrode (dos Santos Raymundo et al. 2007; Jara-Ulloa et al. 2013; Sangeetha and Narayanan 2014; Petković et al. 2015; Liang et al. 2016).

The modified electrode was also used for a successful determination of GA in red wine and white wine within a concentration range of 0 to 3.3×10^{-3} mol L⁻¹. The recorded results of this method showed it was comparable to sensors in the literature, based on its LOD which is far below the maximum permitted GA levels in food sample within the EU and North America.

CHAPTER FOUR

4.0 GRAPHENE OXIDE NANOCOLLOIDS AND SiO₂ NANOPARTICLES MODIFIED GLASSY CARBON ELECTRODE FOR ELECTROCHEMICAL DETERMINATION OF GALLIC ACID

4.1 Introduction

This chapter describes for the first time the use of graphene oxide nanoparticles working in synergy with silica nanoparticles for the electrochemical determination of GA.

Graphene and graphene oxide have attracted very strong scientific and technological interest in the course of the last few years (Murali *et al.* 2010; Artiles, Rout and Fisher 2011; Liu, Dong and Chen 2012; Arvand and Anvari 2013; Chua and Pumera 2014; Gao *et al.* 2014). The compound and its derivatives have shown very important uses in nano and high-frequency electronics (Farmer *et al.* 2011; Hess, Seifert and Garrido 2013), storage of energy and conversion of energy (Brownson, Kampouris and Banks 2011; Sun, Wu and Shi 2011), batteries (Li *et al.* 2018; Al Hassan *et al.* 2019), fuel cells (Farooqui, Ahmad and Hamid 2018; Liu, Choi and Meng 2018), solar cells (Iqbal and Rehman 2018) and other biosciences/technological applications (Gao *et al.* 2014). These have been because of the unique chemical and physical properties of the compound; that includes very high surface area (theoretically 2630 m² g⁻¹) (Geim and Novoselov 2007; Park and Ruoff 2009), very good thermal conductivity (Teweldebrhan *et al.* 2008), strong mechanical strength (Lee *et al.* 2008) and electrical conductivity (Tong, Bohm and Song 2017). Most importantly graphene and graphene oxide have been used for the development of electrochemical sensors used for the determination of organic compounds including antioxidants (Xu, Dai and Chen 2010; Pumera 2011; Arvand and Anvari 2013; Luo *et al.* 2013b; Gao *et al.* 2015; Velmurugan *et al.* 2017). There has also been a lot of work on the use of graphene-based nanomaterials like graphene-based nanocomposites for the determination of antioxidants. However, there has not been any work done using graphene oxide nanocolloids, which is another form of graphene nanomaterial.

Graphene oxide nanocolloids (GON) are graphene oxide nano-sheets synthesised from graphite nanofibers with a uniform size distribution, dispersed in water and

significantly more stable than the powdered graphene oxide (Luo *et al.* 2010). Their physical and chemical properties have led them to be used as core-shell nanoparticles for Raman bioimaging, photothermal and photodynamic therapy (Kim *et al.* 2015). Graphene oxide nanocolloids have not been previously used in any electrochemical determination, hence its use in this work.

The use of nanomaterials such as Ag, Au, SiO₂ and TiO₂ nanoparticles have been previously used for the modification of electrodes for the determination of GA (Tashkhourian *et al.* 2013; Tashkhourian and Nami-Ana 2015), with very good results. However, there has not been any combination between graphene nanocolloids and any of these other nanomaterials for the modification of electrodes for the electrochemical determination of GA. Hence the use of SiO₂ nanoparticles in combination with GON for the electrochemical determination of GA. Silicon dioxide nanoparticles, which is also known as silica nanoparticles have been used in biomedical research. This is because of their stability, low toxicity and their ability to be functionalized with a range of different compounds. Their ability to be functionalized, made them a good base for the graphene oxide nanocolloids.

In this chapter, the physical and chemical properties of GON and those of SiO₂ nanoparticles were harnessed in synergy for the modification of glassy carbon electrode. The modified electrode was used for the determination of GA and the simultaneous analysis of Uric acid (UA) and GA.

4.2 Experimental

4.2.1 Materials and Reagents

The materials and reagents used in this study had earlier been listed (Chapter 2, Table 2.1, pages 46-47). However, for the synthesis and preparation of the modified electrode for this specific study, the following reagents were used.

Tetraethyl orthosilicate (TEOS), ethanol, aqueous ammonia (28-30%), and graphene oxide nanocolloids (nano-GO) were purchased from Sigma Aldrich (London, UK).

4.2.2 Silicon oxide nanoparticles synthesis

The synthesis of silicon oxide nanoparticles has previously been described in Chapter 2, section 2.4.2 in page 50.

4.2.3 Preparation of nano-GO-SiO₂-nanoparticles-GCE

The nano-GO-SiO₂-nanoparticles-GCE was prepared as already described in the working electrode section of this thesis (Chapter 2, section 2.6.1.1, page 57)

4.2.3 Characterisation of nano-GO-SiO₂-nanoparticles

Characterisation of the nano-GO-SiO₂-nanoparticles modified glassy carbon electrode was carried out using SEM (Scanning Electron Microscopy) and EDXA. As described in section 2.5.2, SEM uses electron beams to generate signals from the surface of the mixture. The signals reveal information about the morphology and size distribution of the compound.

The EDX Analysis image showed the chemical composition of the nanoparticles, with the amounts of carbon, oxygen, and silicon on the surface of the modified electrode.

Fourier Transform Infrared spectroscopy (FTIR) was also used to characterise the, SiO₂ nanoparticles, nano-GO, and nano-GO-SiO₂-nanoparticles combination, to show how the compounds attach to each other. The spectra were recorded and analysed accordingly.

4.3. Electrochemical Measurements

All the electrochemical analysis of GA at the nano-GO-SiO₂-nanoparticles were carried out in a 1×10^{-1} mol L⁻¹ phosphate buffer solution at pH 2.0. The CV was scanned within a range of 0.0 V to +1.8 V at a scan rate of 100 mVs⁻¹. The differential pulse voltammograms were recorded in a potential range between 0.0 V and +1.2 V with a pulse amplitude of 0.08 V and pulse period of 0.2s.

Cyclic voltammetry was used for the study of ferrocyanide [Fe(CN)₆]^{3-/4-} (1×10^{-3} mol L⁻¹) on the surface of the modified electrodes, which was swept over a potential range of -0.6 V to 0.6 V at increasing scan rates of 10, 25, 50, 100, 150, 200, 250 and 300 mVs⁻¹. The voltammograms recorded in the course of the study of the [Fe(CN)₆]^{3-/4-} were used for the determination of the electroactive areas of nano-GO-SiO₂-nanoparticles-GCE, the nano-GO-GCE and the bare GCE electrode. This was to understand the effect of the presence of the nanoparticles on the surface of the bare glassy carbon electrode.

Electrochemical impedance spectroscopy was also used to provide information on the impedance changes on the bare and modified electrodes, with the Nyquist

plots of the measurements recorded. The EIS measurements were carried out at a frequency range of 100 KHz – 0.01 Hz (50 points within the frequency range) and a fixed potential of 0.4 V in 0.1 mol L⁻¹ KCl that contains 5 mmol L⁻¹ of [Fe(CN)₆]^{3-/4-} redox solution.

4.3.1 Determination of adsorption time

The time it takes for the adsorption of GA onto the modified electrode was studied using DPV. The voltammograms for the determination of GA (1 x 10⁻³ mol L⁻¹) in phosphate buffer (1 x 10⁻¹ mol L⁻¹, pH 2.0) at room temperature, at a scan rate of 100 mVs⁻¹, were recorded every minute for a duration of seven minutes. The data produced for this experiment were used to determine the time the electrode got saturated with GA, with no further increase in peak current.

4.3.2 Selectivity of the modified electrode

The selectivity of the modified electrode was investigated, using the nano-GO-SiO₂-nanoparticles modified GCE to simultaneously detect GA and Uric acid (UA) using CV in phosphate buffer solution (1 x 10⁻¹ mol L⁻¹, pH 2.0), at a scan rate of 100 mVs⁻¹. The concentration of GA and UA used for this investigation were 0.48 mmol L⁻¹ and 0.36 mmol L⁻¹ respectively. A concentration of 0.48 mmol L⁻¹ of GA was used, because at that concentration a significant distinction between the voltammograms of GA and UA was observed.

This investigation was done by mixing GA (5 mL of 0.48 mmol L⁻¹) with UA (5 mL of 0.36 mmol L⁻¹) into a 10 mL voltammetric cell and vigorously stirred using a magnetic stirrer for two minutes. The voltammograms were then recorded.

4.4 Results and Discussion

4.4.1 Characterisation of nano-GO-SiO₂-nanoparticles modified glassy carbon electrode

The SEM and EDX analysis of the SiO₂ nanoparticles (Figure 4.1) showed the spherical morphology and homogenous size distribution of the synthesised compound (Figure 4.1(A)). The spherical nanoparticles had sizes that ranged from 50 to about 200 nm at magnifications of between 25000X to 100000X.

On the other hand (Figure 4.1(B)), the morphology of the graphene nanocolloids-SiO₂ nanoparticles mixture on the surface of the GCE, shows a substantial increase

in the number of nanoparticles on the surface. The SEM image shows particles of about 100 μm at magnification of 250X, with smaller particles of between 100 nm to 200 nm at magnifications of between 25000X to 100000X. These nanoparticles become apparent as the drop-cast solution dries up on the surface of the GCE. The nanosized SiO_2 nanoparticles on the surface of the GCE as seen in the SEM images create a large active surface area for better transmission performance and high accumulation efficiency as earlier reported by Tashkhourian and Nami-Ana (2015a) and Wang *et al.* (2016).

Meanwhile, Figure 4.1(C), which is the EDX analysis result, shows the elemental composition of the silicon dioxide nanoparticles. The result shows the equal molecular composition of silicon and oxygen.

From the SEM and EDXA analysis of the particles it was seen that the SiO_2 nanoparticles showed a size distribution of 50 to 200 nm, with the SEM images showing sizes of 100 nm. Hence, there was no need to run a DLS analysis, especially with the fact that, the graphene oxide nanocolloids was already in a solution.

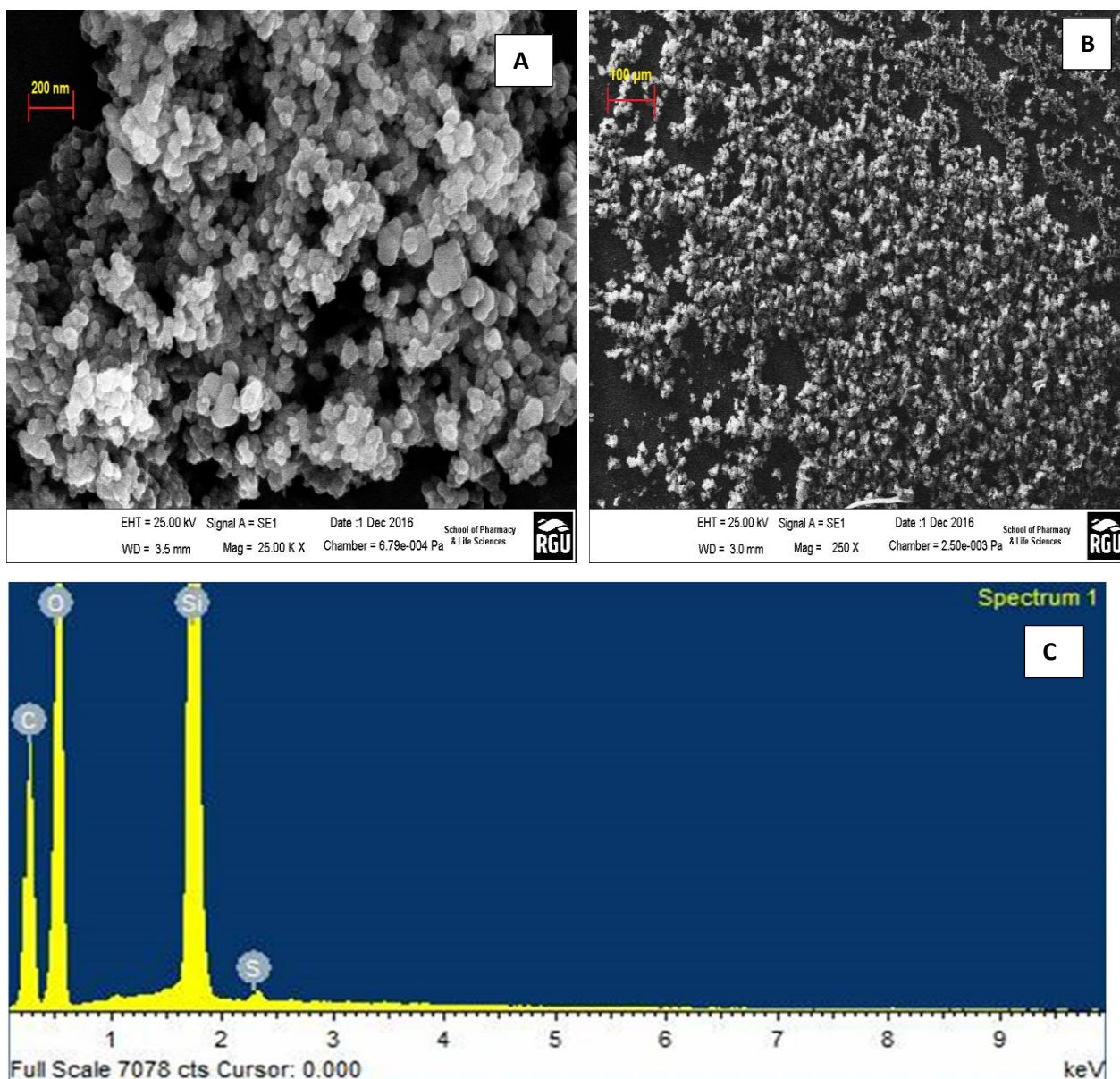


Figure 4. 1. (A) The SEM Image SiO₂ nanoparticles showing the morphology of the nanospheres and the different spectrums used for the EDX, with (B) showing the morphology of the nano-GO-SiO₂ nanocomposite on the electrode surface. (C) The EDX analysis of the SiO₂ nanoparticles and that of the nano-GO-SiO₂ nanocomposite.

4.4.2 Determination of the active surface area of the electrode

The surfaces of the bare glassy carbon electrode, SiO₂-nanoparticles-GCE, nano-GO-GCE and the nano-GO-SiO₂-nanoparticles-GCE were characterised using CV to measure KCl ($1 \times 10^{-1} \text{ mol L}^{-1}$) in $[\text{Fe}(\text{CN})_6]^{3-/4-}$ ($1 \times 10^{-3} \text{ mol L}^{-1}$) with a scan rate of 100 mVs^{-1} . This was used to investigate the electrochemical capacity of the electrodes (Figure 4.2). Comparing the voltammograms obtained from the different modifications, at a scan rate of 100 mVs^{-1} , the nano-GO-SiO₂-nanoparticles GCE presented the highest peak current, followed by the nano-GO-

GCE, SiO₂-nanoparticles-GCE and bare GCE, respectively. This outcome was in line with what was obtained when the electrodes were earlier used for the determination of GA (Figure 4.5). This shows that, the electrochemical effect of the modified electrode was consistent even when used for the measurement of [Fe(CN)₆]^{3-/4-} redox solution.

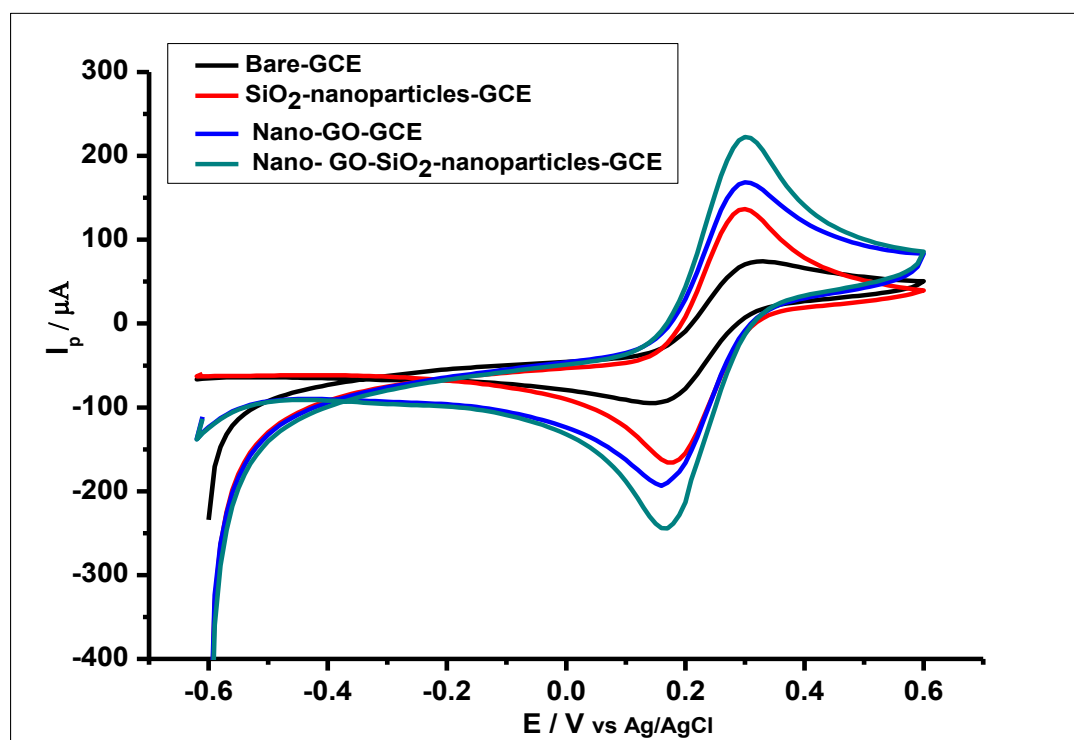


Figure 4. 2. CV voltammograms of $1.0 \times 10^{-3} \text{ mol L}^{-1} [\text{Fe}(\text{CN})_6]^{3-}$ at bare GCE, SiO₂-nanoparticles-GCE, nano-GO-GCE and nano-GO-SiO₂-nanoparticles; scan rate 100 mVs^{-1}

For the calculation of the active surface area of the four electrodes, different scan rates ranging from 10, 25, 50, 100, 150, 200, 250 and 300 mVs⁻¹ were used (Figure 4.3). From Figure 4.2 the highest peak current was obtained from nano-GO-SiO₂-nanoparticles-GCE, showing the possibility of a higher active surface area for the electrode. From the data produced during the study of the different electrodes as demonstrated in Figure 4.3 (page 113), the electroactive surface area was calculated using the Randles-Ševčík equation (Equation 4.1) for a reversible process. Using a diffusion coefficient of $7.6 \times 10^{-6} \text{ cm}^2 \text{ s}^{-1}$ for [Fe(CN)₆]³⁻ and $n=1$. (Bard and Faulkner 2001).

$$I_{pa} = (2.69 \times 10^5) n^{2/3} A D^{1/2} \nu^{1/2} C_0 \dots\dots\dots \text{Equation 4.1}$$

Where I_{pa} is the peak current, A is the electroactive area of the electrode, n is the number of electrons transferred, D is the diffusion coefficient, ν is the scan rate and C the concentration of the redox probe used. From the plot in Figure 4.3(A) inset (page 110), that represents the nano- GO-SiO₂-GCE, the linear regression equation was $I_p (\mu A) = 27.309 \nu^{1/2} (mVs^{-1}) - 58.896$, with $R = 0.9972$. Using the linear regression equations for I_p vs $\nu^{1/2}$ (square root of scan rate) plots of the other electrodes and the Randles-Ševc'ik equation for a reversible process, the electroactive areas for all the electrodes were calculated. Thus, slopes of $0.273 \times 10^{-4} A \nu^{-1/2} D^{1/2}$ for nano-GO-SiO₂-nanoparticles-GCE, $0.227 \times 10^{-4} A \nu^{-1/2} D^{1/2}$ for nano-GO-GCE, $0.047 \times 10^{-4} A \nu^{-1/2} D^{1/2}$ for SiO₂-GCE and $0.193 \times 10^{-4} A \nu^{-1/2} D^{1/2}$ for GCE generated electroactive surface areas of 0.368 cm², 0.306 cm², 0.063 cm² and 0.026 cm² respectively as seen in Table 4.1 (These calculations were done as described in Appendix II, Section 8.2.1, page 212).

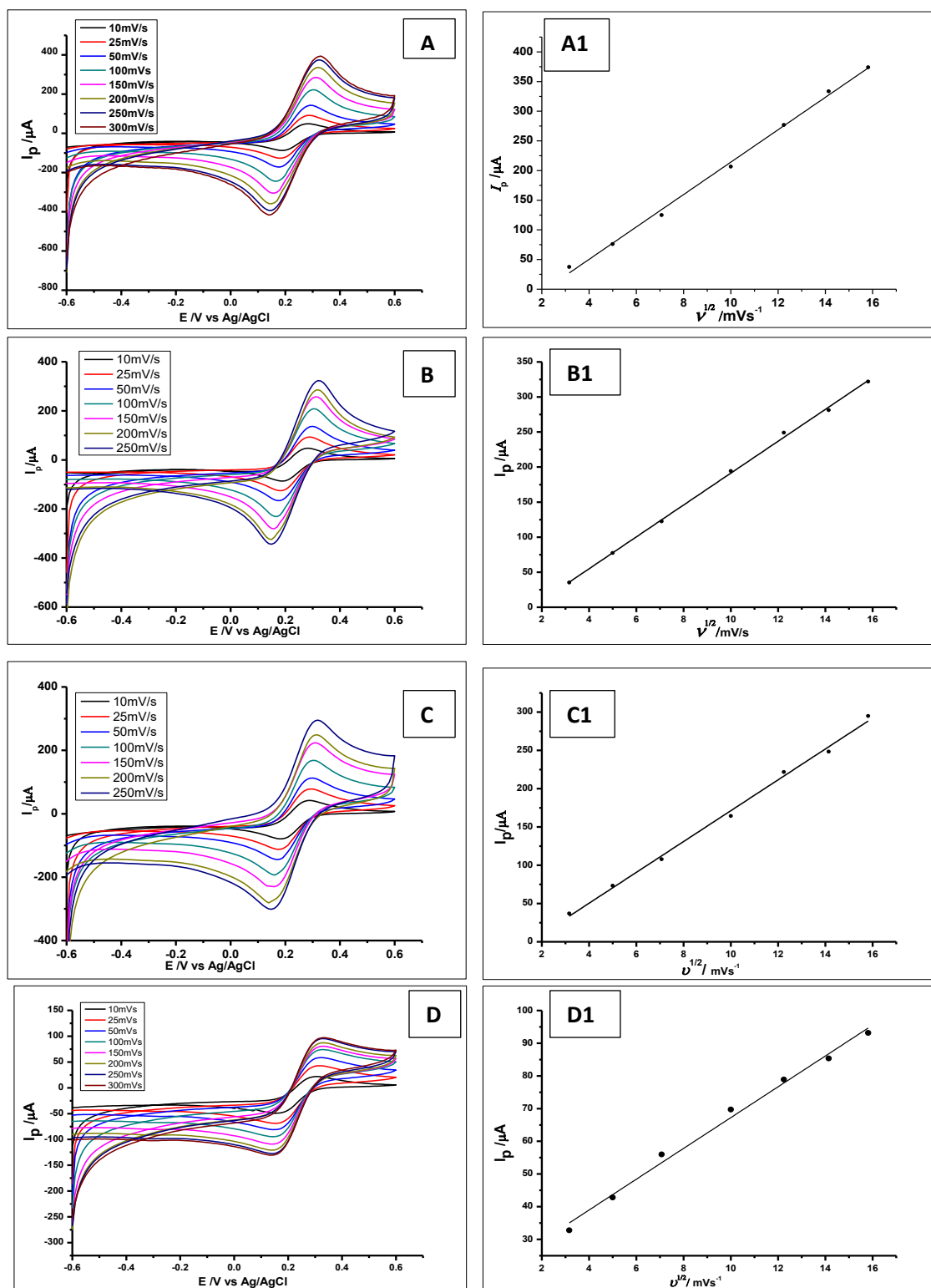


Figure 4. 3. CV voltammograms of $1.0 \times 10^{-3} \text{ mol L}^{-1} [\text{Fe}(\text{CN})_6]^{3-}$ at (A) nano-GO-SiO₂-nanoparticles (B) nano-GO-GCE (C) SiO₂ nanoparticles-GCE and (D) bare GCE; at different scan rates of 10, 25, 50, 100, 150, 200, 250 and 300 mVs^{-1} . (A1, B1, C1 and D1) The plot of peak currents against the square root of the scan rates used to deduce the electroactive surface area of all the individual electrodes using the Randles-Ševcik equation.

Looking at the electroactive surface areas, one can see the increased surface area of the nano-GO-SiO₂-nanoparticles-GCE as compared to the other electrodes. The increased electroactive surface area measured by the CV peak currents method, is expected to be reaction dependent. This is because, the reaction is controlled by the diffusion of the redox solution. Hence, the Nernst diffusion layer, determines the characteristics of the diffusion in the porous electrode and influences the electroactive surface area (Zhu and Zhao 2017). Therefore, the electroactive surface areas as can be seen in Table 4.1, provides increase surface for the GA interaction with the electrode and an increased porosity for the diffusion of the analyte on the surface of the electrode and the modifiers.

Table 4. 1. The different electrodes and their calculated electroactive surface area.

	Bare GCE and the Modified Electrodes	Electroactive surface area (cm²)
1	Nano-GO-SiO ₂ -nanoparticles-GCE	0.368
2	Nano-GO-GCE	0.306
3	SiO ₂ -nanoparticles-GCE	0.063
4	Bare GCE	0.026

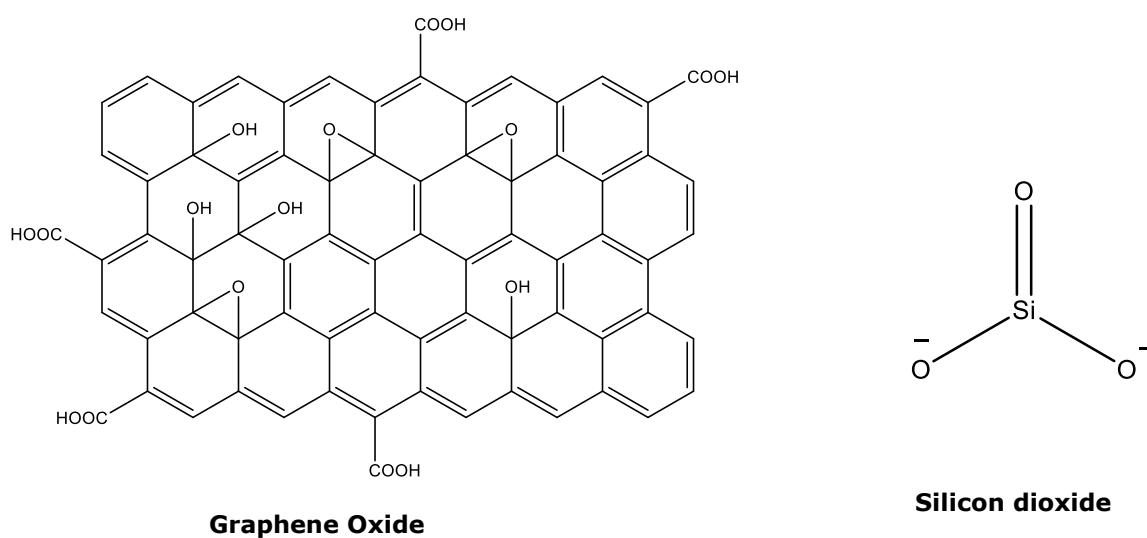
4.4.3 Fourier Transform Infrared Spectroscopy (FTIR)

Fourier Transform Infrared spectroscopy (FTIR) was also used for the characterisation of the SiO₂ nanoparticles, nano-GO (Scheme 4.1, page111) and a combination of both compounds, to show their interaction after they were physically mixed. The spectra were recorded (Figure 4.4, page 112), where the nano-GO and the SiO₂-nanoparticles showed similar spectra to those in the literature (Haeri, Ramezanzadeh and Asghari 2017; Pourhashem, Vaezi and Rashidi 2017).

For the nano-GO (Figure 4.4(A), page 112), the bands around the 3250 and 1408 cm⁻¹ were attributed to the deformed -OH bonds of graphene oxide and C-OH groups, respectively. The other band at around 1039 cm⁻¹ is associated to the C-O bond stretching and then 1724 cm⁻¹ is associated to the stretching vibration of the carbonyl groups as stated by Szabó *et al.* (2006) and Zhang and Choi (2012). Mixing the SiO₂ nanoparticles with the nano-GO (Figure 4.4(C)), created the characteristic peaks of silica nanospheres, formed at the surface of the nano-GO, where the peak at 533 cm⁻¹ and 795 cm⁻¹ are attributed to the Si-O-Si bending

and symmetric stretching vibration respectively. The main strong and broadband at 1066 cm^{-1} with the small shoulder on it is usually that of the transverse optical (TO) and longitudinal optical (LO) modes of the Si-O-Si asymmetric stretching vibration (Lee *et al.* 2010; Musić, Filipović-Vinceković and Sekovanić 2011). Meanwhile, the band observed at 953.59 cm^{-1} found on the SiO_2 nanoparticles spectrum (Figure 4.4(B)) attributed to the silanol group (Si-OH), is seen to have diminished when SiO_2 nanoparticles were combined with the nano-GO. This diminished band can be attributed to the hydrogen bonding between the silanol group (Si-OH) to the GO nanocolloids and the GA.

Furthermore, there was no significant change in the area between $1575 - 1727\text{ cm}^{-1}$ of the nano-GO, which would have demonstrated a reaction of the silica with the carbonyl groups forming Si-O-C bonds; hence confirmation of the possibility of hydrogen bonding between the SiO_2 nanoparticles, nano-GO and the GA molecules.



Scheme 4.1 Chemical Structure of Graphene oxide and Silicon dioxide

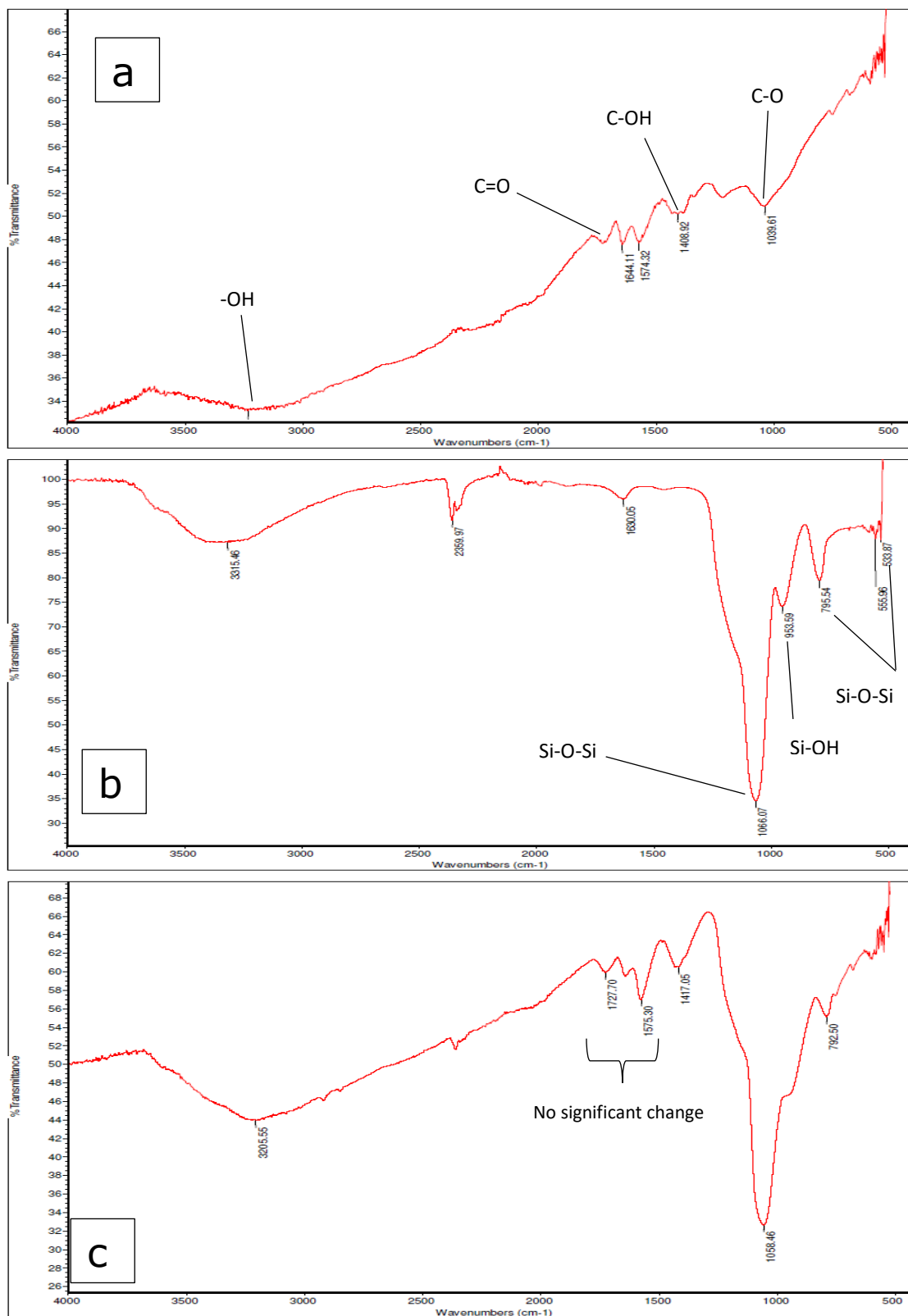


Figure 4. 4. FTIR images showing the spectra of (A) GO-nanocolloids (B) SiO₂ nanoparticles and (C) a combination of the GO-nanocolloids and SiO₂ nanoparticles

4.4.4 Electrochemical Impedance Spectroscopy (EIS)

The electrochemical impedance spectroscopy (EIS) studies of the four modified electrodes were also carried out. This was to provide information on the impedance changes of the electrodes and the electron transfer properties at the electrode interface. This study provides us with evidence of the effect of the modification on the electrode. The EIS results (Figure 4.5) showed changes in impedance at the different electrodes as portrayed by the Nyquist plots obtained. The impedance results showed changes in electron transfer resistance (R_{ct}) at the different electrodes, depicting the barrier for interfacial electron transfer between the electrodes and electrons in the $[\text{Fe}(\text{CN})_6]^{-3/4}$ redox solution. The estimate of the impedance is done by using the diameter of the semicircle, which shows from the results that nano-GO-SiO₂-GCE had a faster interfacial electron transfer due to a reduced R_{ct} .

Meanwhile, the other electrodes in the sequence of nano-GO-GCE, SiO₂-nanoparticles-GCE and bare GCE with increasing R_{ct} show a lesser electron transfer capacity, hence reduced peak currents at the voltammograms (Figure 4.2 and Fig 4.7). Using the equivalent circuit in Fig 4.5 (inset); the various electrodes showed R_{ct} values of 0.75 K Ω for the nano-GO-SiO₂-GCE, 0.85 K Ω for nano-GO-GCE, 0.87 K Ω for SiO₂-nanoparticles-GCE and 0.98 K Ω for the bare-GCE. With the relatively reduced electron transfer resistant (R_{ct}) of the nano-GO-SiO₂-GCE as compared to the other electrodes, electrons are transferred easier and faster. Hence, the increasing peak current as the electron transfer resistance reduces.

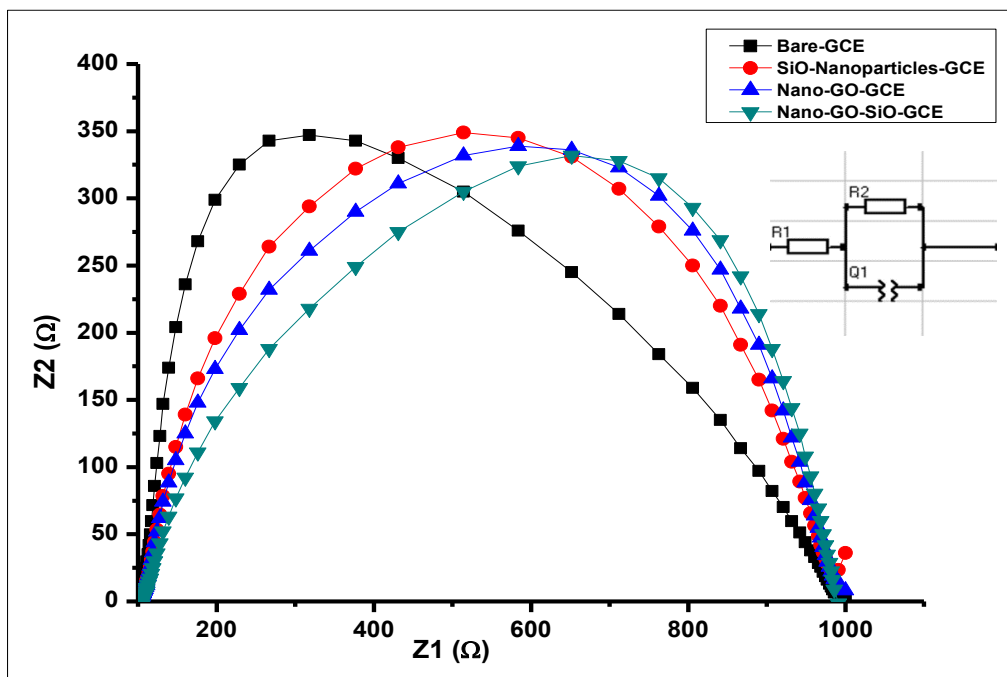


Figure 4. 5. Electrochemical Impedance spectroscopy at the modified electrodes showing the impedance of (A) nano-GO-SiO₂-nanoparticles (B) nano-GO (C) SiO₂-GCE and (D) bare-GCE in a 5 mmol L⁻¹ [Fe(CN)₆]^{3-/4+} redox solution at a frequency range of 100 kHz-0.01 Hz and a potential of 0.3 V (Inset) Equivalent circuit of the measurement

4.4.5 Effect of scan rate on GA determination

The effect and influence of the scan rate were studied towards the electrochemical determination of GA, using CV to record the voltammograms of GA (5×10^{-4} mol L⁻¹) in phosphate buffer (0.1 mol L⁻¹, pH 2.0). This was carried out by increasing the scan rates from 10, 25, 50, 75, 100, 150, 200 to 1300 mVs⁻¹ and the voltammograms recorded (Figure 4.6). With increasing scan rates, the I_p (peak current) of the GA oxidation increased as the scan rate increased. This shows that, the oxidation peak current (I_p) was linear with the scan rate (v), suggesting the reaction process at the electrode was an adsorption-controlled step. The linear regression equation was $I_p (\mu A) = 0.2516 v (mVs^{-1}) + 14$ and $R = 0.9926$. It was also observed that, with the increase in the scan rate, there was a positive shift in the peak potentials which could suggest a kinetic limitation in the reaction (Raouf, Ojani and Kolbadinezhad 2009; Tashkhourian et al. 2013).

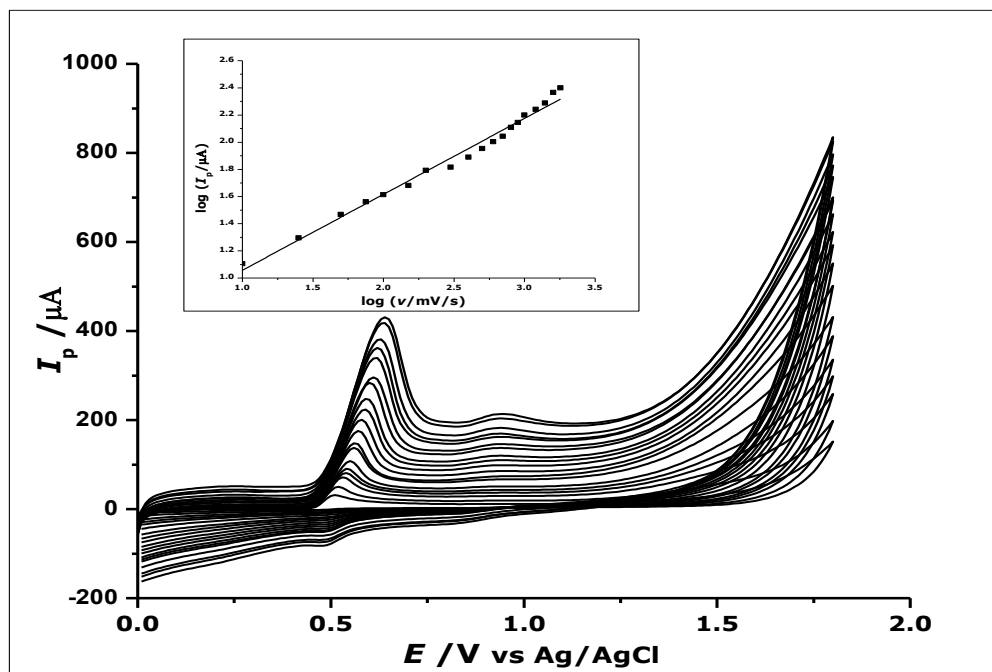


Figure 4. 6. Cyclic Voltammograms of $5.0 \times 10^{-4} \text{ mol L}^{-1}$ gallic acid in phosphate buffer of pH 2.0 determined with a nano-GO-SiO₂-nanoparticles modified glassy carbon electrode at different scan rates from 10 to 1300 mVs⁻¹. (Inset) The plot of $\log I_p$ vs $\log v$ showing a straight line

4.4.6 Oxidation of Gallic acid at bare GCE and nano-GO-SiO₂-nanoparticles modified GCE

The bare and modified GCE respectively were used as the working electrodes in this study while the platinum (Pt) electrode was the counter (auxiliary) electrode and the reference electrode was the Ag/AgCl reference electrode. Cyclic voltammetry was then used to study the oxidation of GA on the surfaces of the bare and modified glassy carbon electrodes. The electrochemical oxidation of GA in an aqueous solution in this case as earlier demonstrated (scheme 3.1, chapter 3, page 84) is a two-reaction process. This is shown in Figure 4.7 as cyclic voltammograms. The electrochemical oxidation of GA is a two electrons reaction and exhibits two peaks due to the formation of a semiquinone radical in the first peak, that gets oxidised to a quinone in the second peak (Souza *et al.* 2011). The GA oxidation mechanism while using the nano-GO-SiO₂-nanoparticles was just the same as described in section 3.4.5 in pages 82-84, where amorphous zirconium oxide nanoparticles was used.

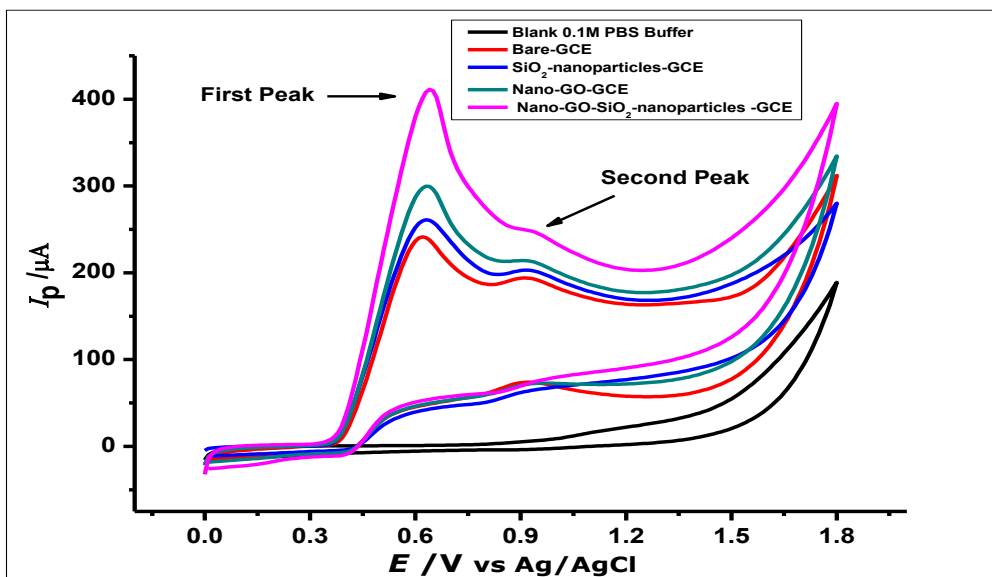


Figure 4. 7. Cyclic voltammograms of $1 \times 10^{-2} \text{ mol L}^{-1}$ GA at nano-GO-SiO₂ nanoparticles-modified GCE, SiO₂ nanoparticles-modified GCE, nano-GO-modified GCE and a bare GCE in 0.1 mol L^{-1} phosphate buffer of pH 2.0 at a scan rate of 100 mVs^{-1} (S/N=3)

The peak currents and potentials observed during the electrochemical oxidation of GA using the different electrodes as seen in Figure 4.7 depict the two equations that make up the scheme in scheme 3.1. The cyclic voltammetry showed the determination of GA ($1.0 \times 10^{-2} \text{ mol L}^{-1}$) using a bare GCE, SiO₂-nanoparticles modified GCE, nano-GO modified GCE and nano-GO-SiO₂-nanoparticles modified GCE. These were carried out in phosphate buffer ($1 \times 10^{-1} \text{ mol L}^{-1}$, pH 2) at a scan rate of 100 mVs^{-1} in an applied potential range of 0.0 to 1.8 V at room temperature. The voltammograms in Figure 4.7 showed peak currents of 241.42 ± 3.8 at 0.63 V for the bare GCE, $261 \pm 1.0 \mu\text{A}$ at 0.63 V for the SiO₂ nanoparticles-GCE, $300 \pm 3 \mu\text{A}$ at 0.63 V for the nano-GO-GCE and $411 \pm 0.9 \mu\text{A}$ at 0.64 V for nano-GO-SiO₂ nanoparticles (Table 4.2).

From the peak currents, it was observed that the bare uncoated glassy carbon electrode produced peak currents which were lower than the peak currents produced by the modified electrodes. On the other hand, no oxidation peak was observed within the potential 0.0 to 1.8 V, specifically over the ranges where we would normally see the oxidation of GA, when 1×10^{-1} phosphate buffer blank was studied with the nano-GO-SiO₂-nanoparticles modified electrode.

Table 4. 2. The peak potential and peak current values of the different electrodes and the corresponding electrolyte analysed

	Electrodes	Peak Potential (V vs Ag/AgCl)	Peak Current Ip (μA)	Electrolyte (mol L⁻¹)
1	Nano-GO-SiO ₂ -GCE	0.63	-	1 x 10 ⁻¹ PBS
2	Bare Glassy Carbon Electrode	0.63	241.42 \pm 3.8	1 x 10 ⁻² GA
3	SiO ₂ nanoparticles modified GCE	0.63	261 \pm 1.0	1 x 10 ⁻² GA
4	Nano-GO-GCE	0.63	300 \pm 3.0	1 x 10 ⁻² GA
5	Nano-GO-SiO ₂ -GCE	0.64	411 \pm 0.9	1 x 10 ⁻² GA

From these voltammograms, one could deduce that, a combination of the SiO₂ nanoparticles and the graphene oxide nanocolloids produced the best peak current. Although, when the individual nanomaterials (SiO₂ and Graphene oxide nanocolloids) were used, they showed an enhancement to the peak current produced by the bare GCE while their combination showed a 41.4% increase in peak current over the bare GCE. The increase in peak current was attributed to the increased surface area and adsorptive ability of the increased nanoparticles on the surface of the glassy carbon electrode.

This study shows that, the GO-SiO₂ combination acted in synergy to enhance the capacity of the GCE to oxidise GA. The increased surface area brought by the nanoparticles and the synergistic effect, enhances electron transfer between the GA-electrode interface. Hence, the increase in peak current as compared to the other two modifications and the bare glassy carbon electrode.

4.4.7 Electrochemical behaviour of Gallic acid at the nano-GO-SiO₂ nanoparticles-GCE

Whilst studying the oxidation of GA on the surface of these modified electrodes, GA showed two peaks during the anodic sweep between the applied potential ranges of 0.0 to 1.8 V. These peaks are found at potentials of 0.64 V and 0.91 V for the first and second peaks respectively, with no noticeable peak on the reverse cathodic sweep. The electrochemical behaviour of GA in this study are similar to other studies Tashkhourian *et al.* (2013), Kahl and Golden (2014), Tashkhourian

and Nami-Ana (2015b), Ghaani *et al.* (2016) and Raja *et al.* (2017). This electrochemical behaviour of GA could be influenced by the pH of the solution, the potential range applied for the determination and possibly the concentration of GA in the solution. This has been demonstrated in the determination of GA by Luo *et al.* (2013) where the effect of the modified electrode on the determination of GA, produced just one peak.

It should be noted that, the electrochemical behaviour of GA on the surface of the nano-GO-SiO₂-nanoparticles modified GCE showed no peaks on the reverse scan, hence showing an irreversible oxidation process. Thus, the number of electrons transferred per molecule (n), could be calculated using the equation 1.11 (Chapter 1, page 16) which states $|E_p - E_{p/2}| = 1.857RT/\alpha nF$, where E_p is the peak potential, $E_{p/2}$ the half peak potential, R the molar gas constant (8.314 JK⁻¹mol⁻¹), T the temperature in Kelvin (298K), α the electron transfer coefficient that is generally between 0.3 and 0.7 and F the Faraday constant (96,487 C mol⁻¹). Looking at Figure 4.2, the value for $|E_p - E_{p/2}|$ was determined to be 46 mV and the number of electrons was calculated to be 2.308 assuming $\alpha = 0.7$.

Hence using the Laviron's equation (Laviron 1974), the determination of electrochemical parameters like the standard electron transfer rate constant (k_s) and the electron transfer coefficient (α) of GA at the modified electrode surface can be calculated using equation 4.2

$$E_p = E^\theta - \frac{RT}{\alpha nF} \ln \frac{RTk_s}{\alpha nF} + \frac{RT}{\alpha nF} \ln v \dots\dots\dots \text{Equation 4.2}$$

Where E^θ is the formal potential (V), α is the charge transfer coefficient, n is the standard heterogeneous electron transfer rate constants. R is the molar gas constant; T is temperature and F is the Faraday constant. Based on the experimental data and voltammograms from Figure 4.7, the plot of the variation of the anodic peak potential and cathodic peak potential vs. the logarithm of the scan rate was produced as shown in Figure 4.8. One observes a straight line from scan rates above 500mVs⁻¹ relative to the logarithm of the scan rate; with a slope of 0.1635 that is equal to $2.303RT/(1-\alpha)nF$. Thus, assuming the electron transfer number is 2 based on the electrode reaction of GA, as shown above; the electron transfer coefficient would be $\alpha = 0.64$. These values demonstrate the symmetry of

the free energy curve (with respect to the reactants and products) and the work done by the nano-GO-SiO₂-nanoparticles as an electron transfer mediator for this oxidation process.

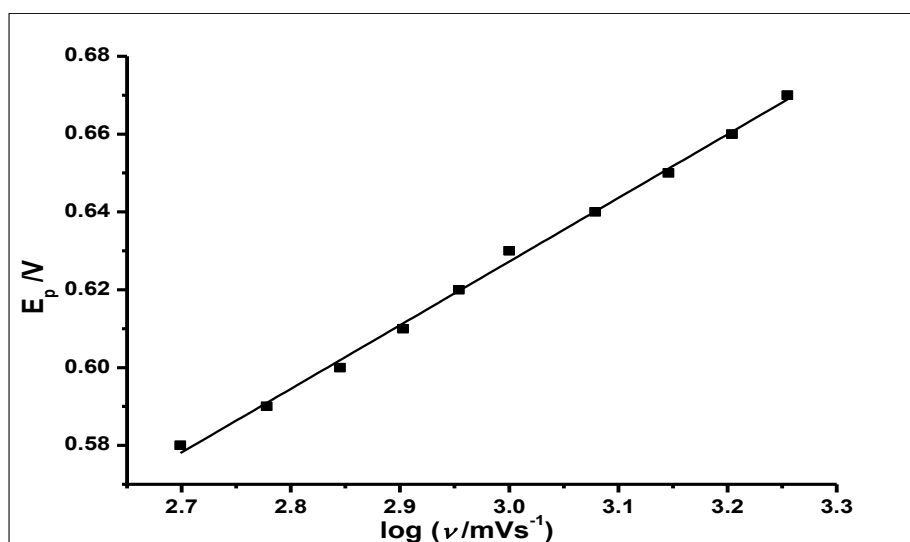


Figure 4. 8. The plot of cathodic peak potential vs log of scan rate, with a regression equation of $y = 0.1635x + 0.1368$, with R^2 value of 0.9975

4.4.8 Effect of nano-GO and SiO₂ nanoparticles concentrations in the modifying mixture

The effect of the changes in concentration of the nano-GO and the SiO₂ nanoparticles in the modifying mixture was investigated. The following concentration combination of graphene oxide nanocolloids and silicon oxide nanoparticles (0.1 mg/mL SiO₂ nanoparticles + 2 mg/mL nano-GO; 1 mg/mL SiO₂ nanoparticles + 0.2 mg/mL GO; 1 mg/mL SiO₂ nanoparticles + 2 mg/mL GO and 5 mg/mL SiO₂ nanoparticles + 2 mg/mL GO) were used for the modification of the glassy carbon electrode and used to determine GA (1×10^{-2} mol L⁻¹). The combinations studied were fixed amounts of nano-GO (2 mg) with changing concentrations of SiO₂ nanoparticles, followed by 1 hr sonication to allow uniform dispersion and bonding of the two compounds. From the results (Figure 4.9), the combination of 1 mg/mL SiO₂ nanoparticles + 2 mg/mL GO-nanocolloids, showed the highest peak current (I_p) of 411.7 μ A; hence it was the combination which was subsequently used for the modification of the GCE.

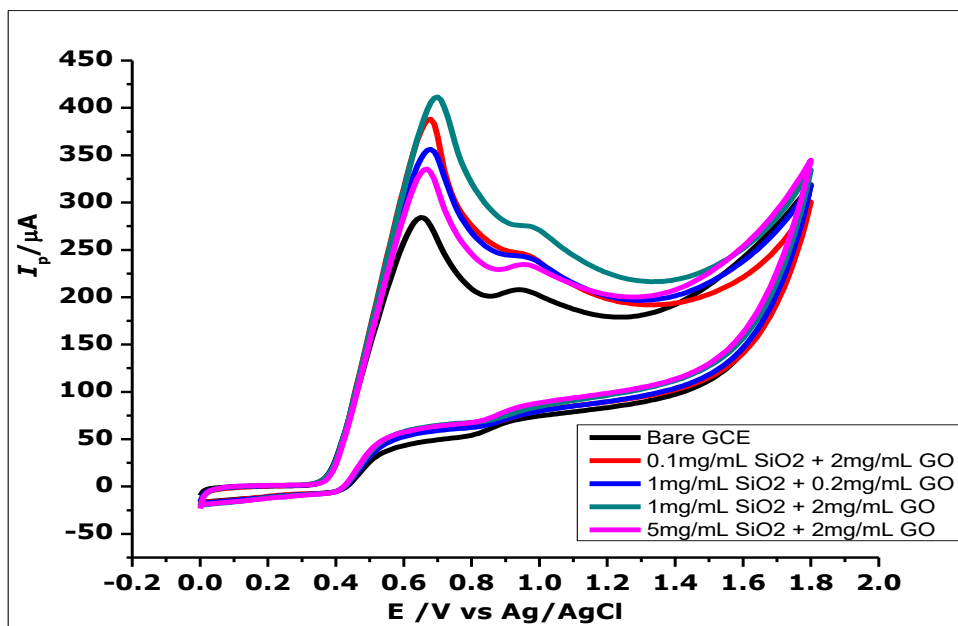


Figure 4. 9. Voltammograms showing changes in the constitution of the nano-GO-SiO₂-nanoparticles used to determine $1 \times 10^{-2} \text{ mol L}^{-1}$ GA in 0.1 mol L^{-1} phosphate buffer at pH 2.0 using CV at a scan rate of 100 mV/s^{-1} .

4.4.9 Effect of volume of nano-GO-SiO₂ nanoparticles on GCE

The amount of nano-GO-SiO₂-nanoparticles drop cast on the glassy carbon electrode and its effect on the determination of GA ($1 \times 10^{-2} \text{ mol L}^{-1}$) in phosphate buffer ($1 \times 10^{-1} \text{ mol L}^{-1}$, pH of 2.0), using CV at a scan rate of 100 mVs^{-1} was investigated. Volumes of $2 \mu\text{L}$ to $5 \mu\text{L}$ of nano-GO-SiO₂-nanoparticles were studied, and it was observed that, the $4 \mu\text{L}$ and $5 \mu\text{L}$ of nano-GO-SiO₂-nanoparticles gave the highest peak currents (I_p) of $403.03 \mu\text{A}$ and $405.18 \mu\text{A}$ respectively (Figure 4.10). The volume of the mixture used for the GCE modification for further experiments was $5 \mu\text{L}$ as further increases of $6 \mu\text{L}$ and $7 \mu\text{L}$ made no difference in peak current.

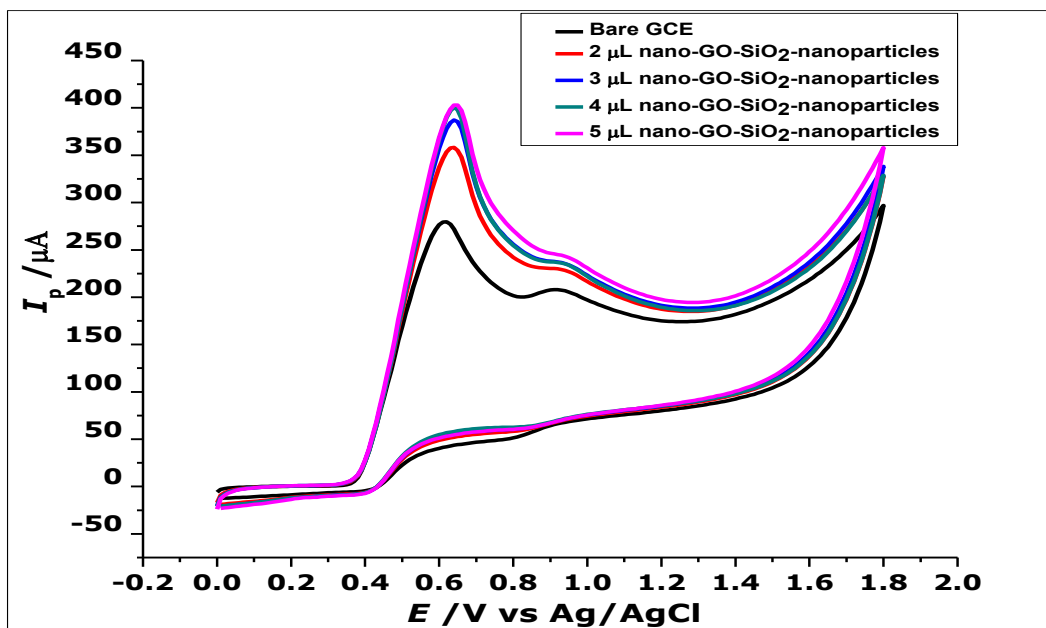


Figure 4. 10. Voltammograms showing the effect of changing volumes of nano-GO-SiO₂-nanoparticles in the determination of $1 \times 10^{-2} \text{ mol L}^{-1}$ GA in a $1 \times 10^{-1} \text{ mol L}^{-1}$ phosphate buffer at pH 2.0 using CV at a scan rate of 100 mVs^{-1}

4.4.10 Effect of adsorption time

The effect of the adsorption of GA to the electrode with time was demonstrated by the detection of GA ($1 \times 10^{-3} \text{ mol L}^{-1}$) in a 0.1 mol L^{-1} phosphate buffer of pH 2.0 at room temperature using DPV at a scan rate of 100 mVs^{-1} .

The voltammograms in Figure 4.11(A) and 4.11(B) demonstrates the adsorption of GA onto the nano-GO-SiO₂-nanoparticles GC electrode by showing a sharp increase after the first scan to an optimum by the 4th to 5th minute, reaching saturation of the GA on the electrode after 6 minutes. This phenomenon confirms the proposed interaction mechanism of GA and the nano-GO-SiO₂-nanoparticles as being an adsorption reaction, and is in agreement with the work of Tashkhourian and Nami-Ana (2015). They suggested an increasing accumulation time up to 5 mins, which reaches a limiting peak current, where further increase in accumulation time shows no change in the current response. Attributing the phenomenon to saturated adsorption of GA on the SiO₂ nanoparticles modified electrode.

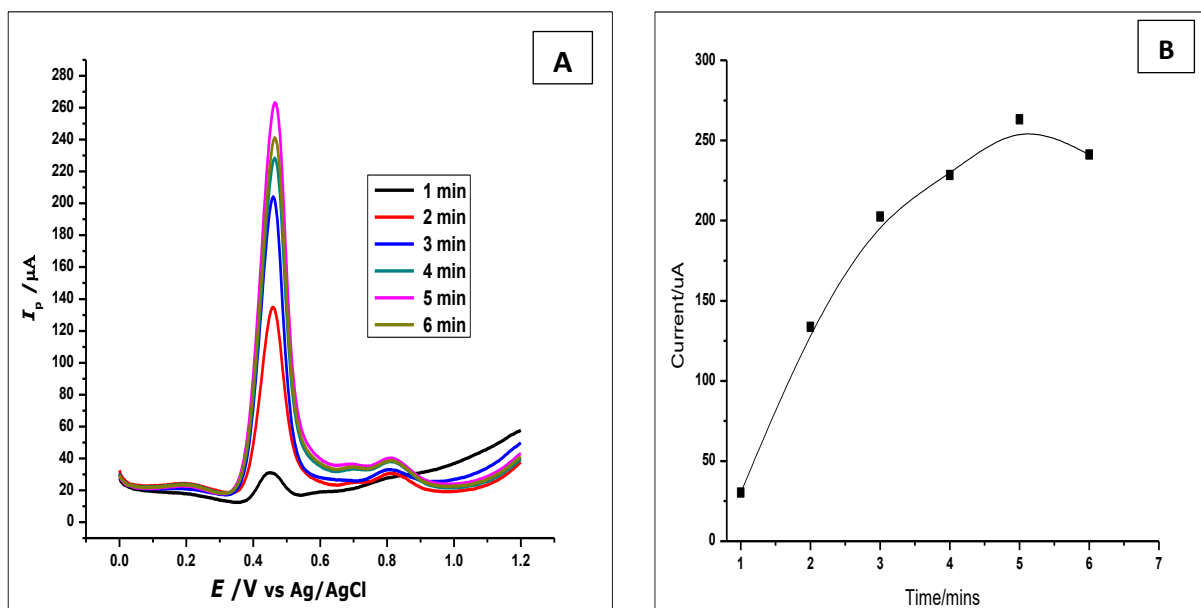


Figure 4. 11. (A) DPV voltammograms showing the effect of adsorption time in the determination of $1 \times 10^{-3} \text{ mol L}^{-1}$ GA in a 0.1 mol L^{-1} phosphate buffer of pH 2.0 at a scan rate of 100 mVs^{-1} (B) and the plots showing the same effect of adsorption time

4.4.11 Effect of pH on Gallic Acid Oxidation

The effect of the pH on the GA solution towards their electrochemical activity and the activity of the nano-GO-SiO₂-GCE was investigated. The electrochemical response of GA ($1 \times 10 \text{ mol L}^{-4}$) was studied with pH ranging from 2.0 to 8.0 using cyclic voltammetry at a scan rate of 100 mVs^{-1} , in phosphate buffer ($1 \times 10^{-1} \text{ mol L}^{-1}$). The oxidation peak and the peak potential (E_p) showed (Figure 4.12), they have been influenced by the pH. From the voltammograms, pH of 2.0 showed a well-shaped oxidation peak, with the highest peak current (I_p) of $33.72 \mu\text{A}$. This can be attributed to the 4.4 pKa of GA, which is a weak organic acid. Hence at a pH of 2.0, the compound tends to be in its most stable form and oxidation reaction would be easier and effective.

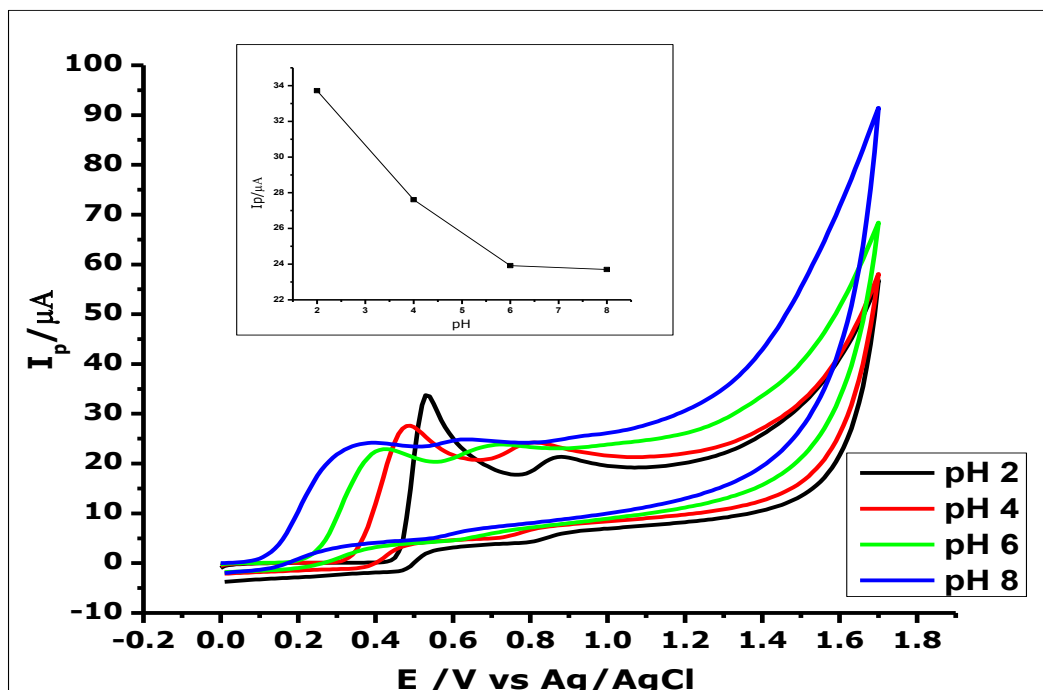


Figure 4. 12. Cyclic Voltammograms showing the effect of pH on the electrochemical behaviour of $1 \times 10^{-4} \text{ mol L}^{-1}$ Gallic Acid. (Inset). The plot of the Peak Current (I_p) against different pH values, showing the effect of pH on the electrochemical behaviour of $1 \times 10^{-4} \text{ mol L}^{-1}$ Gallic acid using bare Glassy Carbon Electrode at a scan rate of 100 mVs^{-1}

On the other hand, as the pH increases, there was a reduction in the peak current (Figure 4.13). For example, at pH 8 the lowest peak current of $23.70 \mu\text{A}$ was observed. There was also a negative shift of the oxidation peak potential from 0.56 V downwards to 0.31 V , as can be seen in Figures 4.12 and 4.13, with a gradual broadening of the oxidation peak/peak area with the increase in pH.

The relationship between the pH and the peak potential E_p shows a good linear relationship as can be seen in Figure 4.13 in the pH range of 2.0 to 8.0, with a linear regression equation of $E_{pa} = 0.705 - 0.0535 \text{ pH}$, with $R^2 = 0.9960$. The slope of the regression line being about 54 mV/pH is comparable to the Nernstian value of 59 mV/pH at 25°C , for an equal number of proton and electron transfer reactions. The pH and peak potential relationship is thus consistent with the two protons/two electrons reaction, which is consistent with other literature data (Tashkhourian *et al.* 2013; Tashkhourian and Nami-Ana 2015). Based on the results, the pH condition selected as the most appropriate for the oxidation of GA in this experiment was, the pH of 2.0. This demonstrates that the oxidation of GA on nano-GO-SiO₂ nanoparticles is at its optimal when done at a pH value of 2.0.

However, Yilmaz, Kekillioglu and Mert (2013) in their work, while using three different types of carbon materials for their carbon paste electrodes, oxidised GA at an optimal pH of 7.0. Meanwhile, Su and Cheng (2015) in the determination of GA using screen-printed carbon electrode modified with poly(melamine) film, carried out the GA oxidation at a pH 3.0. On the other hand Liang *et al.* (2016) determined GA at a pH of 4.0 using a gold microclusters/sulfonate functionalized graphene modified-GCE. Meanwhile, Badea *et al.* (2019) recently used a Lazar ORP-146C reduction-oxidation microsensor and a screen-printed sensor for the electrochemical determination of GA. They tested the two electrodes at pH values of 5.8, 7.0 and 8.0 and found that the redox microsensor was more sensitive at pH 8.0, and the screen-printed electrode showed better sensitivity at pH 7.0. All these confirm the fact that, pH influence of the determination of GA is electrode dependent.

This may be attributed to the fact that, GA with a pKa of 4.4 being a weak organic acid, is most stable or is in its un-dissociated state, at pH 2.0, which was the most appropriate for the adsorption of GA on to SiO₂ as described by Milonjić, Zhigunova and Pavasović (2007).

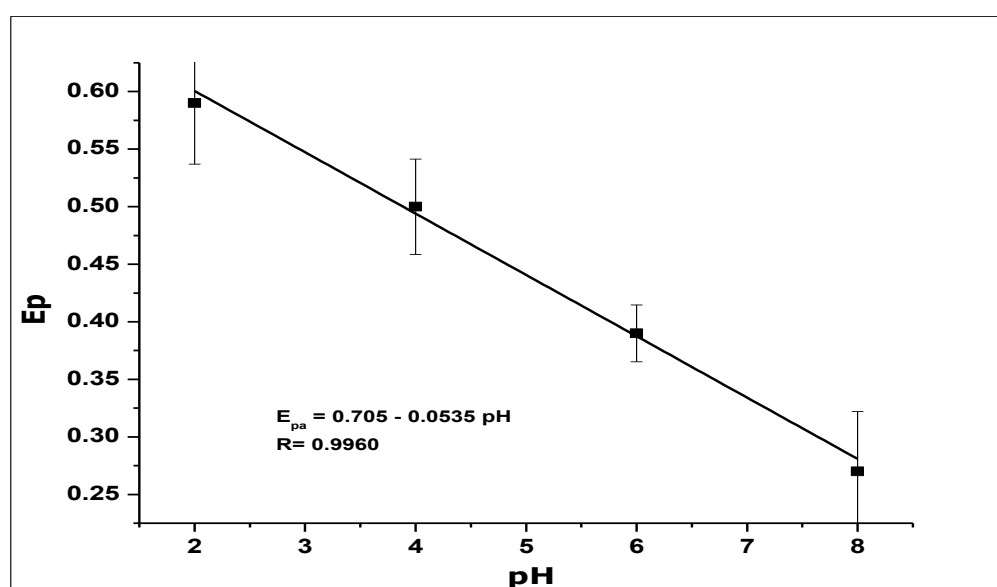


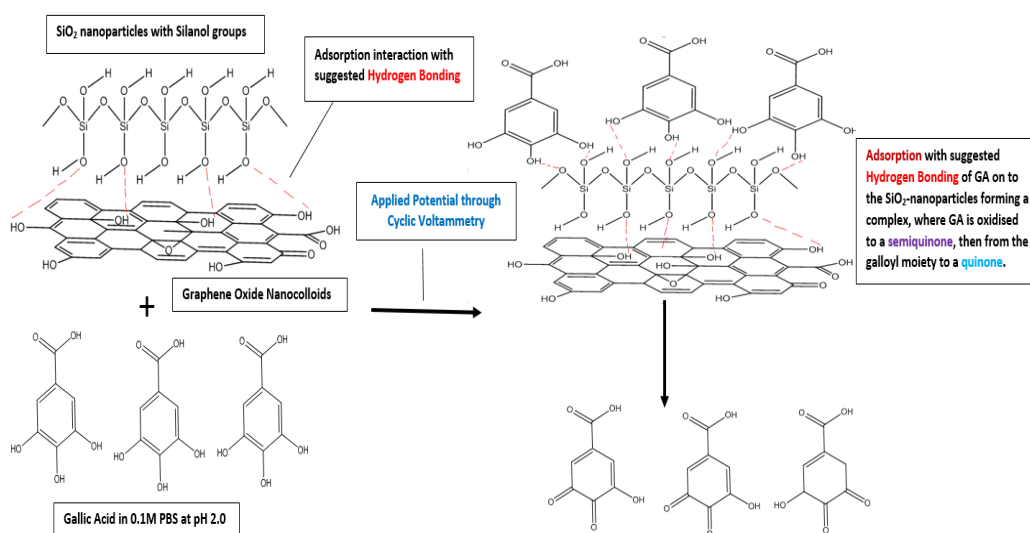
Figure 4. 13. The plot of pH on the Peak Potential E_p on detection of 1×10^{-4} mol L⁻¹ Gallic acid using nano-GO-SiO₂-GCE at a scan rate of 100mVs⁻¹

4.4.12 The Mechanism of the Interaction between nano-GO-SiO₂-nanoparticles-GCE and Gallic Acid solutions

The chemical effect of nano-GO-SiO₂ nanoparticles towards the oxidation of GA and the enhancement of the voltammograms can be attributed to the structural, chemical and physical properties of GO and SiO₂. The SiO₂ nanoparticles with silanol groups bind with the GO-nanocolloids via hydrogen bonding as depicted in Scheme 4.2. The presence of hydrogen bonds on the surface of SiO₂ under aqueous conditions, contributes to the electrical transport properties of graphene oxide on SiO₂ surface structures. While adsorbed on the surface of the graphene oxide nanocolloids, SiO₂ nanoparticles also creates a substrate for the adsorption of GA.

The mechanism proposed for this observation, is based on the work of S. Milonjić (Milonjić 1999; Milonjić, Zhigunova and Pavasović 2007) and colleagues, where they investigated the interaction of SiO₂ and GA. They found that, SiO₂ and GA underwent an adsorption interaction which was linked to the pK_a (4.41) of GA, where the amount of adsorbed GA increases with increasing equilibrium concentration of GA in the solution or decreasing pH of the solution.

Meanwhile, there was a decrease in the amount of GA adsorbed when there was an increase in the pH of the solution.



Scheme 4.2. Scheme showing the interaction of SiO₂ nanoparticles and Graphene oxide nanocolloids as they interact with gallic acid by adsorption with a suggestion of hydrogen bonding, as applied potential is sent through the modified electrode.

The chemical behaviour of SiO₂ and GA was then explained using the pK_a of GA molecules and the surface charge of the silica powder. It should be noted that, the adsorption of weak organic electrolytes like GA on the surface of amphoteric solids like silica depends amongst other things on the degree of dissociation of the electrolyte and the surface charge of the solid; which all depends on the pH of the aqueous solution (Milonjić, Zhigunova and Pavasović 2007). The point of zero charge values (pH_{pzc}), for various forms of SiO₂ lie between the pH range of 2.5-3.6 (Milonjić 1999); Milonjić, Zhigunova and Pavasović 2007); hence, when the pH is below the pH_{pzc} the surface of SiO₂ becomes positively charged, while in a pH higher than the pH_{pzc} the surface becomes negatively charged. With a pK_a of a weak acid, GA at pH values less than 3.5 is mostly un-dissociated or in its stable form and dissociates when the pH increases.

It can, therefore, be interpreted that, the maximum adsorption of GA to SiO₂ occurs at a pH_{pzc} where the silica surface is uncharged, and the GA molecule is un-dissociated. Hence, in a phosphate buffer solution of pH 2.0 < 3.5, where the electrochemical determination took place, GA adsorbed on the SiO₂. Meanwhile, at pH > 3.5, GA's dissociation increases leading to an increase in the negative ion C₆H₂ (OH)₃ COO⁻ concentration and a negatively charged SiO₂ surface. With the increase in the negative molecules and negative surface, the adsorption between GA and SiO₂ nanoparticles decreases due to the repulsive negative-negative forces in the solution.

On the other hand, the GO-nanocolloids possess excellent electrocatalytic properties due to their favourable electron mobility and unique surface properties. This include high specific surface area and one-atom thickness that would accommodate active species like GA and facilitate their electron transfer (Luo *et al.* 2010). The capacity of GO to be chemically or physically functionalised, showing non-covalent π-π (π-stacking), cation-π, van der Waals or hydrogen bonding (Dreyer *et al.* 2015) formed the bases of this proposed mechanism. The SiO₂ nanoparticles physically functionalise the GO-nanocolloids, thus enhancing the availability of the nanosized surface area for electron transfer; whilst the adsorption of the GA to SiO₂ and the nanosized area provides better mass transport of the GA to the electroactive sites on the electrode surface. Moreover, the conductive GO-nanocolloids supports and facilitates the efficient collection and

transfer of electrons to the GCE surface as described by Chen and colleagues (Chen, Feng and Li 2012).

Furthermore, an alternative and plausible explanation for the phenomenon observed in the synergistic effect of the nano-GO and SiO₂ nanoparticles could be that of voltammetry at a three-phase junction, discussed by Oldham and Scholz *et al.* in their work (Oldham 1998; Doménech-Carbó 2015; Scholz, Schröder and Doménech-carbó 2015; Tonle *et al.* 2015). In which, they suggested that, when insoluble insulating crystals like SiO₂ nanoparticles adhere to an electrode, the three-phase junction (where the electrolyte solution, electrode and crystal meet), is the only feasible site for an electrochemical reaction to occur. This might then mean the redox process of GA might have occurred at the three-phase junction between graphene oxide nanocolloids and SiO₂ nanoparticles.

4.4.13 Linear detection range

Differential pulse voltammetry was used for the investigation of different concentrations of GA, to determine the limit of detection (LOD) at a scan rate of 100 mVs⁻¹ and pulse amplitude of 80 mV. With the increase in concentration studied, the detection range was found to be in the range of 6.25 x 10⁻⁶ to 1.0 x 10⁻³ mol L⁻¹; there was a correlated increase in the peak current, whilst using the nano-GO-SiO₂ nanoparticles modified electrode. The measurements produced voltammograms that can be seen in Figure 4.14, the peak current increased proportionally with increasing concentration of GA. Using differential pulse voltammetry in this measurement, produced two oxidation peaks at 0.45 V and 0.8 V since different concentrations of GA were being determined.

Using the first main GA oxidation peak, the analytical calibration graph as seen in Figure 4.15, showed a linear relationship between the peak current and the increase in GA concentration, producing a linear regression equation, where $I_P = 221.02C + 9.426$ (I_P : μA , C : mmol^{-1} and $R^2 = 0.9956$) within a range of 6.25 x 10⁻⁶ to 1.0 x 10⁻³ mol L⁻¹. The limit of detection (LOD) defined as $(3 \times \text{Std}_{\text{Blank}})/m$, where $\text{Std}_{\text{Blank}}$ is the standard deviation of the blank and m is the slope; was found to be 2.09 x 10⁻⁶ mol L⁻¹.

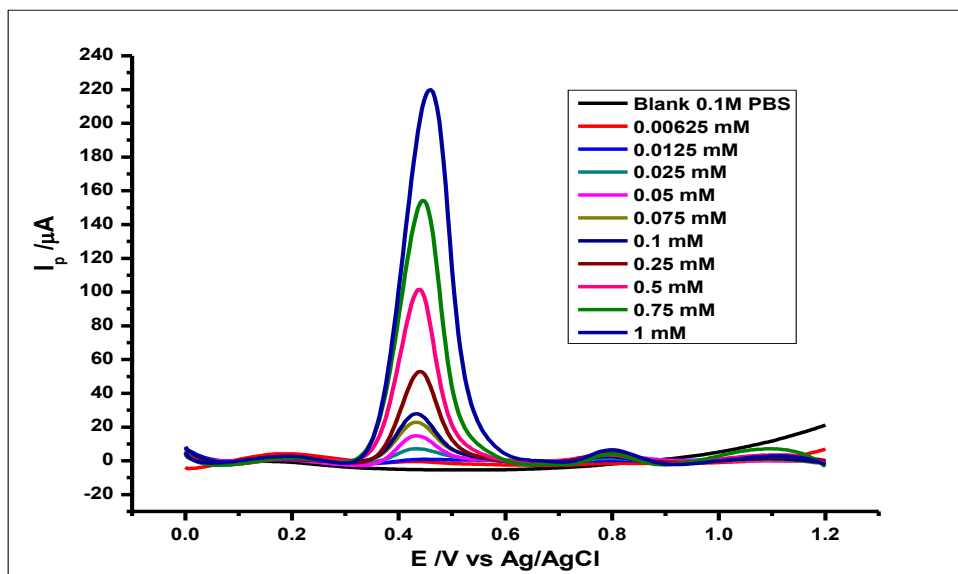


Figure 4. 14. Differential pulse voltammograms of various concentration of GA at nano-GO-SiO₂-nanoparticles in a 0.1 mol L⁻¹ phosphate buffer at pH 2.0 at a scan rate of 100 mVs⁻¹, with voltammograms (a-k) that correspond to the following concentrations a) 0.0, b) 0.00625 mmol L⁻¹, c) 0.0125 mmol L⁻¹, d) 0.025 mmol L⁻¹, e) 0.05 mmol L⁻¹, f) 0.075 mmol L⁻¹, g) 0.1 mmol L⁻¹, h) 0.25 mmol L⁻¹, i) 0.5 mmol L⁻¹, j) 0.75 mmol L⁻¹, k) 1 mmol L⁻¹.

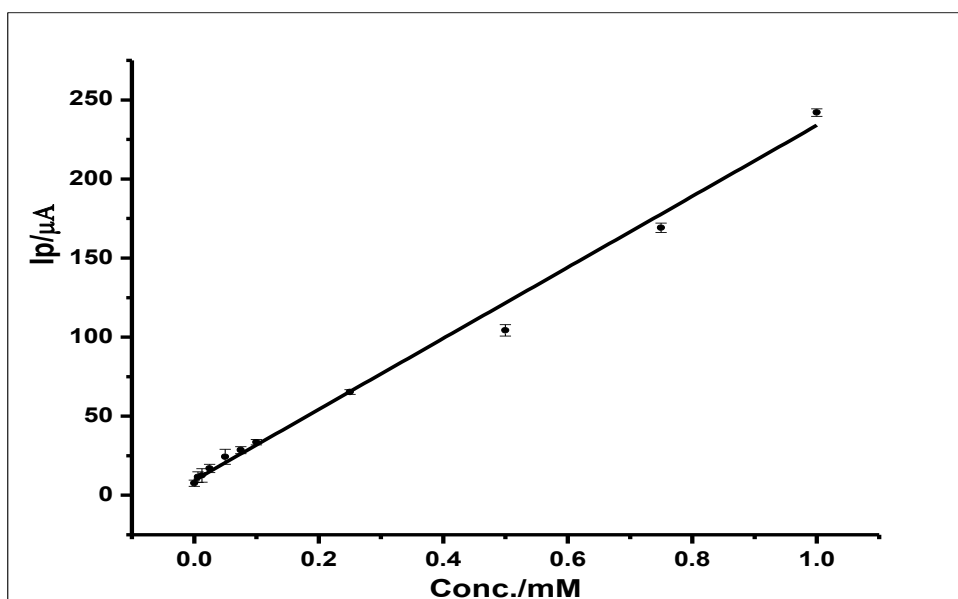


Figure 4. 15. The calibration curve for the determination of Gallic Acid

4.4.14 Reproducibility and repeatability test

The reproducibility of the nano-GO-SiO₂ modified glassy carbon electrode was investigated, by using the modified electrode to determine the oxidation peak current produced by 1.0 × 10⁻³ mol L⁻¹ GA. The oxidation peak currents produced by eight replicates of 1.0 × 10⁻³ mol L⁻¹ GA independently measured with eight different electrodes, produced peak currents with a relative standard deviation of 3.8%, confirming good reproducibility.

Meanwhile, the repeatability of the method was investigated by using a nano-GO-SiO₂-modified glassy carbon electrode, for eight repetitive determination of 1.0 × 10⁻³ mol L⁻¹ GA. The relative standard deviation of the oxidation peak current was found to be 2.92%, thus showing good repeatability of the method.

4.4.15 Stability of the electrode

The stability of the nano-GO-SiO₂-nanoparticles modified glassy carbon electrode was also investigated. The electrodes were stored for 30 days and were subsequently used for the determination of GA (1.0 × 10⁻³ mol L⁻¹). Then the oxidation peak currents produced from the readings of the first day and those of the 30th day showed an RSD of 6.58%; depicting relatively good stability, as shown in Figure 4.16. However, there was a potential shift with the second oxidation peak of GA. This can be attributed to a kinetic limitation at the surface of the electrode due to the time the electrode has been stored. This could also have been because of a slow electron transfer kinetic at the face of the electrode. Although, with the determination of GA using DPV, the first oxidation peak is the peak used for the quantification.

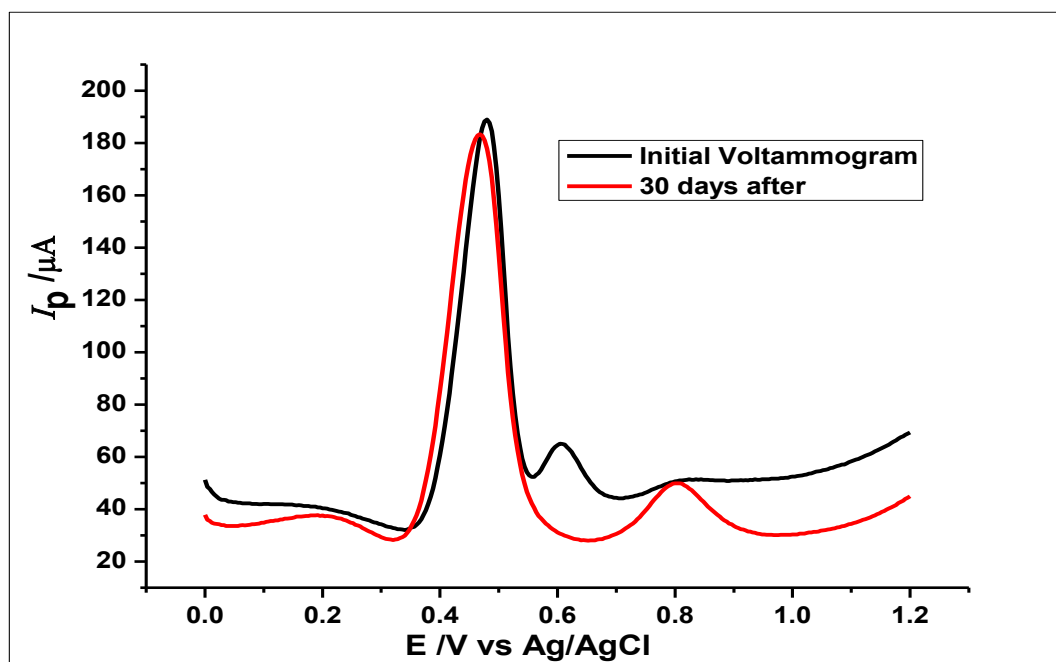


Figure 4. 16. Differential Pulse Voltammograms depicting the stability of the modified electrode after 30 days

4.4.16 Selectivity test

The selectivity of the modified glassy carbon electrode was tested, by the simultaneous detection of GA and Uric acid (UA) in phosphate buffer ($1 \times 10^{-1} \text{ mol L}^{-1}$, pH of 2.0) using CV at a scan rate of 100 mVs^{-1} , at room temperature. This was done by the addition of GA (0.48 mmol L^{-1}) into a 10 mL cell of Uric acid (0.36 mmol L^{-1}) and voltammograms recorded, as seen in Figure 4.17. The concentration of 0.48 mmol L^{-1} of GA was used because, it was at this concentration that, a significant distinction of the voltammograms of GA and UA, was observed (See Figure 4.17). GA and UA showed distinct peaks at approximately 0.51 V and 0.64 V respectively, with the smaller second GA oxidation at a peak potential of 0.88 V. Meanwhile, the voltammogram showing UA on its own without GA, showed an oxidation peak at 0.64 V and GA on its own show oxidation peaks at 0.5 V for the first peak and at 0.88 V for the second smaller peak (Figure 4.17).

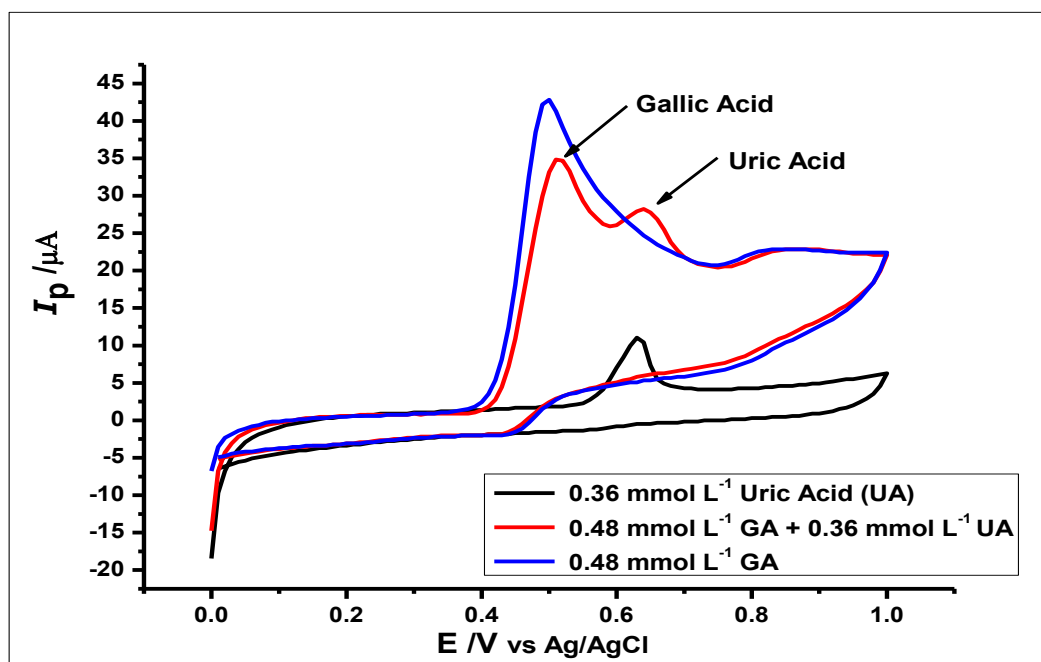


Figure 4. 17. Cyclic Voltammograms showing the 0.36 mmol L⁻¹ Uric acid concentration, 0.48 mmol L⁻¹ GA and a mixture of the two concentrations of GA and UA in a 0.1 mol L⁻¹ phosphate buffer solution at a pH 2.0 at scan rate 100 mVs⁻¹

To confirm the selectivity of the electrode, the UA concentration was kept constant at 0.36 mmol L⁻¹ in a 10 mL voltammetric cell and then aliquots of 100 μ L of 10 mmol L⁻¹ GA were intermittently added and then vigorously stirred for 2 mins. Then voltammograms were recorded, as can be seen in Figure 4.18. In this case, the nano-GO-SiO₂-nanoparticles modified GCE produced voltammograms where increasing GA concentration, showed a proportional increase in the peak current. Hence, Figure 4.18 (inset) shows a linear relationship between the peak current and the increase in GA concentration, producing a linear regression equation, where $I_p = 13.04C + 1.4118$ (I_p : μ A, C: mmol⁻¹ and $R^2 = 0.9915$) within a range of 0.1 mmol L⁻¹ to 0.48 mmol L⁻¹.

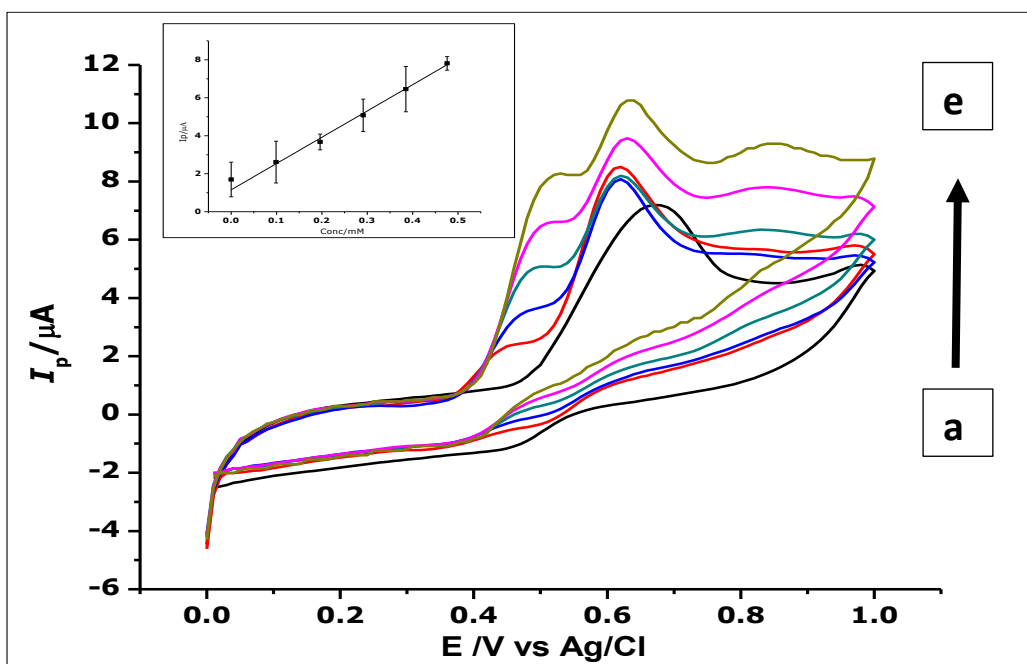


Figure 4. 18. Cyclic Voltammograms showing the constant 0.36 mmol L^{-1} UA concentration and increasing GA concentration from 0.1 to 0.48 mmol L^{-1} (a-e) in a 0.1 mol L^{-1} phosphate buffer at pH 2.0 at a scan rate of 100 mVs^{-1} . (Inset) A graph showing the increasing concentration of GA against the increasing peak current in a constant UA concentration of $3.6 \times 10^{-4} \text{ mol L}^{-1}$

4.4.17 Interference study

The interference of various species in the determination of GA ($1 \times 10^{-3} \text{ mol L}^{-1}$) was also investigated. This was carried out by adding different amounts of foreign ions to a known quantity of the analyte as it was being determined. The foreign species that were used in this case for the investigation of interference were K^+ , Ca^{2+} , Fe^{3+} , and Na^+ , then ascorbic acid, caffeine, caffeic acid and quercetin, respectively. The procedure and the rationale for using the mentioned species for the interference study, were same as earlier discussed, while carrying the interference study on amorphous zirconia nanoparticles-CPE (section 3.4.16, pages 98-99). With relative standard error values of less than 5% (Table 4.3), these ions did not interfere with the determination of GA at the first GA oxidation peak, as depicted in Figure 4.19 and Table 4.3. However, there were some minor changes in the second GA oxidation peak, the latter is not normally used for electrochemical determination of GA, but could be attributed to interference on the second oxidation reaction of GA. Normally the oxidation seen at the first peak is the main GA oxidation. This is attributed to the oxidation of the galloyl group in

GA into a semiquinone radical. The semiquinone radical is further oxidised into a quinone as shown in Chapter 3, Scheme 3.1.

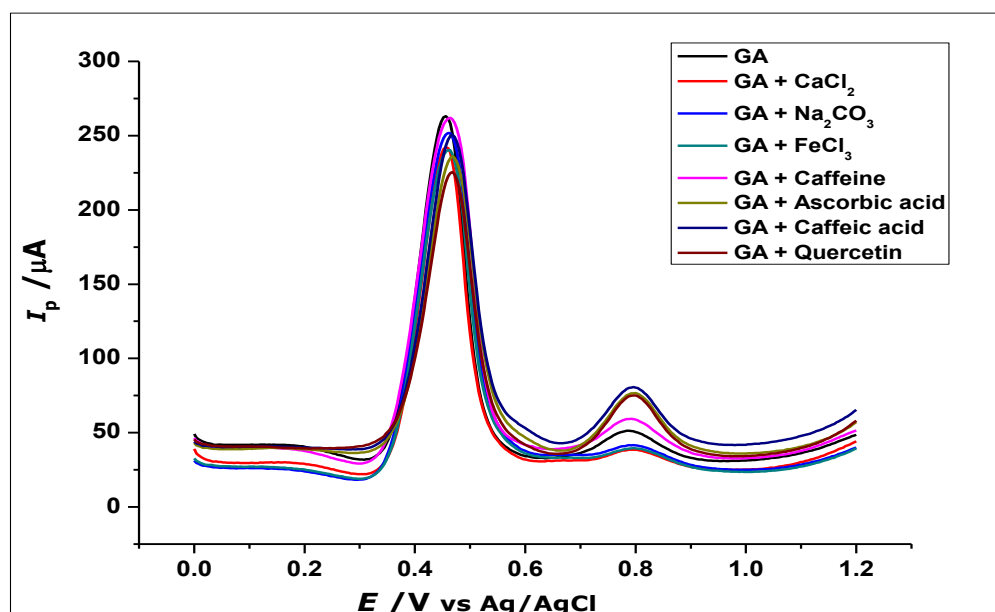


Figure 4. 19. DPV Voltammograms of $1 \times 10^{-3} \text{ mol L}^{-1}$ Gallic acid with different concentrations of some known interfering compounds in 0.1 mol L^{-1} phosphate buffer at pH 2.0 and a scan rate of 100 mVs^{-1}

Table 4. 3. Effects of various substances on the determination of $1 \times 10^{-3} \text{ mol L}^{-1}$ Gallic acid

Interfering Species	Concentration of GA in Solution (mol L^{-1})	Relative Standard Deviation (%)
Ca^{2+}	1×10^{-1}	± 3.70
Na^{+}	1×10^{-1}	± 1.29
Fe^{3+}	1×10^{-1}	± 1.93
Cl^{-}	1×10^{-1}	± 2.01
CO_3^{2-}	1×10^{-1}	± 1.45
Ascorbic acid	1×10^{-3}	± 0.15
Caffeic acid	1×10^{-3}	± 2.80
Caffeine	1×10^{-3}	± 3.89
Quercetin	1×10^{-3}	± 4.64

4.4.18 Analytical application of modified electrode to determine the concentrations of Red/White Wine and Orange juice by using the standard addition method

This analytical method with the nano-GO-SiO₂-nanoparticles modified electrode was used for the determination of GA in red wine, white wine and orange juice as real samples. This was employed to assess the capability of the modified electrode towards the determination of GA in these real sample matrices. Red wine, white wine and orange juice have been known to contain GA as previously recorded by Gao *et al.* (2015), where they used a hybrid material of chitosan, fishbone-shaped Fe₂O₃ and graphene oxide to modify GCE. Then used it for the determination of GA in red and white wine. However, in our work, we used graphene oxide nanocolloids and SiO₂ nanoparticles as modifiers for the GCE.

The determination of GA in red and white wine was validated by the determination of GA in the samples using HPLC (Appendix A) and the results shown in Table 1 in appendix A.

The experiments were done by using 10 mL of the real samples as blanks and then the standard addition of known concentrations of aliquots of GA within a concentration range of 9.1×10^{-4} to 4.7×10^{-3} mol L⁻¹, were added to the cells containing the real samples and the voltammograms recorded and data calculated (Figure 4.20 and Table 4.4).

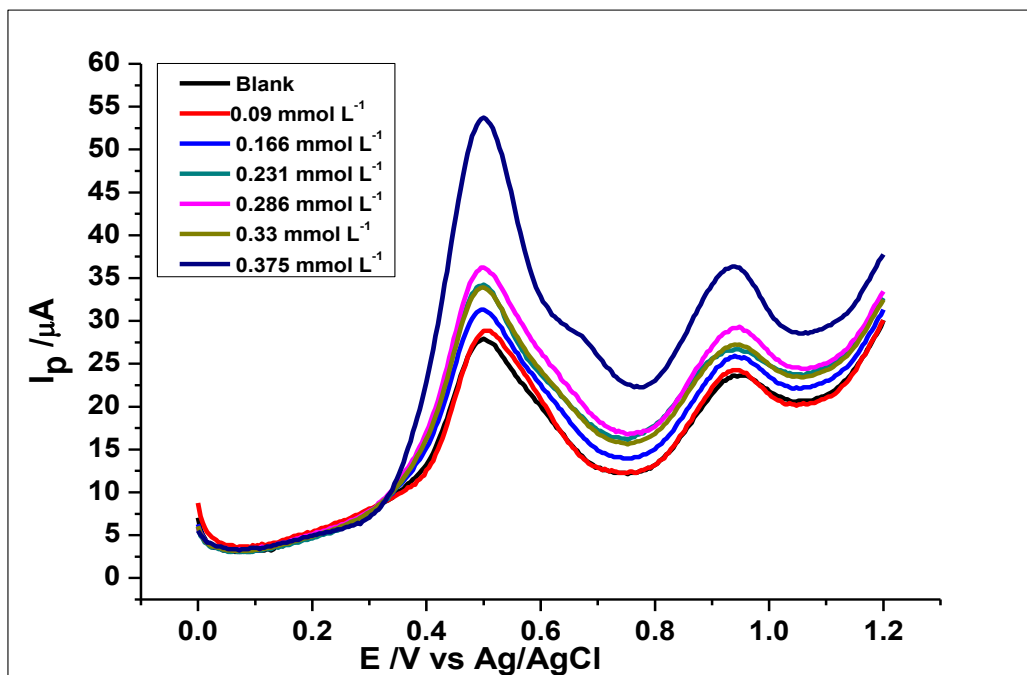


Figure 4. 20. Voltammograms of aliquots of $1 \times 10^{-2} \text{ mol L}^{-1}$ of GA added into Red Wine using a standard addition method.

Table 4. 4 Results of the analysis of GA in spiked Red Wine, White Wine and Orange Juice

Samples	Added (mmol L^{-1})	Found (mmol L^{-1})	Relative Error	Recovery (%)
Red Wine	0.0	0.6300	± 4.05	-
	0.1660	0.1689	± 2.32	102.32
	0.2300	0.2470	± 7.39	107.39
HPLC (Red Wine)		0.5900	± 0.56	
White Wine	0.0	Undetected	-	-
	0.1660	0.1583	± 4.64	95.36
	0.2300	0.242	± 5.65	105.65
Orange Juice	0.0	Undetected	-	-
	0.1700	0.166	± 2.36	97.64
	0.230	0.2379	± 3.44	103.44

4.5 Conclusion

For the first-time graphene oxide nanocolloids mixed with SiO₂ nanoparticles synthesised by the sol-gel method was drop cast on the glassy carbon electrode. The modified electrode was then used for the electrochemical determination of GA (1×10^{-1} mol L⁻¹, phosphate buffer, pH 2.0). The synthesised SiO₂ nanoparticles were characterised using SEM, EDXA and FTIR.

Cyclic and differential pulse voltammetry were applied as the electrochemical techniques and it was found that, graphene nanocolloids mixed with SiO₂ nanoparticles showed an electrochemical effect towards the oxidative determination of GA, within a concentration range of 6.25×10^{-6} to 1.0×10^{-3} mol L⁻¹.

A reaction mechanism was proposed for the interaction of SiO₂ nanoparticles and the graphene oxide nanocolloids towards the electrochemical determination of GA. The modified electrode demonstrated selectivity towards the determination of gallic and uric acid, which is a marked advantage over other electrodes in the literature.

The electrode was found to be a simple, sensitive, fast and cost-effective method for the determination of GA; it showed very good reproducibility, repeatability and a relatively good long-term stability. This is relative to other electrodes developed in the literature as evidenced in section 3.5, page 103.

The electrochemical sensor was successfully applied as a sensitive electrochemical method for the determination of GA in red wine, white wine, and orange juice within the concentration range of 9.1×10^{-4} to 4.7×10^{-3} mol L⁻¹. The results showed the present method to be comparable to some of the other methods in the literature.

CHAPTER FIVE

5.0 THE EFFECT OF ZINC OXIDE NANOPARTICLES ON THE ELECTROCHEMICAL DETERMINATION OF GALLIC ACID USING CARBON PASTE ELECTRODE

5.1 Introduction

In this chapter, zinc oxide nanoparticles (nano-ZnO) were synthesised and used in the modification of carbon paste electrode for the electrochemical determination of GA.

As discussed in Chapter 1 carbon paste electrodes (CPEs) are heterogeneous binary mixtures prepared from carbon powder (graphite) and organic liquid (Paraffin oil) with no electrolytic character. The CPEs and their modified versions have been widely used in electrochemical applications as electrodes for selective and sensitive determination of different organic compounds (Pisoschi et al. 2011; Tashkhourian et al. 2013; Soltani et al. 2015; Tashkhourian and Nami-Ana 2015). The use of nanomaterials and most importantly metal oxide nanoparticles for the development of electrochemical sensors over the last decade, have attracted considerable interest because of their special chemical and physical properties (Qiu, Chen and Yang 2010; Umar *et al.* 2012; Zhou *et al.* 2014). In the development of metal oxide nanoparticles, ZnO nanoparticles have shown a capability to be used in different applications because of their versatile morphology. These include solar cell for energy conversion (Son et al. 2014), photocatalytic activity (Zhang, Shen and Yang 2011) and as a chemical and biological sensor (Tashkhourian *et al.* 2014). The main advantages of these nanostructures of ZnO have been their high surface area to volume ratios, high thermal, mechanical and chemical stability, which is very useful in the design and development of sensors (Afkhami, Kafrahi and Madrakian 2015), and for electrode modification (Tashkhourian *et al.* 2014).

Electrochemical methods with the use of modified electrodes like ZnO nanoparticles modified carbon paste electrodes have generated a lot of interest because they are fast, sensitive, inexpensive, and portable. ZnO nanoparticles, multi-walled carbon nanotubes and polymethyl methacrylate have previously been used for a carbon paste modification in the determination of carbohydrates

(Chekin and Yazdaninia 2014). Meanwhile, Tashkhourian et al. (2014) used ZnO nanoparticles and modified multi-walled carbon nanotubes for the determination of naproxen, with polyglycine. ZnO nanoparticles and multi-walled carbon nanotubes have also been used for the determination of levodopa in the presence of ascorbic acid (Afkhami, Kafrashi and Madrakian 2015). However, they have still not been studied for the determination of antioxidants and specifically GA.

In this section of the work, for the first time ZnO nanoparticles that were synthesised using the solochemical method, were used to modify carbon paste electrode for the determination of GA.

5.2 Experimental

5.2.1 Materials and Reagents

The materials and agents used for the studies in this chapter, had earlier been listed (Chapter 2, Table 2.1, pages 47-478. Although, for the synthesis of ZnO nanoparticles specifically, the following reagents below were used.

Zinc nitrate hexahydrate ($\text{Zn}(\text{NO}_3)_2 \cdot 6\text{H}_2\text{O}$) and Sodium hydroxide (NaOH) were purchased from Sigma Aldrich (London, UK)

5.2.2 Synthesis of ZnO nanoparticles

The synthesis of ZnO nanoparticles has previously been described in Chapter 2, Section 2.4.1, page 50 of this thesis.

5.2.3 Characterisation of the ZnO nanoparticles

The synthesised ZnO nanoparticles were characterised using SEM EDXA, FTIR and electrochemical methods like CV and EIS.

5.3 Results and Discussion

5.3.1 Characterisation of ZnO nanoparticles

From the SEM images (Figure 5.1(A)), the ZnO nanoparticles showed a quasi-spherical structure of the ZnO nanoparticles, lumpy sizes of about 20 μm , which were further ground into the intended nanoparticle sizes of between 40 – 160 nm, which is confirmed in the DLS analysis of the synthesised compound.

Meanwhile, the EDXA data in (Figure 5.1(C)) showed the elemental composition of ZnO nanoparticles to be Zinc and Oxygen atoms at relatively the same amounts.

The nano-ZnO-CPE (Figure 5.1(B)) exhibited a homogenized ZnO-graphite powder in the carbon paste.

The ZnO nanoparticles were analysed DLS analytical method with a Zetasizer (Table 5.1). ZnO nanoparticles (1.0 mg) were dispersed in 10 mL of ethylene glycol and sonicated for 30 mins. Then the results were recorded, and they showed sizes between 40-260 nm. The average particle size distribution, where found to be about 150 nm.

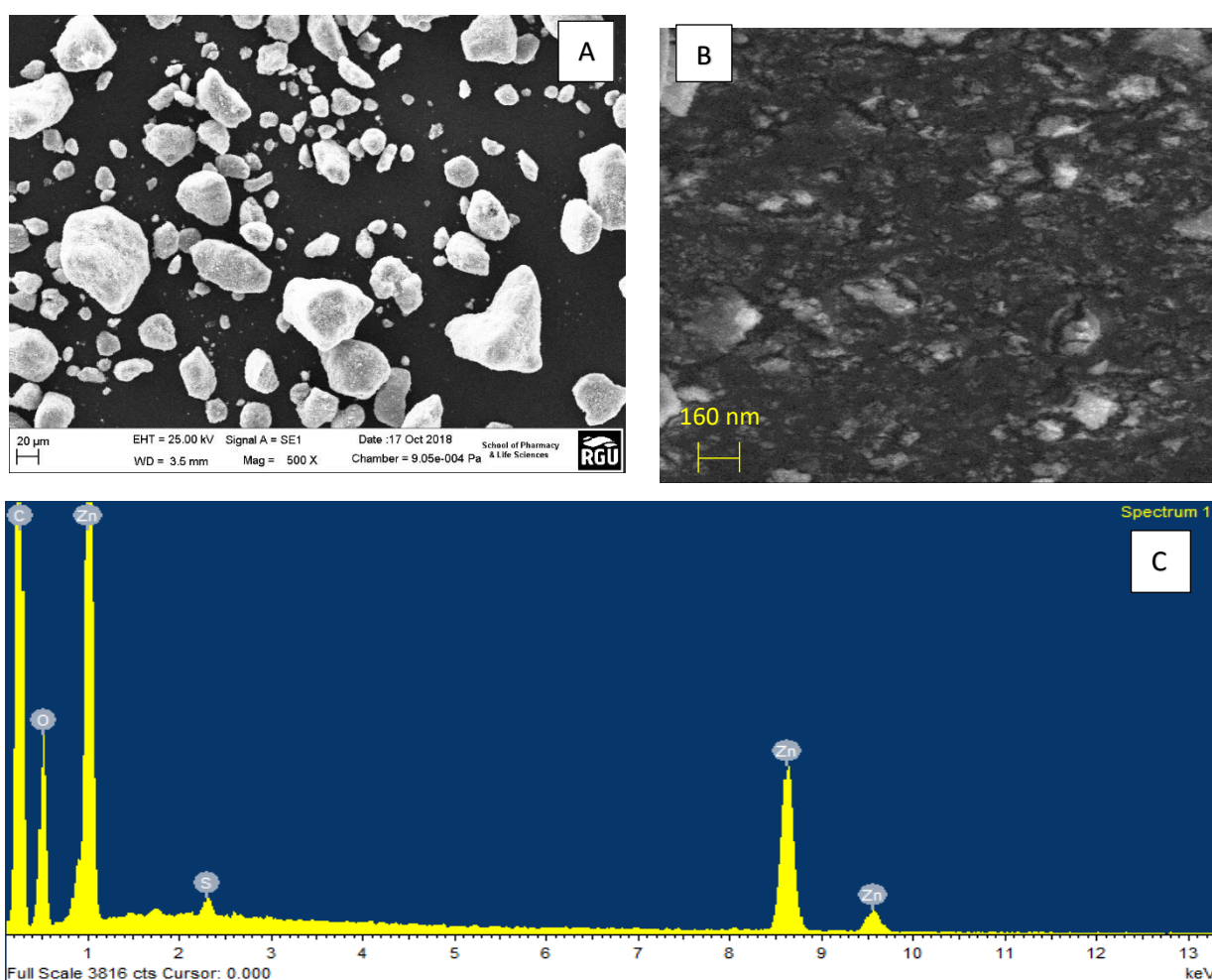


Figure 5. 1. (A) SEM image of ZnO nanoparticles (B) SEM image of ZnO-nanoparticles homogenized in the carbon paste electrode (C) The EDXA analysis of the synthesised compound showing its composition of Zinc and Oxygen

Table 5. 1. The particle size distribution and average size of the synthesised ZnO nanoparticles

	Temp	Z-Ave	Pdl	Peak 1 Mean	Peak 1 Area
	°C	d.nm		d.nm	Percent
ZnO in Ethylene Glycol	25	172.25	0.317	166.9	89.7
ZnO in Ethylene Glycol	25	138.8	0.256	140.6	86.9
ZnO in Ethylene Glycol	25	259.4	0.337	262.3	83.05

5.3.2 Fourier Transform Infrared Spectroscopic analysis

The FTIR spectrum (Figure 5.2) ZnO nanoparticles showed an absorption peak between 500-400 cm^{-1} assigned to the Zn-O bond, while the broad absorption peak between 3300 – 3500 cm^{-1} was attributed to the hydroxyl (OH) group. The FTIR spectrum of ZnO nanoparticles was also compared with the spectrum of a bulk ZnO, which turned up with 96% similarity to the zinc oxide nanoparticles spectrum recorded. This was done just as a confirmation test. The FTIR spectrum is also similar to other ZnO FTIR spectra obtained in literature, like Alwan *et al.* (2015).

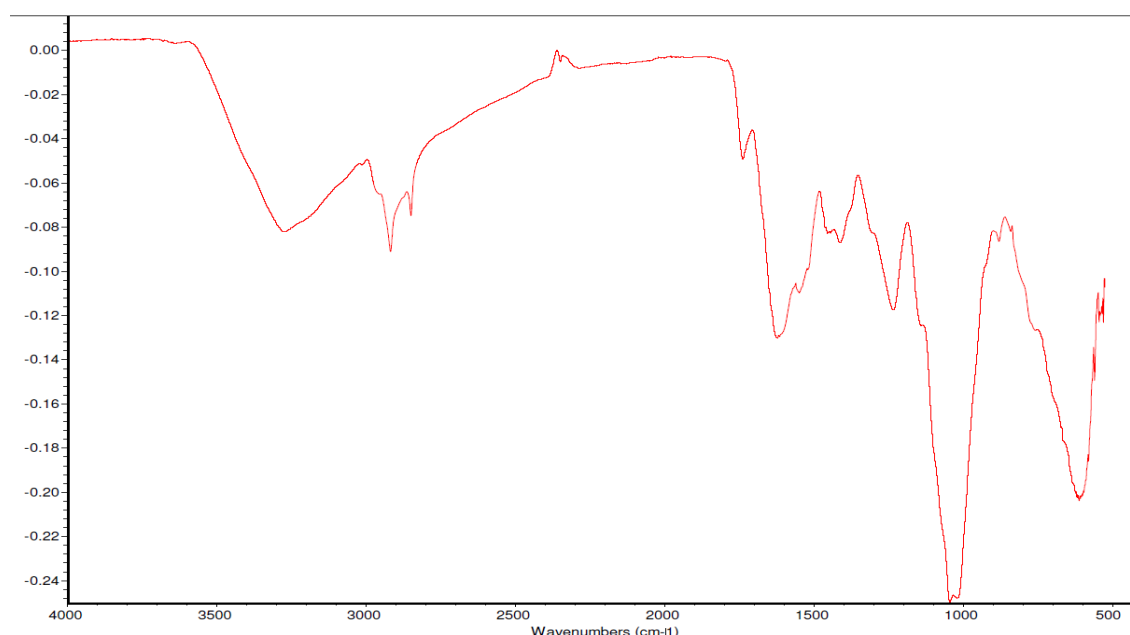


Figure 5. 2. FT-IR spectra of ZnO Nanoparticles

5.3.3 Electrochemical characterisation of the ZnO nanoparticles modified carbon paste electrode

Cyclic voltammetry was used to study the electrochemical interaction between GA and the ZnO nanoparticles modified CPE. Figure 5.3 shows cyclic voltammograms of ZnO nanoparticles-CPE, ZnO-CNT-CPE and bare CPE, in phosphate buffer ($1 \times 10^{-1} \text{ mol L}^{-1}$, pH 2.0) containing GA ($1 \times 10^{-1} \text{ mmol L}^{-1}$) at a scan rate of 100 mV s^{-1} , through an applied potential range of 0 -1.8 V. It was observed that, the nano-ZnO-CPE improved the oxidation current or anodic peak current from about 261 μA for the bare-CPE to 414 μA for the modified electrode. The peak currents were at peak potentials of 0.63 V and 0.68 V respectively for the bare CPE and nano-

ZnO-CPE. The peak potential did not show any negative shift from the bare-CPE to the nano-ZnO-CPE, instead, there was a slight positive shift of about 0.05 V. This suggests that, there was no catalytic effect from the ZnO nanoparticles, as it would have shown a negative peak potential shift if there was a catalytic effect. However, there was an enhancement of the peak current (I_p), because of the increased surface to volume ratio of the ZnO nanoparticles. The blank phosphate buffer ($1 \times 10^{-1} \text{ mol L}^{-1}$, pH 2.0), produced no oxidation peak within the applied range of 0-1.8 V. This showed that, the blank phosphate buffer, showed no peak, even around the potentials where GA is normally oxidised.

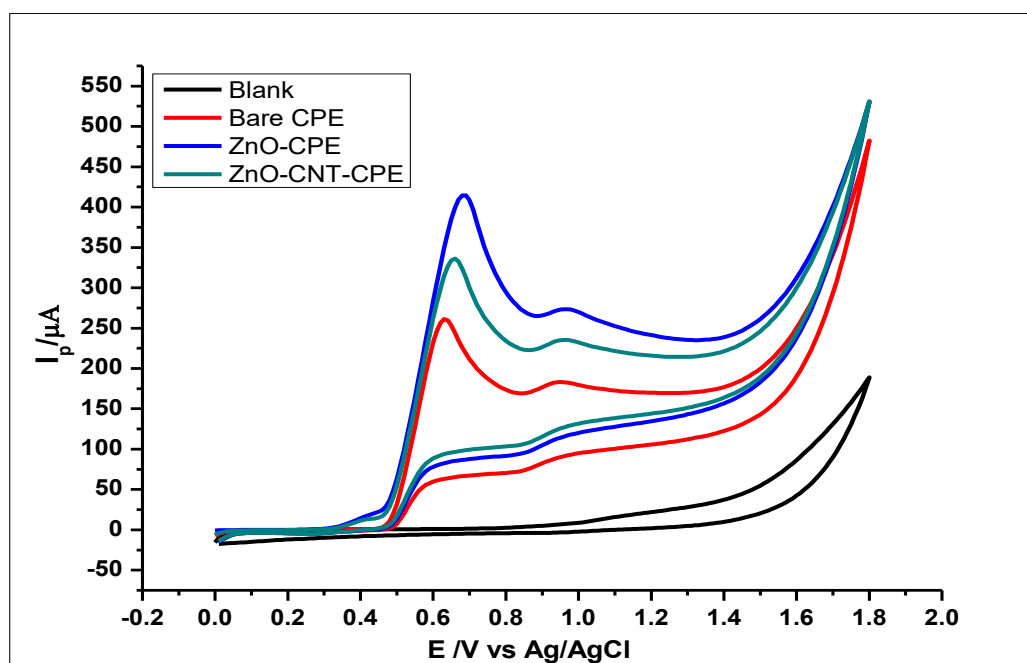


Figure 5. 3. Voltammograms of $1 \times 10^{-2} \text{ mol L}^{-1}$ Gallic acid in a $1 \times 10^{-1} \text{ mol L}^{-1}$ PBS buffer at pH 2.0, determined using a carbon paste electrode, ZnO carbon nanotube-CPE and ZnO nanoparticles modified carbon paste electrode using Cyclic Voltammetry, at a scan rate of 100 mVs^{-1} at room temperature.

Furthermore, carbon nanotube (CNT), was used to modify the carbon paste electrode in the presence and absence of ZnO nanoparticles. CNT have shown remarkable chemical, electrical, mechanical, and structural properties. They are very advantageous in their enhanced electronic properties, rapid electron transfer and a large edge/ basal plane ratio. (Jacobs, Peairs and Venton 2010). These physicochemical properties of CNT have made them very useful in the

development of sensors. Hence their use to enhance the electrochemical properties of the carbon paste electrode.

The results (Figure 5.4 and Table 5.2), showed very different electrochemical behaviours from GA at the different electrodes surfaces. Using just a bare CPE to measure 1×10^{-2} mol L⁻¹ of GA, pH 2.0, at a scan rate of 100 mVs⁻¹; the anodic peak current was at approximately 261 ± 2.07 μ A (Figure 5.4). However, when the CPE was modified using CNT, the anodic peak current increased to about 336 ± 1.9 μ A at a peak potential of 0.69 V. When mixed with ZnO nanoparticles there was a relatively small increase in the peak current to 361 ± 2.4 μ A. Using just the ZnO nanoparticles for the modification the peak current increased even higher to 414 ± 2.5 μ A. From the results, it could be seen that, the ZnO nanoparticles enhanced the electrochemical oxidation of GA at the face of the electrode. This is attributed to the increased surface area created by ZnO nanoparticles. Meanwhile, CNT exhibited its physicochemical properties to increase electron transfer and hence increased peak current. However, the effect of both nanoparticles, relative to either ZnO or CNT; was not complementary. Their individual effects were not reflected by the peak current. Just like Tashkhourian *et al.* (2014) and Tashkhourian and Nami-Ana (2015), the CNT did not give a better effect on the determination of GA as compared to the metal oxide nanoparticles. This could be attributed to the amount of the CNT used in the preparation of the carbon paste electrode; as there is evidence of a synergistic effect between ZnO and CNT in the electrochemical determination of acyclovir (Karim-Nezhad *et al.* 2018). Meanwhile, Fayemi and Adekunle (2015) in their work demonstrated the use of MWCNT and ZnO in the determination of dopamine.

Table 5. 2. The different modified electrodes and the peak currents attained.

	Modified Carbon paste electrodes	Peak Potential (V)	Peak Currents (μA)
1	Bare Carbon paste electrode	0.63	261 ± 0.07
2	CNT modified carbon paste electrode	0.66	336 ± 1.9
3	ZnO-CNT-carbon paste electrode	0.66	361 ± 2.4
4	ZnO-carbon paste electrode	0.68	414 ± 2.5

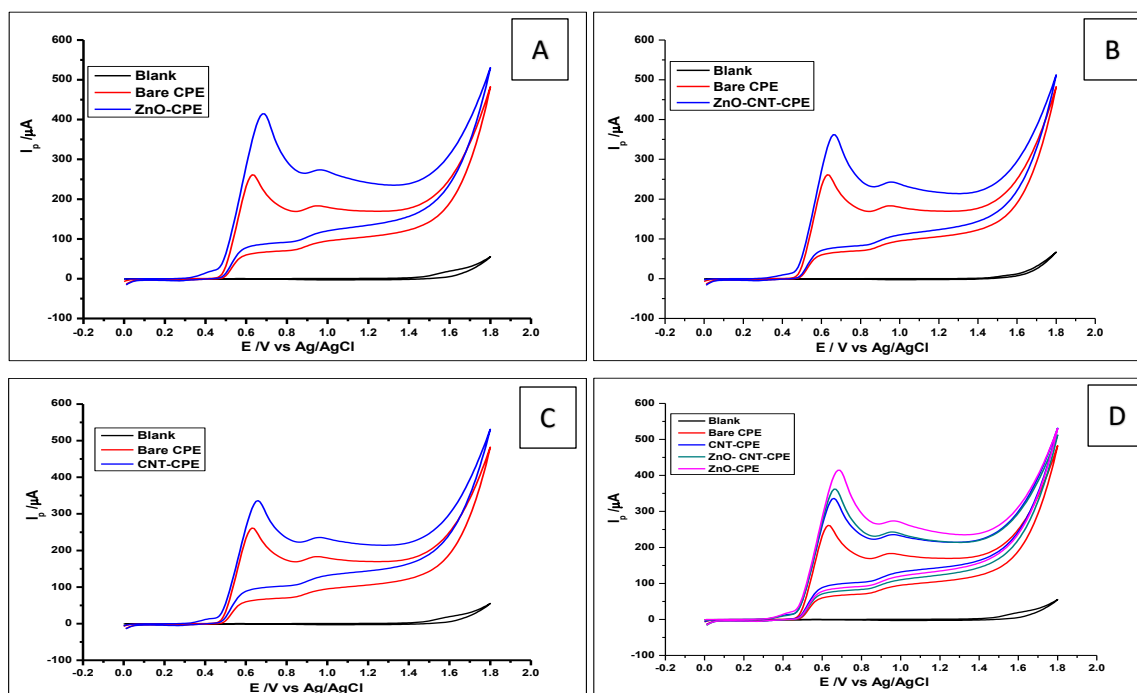


Figure 5. 4. Cyclic voltammograms of the different CPE modifications used to determine 1×10^{-2} mol L^{-1} GA in 1×10^{-1} mol L^{-1} Phosphate buffer at pH 2.0 with a scan rate of 100 mVs^{-1} . (A) ZnO-CPE modification (B) ZnO-CNT-CPE modification, (C) CNT-CPE modification and (D) The different electrodes put together.

5.3.4 Electroactive surface area of ZnO nanoparticles-CPE

The electrochemical performance of the ZnO-nanoparticles-CPE as compared to the bare CPE was studied using electrochemical impedance and CV in $K_3Fe(CN)_6 - K_4Fe(CN)_6$ (5 mmol L^{-1}) (Figure 5.5(A)), where the voltammograms were used to calculate the active surface area of the electrodes (Figure 5.5(B)). The plot of peak current vs the square root of the scan rates (Figure 5.5(C)), produced a linear regression equation thus, $I_{pa} = 14.157v^{1/2} + 2.6323$, with $R^2 = 0.9931$. From the data produced the electroactive surface area was determined using the Randles-Ševcik equation for a reversible process, with a diffusion coefficient of $7.6 \times 10^{-6} \text{ cm}^2 \text{ s}^{-1}$ for $[Fe(CN)_6]^{3-}$ and $n=1$.

$$I_{pa} = (2.69 \times 10^5)n^{2/3} A D^{1/2} v^{1/2} C_0 \quad (5.1)$$

Where n is the number of electrons transferred, A is the electroactive area of the electrode, D is the diffusion coefficient, v is the scan rate and C the concentration of the redox probe used. The electroactive areas were calculated from plots of I_p vs $v^{1/2}$ (square root of scan rate), having slopes of $0.1416 \times 10^{-4} \text{ A v}^{-1/2} D^{1/2}$ for the nano-ZnO-CPE and $0.0471 \times 10^{-4} \text{ A v}^{-1/2} D^{1/2}$ for the bare CPE to give 0.188 cm^2

and 0.063 cm^2 respectively (These calculations were carried out as described in Appendix II, Section 8.2.1, page 212).

From the electroactive surface areas of 0.188 cm^2 for nano-ZnO-CPE and 0.063 cm^2 for the bare CPE, it can be seen that the modified-CPE had a larger surface. This proves the increased surface area influenced the increased peak current observed.

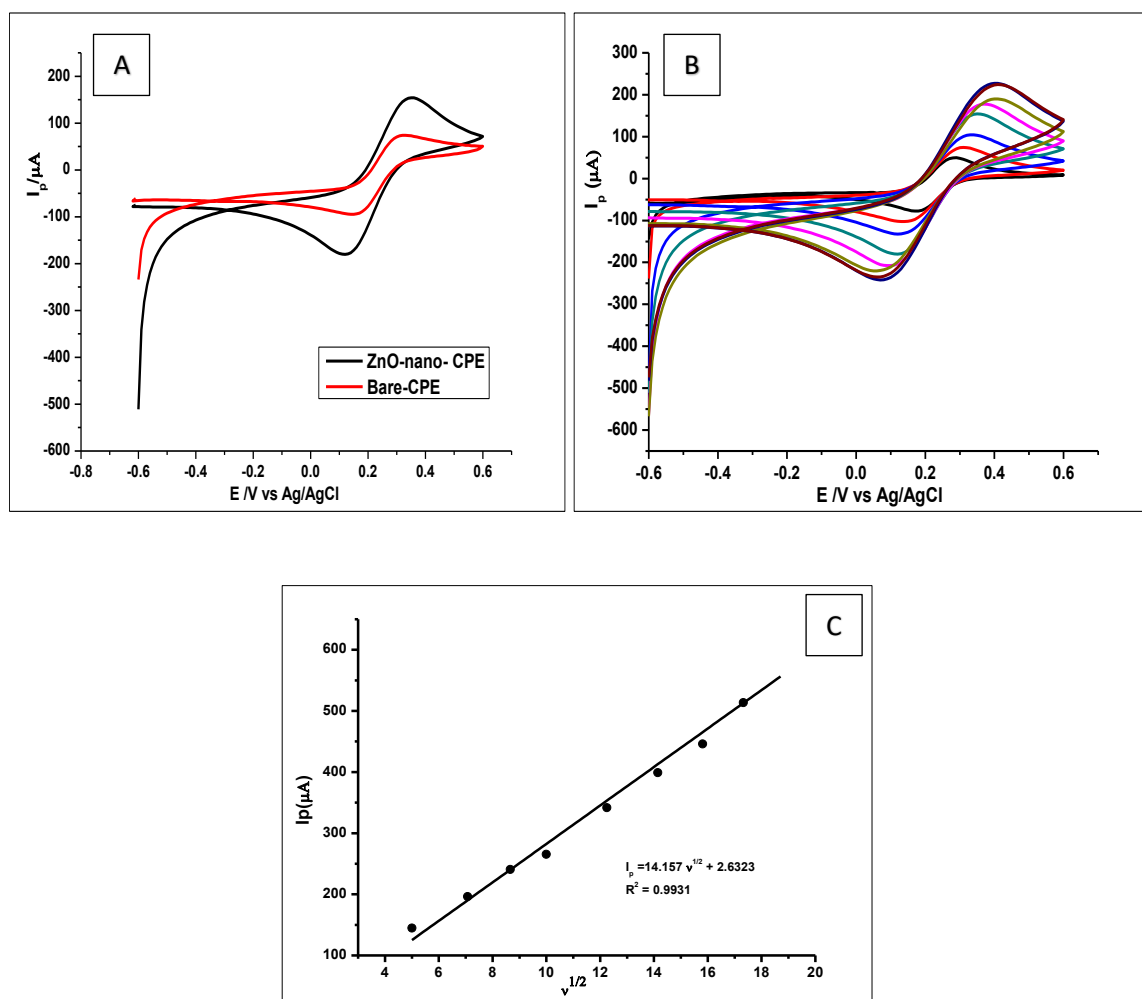


Figure 5. 5. (A) Voltammograms of Nano-ZnO-CPE and bare CPE (B) Voltammograms of 5 mmol L^{-1} of $\text{Fe}[(\text{CN})_6]^{3-/4+}$ at different scan rates used for the calculation of the reactive surface area of the modified CPE.(C) The plot of peak current vs square root of scan rate.

5.3.5 Electrochemical Impedance Spectroscopy (EIS)

EIS was used as a tool to study the interface properties of the ZnO-nanoparticles modified CPE and was used to provide information about the impedance changes of the electrode surface/electrolyte solution interface.

The Nyquist plots of the EIS (Figure 5.6) shows a semi-circular portion which demonstrates an electron transfer limited process, while the linear portion corresponds to a diffusion-limited process. The Nyquist diagram shows the electron transfer resistance (R_{ct}) of both electrodes (bare CPE and Nano-ZnO-CPE), at the bare CPE has a larger R_{ct} and the Nano-ZnO-CPE shows a smaller semicircle, implying a significant acceleration of $\text{Fe}(\text{CN})_6^{3-} / \text{Fe}(\text{CN})_6^{4-}$, which is evidenced in Figure 5.5(A). Here the nano-ZnO-CPE showed an improved peak current as compared to the bare CPE. This is mainly because of the reduced electron transfer resistance of the modified electrode. With a reduced resistance caused by the presence of the ZnO nanoparticles, the electrons transfer faster in higher quantity, hence the improved peak current.

The Nyquist plots were obtained at a fixed potential of 0.3 V vs Ag/AgCl, between the 10 KHz and 1 Hz. Meanwhile, the equivalent circuit that was used for the measurement is shown in Figure 5.6 (inset).

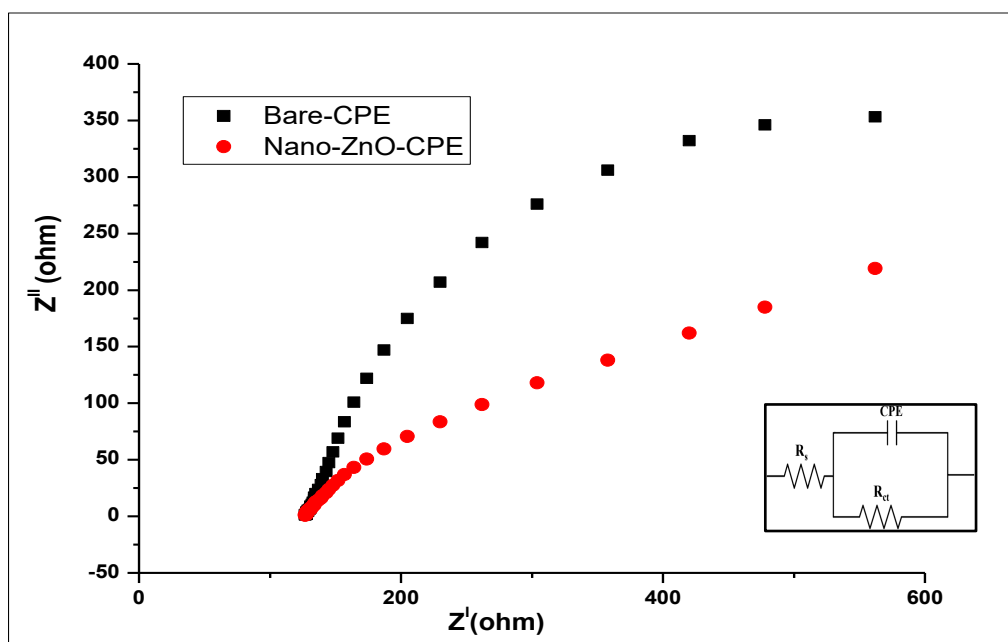


Figure 5. 6. Electrochemical impedance spectroscopy (EIS) at CPE showing the bare CPE and the Nano-ZnO-CPE in a $5 \text{ mmol L}^{-1} \text{ K}_3\text{Fe}[(\text{CN})_6] - \text{K}_4\text{Fe}[(\text{CN})_6]$. Frequency range from 0.01-100kHz.

5.3.5 Effect of pH on GA determination

Further optimisation of the electrochemical condition for GA determination was carried out by studying the effect of pH of buffer towards the determination of GA. Cyclic voltammogram was used to measure GA ($1 \times 10^{-3} \text{ mol L}^{-1}$) in phosphate buffer ($1 \times 10^{-1} \text{ mol L}^{-1}$) at different pH ranging from 2.0 – 8.0, to study the impact of the pH on the peak currents. The peak current of GA peaked at pH 2 and reduced with increasing pH (Figure 5.7). Ultimately, pH 2.0 was chosen as the optimal pH condition for the oxidation of GA. In addition, the linear relationship between the peak current and pH shows an equal number of protons and electrons took part in the oxidation of GA. The negative oxidation peak potential with an increase in pH, suggests the presence of protons in the electrode reaction. As shown in Figure 5.7(B) the peak potential E_p vs. pH gives a good linear relationship in the range pH 2.0-8.0, producing a linear regression equation of $E_p = 0.82 - 0.0585 \text{ pH}$, $R^2 = 0.9909$. From the regression equation, the 58.5 mV/pH slope is close, to the anticipated Nernstian value of 59 mV/pH, at 25°C for an equal number of protons and electrons transfer reaction. This phenomenon of equal proton and electron activity in the electrochemical oxidation of GA, was previously reported (Souza *et al.* 2011; Luo *et al.* 2013).

This shows that the electrochemical oxidation of GA at pH 2.0, involves just one electron at the point of the first oxidation peak as demonstrated in Scheme 3.1 page 79, where GA is first oxidised to the semiquinone radical.

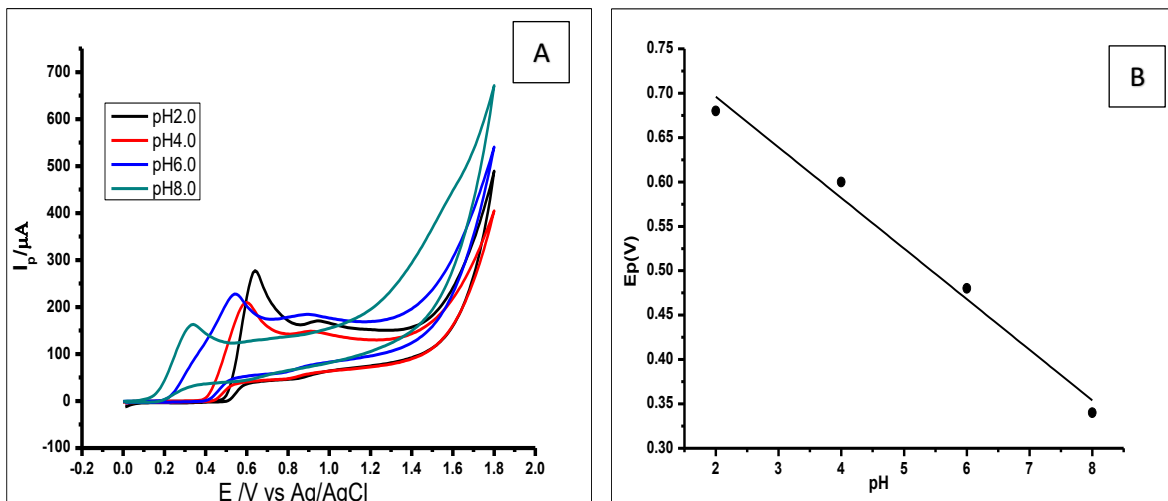


Figure 5. 7. (A). Cyclic Voltammograms showing the effect of pH on the electrochemical behaviour of $1 \times 10^{-4} \text{ mol L}^{-1}$ Gallic Acid. (B). The plot of the Peak Potential (E_p) against different pH values, showing the effect of pH on the electrochemical behaviour of $1 \times 10^{-3} \text{ mol L}^{-1}$ Gallic acid using a ZnO-nanoparticles-CPE at a scan rate of 100 mVs^{-1}

5.3.6 Effect of scan rate on GA determination

Cyclic voltammetric studies were also carried out to investigate the influence of the scan rate at the nano-ZnO-CPE in phosphate buffer ($1 \times 10^{-1} \text{ mol L}^{-1}$, pH 2.0) containing GA ($1 \times 10^{-2} \text{ mol L}^{-1}$) (Figure 5.8). Scan rates from 25 to 350 mVs^{-1} , gave a linear relationship with the peak current (I_p) (Figure 5.8(B)), with the linear regression equation $I_p = 1.3042 v + 131.35$ and $R^2 = 0.9945$. This shows that, the ZnO nanoparticles modified carbon paste electrode had an absorption-controlled reaction.

On the other hand, there was also a linear relationship between the square root of the scan rate and the peak currents (I_p) in the range $25\text{-}1100 \text{ mVs}^{-1}$ (Figure 5.8(C)). The linear regression equation was described as $I_p = -27.408 + 30.809 v^{1/2}$ ($R=0.9944$), validating the oxidation of GA in this case as a diffusion-controlled process.

On the other hand, looking at Figure 5.8(A), there was a positive shift in the peak potentials as the scan rates increased. Thus, the logarithm of the scan rates vs the anodic peak potential (E_p) was shown to have a proportional relationship.

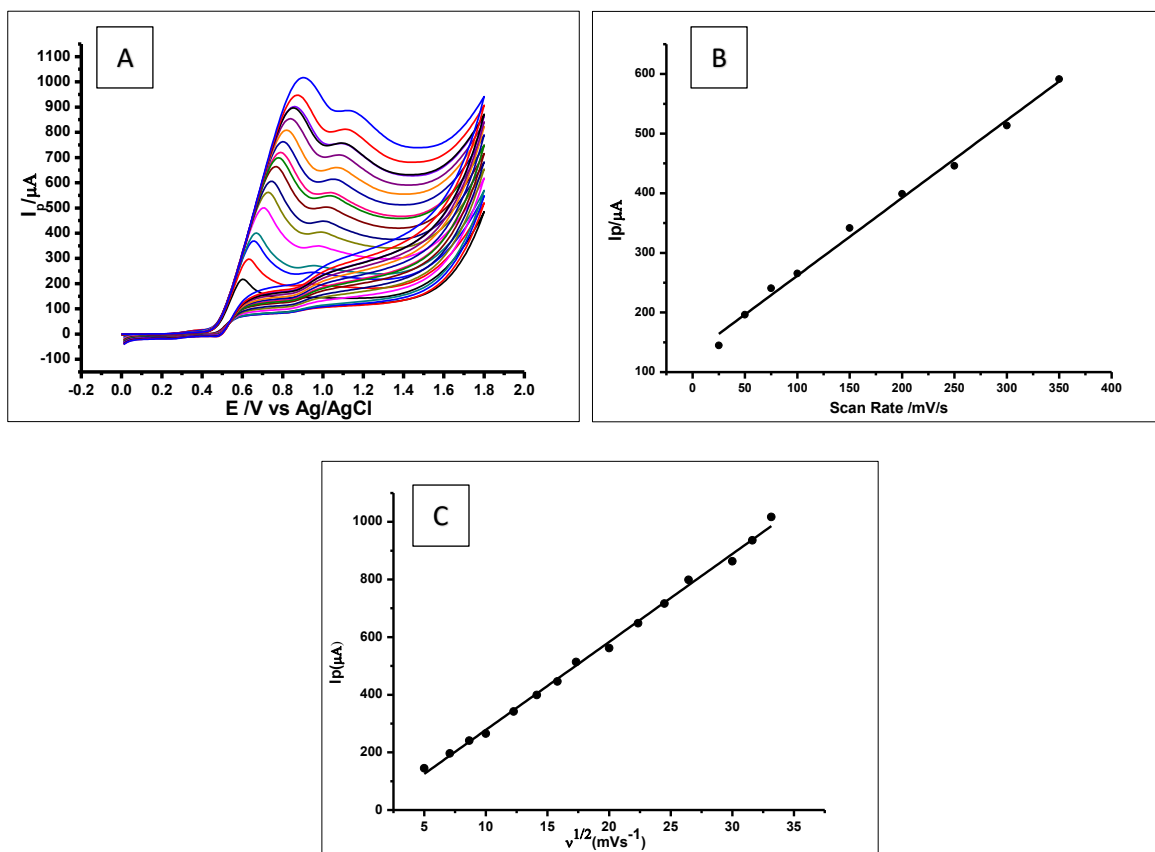


Figure 5. 8. (A) Cyclic voltammograms of nano-ZnO-CPE in a $1 \times 10^{-1} \text{ mol L}^{-1}$ PBS (pH 2.0) with a $1 \times 10^{-2} \text{ mol L}^{-1}$ GA at a scan rate of 25 to 1100 mVs^{-1} (B) the linear relationship between the I_p and the scan rate and (C) the linear relationship between the I_p vs square root of the scan rate.

5.3.7 Effect of concentration and limit of detection for GA determination

The determination of different concentrations of GA at the optimized condition (i.e. nano-ZnO-CPE in a $1 \times 10^{-1} \text{ mol L}^{-1}$ PBS (pH 2.0) at a scan rate of 100 mV s^{-1}) was studied using differential pulse voltammetry (DPV). A linear relationship between the concentrations of GA and the peak current (I_p) was observed (Figure 5.9(A) and (B)). The measurements produced voltammograms in which the peak current increased proportionally with increasing GA concentration. Using DPV in the measurement within the concentration range of 1×10^{-3} to $5 \times 10^{-2} \text{ mmol L}^{-1}$ two oxidation peaks currents were produced at peak potentials of 0.5 V and 0.83 V at different concentrations of GA.

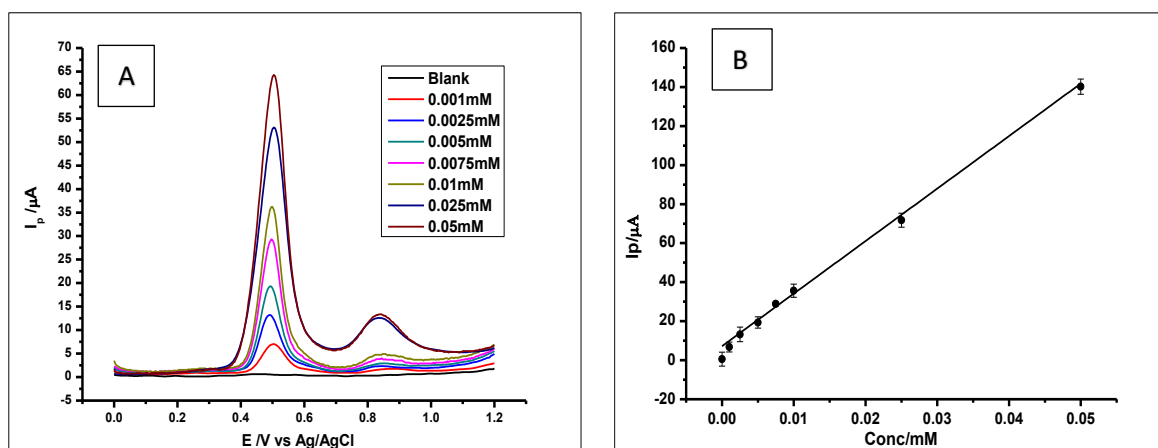


Figure 5. 9. (A) Differential pulse voltammograms of various concentration of GA at ZnO-nanoparticles-CPE in a 0.1 mol L⁻¹ phosphate buffer at pH 2.0 at a scan rate of 100 mVs⁻¹ with voltammograms (a-j) that corresponds to the following concentrations a) 0.0, b) 0.001 mmol L⁻¹, c) 0.0025 mmol L⁻¹, d) 0.005 mmol L⁻¹, e) 0.0075 mmol L⁻¹, f) 0.01 mmol L⁻¹, g) 0.025 mmol L⁻¹, h) 0.05 mmol L⁻¹, i) 0.5 mmol L⁻¹. (B) The calibration curve for the determination of GA.

Using the first main GA oxidation peak as can be seen in Figure 5.9(A), the analytical calibration graph within the concentration range (1×10^{-3} to 5×10^{-2} mmol L⁻¹), showed a linear relationship between the peak current and the increase in GA concentration. This produced a linear regression equation of $I_p = 2708.7 C$ (mmol L⁻¹) + 5.3404 with $R^2=0.9968$. The limit of detection (LOD) defined as $(3 \times Std_{Blank})/m$, where Std_{Blank} is the standard deviation of the blank and m is the slope; was found to be 1.86×10^{-7} mol L⁻¹.

The LOD produced by the ZnO nanoparticles modified is comparable to other limits of detection reported in the literature (Gao et al. 2015); with LODs of 1.5×10^{-7} mol L⁻¹ and 2.09×10^{-6} mol L⁻¹ respectively. The LOD found in this study is also very good for the determination of GA in food samples, because the maximum permitted GA levels in food within the EU and North America ranges from 1.18×10^{-1} mol L⁻¹ to 5.88 mol L⁻¹.

5.3.8 Reproducibility and repeatability of the method

The reproducibility and repeatability of the method using the developed nano-ZnO-CPE were studied. The reproducibility of the method was carried out by producing three different electrodes and used them to measure 8 replicate samples of GA (1×10^{-3} mol L⁻¹) in phosphate buffer (1×10^{-1} mol L⁻¹, pH 2.0). The measurement was done using cyclic voltammetry, at a scan rate of 100 mVs⁻¹ at

room temperature. The voltammograms produced a relative standard deviation (RSD) of 4.9% which showed good reproducibility.

Meanwhile, for the repeatability of the method, 8 different determination of GA ($1 \times 10^{-3} \text{ mol L}^{-1}$) were carried out. The voltammograms produced an RSD of 3.63% showing very good repeatability of the method as can be seen in Figure 5.10(A).

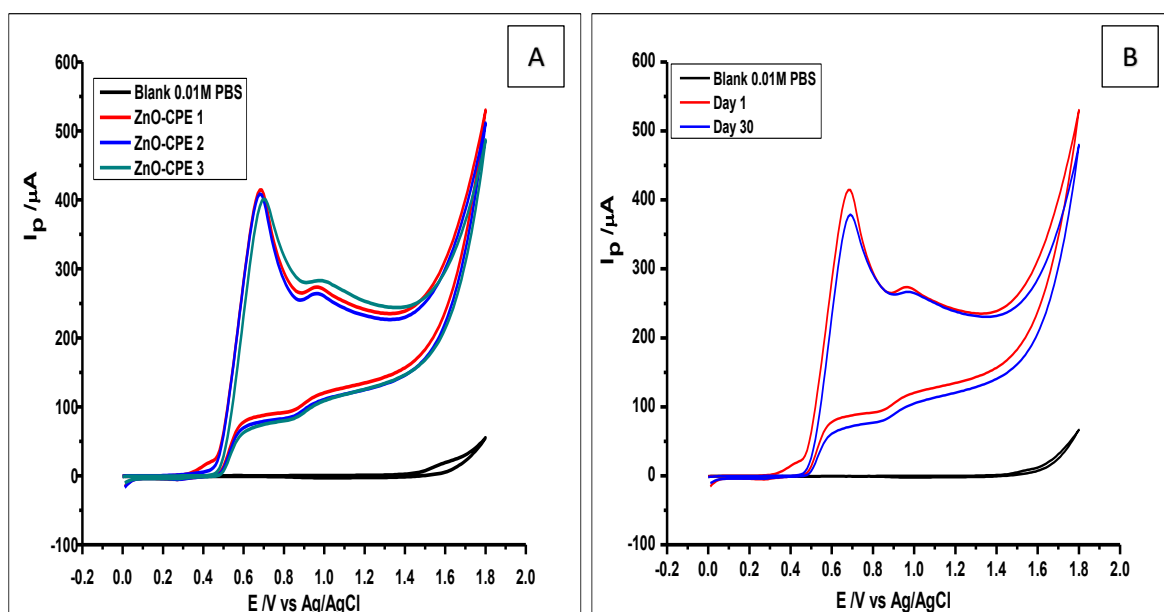


Figure 5. 10. Voltammograms of $1 \times 10^{-3} \text{ mol L}^{-1}$ Gallic acid in a $1 \times 10^{-1} \text{ mol L}^{-1}$ PBS buffer at pH 2.0 measured using nano-ZnO-CPE to measure (A) Repeatability and (B) stability using Cyclic Voltammetry, at a scan rate of 100 mVs^{-1} at room temperature.

5.3.9 Stability of method

Finally, the stability was studied, where 3 electrodes were used to make measurements, and the same electrodes used again a month later to make same measurements. The voltammograms produced an RSD of 4.25%, depicting relatively good stability (Figure 5.10(B)).

5.3.10 Interference study

The interferences of various species in the determination of GA ($1 \times 10^{-3} \text{ mol L}^{-1}$), was investigated by adding different foreign ions (K^+ , Ca^{2+} , Fe^{3+} , and Na^+ then ascorbic acid, caffeic acid and caffeine). The tolerable limits for interference would be the highest amount of the ions that would cause an error of more than 5% in

the determination of GA. Looking at Table 5.2, with RSD values of less than 5% these ions did not interfere with GA.

Table 5. 3. Effects of various substances on the determination of 1×10^{-3} mol L⁻¹ Gallic acid

Interfering Species	Amount in Solution/mol L⁻¹	RSD
Ca ²⁺	1×10^{-1}	±2.08
Na ⁺	1×10^{-1}	±2.16
Fe ³⁺	1×10^{-1}	±1.43
Cl ⁻	1×10^{-1}	±2.08
CO ₃ ²⁻	1×10^{-1}	±2.16
Ascorbic acid	5×10^{-3}	±4.92
Caffeic acid	5×10^{-3}	±3.8
Caffeine	5×10^{-3}	±3.68

5.3.11 Analytical application of the method

The nano-ZnO-CPE was then applied for the determination of GA in red wine. This was done, just to assess the capability of the modified electrode towards the determination of GA in red wine.

The experiment was done just like in the earlier electrodes, by using 10 mL of the 10-fold diluted real samples in 0.1 mol L⁻¹ phosphate buffer, as the blank. Then the standard addition of aliquots of GA was added to the wine. Within a concentration range of 9×10^{-4} to 3.3×10^{-3} mol L⁻¹ the voltammograms were recorded and the results calculated to create a calibration graph (Figure 5.11), with a linear regression equation of $I_p (\mu A) = 4.2306 \text{ Conc (mM)} + 22.003$ and $R^2 = 0.9960$. The analysis was successful with 103% recovery rate.

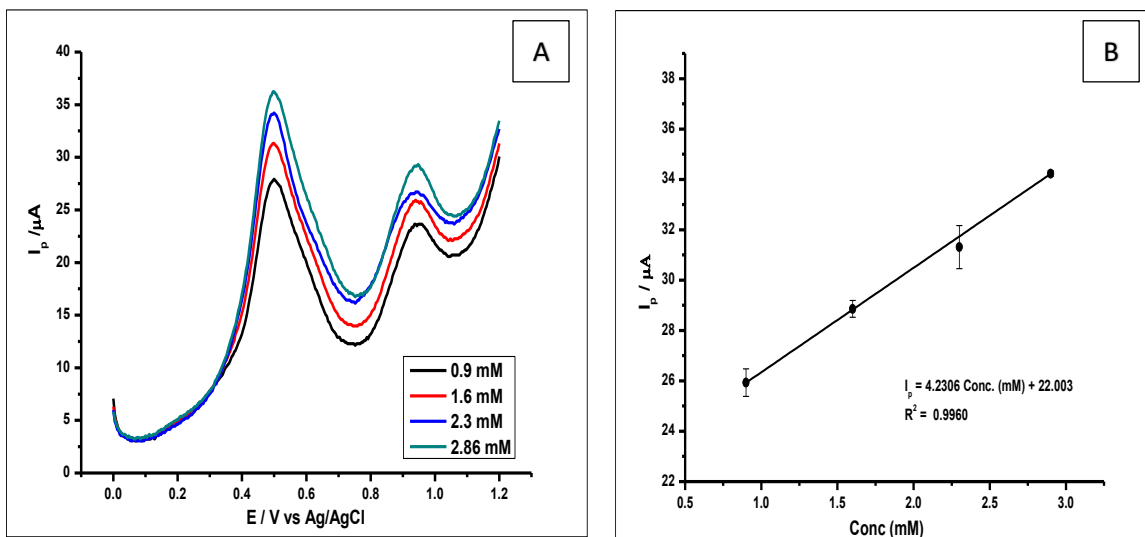


Figure 5. 11. (A) Differential pulse voltammograms of aliquots of $1 \times 10^{-2} \text{ mol L}^{-1}$ of GA added into Red Wine using a standard addition method. (B) Calibration curve created using data from the DPV voltammograms of analysing Red Wine.

Furthermore, just like in all the other electrodes white wine was also analysed using differential pulse voltammetry. The voltammograms produced by the analysis were recorded in Figure 5.12 (A) and a calibration curve was developed from the voltammograms (Figure 5.12 (B)). The voltammograms created a linear regression equation of $I_p (\mu\text{A}) = 5.0622 \text{ Conc. (mM)} + 16.799$ and $R^2 = 0.9995$. Using the standard addition method in the red and white wine, where known concentrations of GA molecules were added to the wine samples; there was a proportional increase in peak current, with increasing GA concentration. This increase in GA concentration happens at the peak potential where the blank wine sample produced an oxidation peak. Hence with the subsequent, three standard addition of GA, it was deduced that the peak at the blank wine sample was GA.

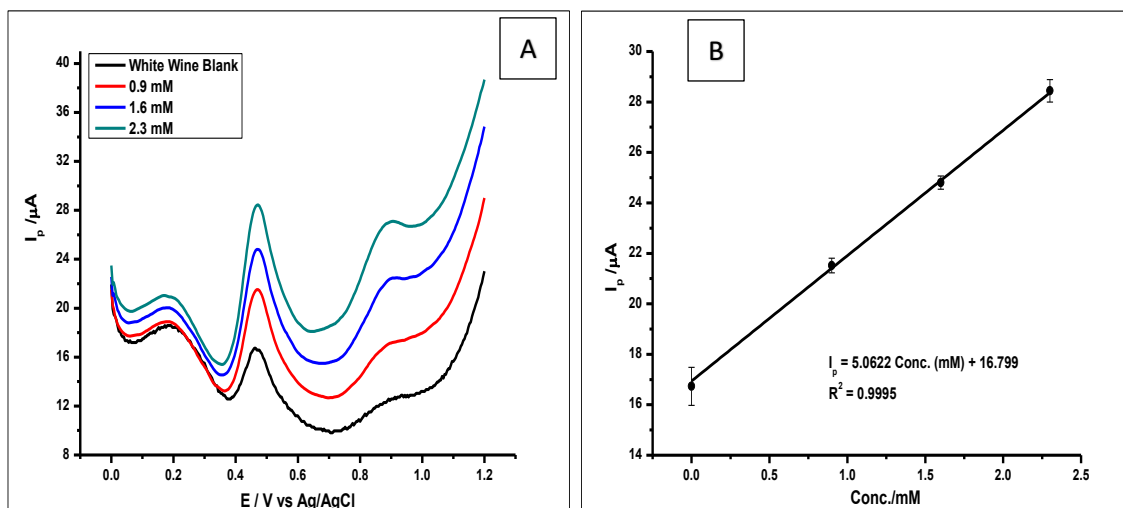


Figure 5. 12. (A) Differential pulse voltammograms of aliquots of $1 \times 10^{-2} \text{ mol L}^{-1}$ of GA added into White Wine using a standard addition method. (B) Calibration curve created using data from the DPV voltammograms of analysing Red Wine.

Table 5. 4. Results of the analysis of GA in spiked Red Wine and White Wine

Samples	Added (mmol^{-1}L)	Found (mmol L^{-1})	% Recovery	Relative Error
Red Wine	0.	1.619	-	-
	0.9	0.929	103.2	± 3.2
	1.6	1.62	101.3	± 1.3
	2.3	2.20	95.7	± 4.3
	2.9	2.89	99.7	± 0.3
White Wine	0	0.0136	-	-
	0.9	0.9325	103.6	± 3.6
	1.6	1.583	98.9	± 1.1
	2.3	2.299	99.5	± 0.5

5.4 Conclusion

In this work, ZnO nanoparticles were synthesised and characterised, then used for the first time in the modification of carbon paste electrode for the electrochemical determination of GA. The ZnO nanoparticles-modified carbon paste electrode was used for the determination of GA in $1 \times 10^{-1} \text{ mol L}^{-1}$ phosphate buffer at a pH 2.0. Cyclic voltammetry and Differential Pulse Voltammetry were used for the characterisation of the electrode and the electrochemical determination of GA. They showed very good electrochemical capability by enhancing the peak currents produced by the oxidation of GA. The modified

electrode showed selectivity as the determination of GA was studied in the presence of different known compounds that could interfere with GA determination.

The electrode was found to be sensitive, fast, cost-effective, and simple for the determination of GA, as compared to other electrodes in the literature with more complex and expensive preparation procedures. Examples include the graphite electrode modified with thionine and nickel hexacyanoferrate for GA determination with an LOD of $1.66 \times 10^{-6} \text{ mol L}^{-1}$ (Sangeetha and Narayanan 2014). Glassy carbon electrode modified with the electrodeposition of Zn-Al-NO₃ layered double hydroxide film for the determination of GA, with an LOD of $1.6 \times 10^{-6} \text{ mol L}^{-1}$ (Kahl and Golden 2014). The fact that, further complex modification procedures have been carried out, with more expensive compounds producing LODs of 10^{-6} to $10^{-9} \text{ mol L}^{-1}$ is a testament to our simple electrode.

The electrode as compared to all the others in the literature also showed relatively good stability, repeatability, and reproducibility.

The modified electrode was also successfully used for the detection of GA in red and white wine, within a concentration range of 9×10^{-4} to $3.3 \times 10^{-3} \text{ mol L}^{-1}$. Meanwhile, these results showed the electrode was comparable to other sensors in the literature, looking at the LOD that shows it is below the maximum GA levels in food samples in the EU and North America.

CHAPTER SIX

6.0 COBALT OXIDE NANOPARTICLES MODIFIED CARBON PASTE ELECTRODE FOR THE ELECTROCHEMICAL DETERMINATION OF GALLIC ACID

6.1 Introduction

In this chapter, the synthesis, characterisation and use of cobalt oxide nanoparticles for the modification of carbon paste electrode for the determination of GA are described and discussed.

Various transition metals and their corresponding oxides in the nanostructured form have been extensively used for the electrochemical determination of many organic compounds. Their popularity has been due to their widely articulated special chemical and physical structures. Cobalt oxide (Co_3O_4) has shown a wide range of usage in the areas of biosensors, as magnetic material, electrocatalyst and lithium batteries (Salimi *et al.* 2008; Karuppiah *et al.* 2014; Yarestani *et al.* 2014), because of their high electroactivity and sensitivity. Cobalt oxide has been used in combination with CNT, MWCNT and rGO in the electrochemical determination of organic compounds. Puangjan and Chaiyasith (2016) reported a novel $\text{ZrO}_2/\text{Co}_3\text{O}_4/\text{rGO}$ composite for the modification of fluorine-doped tin oxide electrode, to be used in the simultaneous determination of GA, caffeic acid and protocatechuic acid. However, the complex and time-consuming electrode preparation still seem like a drawback in their work.

Here a simple co-precipitation method was used for the synthesis of cobalt oxide nanoparticles and used for the first time in the modification of CPE to determine GA in wine samples.

6.2 Experimental

6.2.1 Materials and Reagents

The reagents used for the studies in this chapter had already been listed (Chapter 2, Table 2.1, pages 47-48). For the synthesis of the cobalt oxide nanoparticles the following reagents below were used.

Cobalt (II) nitrate hexahydrate ($\text{Co}(\text{NO}_3)_2 \cdot 6\text{H}_2\text{O}$) and Sodium hydroxide (NaOH) used for cobalt oxide nanoparticles synthesis were purchased from Sigma Aldrich (London, UK).

6.2.2 Synthesis of Cobalt oxide nanoparticles

The procedure for the synthesis of cobalt oxide nanoparticles had previously been described in Chapter 2, section 2.4.4 and page -51 of this thesis.

6.3 Results and discussion

6.3.1 Characterisation of the prepared Cobalt Oxide nanoparticles-modified CPE

The characterisation of the cobalt oxide nanoparticle and CoO-nano-CPE was carried out using SEM and EDXA. This was used to reveal information about the external morphology, chemical composition and crystalline structure of the compounds. The SEM images (Figure 6.1), shows nanoparticles of sizes that range from 60 nm to 288 nm. These nanosized compositions (Figure 6.1 (B)) contributed to the enhancement of peak currents and provided better mass transport when being used for the determination of GA using different electrochemical methods.

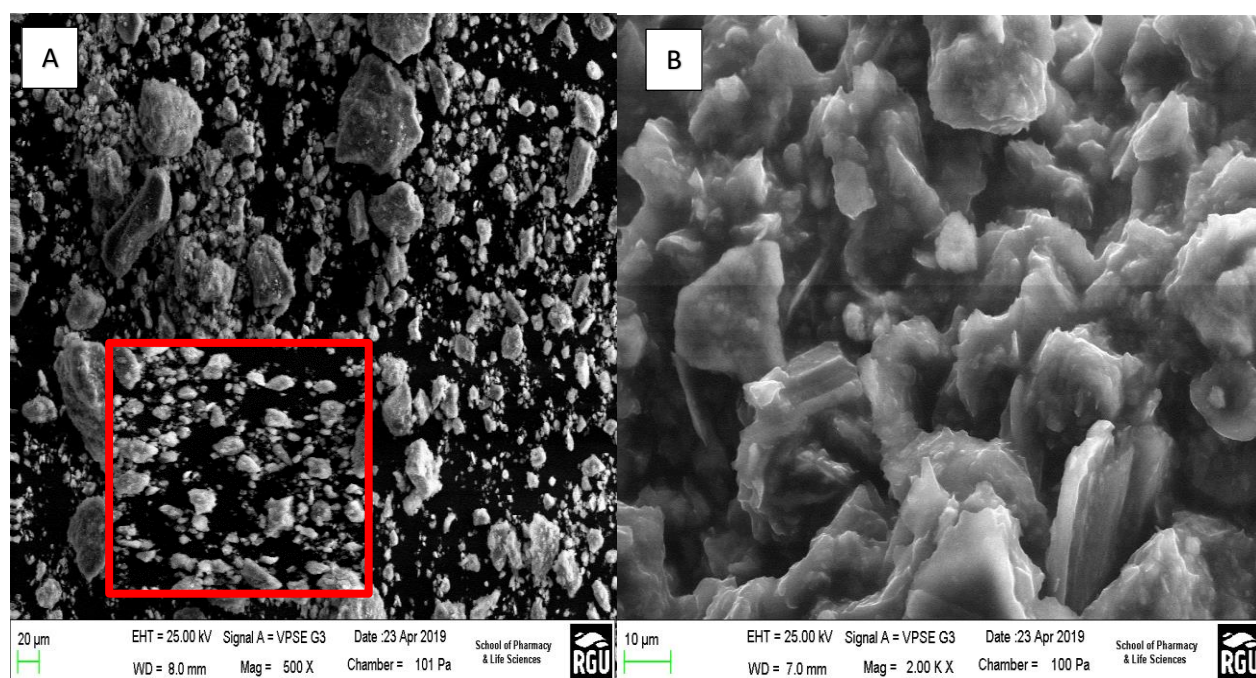


Figure 6. 1. (A) The SEM Image of Cobalt oxide nanoparticles showing the morphology of the nanoparticles with (Inset) Co_3O_4 in 100 nm (B)SEM Image of CoO-nano-CPE, with the paraffin holding the Cobalt oxide nanoparticles and graphite together.

6.3.2 Dynamic Light Scattering (DLS) Analysis

The average particle size, size distribution and poly dispersity index (PDI) of the synthesised cobalt oxide nanoparticles were determined by the dynamic light scattering technique using the Malvern Zetasizer Nano series (Nano Zs) (Figure 6.2). This is run with a Malvern Zetasizer software 7.02 produced by Malvern Instruments Ltd (Malvern, UK). The Zetasizer software loaded on to Microsoft Window XP contains a Macromedia flash© player software by Macromedia Inc. The resulting particle size of the discrete cobalt oxide nanoparticles showed size distribution ranging from 60 nm to 288 nm, with an average particles size of 279.4 nm, which is in agreement with the SEM images showing clusters of nanoparticles of sizes ranging from 10 μm to 20 μm .

Results

	Size (d.nm):	% Intensity:	St Dev (d.n...
Z-Average (d.nm): 279.4	Peak 1: 288.2	83.3	144.5
Pdi: 0.250	Peak 2: 1835	16.7	871.6
Intercept: 0.909	Peak 3: 0.000	0.0	0.000
Result quality : Good			

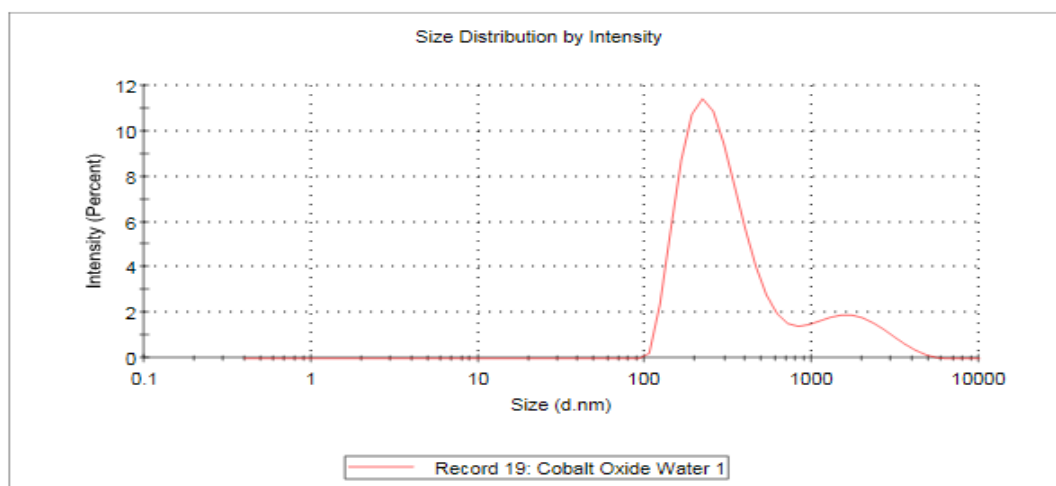


Figure 6. 2 Particle size distribution of synthesized cobalt oxide nanoparticles

6.3.3 Thermogravimetric analysis (TGA)

The thermogravimetric analysis (TGA) of the cobalt oxide nanoparticles was carried out to ascertain the thermal stability of the synthesised nanoparticles (Figure 6.3). The TGA oxygen flow rate was set at 20 mL min⁻¹ and the rate of heating of the sample was 10 °C min⁻¹ using α -alumina crucibles, from temperature room temperature to about 900 °C.

From the TGA analysis the profile shows three main steps downs. The first step started with an initial weight loss from the room temperature to 150 °C mainly attributed to the evaporation of water molecules absorbed on the CoO-NP. The temperature then rises for the second step of weight loss, which happens from 210 °C to 500 °C. This second step of weight loss is attributed to the volatilisation and combustion of organic species with the formation of pyrochlore phases (Chekin, Vahdat and Asadi 2016). The last step of the weight loss from 500 °C to 650 °C is the decomposition of the pyrochlore phases to the CoO-NPs pure phases. The TGA profile continues with no significant weight loss up to 900 °C on the TGA curve, suggesting a decomposed cobalt oxide product.

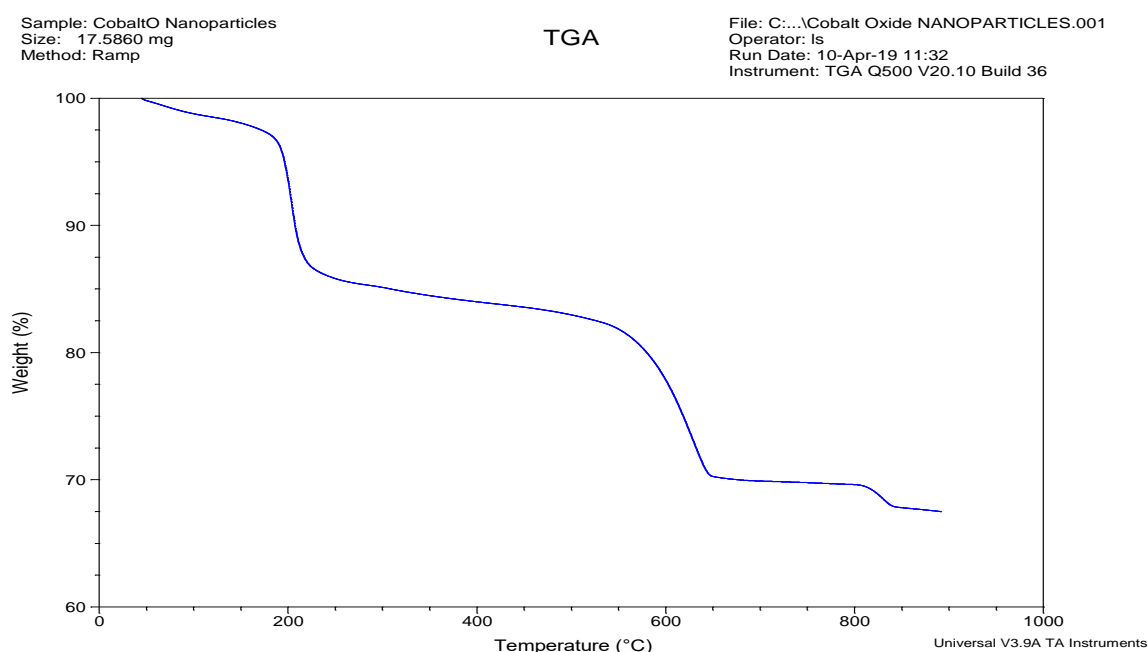


Figure 6. 3 TGA result of the synthesised Cobalt Oxide nanoparticles

6.3.4 Fourier Transform Infrared Spectroscopy (FTIR)

FTIR was also used for the characterisation of the cobalt oxide nanoparticles, with the spectrum range from 400 to 4000 cm^{-1} (Figure 6.4). The absorption peak at 558 cm^{-1} was assigned to the stretching vibration mode of Co-O in which the Co^{3+} is octahedrally coordinated. Meanwhile, the absorption band at 658 cm^{-1} was attributed to the bridging vibration in Co^{2+} , which is tetrahedrally coordinated (Rani, Rani and Kumar 2018). The strong absorbance at 1340 cm^{-1} might be due to traces of un-reacted Na-OH, while the absorption bands between 3400-3600

cm^{-1} are attributed to O-H stretching and banding modes of water absorbed by the Co_3O_4 nanoparticles sample (Estepa and Daudon 1997).



Figure 6. 4. FT-IR Image showing the spectra of Co_3O_4 nanoparticles

6.3.5 Electrochemical behaviour of Gallic acid at the modified carbon paste electrode

The electrochemical behaviour of GA on the CoO-nano-CPE was studied using CV, by measuring GA ($1 \times 10^{-2} \text{ mol L}^{-1}$) in a phosphate buffer ($1 \times 10^{-1} \text{ mol L}^{-1}$, pH 2.0) at a scan rate of 100 mVs^{-1} . All measurements as earlier described were done at room temperature ($\sim 25^\circ\text{C}$). The CoO-nano-CPE was used first, to measure a blank phosphate buffer ($1 \times 10^{-2} \text{ mol L}^{-1}$) and then used to measure the GA solution. Bulk cobalt oxide was also used for the modification of the CPE and then used to measure GA ($1 \times 10^{-2} \text{ mol L}^{-1}$). The bare CPE and GCE, were also used for the measurement of the GA and the voltammograms were overlaid to compare the output of the various electrodes. As can be seen in Figure 6.5, the voltammograms show an increased peak current when cobalt oxide nanoparticles were used to modify the CPE.

The CoO-nano-CPE used for the measurement of GA ($1 \times 10^{-2} \text{ mol L}^{-1}$) produced a peak current of $404 \pm 1.8 \mu\text{A}$ at a peak potential of 0.61 V, bare CPE with peak current of $302 \pm 3.8 \mu\text{A}$ at a peak potential of 0.6 V, bulk Co_3O_4 -CPE produced peak currents of $281 \pm 3.4 \mu\text{A}$ at peak potential 0.67, while the bare GCE electrode

had $309 \pm 2.3 \mu\text{A}$ at peak potential of 0.66 V. With the cobalt oxide nanoparticles modified electrode showing a positive enhancement in peak current and a positive shift in peak potential; the metal oxide nanoparticles modification may not have catalysed the reaction. Hence, the peak current enhancement was not based on electrocatalysis, but on an increase in reactive surface area on the surface of the electrode. This is because of the presence of the increased surface area created by the nanoparticles. The cobalt oxide nanoparticles, in this case, increased the surface area of the modified CPE, hence creating a decreased electron transfer resistance. This decreased electron transfer resistance, increases electron transfer, and thus increased peak current (Figure 6.5, Table 6.1).

Furthermore, on using bulk cobalt oxide powder for the modification of the carbon paste electrode, it was found that, the electrode did not show any peak current enhancement in GA determination (Figure 6.3). There was electron transfer, thus the visible oxidation of GA, but the transfer was a bit restrictive as compared to the other electrodes. The electron transfer restriction caused by the bulk cobalt used for the electrode modification shows, the importance of the nanoparticles in this study.

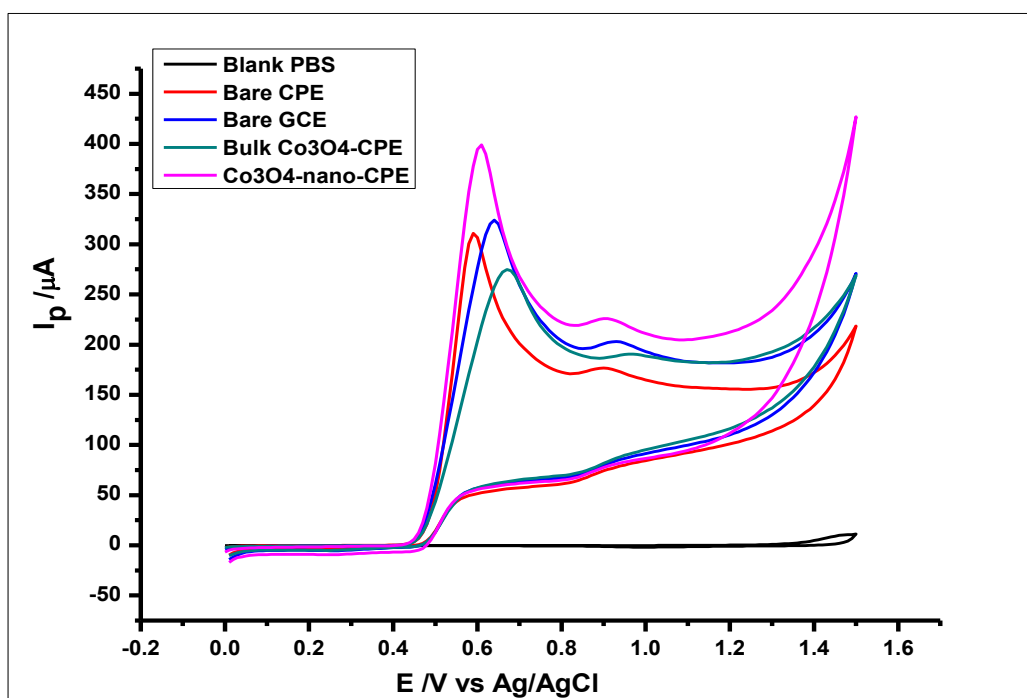


Figure 6. 5. Cyclic voltammograms of $1 \times 10^{-2} \text{ mol L}^{-1}$ GA at Co_3O_4 nanoparticles-modified CPE, bulk Co_3O_4 nanoparticles-modified CPE, bare CPE and bare glassy carbon electrode (GCE) in 0.1 mol L^{-1} phosphate buffer of pH 2.0 at a scan rate of 100 mVs^{-1}

On the other hand, the GA produced two oxidation peaks as earlier reported in the electrochemical oxidation of GA (Tashkhourian et al. 2013; Ziyatdinova and Budnikov 2014). In the course of the anodic sweep from 0.0 to 1.5 V, the voltammograms show two anodic peaks on the forward sweep and the return sweep showing currents of low intensity and no visible peak. The two visible anodic peaks as earlier discussed, tells us that, GA after the first oxidation peak undergoes another reaction that produces the second oxidation peak. On the return sweep, GA does not show any sign of a reduction in the course of using all the electrodes. On measuring just, the phosphate buffer ($1 \times 10^{-1} \text{ mol L}^{-1}$, pH 2.0) at a scan rate of 100 mVs^{-1} the CoO-nano-CPE, did not show any peaks or reactions at the same scan potential range of 0.0 to 1.5 V. Hence, it is concluded that, the cobalt oxide nanoparticles added to the CPE, exhibited a significant effect in the electrochemical determination of GA, which shows an enhancement in the peak current.

Table 6. 1. The peak currents (I_p) and Peak Potentials (E_p) produced by the different electrodes used for the determination of $1 \times 10^{-2} \text{ mol L}^{-1}$ GA in 0.1 mol L^{-1} Phosphate Buffer at pH 2.0 and scan rate 100 mVs^{-1}

	Electrodes	Peak Current/I_p (μA)	Peak Potential/E_p (V vs Ag/AgCl)
1	Bare Carbon Paste Electrode	302 ± 3.8	0.6
2	Bare Glassy Carbon Electrode	309 ± 2.3	0.66
3	Bulk Cobalt Oxide-CPE	281 ± 3.4	0.67
4	Cobalt oxide nanoparticles-CPE	404 ± 1.8	0.61

6.3.6 Effect of pH on Gallic acid oxidation

The effect of the pH on the voltammetric response of GA on the surface of the modified electrode, was investigated in a pH range of 2.0 to 10.0, using CV at a scan rate of 100 mVs^{-1} . Using the CoO-nano-CPE, GA ($1 \times 10^{-3} \text{ mol L}^{-1}$) in phosphate buffer ($1 \times 10^{-1} \text{ mol L}^{-1}$, pH 2.0) was measured and the voltammograms recorded (Figure 6.6(A), 6.4(B) and Table 6.2). The peak currents decreased as the pH was increased from pH 2.0 to 10.0 (Figure 6.6(B) and (C)). The anodic peak current of GA decreased with increasing pH and an increasing negative shift of the peak potential (Figure 6.6(B)), from 0.6 V to 0.2 V.

From the voltammograms seen in these figures, the oxidation peak at pH 2.0 was a well-defined and shaped peak, with the highest peak current of $30.5 \pm 5 \mu\text{A}$ at a

peak potential of 0.54 V, while the other pH of 4.0, 6.0, 8.0 and 10.0 as shown in Table 6.2; showed lower peak currents. This shows a vivid influence of pH towards the electrochemical oxidation of GA at the surface of the CoO-nano-CPE. In subsequent measurements pH, 2.0 was used as the optimum pH for the determination of GA.

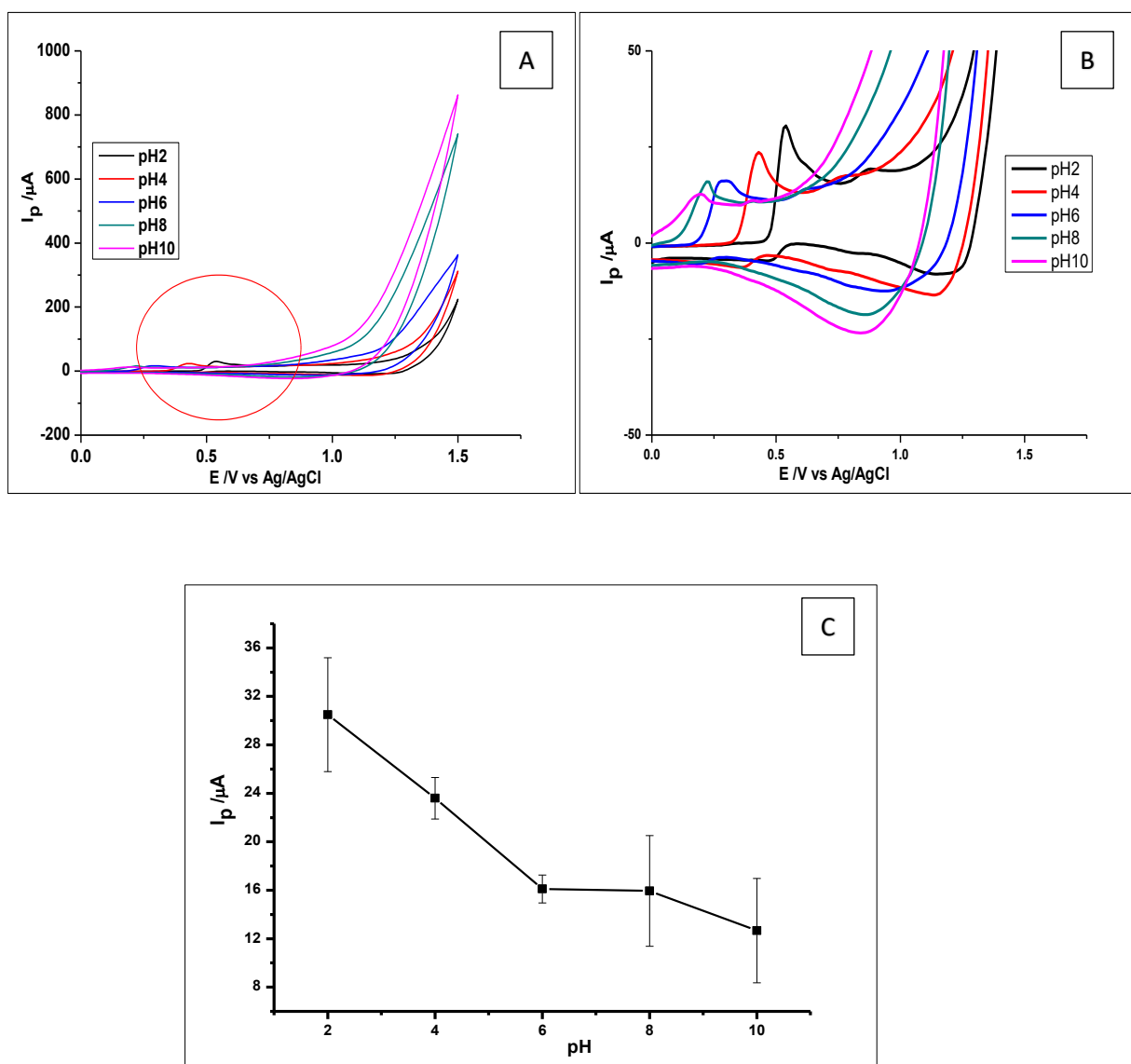


Figure 6. 6. (A) The cyclic voltammograms of 1×10^{-3} mol L⁻¹ GA in the different pH range of 2.0 to 10.0 at a scan rate 100 mVs⁻¹ (B) Zoomed image of the voltammograms (C) A graph of pH against the peak currents.

Table 6. 2. Peak currents and Peak Potentials produced by 1×10^{-3} mol L⁻¹ GA measured by CV using CoO-nano-CPE at different pH and scan rate 100 mVs⁻¹

	pH	Peak Current/ I_p (μ A)	Peak Potential/ E_p (V vs Ag/AgCl)
1	2.0	30.499 ± 4.7	0.54
2	4.0	23.592 ± 1.72	0.43
3	6.0	16.102 ± 1.16	0.28
4	8.0	15.949 ± 4.57	0.22
5	10.0	12.664 ± 4.3	0.2

6.3.7 Effect on the scan rate

The effect of different scan rates on the electrochemical response of GA on the surface of the CoO-nano-CPE was studied, at a range of 50 – 400 mVs⁻¹ using CV. GA at a concentration of 1×10^{-3} mol L⁻¹ in phosphate buffer (1×10^{-1} mol L⁻¹, pH 2.0) was measured at room temperature and the voltammograms recorded as shown in Figure 6.7.

The oxidation peak currents of GA increased linearly as the scan rate was being increased in the range of 50-400 mVs⁻¹. This was expressed in a linear regression equation from the plot on Figure 6.5(B) thus; $I_p = 0.1979 v + 11.831$ with $R^2 = 0.9966$. Meanwhile, the resulting peak potentials show a slight positive shift as the scan range increased (Figure 6.7). This is mainly because the size of the diffusion layer is dependent on the scan rate. At the lower scan rates, the diffusion layer grows further from the electrode surface, as compared to the higher scan rates (Velmurugan et al. 2017). This implies that, the flux is significantly higher at the electrode surface at higher scan rates, creating an internal resistance at the electrode-electrolyte interface; hence, the positive shift in peak potential. From the results, the interaction of GA at the electrode surface was found to be an adsorption-controlled reaction.

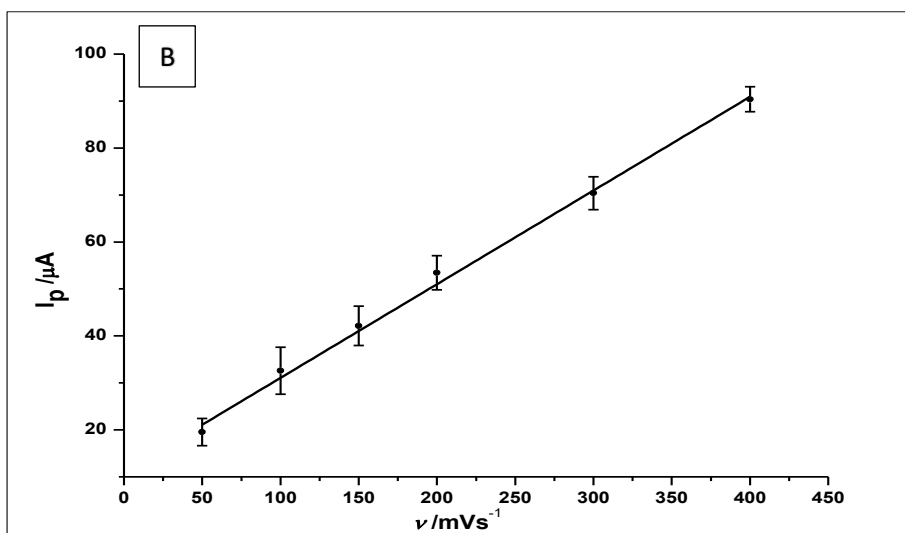
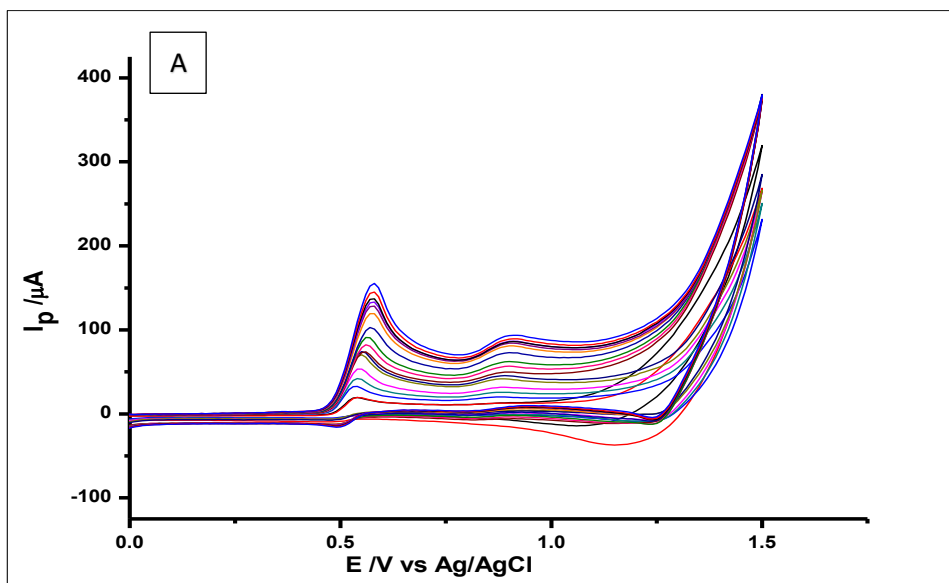


Figure 6. 7. (A) CV voltammograms of $1 \times 10^{-3} \text{ mol L}^{-1}$ GA in $1 \times 10^{-1} \text{ mol L}^{-1}$ Phosphate buffer solution at pH 2.0, showing different scan rates ranging from 50 -1400 mVs^{-1} (B) Plot of the scan rates from 50-400 mVs^{-1} against the peak current.

6.3.8 Effect of concentration changes of Cobalt oxide nanoparticles

The effect of changes in the quantity of Cobalt oxide nanoparticles used in the modification of CPE was studied. As earlier described using amorphous zirconia nanoparticles, 0.5 g, 0.1 g, 0.15 g and 0.2 g of cobalt oxide nanoparticles were weighed and mixed with graphite powder of appropriate ratio. The modified electrode was then used for the electrochemical determination of GA ($1 \times 10^{-2} \text{ mol L}^{-1}$) in phosphate buffer solution ($1 \times 10^{-1} \text{ mol L}^{-1}$, pH 2.0) and a scan rate of 100 mVs^{-1} using CV. From the results shown in (Figure 6.8), the CPE with the 10%

Cobalt oxide nanoparticles showed the highest peak current and a very clear voltammogram. Hence, the 10% cobalt oxide nanoparticles-modified CPE was subsequently used for further measurements.

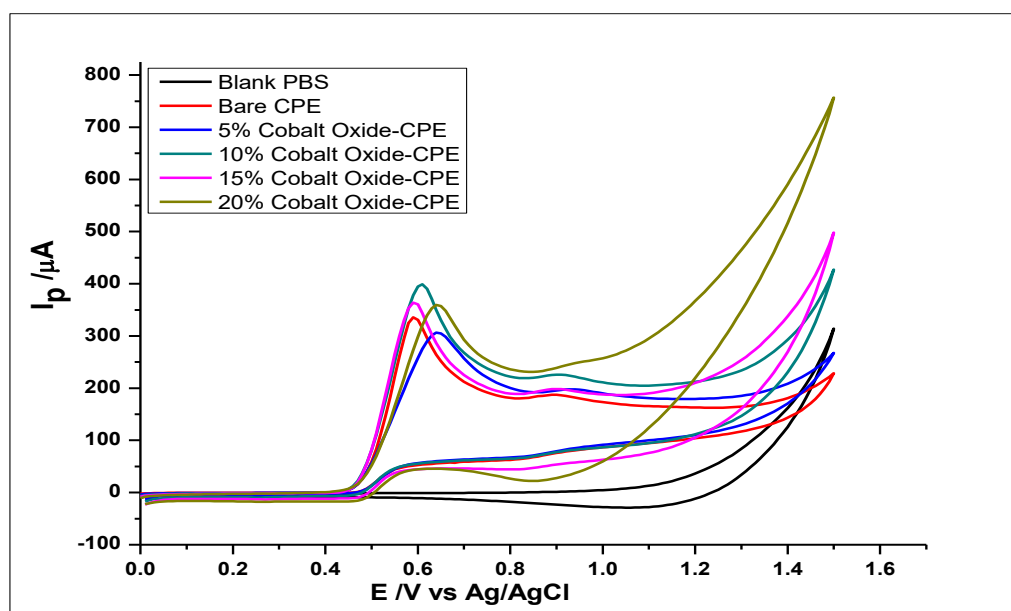


Figure 6. 8. Voltammograms showing changes in the constitution of the carbon paste electrode using 5%, 10%, 15% and 20% Cobalt oxide nanoparticles constituted in the modified CPE. This was used to determine $1 \times 10^{-2} \text{ mol L}^{-1}$ GA in $1 \times 10^{-1} \text{ mol L}^{-1}$ phosphate buffer at pH 2.0 using CV at a scan rate of 100 mVs^{-1}

6.3.9 Effect of time on adsorption of GA

The effect of time on the adsorption of GA on the surface of the CoO-nano-CPE was also studied in this case, by using the optimised electrode for the determination of GA ($1 \times 10^{-3} \text{ mol L}^{-1}$) in a phosphate buffer ($1 \times 10^{-1} \text{ mol L}^{-1}$, pH 2.0) at a scan rate of 100 mVs^{-1} using DPV, at room temperature. Just like in the case of the other metal oxide nanoparticles, the voltammograms produced by the oxidation of GA, every minute for six minutes were analysed. Looking at the voltammograms in Figure 6.9, the peak current increases as the voltammograms are recorded per minute, up to 5 mins in this case, where the peak current does no longer increase; instead with a further increase of the time to 7th minute, the peak currents decreased. This is in line with works carried out by other researchers in the determination of GA (Tashkhourian and Nami-Ana 2015). They suggested that, the phenomenon of no further increase in peak current, with an increase in time; was because of GA saturation at the surface of the modified electrode.

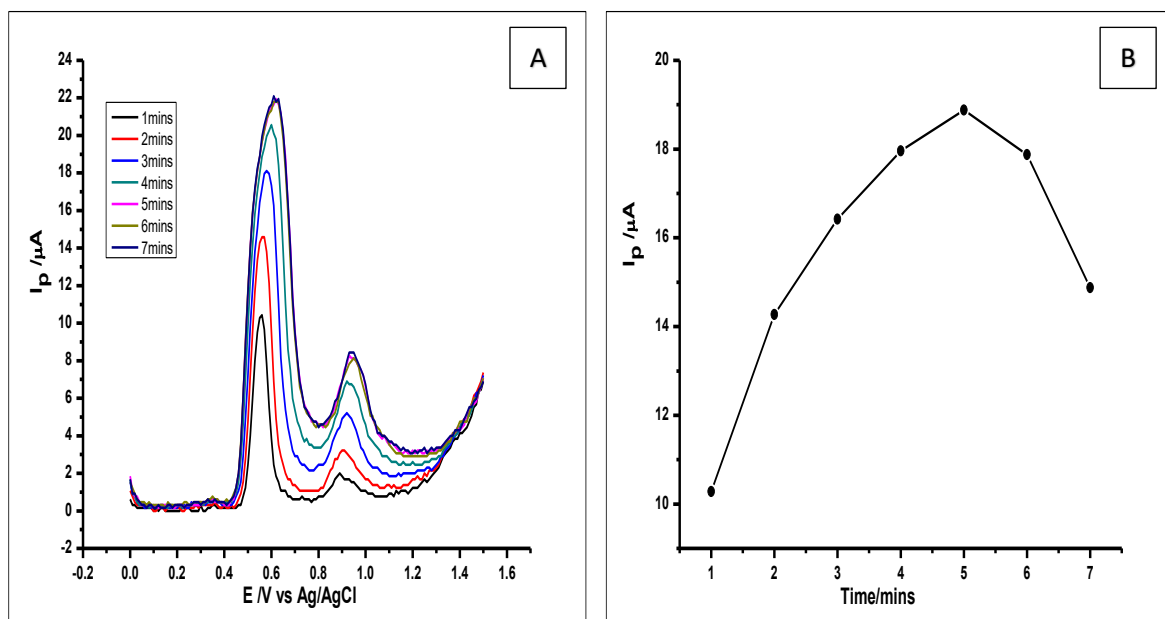


Figure 6. 9. (A) DPV voltammograms showing the effect of time on the adsorption of GA on the surface of CoO-nano-CPE in the determination of $1 \times 10^{-3} \text{ mol L}^{-1}$ GA in a $1 \times 10^{-1} \text{ mol L}^{-1}$ phosphate buffer of pH 2.0 at a scan rate of 100 mVs^{-1} (B) The plots showing the same effect of time on adsorption

6.3.10 Effect of the modified electrode on GA concentration

Differential pulse voltammograms (DPV) was used for the determination of the linear range and the lower limit of GA detection at the surface of the CoO-nano-CPE. DPVs were then obtained by the oxidation of different concentrations of GA in phosphate buffer ($1 \times 10^{-1} \text{ mol L}^{-1}$, pH 2.0) on the surface of the CoO-nano-CPE. The DPV was recorded at a potential range of 0 V to +1.2 V, the scan rate of 100 mVs^{-1} , pulse amplitude of 80 mV and pulse periods of 0.2 s. The recorded results were then used for the determination of the linear range and the LOD of the modified electrode.

There was a proportional increase in peak current as the concentration of GA increased (Figure 6.10). Within the concentration range of 1×10^{-4} to $1 \times 10^{-2} \text{ mol L}^{-1}$, the DPV produced voltammograms of GA with two peaks at peak potentials of 0.55 V and 0.9 V, respectively.

The first and major peak of the voltammograms produced by the different concentrations was used to produce the calibration graph, as can be seen in Figure 6.8 (inset). The calibration plot shows a linear relationship between the peak

current (I_p) and the increasing concentration of GA. However, the linear range was just between 1×10^{-4} to 1×10^{-3} mol L⁻¹, where the linear relationship produced a linear regression equation of $I_p = 11285.86 C - 0.07936$ (I_p : μ A, C : mmol L⁻¹ and $R^2 = 0.9934$) as can be seen in Figure 6.11.

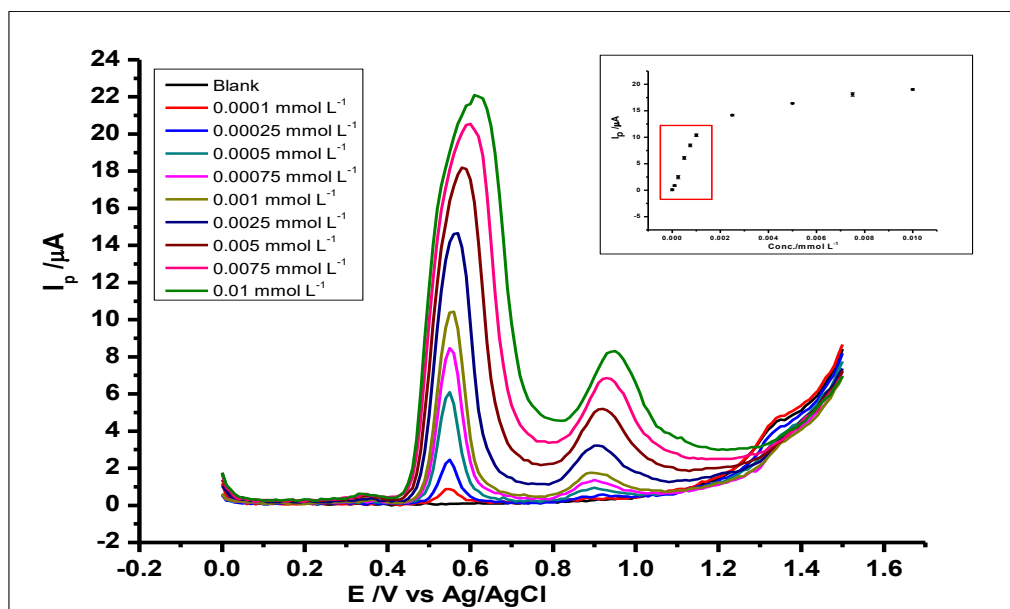


Figure 6. 10. Differential voltammograms of various concentrations of GA at CoO-nano-CPE in a 0.1 mol L⁻¹ phosphate buffer at 2.0 at scan rate of 100 mVs⁻¹, with voltammograms (a-j) that corresponds to the following concentrations a) Blank PBS, b) 1×10^{-4} mmol L⁻¹, c) 2.5×10^{-4} mmol L⁻¹, d) 5×10^{-4} mmol L⁻¹, e) 7.5×10^{-4} mmol L⁻¹, f) 1×10^{-3} mmol L⁻¹, g) 2.5×10^{-3} mmol L⁻¹, h) 5×10^{-3} mmol L⁻¹, i) 7.5×10^{-3} mmol L⁻¹, j) 1×10^{-2} mmol L⁻¹ (inset) Plot of concentration of GA against peak currents.

From the plot shown in Figure 6.11, the linear detection range which is the range at which the CoO-nano-CPE detection of GA is linear with increasing concentration. This range was found to be 1×10^{-4} to 1×10^{-3} mol L⁻¹, while the LOD defined as $(3 \times Std_{Blank})/m$ where Std_{Blank} is the standard deviation of the blank and m is the slope; was found to be 1.52×10^{-6} mol L⁻¹ (0.00152 mmol L⁻¹). With this limit of detection, CoO-nano-CPE is comparable to other electrodes that have been used for the determination of GA as described in Chapter 4. This is because the LOD is below the maximum permitted antioxidant level in food within the EU and North America, which is 1.2×10^{-1} mol L⁻¹ to 6.0 mol L⁻¹ for GA in the guidelines.

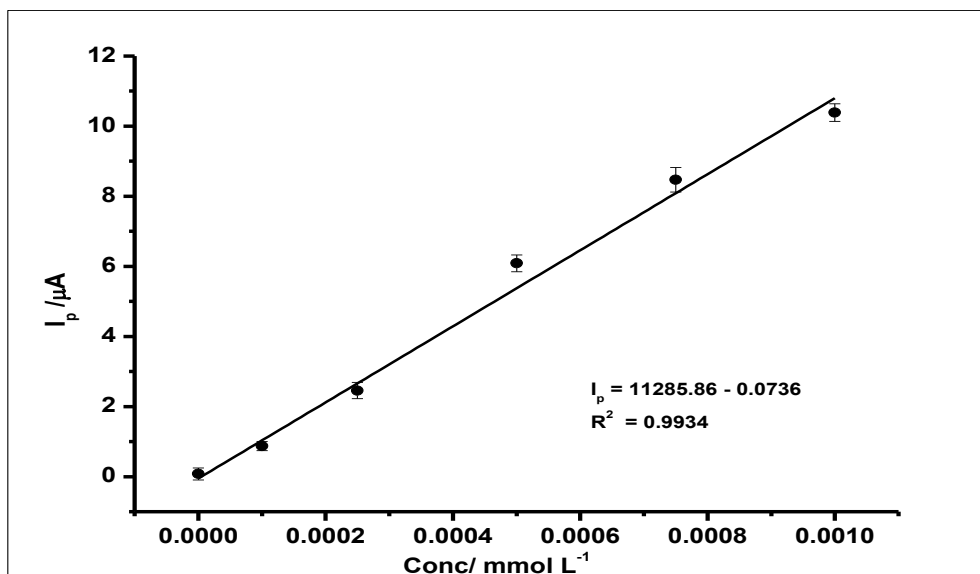


Figure 6. 11. The plot of the Peak Current (I_p) against the concentration of GA, showing the effect of concentration on the electrochemical behaviour of increasing GA concentration, using CoO-nano-CPE at a scan rate of 100 mVs^{-1}

6.3.11 Reproducibility and repeatability of the method

The reproducibility of the determination of GA using the CoO-nano-CPE was carried out, by using the modified electrode for the determination of GA ($5 \times 10^{-4} \text{ mol L}^{-1}$) using DPV. This was done by measuring the GA with six different modified electrodes (prepared on different days). From all the measurements carried out, the relative standard deviation of the peak currents produced was 4.56%, which shows very good reproducibility (Figure 6.12(A)).

The repeatability of the method was also investigated by using the modified electrode for six repeated independent determination of $5 \times 10^{-4} \text{ mol L}^{-1}$ GA using DPV. The relative standard deviation of the voltammograms was 0.66%, showing very good repeatability (Figure 6.12(B)).

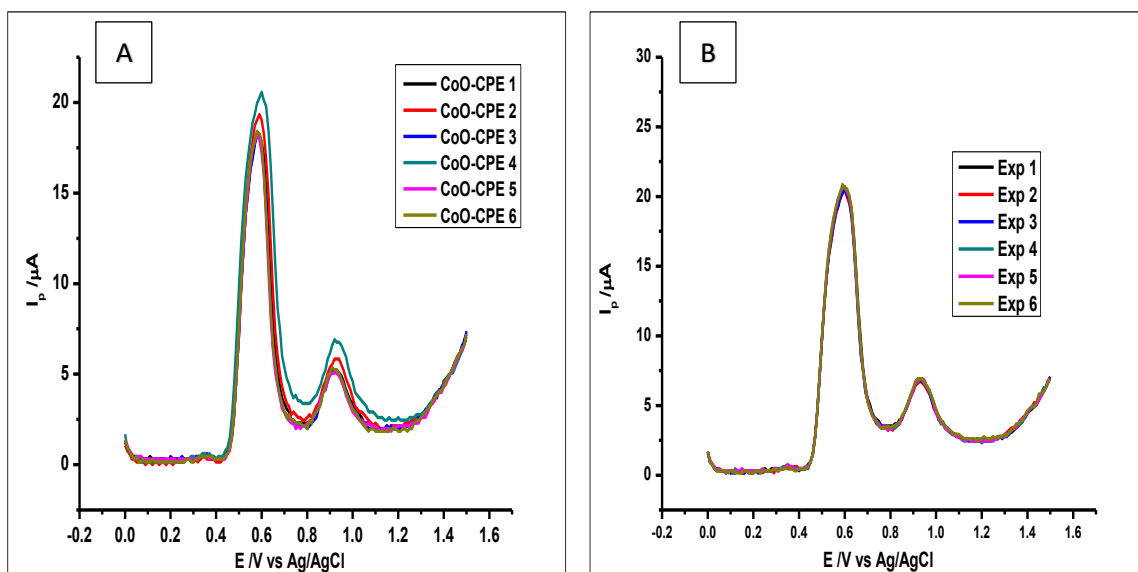


Figure 6. 12 DPV voltammograms of 5×10^{-4} mol L $^{-1}$ Gallic acid showing (A) Reproducibility of the CoO nanoparticles modified CPE (B) Repeatability of the CoO nanoparticles modified CPE

6.3.12 Stability of the method

The stability of the CoO-nano-CPE produced was also studied by the determination of GA (5×10^{-4} mol L $^{-1}$) using DPV. This was done by recording the DPV of the GA with newly prepared modified electrodes, 15 days and 30 days after the first use. The recorded peak currents showed peak currents with RSD of 6.32% (Figure 6.13). Showing very good stability of the modified electrode.

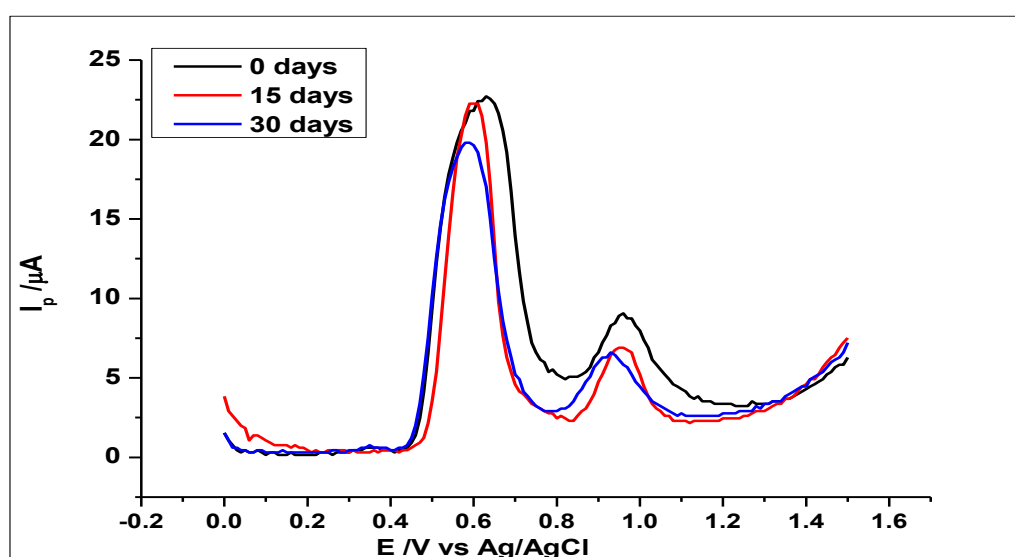


Figure 6. 13. DPV voltammograms of 5×10^{-4} mol L $^{-1}$ Gallic acid, showing voltammograms measured by the same electrodes after 0 days, 15 days and 30 days: showing stability.

6.3.13 Interference study

The CoO-nano-CPE was also used to study the interference, hence the selectivity of the electrode when it is measuring GA in the presence of common interfering species. The interfering species used in this case were caffeine, caffeic acid, ascorbic acid, quercetin and ions like K^+ , Fe^{3+} , Na^+ , Ca^{2+} , Cl^- , and CO_3^{2-} . These species as earlier discussed were selected because of their stated capability in the literature for GA complexation (Fazary, Taha and Ju 2009; Hassanien *et al.* 2011). From voltammograms recorded (Figure 6.14) showing an RSD of 4.9%; the ions and the organic compounds did not interfere with the determination of GA. This is because for there to be interference, the RSD of voltammograms of the mixed solutions (ions + GA) have to be beyond 5%. The tolerable limits of these ions are the amounts of the foreign ion, which would cause a relative standard error of more than 5%. From the results (Figure 6.14) and the RSD, there was no interference recorded.

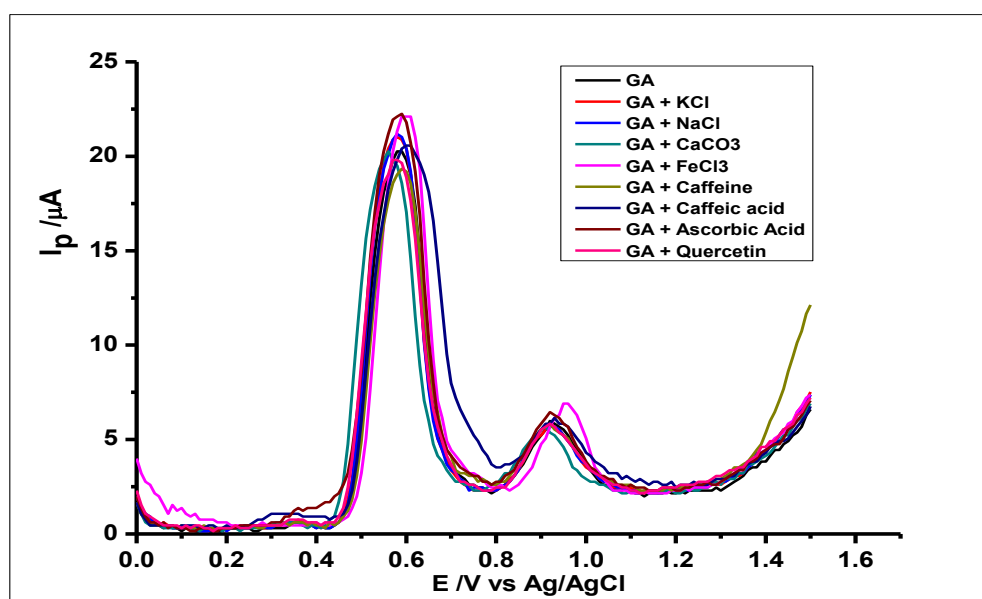


Figure 6. 14. DPV voltammograms of 5×10^{-4} mol L^{-1} Gallic acid with different concentrations of some known interfering compounds in 0.1 mol L^{-1} phosphate buffer at pH 2.0 and a scan rate of 100 mVs^{-1}

6.3.14 Analytical Application of the modified electrode for the determination of GA in Red/White Wine

The modified electrode was used just like in the previous chapters for the electrochemical determination of GA in samples of red wine, white wines, and orange juice.

An appropriate amount of Red Wine was prepared by dilution into 0.01 mol L⁻¹ phosphate buffer and the sample brought to an acidic pH of 2.0, using phosphoric acid (0.1 mol L⁻¹). Then the sample was used as a blank and then studied using DPV at room temperature. The DPV results were then recorded at a potential range of 0 V to +1.6 V, the scan rate of 100 mVs⁻¹, pulse amplitude of 80 mV and a pulse period of 0.2 s.

Aliquots of GA (0.01 mol L⁻¹) were added to the red wine sample using the standard addition method, and then voltammograms recorded. The voltammograms recorded for the red wine can be seen in Figure 6.15(A). The peak current values for the first peak for each of the increasing concentrations of GA in the sample were used to develop a calibration graph of concentration versus peak current as can be seen in Figure 6.15 (B). From the calibration graph, it can be noticed that the increasing concentration of GA showed a linear relationship with the oxidation peak current (I_p). This is demonstrated by the linear regression equation deduced from the calibration; thus, $I_p = 2.254 \text{ Conc. (mmol L}^{-1}) + 1.195$ with $R^2 = 0.9936$. This equation was then used to determine the concentration of GA in the wine sample.

From the voltammograms, in Figure 6.15 the Co₃O₄ nanoparticles modified electrode detected GA in the blank red wine sample. Whilst the addition of GA confirms the fact that, the first determination in the blank sample was actually GA. However, as the concentration of GA in the wine sample increased, there was an unusual third oxidation peak that became noticeable.

It should be noted that, the voltammograms of GA when measured with DPV show two oxidation peaks at peak potential ranges of 0.35 V to 0.6V for the first peak and 0.8 V to 1.0 V for the second peak (Tashkhourian and Nami-Ana 2015).

In the case of this red wine determined by the cobalt oxide modified CPE, the first and the second oxidation peaks are detected at peak potentials of 0.59 V and 1.02 V, while, the third unusual peak is seen at a peak potential of 0.76 V. This third

peak can be attributed to an activation of another organic compound as the GA acid increases in the wine sample.

Looking at HPLC results shown in Appendix Figure 8.7, page 211-212 and results of HPLC analysis of red wine samples by (Tarola, Milano and Giannetti 2007; Ragusa *et al.* 2019); the third peak could be catechin and epicatechin.

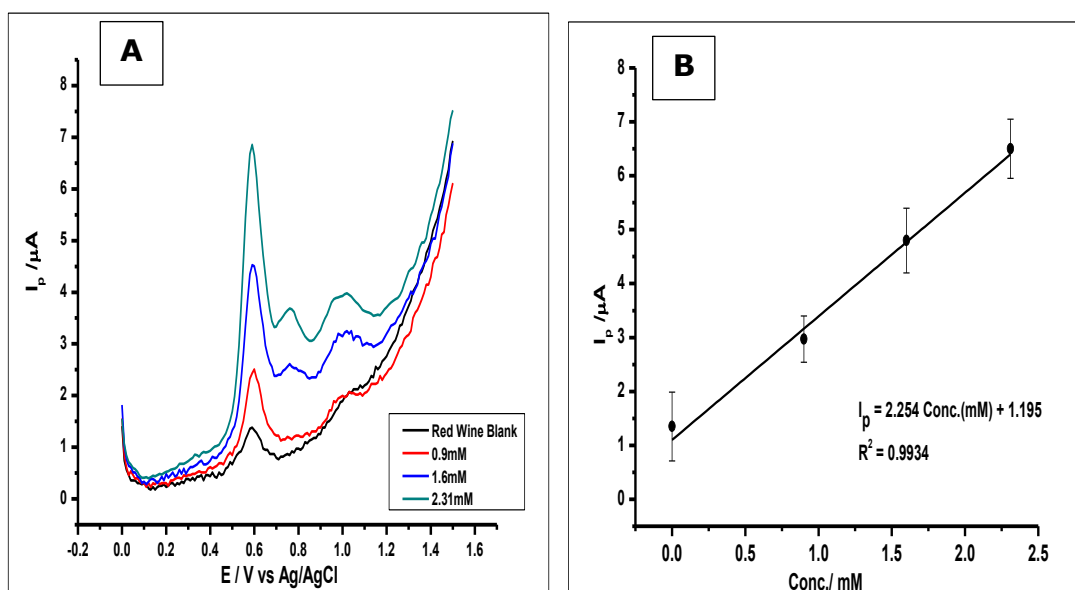


Figure 6. 15. (A) Voltammograms of aliquots of $1 \times 10^{-2} \text{ mol L}^{-1}$ of GA added into Red Wine using a standard addition method (B) Calibration curve of the standard addition of Gallic acid.

Furthermore, as can be seen in Figure 6.16, the cobalt oxide nanoparticles modified electrode was also applied for the determination of GA in white wine sample.

The white wine sample was prepared, just like the red wine earlier described. Then aliquots of GA (0.01 mol L^{-1}) in a phosphate buffer (0.1 mol L^{-1} , pH 2.0), were added by standard addition method to the white wine solution. The mixture was mixed using a magnetic stirrer for about 2 minutes then measured using DPV. The differential pulse voltammograms were then recorded as can be seen in Figure 6.16 (A). From the results, it can be observed that, the cobalt oxide modified carbon paste electrode detected GA in the white wine. The blank white wine sample showed an oxidation peak at a peak potential of 0.61 V.

With the standard addition of GA, it could be noticed that, at almost the same peak potential of 0.61 V, there was a proportional increase in the peak current. This tends to confirm the determination of GA in white wine. Using the peak

current values from the voltammograms, a calibration graph was then produced showing the relationship between the concentration of GA versus the peak current values (Figure 6.16 (B)). The linear relationship demonstrated by the calibration graph, produced a linear regression equation; thus, $I_p = 6.095 \text{ Conc (mmol L}^{-1}) + 4.344$ with $R^2 = 0.9918$. The equation as earlier on, was then used for the quantitative determination of GA contained in the white wine sample.

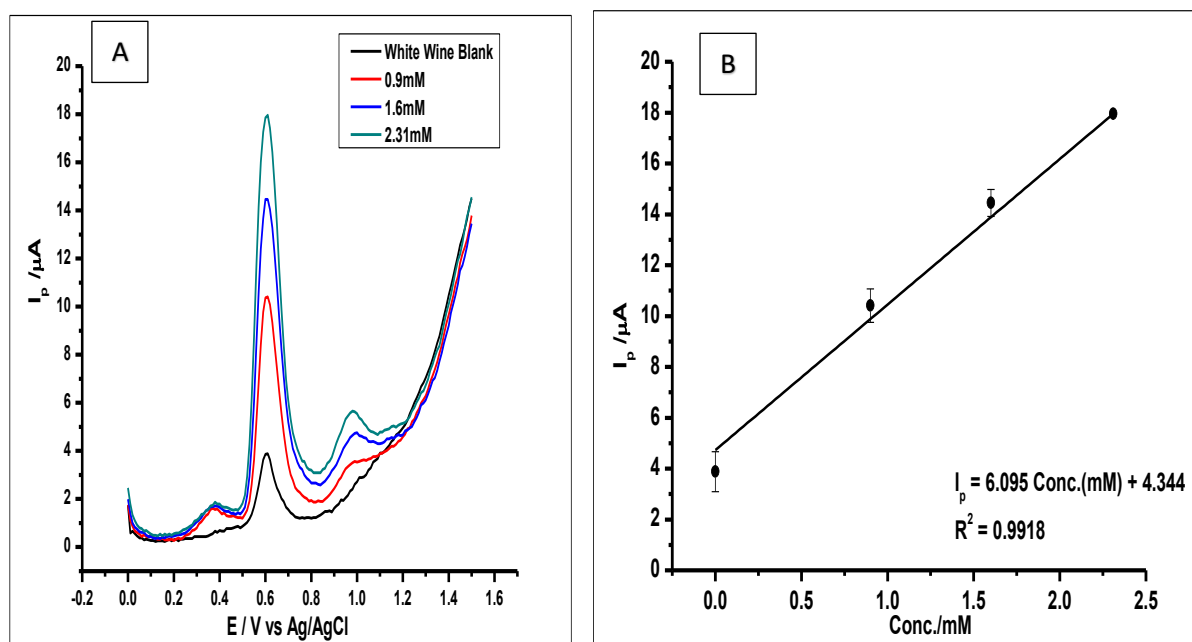


Figure 6. 16. (A) Voltammograms of aliquots of $1 \times 10^{-2} \text{ mol L}^{-1}$ of GA added into White Wine using a standard addition method (B) Calibration curve of the standard addition of Gallic acid.

Finally, the modified CPE was also applied in the determination of GA in the Orange Juice sample. The orange juice was prepared by diluting the appropriate amount of the sample with phosphate buffer solution (0.01 mol L^{-1}) and brought to a pH of 2.0 using 0.1 mol L^{-1} phosphoric acid. Differential pulse voltammetry was then used to measure the blank which is diluted orange juice in this case and then GA was further added to the sample.

Aliquots of GA (0.01 mol L^{-1}) were added to the orange juice samples using the standard addition method. The differential pulse voltammograms were then recorded as was the case in the wine sample. The results can be seen in Figure 6.17, where the usual two oxidation peaks of GA were observed. The first peak current was observed at a peak potential of 0.64 V and the second peak at 0.86 V. Looking at Figure 6.17 (B), a calibration graph of concentration versus peak

current was produced from the increasing concentration of the standard addition of GA. The linear relationship of these two parameters produced a linear regression equation in the format: $I_p = 7.041 \text{ Conc (mol L}^{-1}) + 5.631$ and $R^2 = 0.9911$.

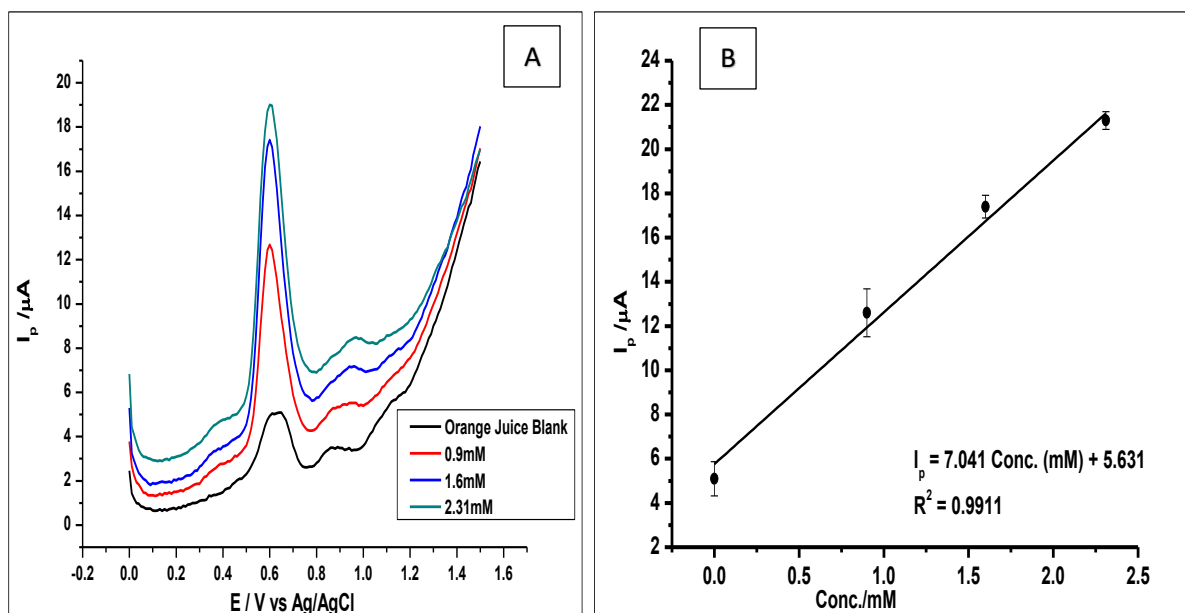


Figure 6. 17. (A) Voltammograms of aliquots of $1 \times 10^{-2} \text{ mol L}^{-1}$ of GA added into Orange Juice using a standard addition method (B) Calibration curve of the standard addition of Gallic acid.

Using all the data produced by these application experiments one could produce the results shown in Table 6.3. The table below shows the quantitative results of the analysis of the samples, which include the amount of GA added to the samples and the amount recovered after analysis. Hence, expressing the amount of GA found in the analysed sample.

Table 6. 3. Results of the analysis of GA in spiked Red Wine, White Wine, and Orange Juice

Samples	Added (mmol L ⁻¹)	Found (mmol L ⁻¹)	Relative Error	Recovery (%)
Red Wine	0.0	0.688	-	
	0.9	0.787	±13	87
	1.6	1.599	±0.7	99.93
	2.31	2.35	±1.73	101.73
White Wine	0.0	0.076	-	-
	0.9	0.995	±10.5	110.5
	1.6	1.658	±3.63	103.63

	2.31	2.23	±3.46	96.54
Orange Juice	0.0	0.0768	-	-
	0.9	0.9897	±9.96	109.96
	1.6	1.671	±4.44	104.44
	2.31	2.225	±3.68	96.32

6.4 Conclusion

This chapter of the thesis presents for the first time, the use of synthesised Co_3O_4 nanoparticles as a metal oxide nanoparticle for the modification of CPE, for GA determination. The metal oxide nanoparticles modified CPE was then used for the electrochemical determination of GA in a phosphate buffer (0.1 mol L^{-1} , pH of 2.0). Cyclic voltammetry and differential pulse voltammetry were then used as the electrochemical technique and it was found that, GA was oxidised on the surface of Co_3O_4 nanoparticles modified carbon paste electrode.

The modified electrode was found to be a simple, sensitive, fast, and cost-effective method for the determination of GA as compared to other electrodes in the literature, where very expensive and complex modifications were used. These electrodes have been listed in Table 1.3, page 41. The electrode also showed very good reproducibility, repeatability, and relatively good long-term stability.

The cobalt modified CPE was successfully applied for the electrochemical determination of GA in red wine, white wine, and orange juice. The results showed that, the modified electrode could test GA in a pure sample. With an unusual third anodic peak when it was used in red wine. This could be as a result of the catalytic strength of the cobalt oxide modified CPE.

CHAPTER SEVEN

7.0 GENERAL CONCLUSIONS AND FUTURE PERSPECTIVE

7.1 Conclusions

The main aim of this Ph.D. research work was to develop a simple, highly sensitive, fast, selective, and cost-effective new material for the electrochemical determination of GA. Metal oxide nanoparticles and/or graphene nanoparticles-based materials were employed to accomplish this aim.

The thesis has described the effect of the different electrode modification on the determination of GA, which is a very important antioxidant. The physicochemical properties of the following nanomaterials were put into effect; graphene oxide nanocolloids, silicon oxide nanoparticles, amorphous zirconium oxide nanoparticles, zinc oxide nanoparticles, and cobalt oxide nanoparticles.

While this study was aimed at seeking new materials for selective and cost-effective electrochemical determination of GA; it provided new insights into the use of graphene oxide nanocolloids and the metal oxide nanoparticles listed above. The study demonstrated the use of graphene oxide nanocolloids for the first time, in the electrochemical determination of an organic compound. By using SEM, EDXA, FTIR, CV and EIS studies, the results demonstrated a synergistic effect between graphene oxide nanocolloids and silicon oxide nanoparticles, towards the electrochemical determination of GA. Whilst using the two nanomaterials for the determination of GA, the following important conclusions were made.

1. Graphene oxide nanocolloids on their own on the surface of the GA, enhanced the electron transfer of GA on to the GCE surface; thus, an enhanced electrochemical response towards the electro-oxidation of GA in aqueous phosphate buffer. The quantity of the graphene oxide on the surface of the glassy carbon electrode was found to have an effect on the electrochemical determination. Where the concentration of graphene oxide nanocolloids drop cast on the surface of the GCE, was optimal only at a volume of 5 μL .
2. The use of silicon dioxide nanoparticles for the modification of the glassy carbon electrode had a poor electrochemical effect compared to the other oxide nanoparticles. However, for the first time an insoluble, insulating

ceramic crystal like SiO₂ nanoparticles have used its physical properties synergistically with graphene oxide nanocolloids.

3. The synergistic interaction between graphene oxide nanocolloids and SiO₂ nanoparticles was also demonstrated for the first time. Where a mechanism, for the interaction was proposed based on hydrogen bonding between nano-GO and SiO₂ nanoparticles. This was followed by the adsorption of GA on to the surface of the silicon oxide nanoparticles. An alternative reason for the synergistic effect was also proposed as the voltammetry three-phase junction between graphene oxide nanocolloids, SiO₂ nanoparticles, and the GA.
4. The study on the effect of pH on the determination of GA, showed decreasing peak current as the pH increased. This was explained using the pKa of GA and its interaction with silicon oxide.
5. With increasing time and increasing number of scans, GA was found to adsorb increasingly on the surface of the modified GCE until a saturation point, where further scans did not affect the peak currents produced by the GA.
6. The combined nanomaterials in this study, however, showed no catalytic effect in the oxidation of GA.

Furthermore, different metal oxide nanoparticles were synthesised and used to modify carbon paste electrode for the electrochemical determination of GA. For the first time in the literature, oxide nanoparticles of zinc, zirconium and cobalt were used for the electrochemical determination of GA. Their individual performance towards the oxidation of GA were studied and the following key conclusions were reached.

1. On the modified surface of the carbon paste electrode, the GA was oxidised producing two anodic peaks when measured using CV and DPV. There was also a confirmation of the transfer of two electrons, as shown by the two anodic peaks. However, on the reverse scan whilst using CV, it was shown that GA underwent an irreversible reaction as no peaks were detected on the reverse scan.
2. For all the metal oxide nanoparticles modified electrodes used, the optimal electrochemical activity for GA was at an acidic pH of 2.0 in phosphate buffer solution (0.1 mol L⁻¹).

3. All the metal oxide nanoparticles modified carbon paste electrodes produced enhanced peak currents as compared to the bare carbon paste electrode. This would be attributed to the increased surface area that is a normal phenomenon with the nanoparticles. Most transition metals and their oxides exhibit catalytic properties, which was not seen in the metal oxides used in this study. This might be attributed to the sizes of the nanoparticles or the quality of the carbon paste electrode.
4. The limit of detection (LOD) of GA as produced from the different metal oxide nanoparticles modified carbon paste electrode was as follows:- ZrO₂ nanoparticles CPE LOD; 1.24×10^{-6} mol L⁻¹ at a range of 1×10^{-6} to 1×10^{-3} mol L⁻¹, ZnO nanoparticles LOD; 1.86×10^{-7} mol L⁻¹ at a range of 1×10^{-3} to 1×10^{-2} mol L⁻¹ and Co₃O₄ nanoparticles LOD; 1.52×10^{-7} mol L⁻¹ at a range of 1×10^{-4} to 1×10^{-3} mol L⁻¹. All the LOD produced by the metal oxide nanoparticles modified CPE are comparable to other LODs of different analytical techniques in the literature.
5. The cobalt oxide nanoparticles modified electrode produced an unusual third oxidation peak, while being used for the determination of GA in the red wine sample.

From the results of the voltammetric determination of GA by the four different modified electrodes, amorphous ZrO₂ nanoparticles modified CPE was adjudged to be the best electrode. This is in terms of the LOD, sensitivity and their analytical application on red and white wine samples. Although Co₃O₄ nanoparticles-modified CPE showed an unusual new third anodic peak in the GA determination of red wine; they showed a limit of detection of 10^{-6} mol L⁻¹ as compared to 10^{-7} mol L⁻¹ for the ZrO₂ nanoparticles. Hence, amorphous ZrO₂ nanoparticles modified CPE, would be able to detect GA at very low concentrations.

However, there was an expectation of electro-catalysis of GA oxidation, having used a transition metal like zirconium. Unfortunately, the GA did not show any electro-catalysis on the surface of the ZrO₂ nanoparticles-modified CPE. This could be because of these possible reasons, which might include the sizes of the nanoparticles, electrode fouling and the electrochemical method used. Or even the possibility that the metal oxides of these compounds do not have the catalytic ability of their respective elements towards GA oxidation.

On the other hand, zinc oxide nanoparticles also showed a relatively good LOD and sensitivity; but did not show any electro-catalysis, like the other electrodes.

From these results, shown by the metal oxide nanoparticles used, there is still potential for further studies, using other analytical equipment and methods. This might include the use of atomic force microscopy (AFM) or X-ray photoelectron spectroscopy (XPS), to study the details of the interaction between the nanoparticles and the carbonaceous materials.

While the thesis deals, with the use of various nanomaterials as electrochemical sensors for the determination of GA, the application of these sensors in the determination of other antioxidants in real-life samples cannot be overemphasised. Hence, they can be used as valuable tools in the understanding of other processes in samples.

In addition, Table 7.1 shows some of the different electrodes that have been developed for the determination of gallic acid in different matrices. It has been previously stated that, the electrodes developed in this work, were simple sensitive, fast, and cost effective. This is when comparing them with the electrodes in table 7.1, with regards to the electrode composition and the limit of detection. From electrode 1 to 11 on the table, the electrode compositions were made up of two or more elements or compounds as compared to the single metal oxide nanoparticles in electrode 12, 14 and 15 developed for this work. This process and method developed from the other electrodes are time consuming and more expensive than ours. Hence, our electrodes are simple, fast, and cost effective.

Regarding the sensitivity of our electrodes, one can observe that, the limit of detection (LOD) ranges from $1 \times 10^{-6} \text{ mol L}^{-1}$ to about $7 \times 10^{-9} \text{ mol L}^{-1}$, for all the electrodes in the table. All the electrodes we developed as shown in Table 7.1 electrodes 12-15, have limits of detections of $1.24 \times 10^{-7} \text{ mol L}^{-1}$ for Am-ZrO₂-CPE, $6.25 \times 10^{-6} \text{ mol L}^{-1}$ for nano-GO-SiO₂-nanoparticles-GCE, $1.86 \times 10^{-7} \text{ mol L}^{-1}$ for nano-ZnO-CPE and $1.52 \times 10^{-2} \text{ mol L}^{-1}$ for nano-CoO-CPE. Their limits of detection fall with the 10^{-6} and $10^{-9} \text{ mol L}^{-1}$, which would be very appropriate for the determination of GA in the food industry. This is because the limit of detections exhibited by our electrodes are comparable to other methods based on the maximum permitted antioxidant levels in food within the European Union and North America. The guideline prescribes ranges of 20 to 1000 ppm (20 to 1000 mg L⁻¹); which for GA, gives the permitted range of $1.2 \times 10^{-1} \text{ mol L}^{-1}$ to 5.9 mol L^{-1} . Thus, with our electrodes exhibiting these LODs, which far below these standard permitted levels, the electrodes are definitely comparable to others in the literature.

Table 7. 1. Metal Oxide Nanoparticles and Metal Nanoparticles composites in different electrochemical sensor systems for the determination of Gallic acid and our electrodes

	MO NPs and MNPs Electrode	Electrochemical technique	Analytes	Limit of Detection (mol L⁻¹)	Linear Response (mol L⁻¹)	Ref.
1	Zn-Al-NO ₃ /LDHf/GCE	DPV	Gallic acid	1.6 x 10 ⁻⁶	4.0 x 10 ⁻⁶ – 6.0 x 10 ⁻⁴	(Kahl and Golden 2014)
2	TH/NiHCF	DPV CA	Gallic acid	1.66 x 10 ⁻⁶	5 x 10 ⁻⁶ – 1.2 x 10 ⁻³	(Sangeetha and Narayanan 2014)
3	S _{DBD} AuNP-LB	CV	Gallic acid	5.6 x 10 ⁻⁶	1.0 x 10 ⁻⁷ –1.0 x 10 ⁻⁵	(Medina-Plaza <i>et al.</i> 2015)
4	CS-fFe ₂ O ₃ -ERGO/GCE	DPV	Gallic acid	1.5 x 10 ⁻⁷	1.0 x 10 ⁻⁶ – 1.0 x 10 ⁻⁴	(Gao <i>et al.</i> 2015)
5	[Cu ₂ tpmc](ClO ₄) ₄ /CGCE or CGE	DPV	Gallic acid	0.15-CGE 4.6 – CGCE	2.5 x 10 ⁻⁷ – 1.0 x 10 ⁻⁴	(Petković <i>et al.</i> 2015)
6	AuMCs/SF-GR/GCE	DPV	Gallic acid	1.09 x 10 ⁻⁸	5.0 x 10 ⁻⁸ – 8.0 x 10 ⁻⁶	(Liang <i>et al.</i> 2016)
7	AgNP/Delph/GCE	Amperometry	Gallic acid	2.8 x 10 ⁻⁷	6 x 10 ⁻⁷ –8.68 x 10 ⁻⁶	(Ghaani <i>et al.</i> 2016)
8	PDDA-GR-Pt/GCE	SWV	Gallic acid	7.0 x 10 ⁻⁹	3 x 10 ⁻⁸ – 1.0 x 10 ⁻⁶	(Gao <i>et al.</i> 2016)
9	ZrO ₂ /Co ₃ O ₄ /rGO/FTO	DPV	Gallic acid, Caffeic acid, Protocatechuic acid	-	-	(Puangjan and Chaiyasith 2016)
10	Bi ₂ MoO ₆ /Bi ₂ S ₃ Nanobelts	Photo electro-chemistry	Gallic acid	-	-	(Wang <i>et al.</i> 2017)
11	ZrO ₂ -ChCl-AuNPs/CPE	DPV	Gallic acid	2.5 x 10 ⁻⁸	2.2 x 10 ⁻⁷ –5.5 x 10 ⁵	(Shahamirifard <i>et al.</i> 2018)
12	Am-ZrO ₂ -CPE	DPV	Gallic Acid	1.24 x 10 ⁻⁷	1 x 10 ⁻⁶ - 1 x 10 ⁻³	This work
13	Nano-GO-SiO ₂ -nanoparticles-GCE	DPV	Gallic acid	6.25 x 10 ⁻⁶	1 x 10 ⁻⁶ - 1 x 10 ⁻³	This work
13	Nano ZnO-CPE	DPV	Gallic acid	1.86 x 10 ⁻⁷	1 x 10 ⁻³ - 1 x 10 ⁻²	This work
14	Nano-CoO-CPE	DPV	Gallic acid	1.52 x 10 ⁻⁶	1 x 10 ⁻⁴ - 1 x 10 ⁻²	This work

7.2 Future Perspective

The study described in this thesis and the results thereof, provides a broad foundation for continued research and development in the area of electrochemical analysis of organic compounds.

The study provides an avenue for the use of graphene oxide nanocolloids for further work in the modification of electrochemical sensors. Their further use as composites with metal oxide nanoparticles could be explored for the determination of other antioxidants.

One can also propose a further investigation into the interaction between graphene oxide nanocolloids and SiO₂ nanoparticles or other metal oxide nanoparticles. This is to tap on their synergistic effect, for use in other electrochemical sensors or electrochemical applications. With the luxury of time and funding, one could have gone further to investigate the interaction between graphene oxide nanocolloids and SiO₂ nanoparticles using some further techniques. Although, there are techniques like the Atomic force microscopy (AFM) and X-ray photoelectron spectroscopy (XPS) (Johns *et al.* 2013), which we could have used, to show some of the regularly sized nanoparticles on the surface of GO nanocolloids. XPS is a way to confirm the chemical identity of the nanoparticles; however, the interaction, may have still been elusive. Hence, the techniques proposed by Chowdhury *et al.* (2014), where they investigated the interaction of graphene oxide nanomaterials with natural organic matter and metal oxide surfaces. They used a quartz crystal microbalance with dissipation monitoring (QCM-D), where they deposited and released GO on different surfaces and used QCM-D to study them. Meanwhile, Sotirelis and Chrysikopoulos (2015) in their study, evaluated by using electrophoretic mobility measurements, the interaction of graphene oxide and quartz sand. They constructed Derjaguin-Landau-Verwey-Overbeek (DLVO) potential energy profiles, using zeta potentials for the experimental conditions. Furthermore, Xu *et al.* (2014) tried to understand the interaction between the components of graphene-based composites. They studied the interfacial interactions of semiconductors with graphene and reduced graphene oxide, using CeO₂ as a case study. They used computational measurements, where density functional theory (DFT) calculations were done by using the Vienna ab initio simulation package (VASP). Meanwhile, to explore the interaction between CeO₂ and graphene (GR), they calculated the density of states (DOSs) of individual CeO₂ and GR sheet before and after the formation of the hybrids. These different methods and techniques could have been used to probe further on the interaction between graphene oxide nanocolloids and SiO₂ nanoparticles, with possibly more metal oxide nanoparticles. For the metal oxide nanoparticles, they provide the basis for further use in the modification of electrodes for specific organic compound determination.

The studies also provide a base to understand why the transition metal oxide nanoparticles did not exhibit the catalytic properties they are normally known for and if there are possibilities to further optimise that property.

Overall, the whole study provides the bases for further studies on the use of metal oxide nanoparticles in the modification of carbon-based compounds for cheap and selective electrochemical sensor.

REFERENCES

ABDEL-HAMID, R. and NEWAIR, E.F., 2013. Adsorptive stripping voltammetric determination of gallic acid using an electrochemical sensor based on polyepinephrine/glassy carbon electrode and its determination in black tea sample. *Journal of Electroanalytical Chemistry*, 704, pp. 32–37. Available from: <http://dx.doi.org/10.1016/j.jelechem.2013.06.006>.

AFKHAMI, A., KAFRASHI, F. and MADRAKIAN, T., 2015. Electrochemical determination of levodopa in the presence of ascorbic acid by polyglycine/ZnO nanoparticles/multi-walled carbon nanotubes-modified carbon paste electrode. *Ionics*, 21(10), pp. 2937–2947.

AGÜÍ, L., YÁÑEZ-SEDEÑO, P. and PINGARRÓN, J.M., 2008. Role of carbon nanotubes in electroanalytical chemistry. A review. *Analytica Chimica Acta*, 622(1–2), pp. 11–47.

ALWAN, R.M. et al., 2015. Synthesis of Zinc Oxide Nanoparticles via Sol – Gel Route and Their Characterization. *Nanoscience and Nanotechnology*, 5(1), pp. 1–6.

ANDREI, V. et al., 2016. A single use electrochemical sensor based on biomimetic nanocerium for the detection of wine antioxidants. *Talanta*, 156–157, pp. 112–118. Available from: <http://dx.doi.org/10.1016/j.talanta.2016.04.067>.

ARMBRUSTER, D.A. and PRY, T., 2008. Limit of blank, limit of detection and limit of quantitation. *Clinical Biochemical Reviews*, 29(Suppl. 1), p. S49.

ARTILES, M.S., ROUT, C.S. and FISHER, T.S., 2011. Graphene-based hybrid materials and devices for biosensing. *Advanced Drug Delivery Reviews*, 63(14–15), pp. 1352–1360. Available from: <http://dx.doi.org/10.1016/j.addr.2011.07.005>.

ARVAND, M. and ANVARI, M., 2013. A graphene-based electrochemical sensor for sensitive detection of quercetin in foods. *Journal of the Iranian Chemical Society*, 10(5), pp. 841–849.

BADEA, M. et al., 2019. Electrochemical strategies for gallic acid detection:

Potential for application in clinical, food or environmental analyses. *Science of the Total Environment*, 672, pp. 129–140.

BADHANI, B., SHARMA, N. and KAKKAR, R., 2015. Gallic acid: A versatile antioxidant with promising therapeutic and industrial applications. *RSC Advances*, 5(35), pp. 27540–27557.

BAJPAI, B. and PATIL, S., 2008. A new approach to microbial production of gallic acid. *Brazilian Journal of Microbiology: [Publication of the Brazilian Society for Microbiology]*, 39(4), pp. 708–711. Available from: <http://www.ncbi.nlm.nih.gov/pubmed/24031294><http://www.pubmedcentral.nih.gov/articlerender.fcgi?artid=PMC3768451>.

BARD, A.J. and FAULKNER, L.R., 2001. *Electrochemical Methods: Fundamentals and Applications*. Electrochemistry. I. Faulkner, Larry R.

BATCHELOR-MCAULEY, C. et al., 2008. Copper oxide nanoparticle impurities are responsible for the electroanalytical detection of glucose seen using multiwalled carbon nanotubes. *Sensors and Actuators, B: Chemical*, 132(1), pp. 356–360.

BATCHELOR-MCAULEY, C. et al., 2015. Recent Advances in Voltammetry. *ChemistryOpen*, 4(3), pp. 224–260.

BECERRA-HERRERA, M. et al., 2015. Extraction and Determination of Phenolic Compounds in the Berries of *Sorbus americana* Marsh and *Lonicera oblongifolia* (Goldie) Hook. *Food Analytical Methods*, 8(10), pp. 2554–2559.

BENIWAL, V. et al., 2013. Recent Advances in Industrial Application of Tannases: A Review. *Recent Patents on Biotechnology*, 7(3), pp. 228–233. Available from: <http://www.eurekaselect.com/openurl/content.php?genre=article&issn=1872-2083&volume=7&issue=3&spage=228>.

BENVIDI, A. et al., 2016. Electrocatalytic oxidation of hydrazine on magnetic bar carbon paste electrode modified with benzothiazole and iron oxide nanoparticles: Simultaneous determination of hydrazine and phenol. *Cuihua Xuebao/Chinese Journal of Catalysis*, 37(4), pp. 549–560.

BROWNSON, D. a. C. and BANKS, C.E., 2014. *The Handbook of Graphene*

Electrochemistry - Chapter 2 - Interpreting Electrochemistry. Available from: <http://link.springer.com/10.1007/978-1-4471-6428-9>.

BROWNSON, D.A.C., KAMPOURIS, D.K. and BANKS, C.E., 2011. An overview of graphene in energy production and storage applications. *Journal of Power Sources*, 196(11), pp. 4873–4885. Available from: <http://dx.doi.org/10.1016/j.jpowsour.2011.02.022>.

BURKE, L.D. and MURPHY, O.J., 1979. Cyclic voltammetry as a technique for determining the surface area of RuO₂ electrodes. *Journal of Electroanalytical Chemistry*, 96(1), pp. 19–27.

CAMPBELL, F.W. and COMPTON, R.G., 2010. The use of nanoparticles in electroanalysis: An updated review. *Analytical and Bioanalytical Chemistry*, 396(1), pp. 241–259.

CAROCHO, M. and FERREIRA, I.C.F.R., 2013. A review on antioxidants, prooxidants and related controversy: Natural and synthetic compounds, screening and analysis methodologies and future perspectives. *Food and Chemical Toxicology*, 51(1), pp. 15–25.

CHANG, J. et al., 2014. Graphene-based sensors for detection of heavy metals in water: A review Chemosensors and Chemoreception. *Analytical and Bioanalytical Chemistry*, 406(16), pp. 3957–3975.

CHEEMALAPATI, S., 2018. Chemically modified electrodes-metal nanoparticles., 2(1), pp. 2017–2018.

CHEKIN, F., VAHDAT, S.M. and ASADI, M.J., 2016. Green synthesis and characterization of cobalt oxide nanoparticles and its electrocatalytic behavior. *Russian Journal of Applied Chemistry*, 89(5), pp. 816–822.

CHEKIN, F. and YAZDANINIA, M., 2014. A sensor based on incorporating Ni²⁺ into ZnO nanoparticles-multi wall carbon nanotubes-poly methyl metacrylat nanocomposite film modified carbon paste electrode for determination of carbohydrates. *Russian Journal of Electrochemistry*, 50(10), pp. 967–973. Available from: <http://link.springer.com/10.1134/S1023193514040041>.

Chemistry Glossary, 2018. [online]. Croatian-English Chemistry Dictionary & Glossary. Available from: <https://glossary.periodni.com/dictionary.php?en=alotropska+modifikacija> [Accessed 2 Nov 2019].

CHEN, D., FENG, H. and LI, J., 2012. Graphene oxide: Preparation, functionalization, and electrochemical applications. *Chemical Reviews*, 112(11), pp. 6027–6053.

CHEN, Z., BERTIN, R. and FROLDI, G., 2013. EC50 estimation of antioxidant activity in DPPH* assay using several statistical programs. *Food Chemistry*, 138(1), pp. 414–420. Available from: <http://dx.doi.org/10.1016/j.foodchem.2012.11.001>.

CHEVION, S., ROBERTS, M.A. and CHEVION, M., 2000. The use of cyclic voltammetry for the evaluation of antioxidant capacity. *Free Radical Biology and Medicine*, 28(6), pp. 860–870.

CHIA, Y.C. et al., 2010. Anti-Neoplastic effects of gallic acid, a major component of toona sinensis leaf extract, on oral squamous carcinoma cells. *Molecules*, 15(11), pp. 8377–8389.

CHIKERE, C. et al., 2019a. Zinc oxide nanoparticles modified-carbon paste electrode used for the electrochemical determination of Gallic acid. *Journal of Physics: Conference Series*, 1310, p. 012008. Available from: <https://iopscience.iop.org/article/10.1088/1742-6596/1310/1/012008>.

CHIKERE, C.O. et al., 2019b. The synergistic effect between graphene oxide nanocolloids and silicon dioxide nanoparticles for gallic acid sensing. *Journal of Solid State Electrochemistry*, 23(6), pp. 1795–1809. Available from: <https://doi.org/10.1007/s10008-019-04267-9>.

CHOWDHURY, I. et al., 2014. Interactions of graphene oxide nanomaterials with natural organic matter and metal oxide surfaces. *Environmental Science and Technology*, 48(16), pp. 9382–9390.

CHRISTENSEN, A. and CARTER, E.A., 1998. First-principles study of the surfaces of zirconia. *Physical Review B - Condensed Matter and Materials Physics*, 58(12),

pp. 1–15. Available from: papers2://publication/uuid/BC6EEC15-2082-4245-956E-813AB1175FCE.

CHUA, C.K. and PUMERA, M., 2014. Chemical reduction of graphene oxide: a synthetic chemistry viewpoint. *Chem. Soc. Rev.*, 43(1), pp. 291–312. Available from: <http://xlink.rsc.org/?DOI=C3CS60303B>.

CLIMENT, V. and FELIU, J.M., 2015. *Cyclic Voltammetry. Reference Module in Chemistry, Molecular Sciences and Chemical Engineering*. Elsevier Inc. Available from: <http://linkinghub.elsevier.com/retrieve/pii/B9780124095472107644>.

COUTO, A.G. et al., 2013. Anti-inflammatory, antiallodynic effects and quantitative analysis of gallic acid in spray dried powders from *Phyllanthus niruri* leaves, stems, roots and whole plant. *Brazilian Journal of Pharmacognosy*, 23(1), pp. 124–131. Available from: <http://dx.doi.org/10.1590/S0102-695X2012005000133>.

DALLA PELLEGRINA, C. et al., 2005. Anti-tumour potential of a gallic acid-containing phenolic fraction from *Oenothera biennis*. *Cancer Letters*, 226(1), pp. 17–25.

DANIEL, M.C. and ASTRUC, D., 2004. Gold Nanoparticles: Assembly, Supramolecular Chemistry, Quantum-Size-Related Properties, and Applications Toward Biology, Catalysis, and Nanotechnology. *Chemical Reviews*, 104(1), pp. 293–346. Available from: <https://pubs.acs.org/doi/abs/10.1021/cr030698+>.

DANILEWICZ, J.C., 2015. Folin-Ciocalteu, FRAP, and DPPH• assays for measuring polyphenol concentration in white wine. *American Journal of Enology and Viticulture*, 66(4), pp. 463–471.

DARMANYAN, A.P. et al., 1998. Quenching of Singlet Oxygen by Oxygen- and Sulfur-Centered Radicals: Evidence for Energy Transfer to Peroxyl Radicals in Solution. *Journal of the American Chemical Society*, 120(2), pp. 396–403. Available from: <http://pubs.acs.org/doi/abs/10.1021/ja9730831>.

DOMÉNECH-CARBÓ, A., 2015. Theoretical scenarios for the electrochemistry of porous silicate-based materials: an overview. *Journal of Solid State Electrochemistry*, 19(7), pp. 1887–1903.

DREYER, D.R. et al., 2015. The chemistry of graphene oxide. *Graphene Oxide: Reduction Recipes, Spectroscopy, and Applications*, pp. 61–95.

EGUÍLAZ, M. et al., 2016. Covalent functionalization of single-walled carbon nanotubes with polytyrosine: Characterization and analytical applications for the sensitive quantification of polyphenols. *Analytica Chimica Acta*, 909, pp. 51–59.

ELGRISHI, N. et al., 2018. A Practical Beginners's Guide to Cyclic Voltammetry. *Journal of Chemical Education*, 95, pp. 197–206.

ER-RAKI, S. et al., 1998. Using of the FAO-56 model for estimating actual evapotranspiration of olives orchards in semi arid region . *Computing*, 30(6), pp. 1052–1055.

EREMIA, S.A.V. et al., 2013. Disposable biosensor based on platinum nanoparticles-reduced graphene oxide-laccase biocomposite for the determination of total polyphenolic content. *Talanta*, 110, pp. 164–170. Available from: <http://dx.doi.org/10.1016/j.talanta.2013.02.029>.

ESLAMI, A.C. et al., 2010. Free radicals produced by the oxidation of gallic acid: An electron paramagnetic resonance study. *Chemistry Central Journal*, 4(1), pp. 1–4.

ESTEPA, L. and DAUDON, M., 1997. Contribution of Fourier transform infrared spectroscopy to the identification of urinary stones and kidney crystal deposits. *Biospectroscopy*, 3(5), pp. 347–369.

EZHIL VILIAN, A.T., RAJKUMAR, M. and CHEN, S.M., 2014. In situ electrochemical synthesis of highly loaded zirconium nanoparticles decorated reduced graphene oxide for the selective determination of dopamine and paracetamol in presence of ascorbic acid. *Colloids and Surfaces B: Biointerfaces*, 115, pp. 295–301. Available from: <http://dx.doi.org/10.1016/j.colsurfb.2013.12.014>.

FACHINGER, J., 2012. Graphite. In: R. KONINGS and R. STOLLER, eds. *Comprehensive Nuclear Materials*. Amsterdam: Elsevier. pp. 539–561. Available from: <https://linkinghub.elsevier.com/retrieve/pii/B9780080560335001105>.

FAN, Y. et al., 2011. TiO₂-graphene nanocomposite for electrochemical sensing of

adenine and guanine. *Electrochimica Acta*, 56(12), pp. 4685–4690. Available from: <http://dx.doi.org/10.1016/j.electacta.2011.02.114>.

FARMER, D.B. et al., 2011. High-frequency, scaled graphene transistors on diamond-like carbon. *Nature*, 472(7341), pp. 74–78. Available from: <http://dx.doi.org/10.1038/nature09979>.

FAROOQUI, U.R., AHMAD, A.L. and HAMID, N.A., 2018. Graphene oxide: A promising membrane material for fuel cells. *Renewable and Sustainable Energy Reviews*, 82(September 2017), pp. 714–733. Available from: <http://dx.doi.org/10.1016/j.rser.2017.09.081>.

FAYEMI, O.E. and ADEKUNLE, A.S., 2015. Metal Oxide Nanoparticles/Multi-walled Carbon Nanotube Nanocomposite Modified Electrode for the Detection of Dopamine: Comparative Electrochemical Study. *Journal of Biosensors & Bioelectronics*, 06(04), p. 190.

FAZARY, A.E., TAHA, M. and JU, Y.H., 2009. Iron complexation studies of gallic acid. *Journal of Chemical and Engineering Data*, 54(1), pp. 35–42.

FERNANDES, D.M. et al., 2014. Novel electrochemical sensor based on N-doped carbon nanotubes and Fe₃O₄ nanoparticles: Simultaneous voltammetric determination of ascorbic acid, dopamine and uric acid. *Journal of Colloid and Interface Science*, 432, pp. 207–213. Available from: <http://dx.doi.org/10.1016/j.jcis.2014.06.050>.

FERNANDES, F.H.A. and SALGADO, H.R.N., 2016. Gallic Acid: Review of the Methods of Determination and Quantification. *Critical Reviews in Analytical Chemistry*, 46(3), pp. 257–265. Available from: <http://dx.doi.org/10.1080/10408347.2015.1095064>.

GAFFNEY, J.S., MARLEY, N.A. and JONES, D.E., 2002. Fourier Transform Infrared (FTIR) Spectroscopy. In: *Characterization of Materials*. pp. 1–33.

GAO, F.F. et al., 2015. An electrochemical sensor for gallic acid based on Fe₂O₃/electro-reduced graphene oxide composite: Estimation for the antioxidant capacity index of wines. *Materials Science and Engineering C*, 57, pp. 279–287. Available from: <http://dx.doi.org/10.1016/j.msec.2015.07.025>.

GAO, L. et al., 2014. Graphene oxide-DNA based sensors. *Biosensors and Bioelectronics*, 60, pp. 22–29. Available from: <http://dx.doi.org/10.1016/j.bios.2014.03.039>.

GAO, Y. et al., 2016. Highly sensitive determination of gallic acid based on a Pt nanoparticle decorated polyelectrolyte-functionalized graphene modified electrode. *Analytical Methods*, 8(48), pp. 8474–8482. Available from: <http://dx.doi.org/10.1039/C6AY02583H>.

GEIM, A.K. and NOVOSELOV, K.S., 2007. The rise of graphene. *Nanoscience and Technology*, pp. 11–19.

GEORGE, J.M., ANTONY, A. and MATHEW, B., 2018. Metal oxide nanoparticles in electrochemical sensing and biosensing: a review. *Microchimica Acta*, 185(7).

GHAANI, M. et al., 2016. Development of an electrochemical nanosensor for the determination of gallic acid in food. *Analytical Methods*, 8(5), pp. 1103–1110.

GHADIMI, H. et al., 2017. Chapter 1 – Introduction. In: *Electrochemistry of Dihydroxybenzene Compounds*. Chennai, India: Elsevier.

GOLDSTEIN, J.I. et al., 2017. *Scanning electron microscopy and x-ray microanalysis*. 4th ed. *Technology & Engineering*. Springer.

GOLUMBIC, C. and MATTILL, H.A., 1942. The antioxidant properties of gallic acid and allied compounds. *Oil & Soap*, 19(8), pp. 144–145.

GÓMEZ-NAVARRO, C. et al., 2010. Atomic structure of reduced graphene oxide. *Nano Letters*, 10(4), pp. 1144–1148.

GOYAL, R.N., CHATTERJEE, S. and RANA, A.R.S., 2010. The effect of modifying an edge-plane pyrolytic graphite electrode with single-wall carbon nanotubes on its use for sensing diclofenac. *Carbon*, 48(14), pp. 4136–4144. Available from: <https://www.sciencedirect.com/science/article/pii/S0008622310005178>.

GRIS, E.F. et al., 2013. Phenolic profile and effect of regular consumption of Brazilian red wines on in vivo antioxidant activity. *Journal of Food Composition and Analysis*, 31(1), pp. 31–40. Available from: <http://dx.doi.org/10.1016/j.jfca.2013.03.002>.

GÜLÇİN, I., 2012. Antioxidant activity of food constituents: An overview. *Archives of Toxicology*, 86(3), pp. 345–391.

GUNCKEL, S. et al., 1998. Antioxidant activity of gallates: an electrochemical study in aqueous media. *Chemico-Biological Interactions*, 114(1–2), pp. 45–59.

GUSATTI, M. et al., 2009. Synthesis of ZnO nanostructures in Low Reaction Temperature. *Chemical Engineering Transaction*, 17, pp. 1017–1022.

HAERI, S.Z., RAMEZANZADEH, B. and ASGHARI, M., 2017. A novel fabrication of a high performance SiO₂-graphene oxide (GO) nanohybrids: Characterization of thermal properties of epoxy nanocomposites filled with SiO₂-GO nanohybrids. *Journal of Colloid and Interface Science*, 493, pp. 111–122. Available from: <http://dx.doi.org/10.1016/j.jcis.2017.01.016>.

HALLIWELL, B. and GUTTERIDGE, J.M.C., 1995. Letters to the Editors THE DEFINITION AND MEASUREMENT OF ANTIOXIDANTS IN. *Free Radical Biology and Medicine*, 18(1), pp. 125–126.

AL HASSAN, M.R. et al., 2019. Emergence of graphene as a promising anode material for rechargeable batteries: a review. *Materials Today Chemistry*, 11, pp. 225–243. Available from: <https://doi.org/10.1016/j.mtchem.2018.11.006>.

HASSANIEN, M.M. et al., 2011. Extraction of gallium, indium and thallium from aquatic media using amino silica gel modified by gallic acid. *Microchimica Acta*, 172(1), pp. 137–145.

HEIM, K.E., TAGLIAFERRO, A.R. and BOBILYA, D.J., 2002. Flavonoid antioxidants: Chemistry, metabolism and structure-activity relationships. *Journal of Nutritional Biochemistry*, 13(10), pp. 572–584.

HENZE, G., 2001. Stripping-Verfahren [1--7]. In: *Polarographie Und Voltammetrie: Grundlagen Und Analytische Praxis*. Berlin, Heidelberg: Springer Berlin Heidelberg. pp. 154–225. Available from: https://doi.org/10.1007/978-3-642-56492-5_5.

HESS, L.H., SEIFERT, M. and GARRIDO, J.A., 2013. Graphene transistors for bioelectronics. *Proceedings of the IEEE*, 101(7), pp. 1780–1792.

HOLZE, R., 2016. Understanding voltammetry: Simulation of electrode processes. *Journal of Solid State Electrochemistry*, 20(1), pp. 305–306. Available from: <http://link.springer.com/10.1007/s10008-015-3033-2>.

HOYOS-ARBELÁEZ, J., VÁZQUEZ, M. and CONTRERAS-CALDERÓN, J., 2017. Electrochemical methods as a tool for determining the antioxidant capacity of food and beverages: A review. *Food Chemistry*, 221, pp. 1371–1381. Available from: <http://dx.doi.org/10.1016/j.foodchem.2016.11.017>.

HUGO, P.C. et al., 2012. Antioxidant interactions between major phenolic compounds found in 'Ataulfo' mango pulp: Chlorogenic, gallic, protocatechuic and vanillic acids. *Molecules*, 17(11), pp. 12657–12664.

IQBAL, M.Z. and REHMAN, A.U., 2018. Recent progress in graphene incorporated solar cell devices. *Solar Energy*, 169(May), pp. 634–647. Available from: <https://doi.org/10.1016/j.solener.2018.04.041>.

JACOBS, C.B., PEAIRS, M.J. and VENTON, B.J., 2010. Review: Carbon nanotube based electrochemical sensors for biomolecules. *Analytica Chimica Acta*, 662(2), pp. 105–127.

JARA-ULLOA, P. et al., 2013. Polypyrrole Molecularly Imprinted Modified Glassy Carbon Electrode for the Recognition of Gallic Acid. *Journal of the Electrochemical Society*, 160(4), pp. H243–H246. Available from: <http://jes.ecsdl.org/cgi/doi/10.1149/2.001306jes>.

JAYAMANI, J. and SHANMUGAM, G., 2014. Gallic acid, one of the components in many plant tissues, is a potential inhibitor for insulin amyloid fibril formation. *European Journal of Medicinal Chemistry*, 85, pp. 352–358. Available from: <http://dx.doi.org/10.1016/j.ejmech.2014.07.111>.

JENG DONG, H. et al., 2011. Gallic acid induces G2/M phase arrest of breast cancer cell MCF-7 through stabilization of p27Kip1 attributed to disruption of p27 Kip1/Skp2 complex. *Journal of Agricultural and Food Chemistry*, 59(5), pp. 1996–2003.

JI, H.F., ZHANG, H.Y. and SHEN, L., 2006. Proton dissociation is important to understanding structure-activity relationships of gallic acid antioxidants.

Bioorganic and Medicinal Chemistry Letters, 16(15), pp. 4095–4098.

JOHNS, J.E. et al., 2013. Metal oxide nanoparticle growth on graphene via chemical activation with atomic oxygen. *Journal of the American Chemical Society*, 135(48), pp. 18121–18125.

KAHL, M. and GOLDEN, T.D., 2014. Electrochemical determination of phenolic acids at a Zn/Al layered double hydroxide film modified glassy carbon electrode. *Electroanalysis*, 26(8), pp. 1664–1670.

KANCHEVA, V.D., 2009. Phenolic antioxidants - radical-scavenging and chain-breaking activity: A comparative study. *European Journal of Lipid Science and Technology*, 111(11), pp. 1072–1089. Available from: <http://doi.wiley.com/10.1002/ejlt.200900005>.

KARIM-NEZHAD, G. et al., 2018. Synergistic effect of ZnO nanoparticles and carbon nanotube and polymeric film on electrochemical oxidation of acyclovir. *Iranian Journal of Pharmaceutical Research*, 17(1), pp. 52–62.

KARIUKI, J., ERVIN, E. and OLAFSON, C., 2015. Development of a novel, low-cost, disposable wooden pencil graphite electrode for use in the determination of antioxidants and other biological compounds. *Sensors (Switzerland)*, 15(8), pp. 18887–18900.

KARUPPIAH, C. et al., 2014. A novel enzymatic glucose biosensor and sensitive non-enzymatic hydrogen peroxide sensor based on graphene and cobalt oxide nanoparticles composite modified glassy carbon electrode. *Sensors and Actuators, B: Chemical*, 196, pp. 450–456. Available from: <http://dx.doi.org/10.1016/j.snb.2014.02.034>.

KATZ, E., WILLNER, I. and WANG, J., 2004. Electroanalytical and Bioelectroanalytical Systems Based on Metal and Semiconductor Nanoparticles. *Electroanalysis*, 16(12), pp. 19–44.

KHOSHESAB, Z.M., 2015. Simultaneous electrochemical determination of acetaminophen, caffeine and ascorbic acid using a new electrochemical sensor based on CuO-graphene nanocomposite. *RSC Advances*, 5(115), pp. 95140–95148.

KILMARTIN, P.A. and HSU, C.F., 2003. Characterisation of polyphenols in green, oolong, and black teas, and in coffee, using cyclic voltammetry. *Food Chemistry*, 82(4), pp. 501–512.

KILMARTIN, P.A., ZOU, H. and WATERHOUSE, A.L., 2002. Correlation of wine phenolic composition versus cyclic voltammetry response. *American Journal of Enology and Viticulture*, 53(4), pp. 294–302.

KILMARTIN, P. a, ZOU, H. and WATERHOUSE, A.L., 2001. A Cyclic Voltammetry Method Suitable for Characterizing Antioxidant Properties of Wine and Wine Phenolics A Cyclic Voltammetry Method Suitable for Characterizing Antioxidant Properties of Wine and Wine Phenolics. *Journal of Agricultural and Food Chemistry*, 49, pp. 1957–1965.

KIM, J. et al., 2010. Graphene oxide sheets at interfaces Supporting information. *Journal of the American Chemical Society*, 132(14), p. 8180. Available from: <http://pubs.acs.org/doi/abs/10.1021/ja102777p>.

KIM, J.-S. et al., 2009. Synthesis and microstructure of zirconia nanopowders by glycothermal processing. *Transactions of Nonferrous Metals Society of China*, 19, pp. s88–s91.

KIM, Y.-J., 2007. Antimelanogenic and Antioxidant Properties of Gallic Acid. *Biological & Pharmaceutical Bulletin*, 30(6), pp. 1052–1055. Available from: <http://joi.jlc.jst.go.jp/JST.JSTAGE/bpb/30.1052?from=CrossRef>.

KIM, Y.K. et al., 2015. One-pot synthesis of multifunctional Au@Graphene oxide nanocolloid core@shell nanoparticles for raman bioimaging, photothermal, and photodynamic therapy. *Small*, 11(21), pp. 2527–2535.

KOUVA, S. et al., 2015. Review: Monoclinic zirconia, its surface sites and their interaction with carbon monoxide. *Catalysis Science and Technology*, 5(7), pp. 3473–3490.

KRATZ, J.M. et al., 2008. Anti-HSV-1 and anti-HIV-1 activity of gallic acid and pentyl gallate. *Memorias Do Instituto Oswaldo Cruz*, 103(5), pp. 437–442.

KRIMMEL, B. et al., 2010. OH-radical induced degradation of hydroxybenzoic- and

hydroxycinnamic acids and formation of aromatic products-A gamma radiolysis study. *Radiation Physics and Chemistry*, 79(12), pp. 1247–1254.

KUBO, I. et al., 2003. Non-antibiotic Antibacterial Activity of Dodecyl Gallate(2003- Kubo_Isao).pdf, 11(May 2002), pp. 573–580.

LAVIRON, E., 1974. Adsorption, autoinhibition and autocatalysis in polarography and in linear potential sweep voltammetry. *Journal of Electroanalytical Chemistry*, 52(3), pp. 355–393.

LEE, C. et al., 2008. Measurement of the elastic properties and intrinsic strength of monolayer graphene. *Science*, 321(5887), pp. 385–388.

LEE, K.G. et al., 2010. Functionalization effects of single-walled carbon nanotubes as templates for the synthesis of silica nanorods and study of growing mechanism of silica. *ACS Nano*, 4(7), pp. 3933–3942.

LI, F. et al., 2011. Electrochemical behavior of graphene doped carbon paste electrode and its application for sensitive determination of ascorbic acid. *Sensors and Actuators, B: Chemical*, 157(1), pp. 110–114.

LI, X. et al., 2018. Graphene and its derivatives in lithium–sulfur batteries. *Materials Today Energy*, 9, pp. 319–335. Available from: <https://doi.org/10.1016/j.mtener.2018.06.001>.

LI, Y. et al., 2001. Effect of calcium salts on isosynthesis over ZrO₂ catalysts. *Journal of Molecular Catalysis A: Chemical*, 175(1–2), pp. 267–275.

LI, Y., SCHLUESENER, H.J. and XU, S., 2010. Gold nanoparticle-based biosensors. *Gold Bulletin*, 43(1), pp. 29–41.

LIAN, P. et al., 2010. Enhanced cycling performance of Fe₃O₄-graphene nanocomposite as an anode material for lithium-ion batteries. *Electrochimica Acta*, 56(2), pp. 834–840.

LIANG, C. et al., 2012. Gallic Acid Induces the Apoptosis of Human Osteosarcoma Cells *In Vitro* and *In Vivo* via the Regulation of Mitogen-Activated Protein Kinase Pathways. *Cancer Biotherapy & Radiopharmaceuticals*, 27(10), pp. 701–710. Available from: <http://online.liebertpub.com/doi/abs/10.1089/cbr.2012.1245>.

LIANG, Z. et al., 2016. A simple, ultrasensitive sensor for gallic acid and uric acid based on gold microclusters/sulfonate functionalized graphene modified glassy carbon electrode. *Sensors and Actuators, B: Chemical*, 224, pp. 915–925. Available from: <http://dx.doi.org/10.1016/j.snb.2015.10.101>.

LINO, F.M.A. et al., 2014. Voltammetric and spectrometric determination of antioxidant capacity of selected wines. *Electrochimica Acta*, 128, pp. 25–31.

LIU, J., CHOI, H.J. and MENG, L.Y., 2018. A review of approaches for the design of high-performance metal/graphene electrocatalysts for fuel cell applications. *Journal of Industrial and Engineering Chemistry*, 64, pp. 1–15. Available from: <https://doi.org/10.1016/j.jiec.2018.02.021>.

LIU, Y. et al., 2013. Gallic acid is the major component of grape seed extract that inhibits amyloid fibril formation. *Bioorganic and Medicinal Chemistry Letters*, 23(23), pp. 6336–6340. Available from: <http://dx.doi.org/10.1016/j.bmcl.2013.09.071>.

LIU, Y. et al., 2014. Gallic acid interacts with α -synuclein to prevent the structural collapse necessary for its aggregation. *Biochimica et Biophysica Acta - Proteins and Proteomics*, 1844(9), pp. 1481–1485. Available from: <http://dx.doi.org/10.1016/j.bbapap.2014.04.013>.

LIU, Y., DONG, X. and CHEN, P., 2012. Biological and chemical sensors based on graphene materials. *Chem. Soc. Rev.*, 41(6), pp. 2283–2307. Available from: <http://xlink.rsc.org/?DOI=C1CS15270J>.

LÓPEZ-COBO, A. et al., 2015. Determination of phenolic compounds and antioxidant activity of a Mediterranean plant: The case of *Satureja montana* subsp. *kitaibelii*. *Journal of Functional Foods*, 18, pp. 1167–1178.

LÓPEZ-VÉLEZ, M., MARTÍNEZ-MARTÍNEZ, F. and VALLE-RIBES, C. Del, 2003. The Study of Phenolic Compounds as Natural Antioxidants in Wine. *Critical Reviews in Food Science and Nutrition*, 43(2), pp. 233–244. Available from: <http://www.tandfonline.com/doi/abs/10.1080/10408690390826509>.

LUNSFORD, S.K. et al., 2013. Electrochemistry Experiments to Develop Novel Sensors for Real-World Applications. *Systematics, Cybernetics and Informatics*,

11(6), pp. 32–35.

LUO, J. et al., 2010. Graphene oxide nanocolloids. *Journal of the American Chemical Society*, 132(50), pp. 17667–17669.

LUO, J.H. et al., 2013a. Sensitive detection of gallic acid based on polyethyleneimine- functionalized graphene modified glassy carbon electrode. *Sensors and Actuators, B: Chemical*, 186, pp. 84–89.

LUO, J.H. et al., 2013b. Sensitive detection of gallic acid based on polyethyleneimine-functionalized graphene modified glassy carbon electrode. *Sensors and Actuators B: Chemical*, 186, pp. 84–89. Available from: <http://linkinghub.elsevier.com/retrieve/pii/S0925400513006576>.

LUO, X. et al., 2006. Application of nanoparticles in electrochemical sensors and biosensors. *Electroanalysis*, 18(4), pp. 319–326.

MA, W. et al., 2013. Rapid and specific sensing of gallic acid with a photoelectrochemical platform based on polyaniline–reduced graphene oxide–TiO₂. *Chemical Communications*, 49(71), p. 7842. Available from: <http://xlink.rsc.org/?DOI=c3cc43540g>.

MAKHOTKINA, O. and KILMARTIN, P.A., 2009. Uncovering the influence of antioxidants on polyphenol oxidation in wines using an electrochemical method: Cyclic voltammetry. *Journal of Electroanalytical Chemistry*, 633(1), pp. 165–174. Available from: <http://dx.doi.org/10.1016/j.jelechem.2009.05.007>.

MAKHOTKINA, O. and KILMARTIN, P.A., 2010. The use of cyclic voltammetry for wine analysis: Determination of polyphenols and free sulfur dioxide. *Analytica Chimica Acta*, 668(2), pp. 155–165. Available from: <http://dx.doi.org/10.1016/j.aca.2010.03.064>.

MAKHOTKINA, O. and KILMARTIN, P.A., 2012. The phenolic composition of Sauvignon blanc juice profiled by cyclic voltammetry. *Electrochimica Acta*, 83, pp. 188–195. Available from: <http://dx.doi.org/10.1016/j.electacta.2012.07.101>.

MAKHOTKINA, O. and KILMARTIN, P.A., 2013. Electrochemical oxidation of wine polyphenols in the presence of sulfur dioxide. *Journal of Agricultural and Food*

Chemistry, 61(23), pp. 5573–5581.

MATSUDA, H. and AYABE, Y., 1955. Theoretical Analysis of Polarographic Waves . I . Metal Ions Reduction of Simple By Hiroaki MATSUDA and Yuzo AYABE (Received December. *Bulletin of the Chemical Society of Japan*, Vol 28(6), pp. 422–428.

MCCREERY, R.L., 2017. Electrochemical properties of carbon surfaces. In: A. WIECKOWSKI, ed. *Interfacial Electrochemistry: Theory: Experiment, and Applications*. CRC Press. p. 631.

MEDINA-PLAZA, C. et al., 2015. Analysis of organic acids and phenols of interest in the wine industry using Langmuir-Blodgett films based on functionalized nanoparticles. *Analytica Chimica Acta*, 853(1), pp. 572–578.

MEI, L.P. et al., 2016. A glassy carbon electrode modified with porous Cu₂O nanospheres on reduced graphene oxide support for simultaneous sensing of uric acid and dopamine with high selectivity over ascorbic acid. *Microchimica Acta*, 183(6), pp. 2039–2046. Available from: <http://dx.doi.org/10.1007/s00604-016-1845-0>.

MENG, Z., ZHENG, J. and LI, Q., 2015. A nitrite electrochemical sensor based on electrodeposition of zirconium dioxide nanoparticles on carbon nanotubes modified electrode. *Journal of the Iranian Chemical Society*, 12(6), pp. 1053–1060. Available from: <http://dx.doi.org/10.1007/s13738-014-0565-9>.

MILONJIĆ, S.K., ZHIGUNOVA, L.K. and PAVASOVIĆ, V.L., 2007. Adsorption of some weak organic electrolytes from aqueous solutions on silica. *Materials Science Forum*, 555, pp. 195–200.

MILONJIĆ, S.K., 1999. Surface properties of metal ions modified silicas. *Colloids and Surfaces A: Physicochemical and Engineering Aspects*, 149(1–3), pp. 461–466. Available from: <https://www.sciencedirect.com/science/article/pii/S0927775798005639> [Accessed 1 Mar 2018].

MIN, D.B. and BOFF, J.M., 2002. Chemistry and Reaction of Singlet Oxygen in Foods. *Comprehensive Reviews in Food Science and Food Safety*, 1(2), pp. 58–72. Available from: <http://doi.wiley.com/10.1111/j.1541-4337.2002.tb00007.x>.

MINUSSI, R.C. et al., 2003. Phenolic compounds and total antioxidant potential of commercial wines. *Food Chemistry*, 82(3), pp. 409–416.

MISHRA, K., OJHA, H. and CHAUDHURY, N.K., 2012. Estimation of antiradical properties of antioxidants using DPPH- assay: A critical review and results. *Food Chemistry*, 130(4), pp. 1036–1043.

MOLODETSKY, I. et al., 2000. Energetics of X-ray-amorphous zirconia and the role of surface energy in its formation. *Journal of Non-Crystalline Solids*, 262(1–3), pp. 106–113.

MUDNIC, I. et al., 2010. Antioxidative and vasodilatory effects of phenolic acids in wine. *Food Chemistry*, 119(3), pp. 1205–1210. Available from: <http://dx.doi.org/10.1016/j.foodchem.2009.08.038>.

MURALI, S. et al., 2010. Graphene and Graphene Oxide: Synthesis, Properties, and Applications. *Advanced Materials*, 22(35), pp. 3906–3924.

MUSIĆ, S., FILIPOVIĆ-VINCEKOVIĆ, N. and SEKOVANIĆ, L., 2011. Precipitation of amorphous SiO₂ particles and their properties. *Brazilian Journal of Chemical Engineering*, 28(1), pp. 89–94.

NAIK, K.K. and ROUT, C.S., 2015. Electrodeposition of ZnCo₂O₄ nanoparticles for biosensing applications. *RSC Advances*, 5(97), pp. 79397–79404.

NOVAK, I., ŠERUGA, M. and KOMORSKY-LOVRIĆ, Š., 2009. Electrochemical characterization of epigallocatechin gallate using square-wave voltammetry. *Electroanalysis*, 21(9), pp. 1019–1025.

OLDHAM, K.B., 1998. Voltammetry at a three-phase junction. *Journal of Solid State Electrochemistry*, 2(6), pp. 367–377.

OLDHAM, K.B. and ZOSKI, C.G., 1986. Chapter 2 Mass Transport to Electrodes. *Comprehensive Chemical Kinetics*, 26(C), pp. 79–143.

OLIVEIRA-NETO, J.R. et al., 2016. Electrochemical behavior and determination of major phenolic antioxidants in selected coffee samples. *Food Chemistry*, 190, pp. 506–512. Available from: <http://dx.doi.org/10.1016/j.foodchem.2015.05.104>.

ÖZCAN, L., ŞAHİN, M. and ŞAHİN, Y., 2008. Electrochemical preparation of a molecularly imprinted polypyrrole-modified pencil graphite electrode for determination of ascorbic acid. *Sensors*, 8(9), pp. 5792–5805.

PANIZZA, M. and CERISOLA, G., 2009. Electrochemical degradation of gallic acid on a BDD anode. *Chemosphere*, 77(8), pp. 1060–1064. Available from: <http://dx.doi.org/10.1016/j.chemosphere.2009.09.007>.

PARK, S., VOHS, J.M. and GORTE, R.J., 2000. Direct oxidation of hydrocarbons in a solid-oxide fuel cell. *Nature*, 404(6775), pp. 265–267.

PARK, S. and RUOFF, R.S., 2009. Chemical methods for the production of graphenes. *Nature Nanotechnology*, 4(4), p. 217.

PARVEEN, S. et al., 2013. *Electrogenerated chemiluminescence protocols and applications*. Springer Berlin Heidelberg.

PEI, L.Z. et al., 2013. Synthesis and formation process of zirconium dioxide nanorods. *Materials Science- Poland*, 31(2), pp. 186–192.

PENG, J., HOU, C. and HU, X., 2012. A graphene-based electrochemical sensor for sensitive detection of vanillin. *International Journal of Electrochemical Science*, 7(2), pp. 1724–1733.

PENN, S.G., HE, L. and NATAN, M.J., 2003. Nanoparticles for bioanalysis. *Current Opinion in Chemical Biology*, 7(5), pp. 609–615.

PERRON, N.R. et al., 2010. Kinetics of iron oxidation upon polyphenol binding. *Dalton Transactions*, 39(41), pp. 9982–9987.

PETKOVIĆ, B.B. et al., 2015. Dinuclear copper(II) octaazamacrocyclic complex in a PVC coated GCE and graphite as a voltammetric sensor for determination of gallic acid and antioxidant capacity of wine samples. *Talanta*, 132, pp. 513–519.

PEYRAT-MAILLARD, M.N., BONNELLY, S. and BERSSET, C., 2000. Determination of the antioxidant activity of phenolic compounds by coulometric detection. *Talanta*, 51(4), pp. 709–716.

PILJAC-ŽEGARAC, J. et al., 2010. Electrochemical determination of antioxidant

capacity of fruit tea infusions. *Food Chemistry*, 121(3), pp. 820–825.

PINCHUK, I. et al., 2012. Evaluation of antioxidants: Scope, limitations and relevance of assays. *Chemistry and Physics of Lipids*, 165(6), pp. 638–647. Available from: <http://dx.doi.org/10.1016/j.chemphyslip.2012.05.003>.

PISOSCHI, A.M. et al., 2011. Determination of ascorbic acid content of some fruit juices and wine by voltammetry performed at Pt and carbon paste electrodes. *Molecules*, 16(2), pp. 1349–1365.

PISOSCHI, A.M. et al., 2016. Antioxidant capacity determination in plants and plant-derived products: A review. *Oxidative Medicine and Cellular Longevity*, 2016.

PISOSCHI, A.M., CIMPEANU, C. and PREDOI, G., 2015. Electrochemical Methods for Total Antioxidant Capacity and its Main Contributors Determination: A review. *Open Chemistry*, 13(1), pp. 824–856.

POKORNÝ, J., 2007. Are natural antioxidants better - and safer - Than synthetic antioxidants? *European Journal of Lipid Science and Technology*, 109(6), pp. 629–642.

PORGALI, E. and BÜYÜKTUNCEL, E., 2012. Determination of phenolic composition and antioxidant capacity of native red wines by high performance liquid chromatography and spectrophotometric methods. *Food Research International*, 45(1), pp. 145–154.

POURHASHEM, S., VAEZI, M.R. and RASHIDI, A., 2017. Investigating the effect of SiO₂-graphene oxide hybrid as inorganic nanofiller on corrosion protection properties of epoxy coatings. *Surface and Coatings Technology*, 311, pp. 282–294. Available from: <http://dx.doi.org/10.1016/j.surfcoat.2017.01.013>.

PRAKASHBABU, D. et al., 2014. Low temperature synthesis of pure cubic ZrO₂ nanopowder: Structural and luminescence studies. *Spectrochimica Acta - Part A: Molecular and Biomolecular Spectroscopy*, 122, pp. 216–222. Available from: <http://dx.doi.org/10.1016/j.saa.2013.11.043>.

PRIETO-SIMÓN, B. et al., 2008. Electrochemical biosensors as a tool for

antioxidant capacity assessment. *Sensors and Actuators, B: Chemical*, 129(1), pp. 459–466.

PUANGJAN, A. and CHAIYASITH, S., 2016. An efficient ZrO₂/Co₃O₄/reduced graphene oxide nanocomposite electrochemical sensor for simultaneous determination of gallic acid, caffeic acid and protocatechuic acid natural antioxidants. *Electrochimica Acta*, 211, pp. 273–288. Available from: <http://dx.doi.org/10.1016/j.electacta.2016.04.185>.

PUMERA, M., 2011. Graphene in biosensing. *Materials Today*, 14(7–8), pp. 308–315. Available from: [http://dx.doi.org/10.1016/S1369-7021\(11\)70160-2](http://dx.doi.org/10.1016/S1369-7021(11)70160-2).

QIU, Y., CHEN, W. and YANG, S., 2010. Facile hydrothermal preparation of hierarchically assembled, porous single-crystalline ZnO nanoplates and their application in dye-sensitized solar cells. *Journal of Materials Chemistry*, 20(5), pp. 1001–1006.

RADHA, A. V. et al., 2009. Surface enthalpy, enthalpy of water adsorption, and phase stability in nanocrystalline monoclinic zirconia. *Journal of the American Ceramic Society*, 92(1), pp. 133–140.

RAGUSA, A. et al., 2019. HPLC analysis of phenols in Negroamaro and primitivo red wines from salento. *Foods*, 8(2), p. 45.

RAJA, N. et al., 2017. Amperometric detection of gallic acid based on electrochemically activated screen printed carbon electrode. *International Journal of Electrochemical Science*, 12(6), pp. 4620–4629.

RANI, N., RANI, G. and KUMAR, M., 2018. Green synthesis , characterization and optical properties of cobalt oxide nanoparticles by co-precipitation method. *International Journal of Advanced Research and Development*, 3(2), pp. 1195–1198.

RAOOF, J.B., OJANI, R. and KOLBADINEZHAD, M., 2009. Voltammetric sensor for glutathione determination based on ferrocene-modified carbon paste electrode. *Journal of Solid State Electrochemistry*, 13(9), pp. 1411–1416.

RASSAEI, L. et al., 2011. Nanoparticles in electrochemical sensors for

environmental monitoring. *TrAC - Trends in Analytical Chemistry*, 30(11), pp. 1704–1715.

REBELO, M.J. et al., 2013. Comparative study of the antioxidant capacity and polyphenol content of Douro wines by chemical and electrochemical methods. *Food Chemistry*, 141(1), pp. 566–573. Available from: <http://dx.doi.org/10.1016/j.foodchem.2013.02.120>.

SAAD AL FARHAN, B., 2017. Characterization of ZrO₂ Nano Particles Prepared by Glycothermal Method and their Efficiency as Adsorbent of As(III) and As(V) from Waste Water. *Journal of Environmental & Analytical Toxicology*, 7(6), pp. 5325–5533.

SAINSBURY, T. and FITZMAURICE, D., 2004. Templated assembly of semiconductor and insulator nanoparticles at the surface of covalently modified multiwalled carbon nanotubes. *Chemistry of Materials*, 16(9), pp. 3780–3790.

SAJID, M. et al., 2016. Chemically modified electrodes for electrochemical detection of dopamine in the presence of uric acid and ascorbic acid: A review. *TrAC - Trends in Analytical Chemistry*, 76, pp. 15–29. Available from: <http://dx.doi.org/10.1016/j.trac.2015.09.006>.

SALIMI, A. et al., 2008. Electrochemical detection of trace amount of arsenic(III) at glassy carbon electrode modified with cobalt oxide nanoparticles. *Sensors and Actuators, B: Chemical*, 129(1), pp. 246–254.

SANGEETHA, N.S. and NARAYANAN, S.S., 2014. A novel bimediator amperometric sensor for electrocatalytic oxidation of gallic acid and reduction of hydrogen peroxide. *Analytica Chimica Acta*, 828, pp. 34–45. Available from: <http://dx.doi.org/10.1016/j.aca.2014.04.041>.

DOS SANTOS RAYMUNDO, M. et al., 2007. Quantitative determination of the phenolic antioxidants using voltammetric techniques. *LWT - Food Science and Technology*, 40(7), pp. 1133–1139.

SARAJI, M. and MOUSAVI, F., 2010. Use of hollow fibre-based liquid-liquid-liquid microextraction and high-performance liquid chromatography-diode array detection for the determination of phenolic acids in fruit juices. *Food Chemistry*,

123(4), pp. 1310–1317. Available from:
<http://dx.doi.org/10.1016/j.foodchem.2010.06.012>.

SCHOLZ, F., 2010. *Electroanalytical Methods*. Springer, vol. 1.

SCHOLZ, F., SCHRÖDER, U. and DOMÉNECH-CARBÓ, A., 2015. *Electrochemistry of Immobilized Particles and Droplets*. Springer International Publishing.

SCIMECA, M. et al., 2018. Energy Dispersive X-ray (EDX) microanalysis: A powerful tool in biomedical research and diagnosis. *European Journal of Histochemistry*, 62(1), p. 2841.

SHAHAMIRIFARD, S.A. et al., 2018. A simple ultrasensitive electrochemical sensor for simultaneous determination of gallic acid and uric acid in human urine and fruit juices based on zirconia-choline chloride-gold nanoparticles-modified carbon paste electrode. *Biosensors and Bioelectronics*, 114(January), pp. 30–36.

SHANG, L., ZHAO, F. and ZENG, B., 2014. Sensitive voltammetric determination of vanillin with an AuPd nanoparticles-graphene composite modified electrode. *Food Chemistry*, 151, pp. 53–57. Available from:
<http://dx.doi.org/10.1016/j.foodchem.2013.11.044>.

SHAO, Y. et al., 2010a. Facile and controllable electrochemical reduction of graphene oxide and its applications. *Journal of Materials Chemistry*, 20(4), pp. 743–748.

SHAO, Y. et al., 2010b. Graphene based electrochemical sensors and biosensors: A review. *Electroanalysis*, 22(10), pp. 1027–1036.

SHOLZ, F., 2010. Electrolytes. In: *Electroanalytical Methods*. Berlin: Springer. p. 366.

SILVA JUNIOR, E., ANTONIO, S.G. and LONGO, E., 2018. Synthesis and structural evolution of partially and fully stabilized ZrO₂ from a versatile method aided by microwave power. *Ceramics International*, 44(3), pp. 3517–3522.

SOCHOR, J. et al., 2013. Electrochemistry as a tool for studying antioxidant properties. *International Journal of Electrochemical Science*, 8(6), pp. 8464–8489.

ŠOLC, R. et al., 2014. Radical sites in humic acids: A theoretical study on protocatechuic and gallic acids. *Computational and Theoretical Chemistry*, 1032, pp. 42–49.

SOLTANI, N. et al., 2015. Simultaneous determination of acetaminophen, dopamine and ascorbic acid using a PbS nanoparticles Schiff base-modified carbon paste electrode. *Comptes Rendus Chimie*, 18(4), pp. 438–448. Available from: <http://dx.doi.org/10.1016/j.crci.2014.07.001>.

SON, D.Y. et al., 2014. 11% efficient perovskite solar cell based on ZnO nanorods: An effective charge collection system. *Journal of Physical Chemistry C*, 118(30), pp. 16567–16573.

SOTIRELIS, N.P. and CHRYSIKOPOULOS, C. V., 2015. Interaction Between Graphene Oxide Nanoparticles and Quartz Sand. *Environmental Science and Technology*, 49(22), pp. 13413–13421.

SOUZA, L.P. et al., 2011. Voltammetric Determination of the Antioxidant Capacity in Wine Samples Using a Carbon Nanotube Modified Electrode. *Journal of Agricultural and Food Chemistry*, 59(14), pp. 7620–7625. Available from: <http://pubs.acs.org/doi/abs/10.1021/jf2005589>.

STANKOVIĆ, D.M. et al., 2017. Design of titanium nitride- and wolfram carbide-doped RGO/GC electrodes for determination of gallic acid. *Analytical Biochemistry*, 539(March), pp. 104–112.

STANKOVICH, S. et al., 2006. Graphene-based composite materials. *Nature*, 442(7100), pp. 282–286.

STRADIOTTO, N.R., YAMANAKA, H. and ZANONI, M.V.B., 2003. Electrochemical sensors: A powerful tool in analytical chemistry. *Journal of the Brazilian Chemical Society*, 14(2), pp. 159–173.

SU, Y.L. and CHENG, S.H., 2015. Sensitive and selective determination of gallic acid in green tea samples based on an electrochemical platform of poly(melamine) film. *Analytica Chimica Acta*, 901, pp. 41–50. Available from: <http://dx.doi.org/10.1016/j.aca.2015.10.026>.

SUN, Y., WU, Q. and SHI, G., 2011. Graphene based new energy materials. *Energy and Environmental Science*, 4(4), pp. 1113–1132.

ŠVANCARA, I. et al., 2001. Carbon Paste Electrodes in Modern Electroanalysis. *Critical Reviews in Analytical Chemistry*, 31(4), pp. 311–345. Available from: <http://www.tandfonline.com/doi/abs/10.1080/20014091076785>.

SZABÓ, T. et al., 2006. Evolution of Surface Functional Groups in a Series of Progressively Oxidized Graphite Oxides Evolution of Surface Functional Groups in a Series of Progressively Oxidized Graphite Oxides. *Chemistry of Materials*, 18(11), pp. 2740–2749. Available from: <http://pubs.acs.org/doi/abs/10.1021/cm060258%2B>.

TAKO, E. et al., 2014. Polyphenolic compounds appear to limit the nutritional benefit of biofortified higher iron black bean (*Phaseolus vulgaris* L.). *Nutrition Journal*, 13(1), pp. 1–9.

TAROLA, A.M., MILANO, F. and GIANNETTI, V., 2007. Simultaneous determination of phenolic compounds in red wines by HPLC-UV. *Analytical Letters*, 40(12), pp. 2433–2445.

TASHKHOURIAN, J. et al., 2013. Construction of a modified carbon paste electrode based on TiO₂ nanoparticles for the determination of gallic acid. *Journal of Solid State Electrochemistry*, 17(1), pp. 157–165.

TASHKHOURIAN, J. et al., 2014. ZnO nanoparticles and multiwalled carbon nanotubes modified carbon paste electrode for determination of naproxen using electrochemical techniques. *Journal of Electroanalytical Chemistry*, 714–715, pp. 103–108.

TASHKHOURIAN, J. and NAMI-ANA, S.F.F., 2015. A sensitive electrochemical sensor for determination of gallic acid based on SiO₂nanoparticle modified carbon paste electrode. *Materials Science and Engineering C*, 52, pp. 103–110. Available from: <http://linkinghub.elsevier.com/retrieve/pii/S092849311500199X>.

TASIOULA-MARGARI, M. and TSABOLATIDOU, E., 2015. Extraction, Separation, and Identification of Phenolic Compounds in Virgin Olive Oil by HPLC-DAD and HPLC-MS. *Antioxidants*, 4(3), pp. 548–562. Available from:

<http://www.mdpi.com/2076-3921/4/3/548/>.

TERKI, R. et al., 2006. Structural and electronic properties of zirconia phases: A FP-LAPW investigations. *Materials Science in Semiconductor Processing*, 9(6), pp. 1006–1013.

TERPINC, P. et al., 2011. Antioxidant properties of 4-vinyl derivatives of hydroxycinnamic acids. *Food Chemistry*, 128(1), pp. 62–69.

TEWELDEBRHAN, D. et al., 2008. Superior Thermal Conductivity of Single-Layer Graphene. *Nano Letters*, 8(3), pp. 902–907.

TEYMOURIAN, H. et al., 2014. One-pot hydrothermal synthesis of zirconium dioxide nanoparticles decorated reduced graphene oxide composite as high performance electrochemical sensing and biosensing platform. *Electrochimica Acta*, 143, pp. 196–206. Available from: <http://dx.doi.org/10.1016/j.electacta.2014.08.007>.

THAIPONG, K. et al., 2006. Comparison of ABTS, DPPH, FRAP, and ORAC assays for estimating antioxidant activity from guava fruit extracts. *Journal of Food Composition and Analysis*, 19(6–7), pp. 669–675.

TIAN, L. et al., 2014. Determination of quercetin using a photo-electrochemical sensor modified with titanium dioxide and a platinum(II)-porphyrin complex. *Microchimica Acta*, 182(3–4), pp. 687–693.

TONG, Y., BOHM, S. and SONG, M., 2017. The capability of graphene on improving the electrical conductivity and anti-corrosion properties of Polyurethane coatings. *Applied Surface Science*, 424, pp. 72–81. Available from: <http://dx.doi.org/10.1016/j.apsusc.2017.02.081>.

TONLE, I.K. et al., 2015. Organoclay-modified electrodes: preparation, characterization and recent electroanalytical applications. *Journal of Solid State Electrochemistry*, 19(7), pp. 1949–1973.

TSYGANENKO, A.A. and FILIMONOV, V.N., 1973. Infrared spectra of surface hydroxyl groups and crystalline structure of oxides. *Journal of Molecular Structure*, 19(2), pp. 579–589.

UMAR, A. et al., 2012. Hydrothermally grown ZnO nanoflowers for environmental remediation and clean energy applications. *Materials Research Bulletin*, 47(9), pp. 2407–2414.

VASILESCU, I. et al., 2015. Determination of the antiradical properties of olive oils using an electrochemical method based on DPPH radical. *Food Chemistry*, 166, pp. 324–329. Available from: <http://dx.doi.org/10.1016/j.foodchem.2014.06.042>.

VELMURUGAN, M. et al., 2017. Electrochemical preparation of activated graphene oxide for the simultaneous determination of hydroquinone and catechol. *Journal of Colloid and Interface Science*, 500, pp. 54–62. Available from: <http://dx.doi.org/10.1016/j.jcis.2017.03.112>.

VELMURUGAN, M. and CHEN, S.M., 2017. Synthesis and characterization of porous MnCo₂O₄ for electrochemical determination of cadmium ions in water samples. *Scientific Reports*, 7(1), pp. 1–8. Available from: <http://dx.doi.org/10.1038/s41598-017-00748-x>.

VENKATATHRI, N., 2007. Preparation of silica nanoparticle through coating with octyldecyltrimethoxy silane. *Indian Journal of Chemistry - Section A Inorganic, Physical, Theoretical and Analytical Chemistry*, 46(12), pp. 1955–1958.

VILAS-BOAS, Â. et al., 2019. Evaluation of total polyphenol content of wines by means of voltammetric techniques: Cyclic voltammetry vs differential pulse voltammetry. *Food Chemistry*, 276(October 2018), pp. 719–725. Available from: <https://doi.org/10.1016/j.foodchem.2018.10.078>.

VILIAN, A.T.E. and CHEN, S.M., 2015. Preparation of carbon nanotubes decorated with manganese dioxide nanoparticles for electrochemical determination of ferulic acid. *Microchimica Acta*, 182(5–6), pp. 1103–1111.

WADEKAR, K.F., NEMADE K.R. and WAGHULEY S.A., 2017. Chemical synthesis of cobalt oxide (Co₃O₄) nanoparticles using Co-precipitation method. *Research Journal of Chemical International Science Community Association Research Journal of Chemical Sciences Res. J. Chem. Sci*, 7(71), pp. 53–55. Available from: <http://www.isca.in/rjcs/Archives/v7/i1/9.ISCA-RJCS-2016-055.pdf>.

WANG, F. and HU, S., 2009. Electrochemical sensors based on metal and semiconductor nanoparticles. *Microchimica Acta*, 165(1-2), pp. 1-22.

WANG, J., 2006. *Analytical Electrochemistry, Third Edition*. JOHN WILEY & SONS, INC., PUBLICATION. New York: Wiley.

WANG, L. et al., 2017. Tailoring heterostructured Bi₂MoO₆/Bi₂S₃ nanobelts for highly selective photoelectrochemical analysis of gallic acid at drug level. *Biosensors and Bioelectronics*, 94(February), pp. 107-114.

WANG, S. et al., 2016a. Simultaneous Electrochemical Determination of Dopamine and Serotonin in Rat Cerebrospinal Fluid Using Screen-Printed Electrode Modified with MWNTs-SiO₂-chitosan Composites. *Biosensors and Bioelectronics*, 11, pp. 2360-2376. Available from: <http://linkinghub.elsevier.com/retrieve/pii/S0956566314007945>.

WANG, X. et al., 2014. Highly dispersible and stable copper terephthalate metal-organic framework-graphene oxide nanocomposite for an electrochemical sensing application. *ACS Applied Materials and Interfaces*, 6(14), pp. 2407-2414.

WANG, Y. et al., 2015. A novel electrochemical sensor based on zirconia/ordered macroporous polyaniline for ultrasensitive detection of pesticides. *Analyst*, 140(2), pp. 560-566.

WANG, Z. et al., 2016b. Carbon nanomaterials-based electrochemical aptasensors. *Biosensors and Bioelectronics*, 79, pp. 136-149.

WATERHOUSE, A.L., 2002. Wine phenolics. *Annals of the New York Academy of Sciences*, 957, pp. 21-36.

WĘGIEL, J., BURNAT, B. and SKRZYPEK, S., 2018. A graphene oxide modified carbon ceramic electrode for voltammetric determination of gallic acid. *Diamond and Related Materials*, 88(July), pp. 137-143.

WEI, C. et al., 2007. Electrocatalysis of horseradish peroxidase immobilized on cobalt nanoparticles modified ITO electrode. *Analytical Letters*, 40(17), pp. 3182-3194.

WRIGHT, J.S., JOHNSON, E.R. and DILABIO, G.A., 2001. Predicting the activity of

phenolic antioxidants: Theoretical method, analysis of substituent effects, and application to major families of antioxidants. *Journal of the American Chemical Society*, 123(6), pp. 1173–1183.

WRIGHT, P.K. and EVANS, A.G., 1999. Mechanisms governing the performance of thermal barrier coatings. *Current Opinion in Solid State and Material Science*, 4, pp. 255–265.

XIE, J. et al., 2013. Co₃O₄-reduced graphene oxide nanocomposite as an effective peroxidase mimetic and its application in visual biosensing of glucose. *Analytica Chimica Acta*, 796, pp. 92–100. Available from: <http://dx.doi.org/10.1016/j.aca.2013.08.008>.

XIONG, C. et al., 2017. Highly sensitive detection of gallic acid based on organic electrochemical transistors with poly(diallyldimethylammonium chloride) and carbon nanomaterials nanocomposites functionalized gate electrodes. *Sensors and Actuators, B: Chemical*, 246, pp. 235–242. Available from: <http://dx.doi.org/10.1016/j.snb.2017.02.025>.

XIONG, L. et al., 2012. An electrochemical thermometer: Voltammetric measurement of temperature and its application to amperometric gas sensing. *Analyst*, 137(11), pp. 2567–2573.

XU, H., DAI, H. and CHEN, G., 2010. Direct electrochemistry and electrocatalysis of hemoglobin protein entrapped in graphene and chitosan composite film. *Talanta*, 81(1–2), pp. 334–338. Available from: <http://dx.doi.org/10.1016/j.talanta.2009.12.006>.

XU, L. et al., 2014. Interfacial interactions of semiconductor with graphene and reduced graphene oxide: CeO₂ as a case study. *ACS Applied Materials and Interfaces*, 6(22), pp. 20350–20357.

YAKOVLEVA, K.E. et al., 2007. Characterization of plant phenolic compounds by cyclic voltammetry. *Applied Biochemistry and Microbiology*, 43(6), pp. 661–668. Available from: <http://link.springer.com/10.1134/S0003683807060166>.

YANG, S. et al., 2015. Synthesis of Mn₃O₄ nanoparticles/nitrogen-doped graphene hybrid composite for nonenzymatic glucose sensor. *Sensors and*

Actuators, B: Chemical, 221, pp. 172–178. Available from: <http://dx.doi.org/10.1016/j.snb.2015.06.110>.

YARDIM, Y., GULCAN, M. and ŞENTURK, Z., 2013. Determination of vanillin in commercial food product by adsorptive stripping voltammetry using a boron-doped diamond electrode. *Food Chemistry*, 141(3), pp. 1821–1827.

YARESTANI, M. et al., 2014. Hydrothermal synthesis of cobalt oxide nanoparticles: Its optical and magnetic properties. *Journal of Sciences, Islamic Republic of Iran*, 25(4), pp. 339–343.

YEDURKAR, S., MAURYA, C. and MAHANWAR, P., 2016. Biosynthesis of Zinc Oxide Nanoparticles Using *Ixora Coccinea* Leaf Extract—A Green Approach. *Open Journal of Synthesis Theory and Applications*, 05(01), pp. 1–14.

YEN, G.C., DUH, P. Der and TSAI, H.L., 2002. Antioxidant and pro-oxidant properties of ascorbic acid and gallic acid. *Food Chemistry*, 79(3), pp. 307–313.

YILMAZ, Ü.T., KEKILLIOGLU, A. and MERT, R., 2013. Determination of Gallic acid by differential pulse polarography: Application to fruit juices. *Journal of Analytical Chemistry*, 68(12), pp. 1064–1069. Available from: <http://link.springer.com/10.1134/S1061934813120113>.

ZARE, H.R. and CHATRAEI, F., 2011. Preparation and electrochemical characteristics of electrodeposited acetaminophen on ruthenium oxide nanoparticles and its role as a sensor for simultaneous determination of ascorbic acid, dopamine and N-acetyl-L-cysteine. *Sensors and Actuators, B: Chemical*, 160(1), pp. 1450–1457. Available from: <http://dx.doi.org/10.1016/j.snb.2011.10.012>.

ZHANG, G., SHEN, X. and YANG, Y., 2011. Facile synthesis of monodisperse porous ZnO spheres by a soluble starch-assisted method and their photocatalytic activity. *Journal of Physical Chemistry C*.

ZHANG, Q. et al., 2000. Sol-gel derived ZrO₂-SiO₂ highly reflective coatings.pdf, 2(July 1999), pp. 319–323.

ZHANG, W.L. and CHOI, H.J., 2012. Silica-graphene oxide hybrid composite

particles and their electroresponsive characteristics. *Langmuir*, 28(17), pp. 7055–7062.

ZHANG, X. et al., 2014. Electrochemical sensor based on carbon-supported NiCoO₂ nanoparticles for selective detection of ascorbic acid. *Biosensors and Bioelectronics*, 55, pp. 446–451.

ZHENG, D. et al., 2010. Preparation and application of a novel vanillin sensor based on biosynthesis of Au-Ag alloy nanoparticles. *Sensors and Actuators, B: Chemical*, 148(1), pp. 247–252. Available from: <http://dx.doi.org/10.1016/j.snb.2010.04.031>.

ZHOU, Y. et al., 2014. Synthesis of ZnO micro-pompons by soft template-directed wet chemical method and their application in electrochemical biosensors. *Electrochimica Acta*, 115, pp. 277–282.

ZHU, C. et al., 2015. Electrochemical sensors and biosensors based on nanomaterials and nanostructures. *Analytical Chemistry*, 87(1), pp. 230–249.

ZHU, P. and ZHAO, Y., 2017. Effects of electrochemical reaction and surface morphology on electroactive surface area of porous copper manufactured by Lost Carbonate Sintering. *RSC Advances*, 7(42), pp. 26392–26400.

ZIYATDINOVA, G.K. and BUDNIKOV, H.C., 2014. Evaluation of the antioxidant properties of spices by cyclic voltammetry. *Journal of Analytical Chemistry*, 69(10), pp. 990–997. Available from: <http://link.springer.com/10.1134/S1061934814100189>.

ZOSKI, C.G., 2007. *Handbook of electrochemistry*. 1st ed. Elsevier.

APPENDIX I

8.1. PUBLICATION PAGES

Journal of Solid State Electrochemistry (2019) 23:1795–1809
<https://doi.org/10.1007/s10008-019-04267-9>

ORIGINAL PAPER



The synergistic effect between graphene oxide nanocolloids and silicon dioxide nanoparticles for gallic acid sensing

Chrys O. Chikere¹ · Nadimul Haque Faisal² · Paul Kong Thoo Lin¹ · Carlos Fernandez¹

Received: 10 January 2019 / Revised: 28 March 2019 / Accepted: 29 March 2019 / Published online: 10 May 2019
© The Author(s) 2019

Abstract

For the first time, the synergistic effect of graphene oxide nanocolloids (nano-GO) and silicon dioxide (silica) nanoparticles (SiO₂-nanoparticles) has been used to modify a glassy carbon electrode (GCE) for the determination of gallic acid (GA). The modified electrode surface was characterised by using scanning electron microscopy (SEM), energy-dispersive X-ray spectroscopy (EDXA) and Fourier transform infrared spectroscopy (FTIR). The electrochemical behaviour of the modified electrode was then studied, using cyclic voltammetry (CV) and differential pulse voltammetry (DPV), showing that the electrode was sensitive to GA in a concentration range of 6.25×10^{-6} to 1.0×10^{-3} mol L⁻¹, with a correlation coefficient R^2 of 0.9956 and a limit of detection of 2.09×10^{-6} mol L⁻¹ (S/N = 3). The proposed method was successfully used for the determination of GA in red wine, white wine and orange juice, with recoveries of 102.3, 95.4 and 97.6%, respectively.

Keywords Graphene oxide nanocolloids · Gallic acid · SiO₂ nanoparticles · Electrochemistry · Cyclic voltammetry · Differential pulse voltammetry

Introduction

Gallic acid (2,3,4-trihydroxybenzoic acid) (GA) is a naturally occurring phenolic compound in plants and is a natural antioxidant with several biological activities. The compound has shown its capacity as a reducing agent in the pharmaceutical industry and also as a homeopathic drug that can be found in tea, red wine, fruits (bananas, blueberries, grapes), beverages and several medicinal plants [1]. In the pharmaceutical industry, it is widely used as a reducing agent in products like Dermatol, Aiol and bismuth salts of gallic acid [2]. Several studies had shown GA to have anti-carcinogenic, anti-mutagenic and anti-oxidative properties [3]; hence, it is recommended usage as an antioxidant in human diet. This is because it can reduce the risk of disease development, by the

prevention or slowing down of molecular oxidation in the body [4], known as oxidative stress. Furthermore, oxidative stress has been linked to human diseases like Alzheimer's disease, cardiovascular diseases, Parkinson's disease, diabetes and cancer [5, 6].

With the increasing importance of antioxidants in our diets and our health, especially natural antioxidants like vitamins, carotenoids and phenolic or flavonoid compounds in the reduction of oxidative stress, many *in vitro* chemically based assays have been developed for the determination of the capacity of these antioxidants. The study of antioxidant properties has been mainly carried out by spectrophotometric methods [7, 8], chromatographic [9, 10], flow injection-chemiluminescence [11] and electrochemical methods [12–14]. However, the main drawbacks to the chromatographic and spectrophotometric methods have been the cost of equipment, coupled with the extensive time-consuming sample preparation procedures as well as the use of expensive and toxic reagents which are detrimental to the environment.

Amongst all the available methods, electrochemical techniques have generated a lot of interest due to their many advantages, including being fast, sensitive, selective, inexpensive and portable, with little or no sample pre-treatment

Electronic supplementary material The online version of this article (<https://doi.org/10.1007/s10008-019-04267-9>) contains supplementary material, which is available to authorized users.

✉ Carlos Fernandez
c.fernandez@rgu.ac.uk

IOPscience

This site uses cookies. By continuing to use this site you agree to our use of cookies. To find out more, see our Privacy and Cookies policy. 

PAPER • OPEN ACCESS

Zinc oxide nanoparticles modified-carbon paste electrode used for the electrochemical determination of Gallic acid

C Chikere¹, N H Faisal², P K T Lin¹ and C Fernandez¹

Published under licence by IOP Publishing Ltd

Journal of Physics: Conference Series, Volume 1310, conference 1

c.fernandez@rgu.ac.uk

¹ School of Pharmacy of Pharmacy and Life Sciences, Robert Gordon University, Aberdeen, United Kingdom

² School of Engineering, Robert Gordon University, Aberdeen, United Kingdom Tel. +44(0)1224262559.

C Chikere *et al* 2019 *J. Phys.: Conf. Ser.* **1310** 012008

<https://doi.org/10.1088/1742-6596/1310/1/012008>

Buy this article in print



Article

Interaction between Amorphous Zirconia Nanoparticles and Graphite: Electrochemical Applications for Gallic Acid Sensing Using Carbon Paste Electrodes in Wine

Chrys. O. Chikere¹, Nadimul Haque Faisal² , Paul Kong-Thoo-Lin¹ and Carlos Fernandez^{1,*}

¹ School of Pharmacy and Life Sciences, Robert Gordon University, Garthdee Road, Aberdeen AB10 7GJ, UK; c.o.chikere@rgu.ac.uk (C.O.C.); p.v.s.kong-thoo-lin@rgu.ac.uk (P.K.-T.-L.)

² School of Engineering, the Robert Gordon University, Garthdee Road, Aberdeen AB10 7GJ, UK; N.H.Faisal@rgu.ac.uk

* Correspondence: c.fernandez@rgu.ac.uk; Tel.: +44-(0)-1224-262559

Received: 31 January 2020; Accepted: 10 March 2020; Published: 17 March 2020



Abstract: Amorphous zirconium oxide nanoparticles (ZrO_2) have been used for the first time, to modify carbon paste electrode (CPE) and used as a sensor for the electrochemical determination of gallic acid (GA). The voltammetric results of the ZrO_2 nanoparticles-modified CPE showed efficient electrochemical oxidation of gallic acid, with a significantly enhanced peak current from $261 \mu A \pm 3$ to about $451 \mu A \pm 1$. The modified surface of the electrode and the synthesised zirconia nanoparticles were characterised by scanning electrode microscopy (SEM), Energy-dispersive x-ray spectroscopy (EDXA), X-ray powdered diffraction (XRD) and Fourier-transform infrared spectroscopy (FTIR). Meanwhile, the electrochemical behaviour of GA on the surface of the modified electrode was studied using differential pulse voltammetry (DPV), showing a sensitivity of the electrode for GA determination, within a concentration range of $1 \times 10^{-6} \text{ mol L}^{-1}$ to $1 \times 10^{-3} \text{ mol L}^{-1}$ with a correlation coefficient of R^2 of 0.9945 and a limit of detection of $1.24 \times 10^{-7} \text{ mol L}^{-1}$ ($S/N = 3$). The proposed ZrO_2 nanoparticles modified CPE was successfully used for the determination of GA in red and white wine, with concentrations of $0.103 \text{ mmol L}^{-1}$ and $0.049 \text{ mmol L}^{-1}$ respectively.

Keywords: amorphous materials; zirconium oxide nanoparticles; carbon paste electrode; phenolic acid; gallic acid; electrochemistry; cyclic voltammetry; differential pulse voltammetry

Highlights:

- For the first time, synthesised amorphous zirconium dioxide nanoparticles modified CPE has been used for the electrochemical determination of gallic acid
- Interaction of amorphous ZrO_2 nanoparticles with graphite has been proposed
- Amorphous ZrO_2 nanoparticles modified CPE has been used for the detection of gallic acid in wine samples.

1. Introduction

Nanoparticles and nanomaterials exhibit unique chemical, physical and electrochemical properties due to their very small sizes (between 1–500 nm), which are different from the bulk of the same compounds [1]. Based on these different properties, which include size, shape, crystal structure,



Dynamics of nanointerfaces: general discussion

Hassan Alzahrani, Cameron Bentley,  Rob Burrows,  Chan Cao, Qiong Cai,  Chrys Chikere,  Richard M. Crooks, Johan Dunevall, Martin Edwards,  Andrew Ewing, Rui Gao, Robert Hillman, Mohi Kahram, Frederic Kanoufi, Christine Kranz, Jean-François Lemineur, Yitao Long,  Kim McKelvey, Michael Mirkin, Stacy Moore,  Wojciech Nogala, Hang Ren, Wolfgang Schuhmann,  Patrick Unwin,  Andrea Vezzoli, Henry White,  Katherine Willets, Zhugen Yang and Yilun Ying 

DOI: 10.1039/C8FD90026D

Martin Edwards opened the discussion of the paper by Andrew Ewing: You mentioned leakage from the vesicles as an explanation for why extracellular vesicles display a slightly lower dopamine content than those measured in intracellular VIEC. Do you have any evidence for where this occurs? Is it a function of time? Would repeating the preparation procedures, either completely or only some of the stages, allow you to determine this? If you knew the losses by preparation step, you might be able to work back and calculate the intracellular concentration.

Energy conversion at nanointerfaces: general discussion

Hassan Alzahrani, Cameron Bentley, Paul W. Bohn, [Chrys Chikere](#), Daniel Commandeur, Richard M. Crooks, Cyril Ehi-Eromosele, Andrew Ewing, Alina Galejeva, Thom Hersbach, [Robert Hillman](#), Frederic Kanoufi, Marc Koper, Christine Kranz, Tobias Löffler, [Yitao Long](#), [Julie MacPherson](#), Kim McKelvey, Shelley Minter, [Michael Mirkin](#), Richard Nichols, [Wojciech Nogala](#), Denis Öhl, Juan Pelta, Hang Ren, [Jennifer Rudd](#), Wolfgang Schuhmann, [Zhongqun Tian](#), Patrick Unwin, Andrea Vezzoli, Katherin Willets, Yanfang Wu, [Zhugen Yang](#), Dongping Zhan and Chuan Zhao

DOI: 10.1039/c8fd90025f

Julie MacPherson opened discussion of the paper by Richard M. Crooks: What happens if you apply a continuous potential, as opposed to a pulsed potential, in terms of the morphology of the Pt deposit? Why did you choose such a high frequency; what's the rationale behind this? For the frequencies chosen, how much of the current response is dominated by capacitive charging? Each pulse is only 1 ms long (for a 1000 Hz frequency), but you have a very small electrode area, which is in your favour for minimising capacitive contributions.



DISCUSSIONS

[View Article Online](#)
[View Journal](#) | [View Issue](#)

Processes at nanopores and bio-nanointerfaces: general discussion

Hassan Alzahrani, Christophe Antoine, Lane Baker, Sebastien Balme,  Gourav Bhattacharya,  Paul W. Bohn, Qiong Cai,  Chrys Chikere, Richard M. Crooks, Naren Das, Martin Edwards,  Cyril Ehi-Eromosele, Niklas Ermann, Lei Jiang, Frederic Kanoufi, Christine Kranz, Yitao Long,  Julie MacPherson, Kim McKelvey,  Michael Mirkin, Richard Nichols, Wojciech Nogala, Juan Pelta, Hang Ren, Jennifer Rudd,  Wolfgang Schuhmann, Zuzanna Siwy, Zhongqun Tian, Patrick Unwin,  Liping Wen, Henry White,  Katherine Willets,  Yanfang Wu  and Yilun Ying 

DOI: 10.1039/C8FD90023J

Paul W. Bohn opened a discussion of the introductory lecture by Henry S. White: The problem of limits to the measurement of fast dynamics is determined by (1) the geometry and size of the structure, and (2) the nature of the electrolyte. Could you sensibly reduce the RC time constant by eliminating the supporting electrolyte? Even if the resistance is increased, could you get around the problem by confining the system to an ultra-small volume?

APPENDIX II

8.2 General Calculations

8.2.1 Electrochemical Calculations

8.2.1.1 Electroactive Surface Area

The calculations for the electroactive surface area were carried out, using the Randles-Ševčík equation thus $I_{pa} = (2.69 \times 10^5)n^{2/3} A D^{1/2} \nu^{1/2} C_0$

Using the Randles-Ševčík equation:-

A (Electroactive surface area) = $\frac{I_{pa}}{(2.69 \times 10^5)n^{2/3}D^{1/2}\nu^{1/2}C_0}$ From the data produced

by the redox reaction, n = number of electrons = 1, D which is diffusion coefficient of the redox solution = $7.6 \times 10^{-6} \text{ cm}^2 \text{ s}^{-1}$

Meanwhile for the data produced by the different electrodes in their determination of the $[\text{Fe}(\text{CN})_6]^{4+/3-}$ redox solution, linear regression equations were produced in the format = $I_p (\mu\text{A}) = 27.309 \nu^{1/2} (\text{mVs}^{-1}) - 58.896$ where $I_{pa}/\nu^{1/2}$ could be deduced.

8.2.1.2 Number of electrons involved in GA oxidation

The number of electrons involved in the oxidation of GA was calculated using the following equation $i_p = \frac{nFQ\nu}{4RT}$ where i_p is the anodic peak current, Q is the amount of charge integrated from the area of the CV peak, T is temperature in Kelvin, R is the universal gas constant ($8.314 \text{ Jmol}^{-1}\text{K}^{-1}$) and F is the Faraday constant (96500 Cmol^{-1}), ν is the scan rate, while n is the number of electrons to be calculated.

Hence n was calculated by $n = \frac{i_p \times 4RT}{FQ\nu}$ From this equation and the slope of the linear regression of voltammograms of I_p vs ν , which is I_p/ν ; the number of electrons can then be deduced.

8.2.2 Statistical analysis

8.2.2.1 Standard Deviation

The standard deviation (STD) of the recorded peak currents was measured using Microsoft excel, producing values subsequently used for relative standard deviation

8.2.2.2 Relative Standard Deviation

The relative standard deviation (RSD) calculations were also carried out using Microsoft Excel, using the following formula

$$RSD = \frac{STD(range)}{Average\ range} \times 100\%$$

8.2.2.3 Variance

The variance was also calculated using the Microsoft Excel, where the STD was square:

$$Variance = (RSD)^2$$

8.2.2.4 T-test

The T-test was calculated by using the following equation:

$$\frac{\textit{Difference between the means of the group}}{\textit{Variability of the groups}}$$

which was defined using the following equation:

$$t - test = \frac{\bar{X}_A - \bar{X}_B}{\sqrt{\frac{Var_A}{n} + \frac{Var_B}{n}}}$$

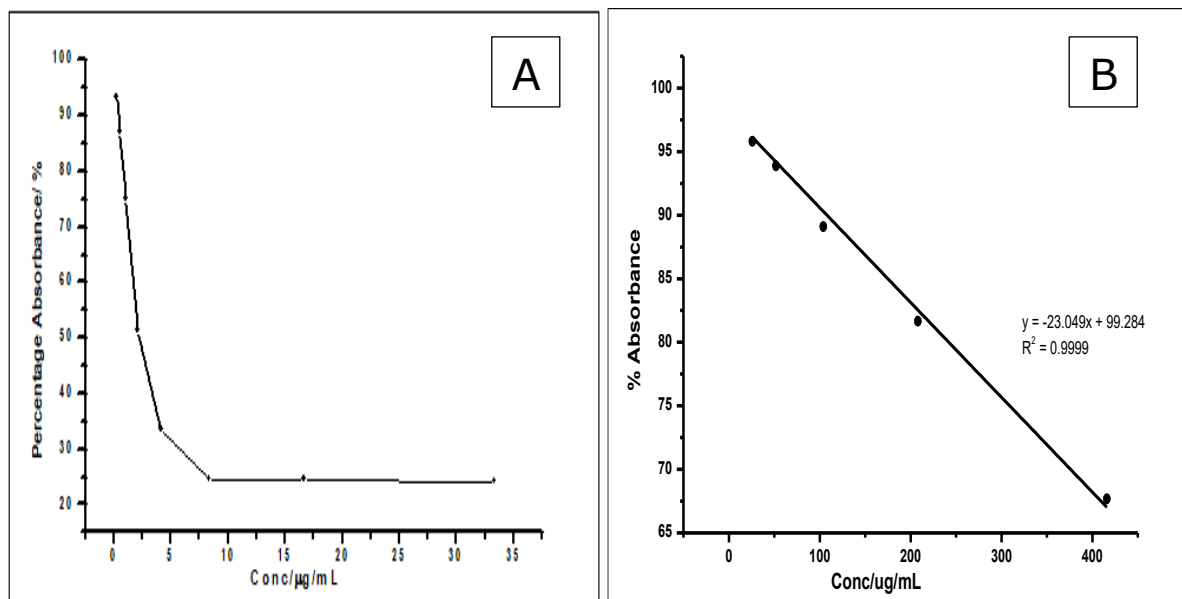
Where $\bar{X}_A - \bar{X}_B$ is the difference between the means of the group, while Var_A and Var_B are variances of the groups of results and n is the number of outcomes in A and in B.

APPENDIX III

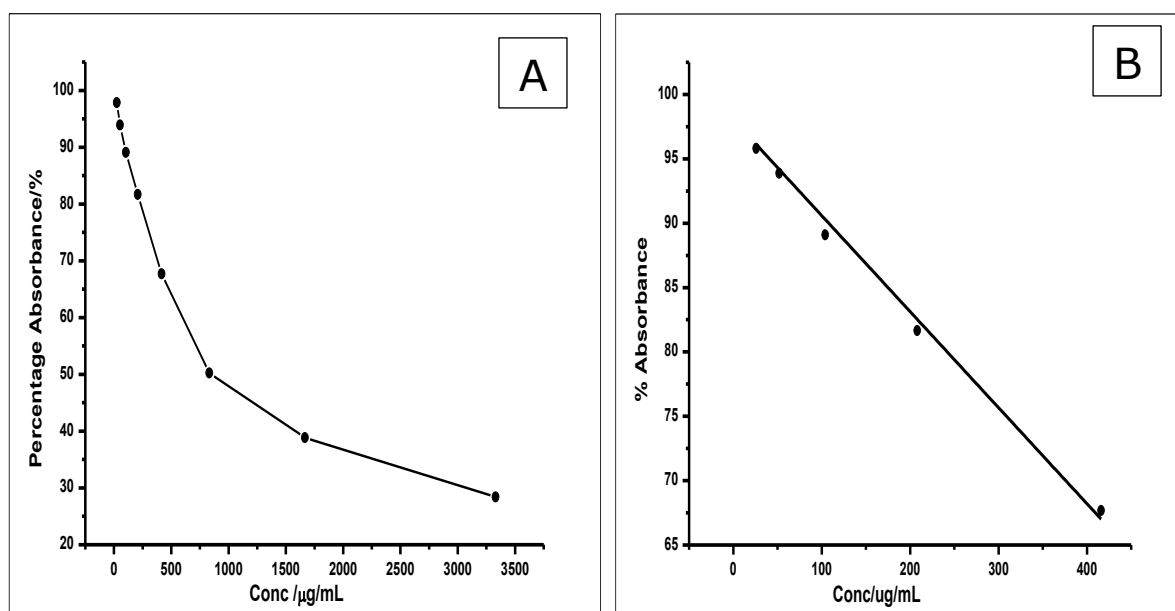
8.3 DPPH Assay

DPPH was used to measure the scavenging capacity or the antioxidant capacity of the following antioxidants, Gallic acid, Ascorbic acid, Trolox and Vanillin. As earlier discussed, the assay functions by electron transfer reactions between the DPPH and the antioxidants being analysed. DPPH being a radical is being scavenged by the antioxidants; hence the strength of the scavenging power of the antioxidant is being measured. This measurement is done by measuring the change of colour from deep purple to light purple, as there is a donation of electrons or hydrogen atoms to the unstable DPPH radical (Mishra, Ojha and Chaudhury 2012).

This can be seen in the IC₅₀ results in Appendix Figure 8.1, 8.2 and Table 8.1, which shows AA, TR, GA and VA.



Appendix Figure 8. 1. (A) Graph showing the IC₅₀ of Gallic acid, which is the amount Gallic acid needed to scavenge 50% of the free radical, which in this case is DPPH. (B) The linear plot used to deduce the IC₅₀



Appendix Figure 8. 2 (A) Graph showing the IC₅₀ of Vanillin, which is the amount of Vanillin needed to scavenge 50% of the free radical, which in this case is DPPH. (B) The linear plot used to deduce the IC₅₀

From these results Appendix Figure 8.1(B) and 8.2(B), GA showed a high scavenging capacity, thus a less concentration to scavenge 50% of the DPPH radical as compared to vanillin. The results show that GA has an IC₅₀ of 2.13 µg mL⁻¹, while VA is 644 µg mL⁻¹, showing that the lower the IC₅₀ the higher the antioxidant capacity.

Comparing these results with the proposed electrochemical method, GA tends to be more electroactive than the VA and some of the antioxidants (Appendix Table 8.1)

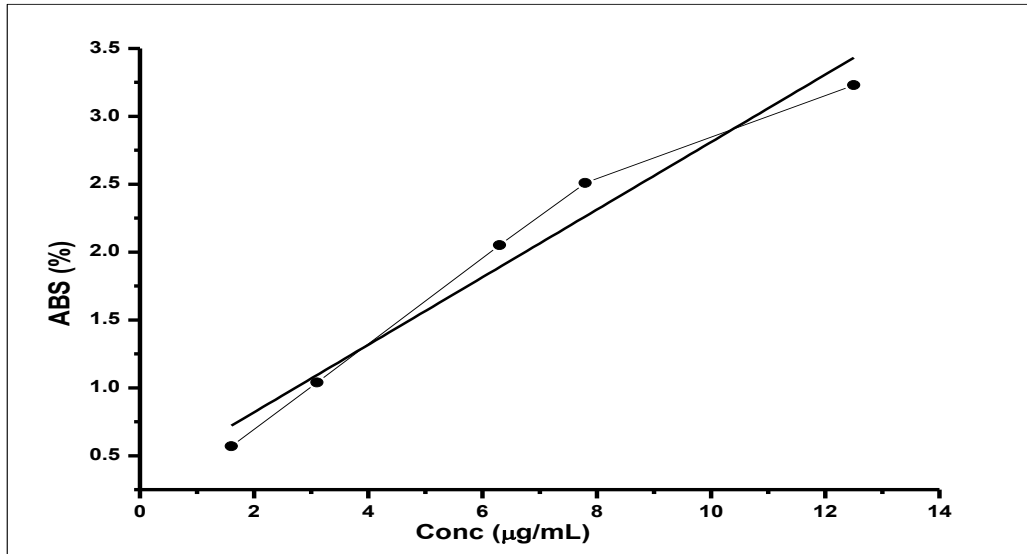
Appendix Table 8. 1 The antioxidant scavenging activity of GA, TR, AA and VA analysed using DPPH Assay

	Gallic Acid	Trolox	Ascorbic Acid	Vanillin
IC₅₀ (µg/mL)	2.13	6.7	5.93	644
Activity (µM)	12.05	27.89	33.67	4236

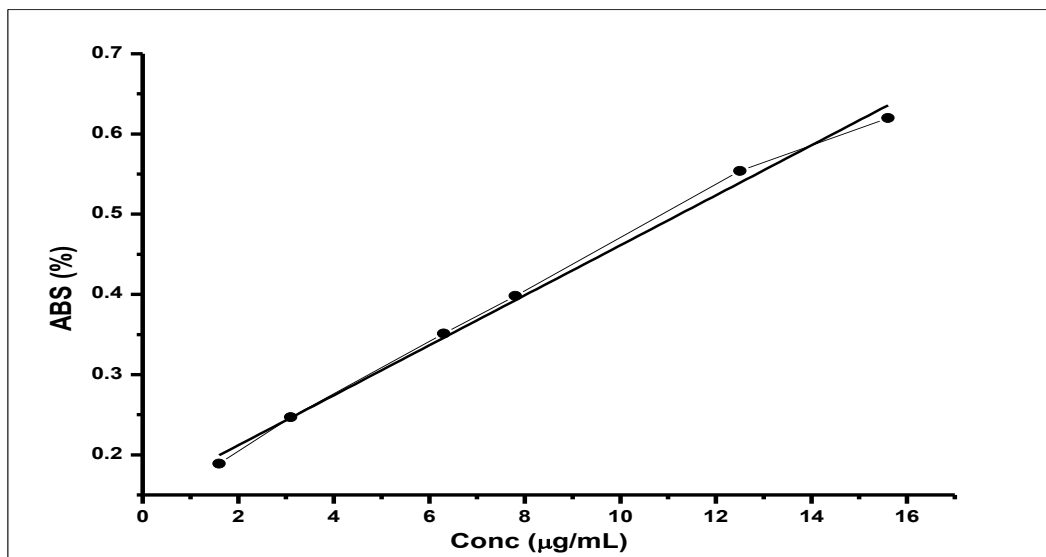
8.4 FRAP Assay

FRAP assay was also used to study the antioxidant capacity of GA, VA and AA (Appendix Figure 8.3, 8.4 and 8.5).

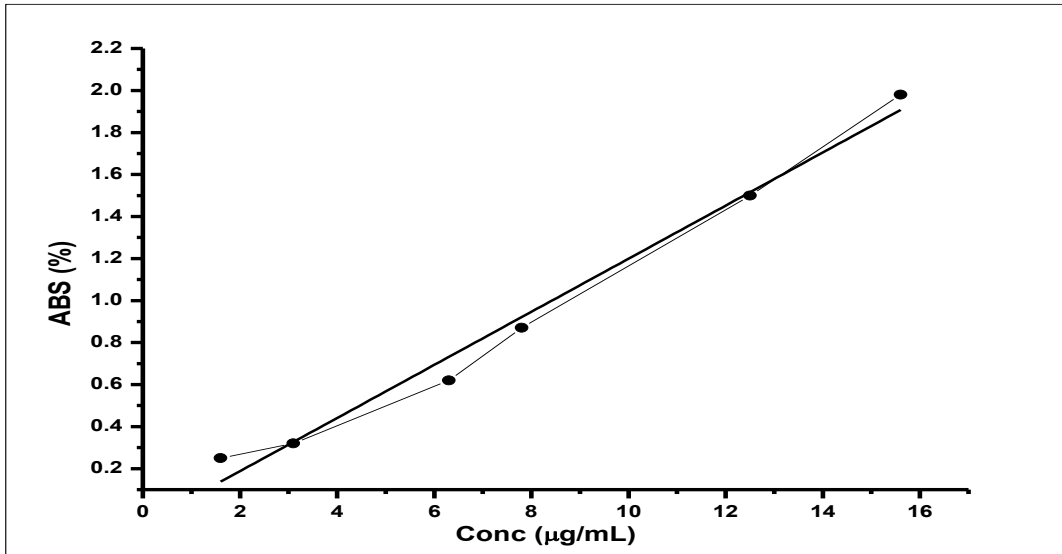
Trolox, which is used as the standard in FRAP assay analysis, showed a linear range of 1 µg mL⁻¹ to 16 µg mL⁻¹, where results are expressed in µmol L⁻¹ Trolox Equivalent (TE)/100 µg. The results of the FRAP measurement show Ascorbic acid 116 µmol L⁻¹ TE/100 µg, Vanillin 33.6 µmol L⁻¹ TE/100 µg and GA was 585 µmol L⁻¹ TE/100 µg. These are in line with the earlier DPPH measurements.



Appendix Figure 8. 3 The plot of the antioxidant activity of Gallic Acid using FRAP



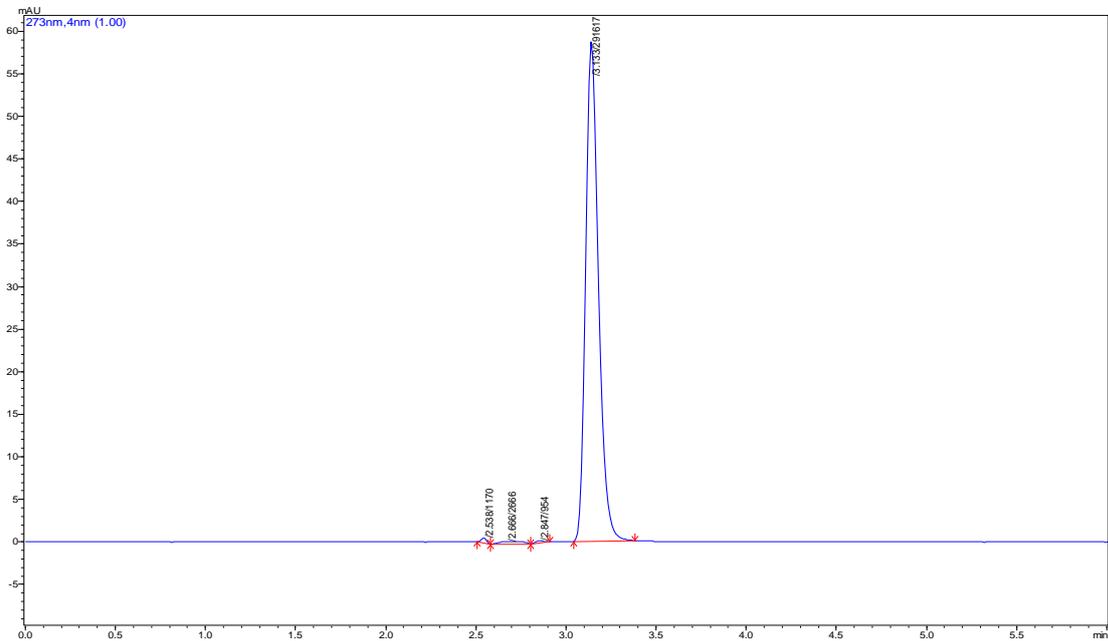
Appendix Figure 8. 4 The plot of the antioxidant activity of Vanillin determined using FRAP



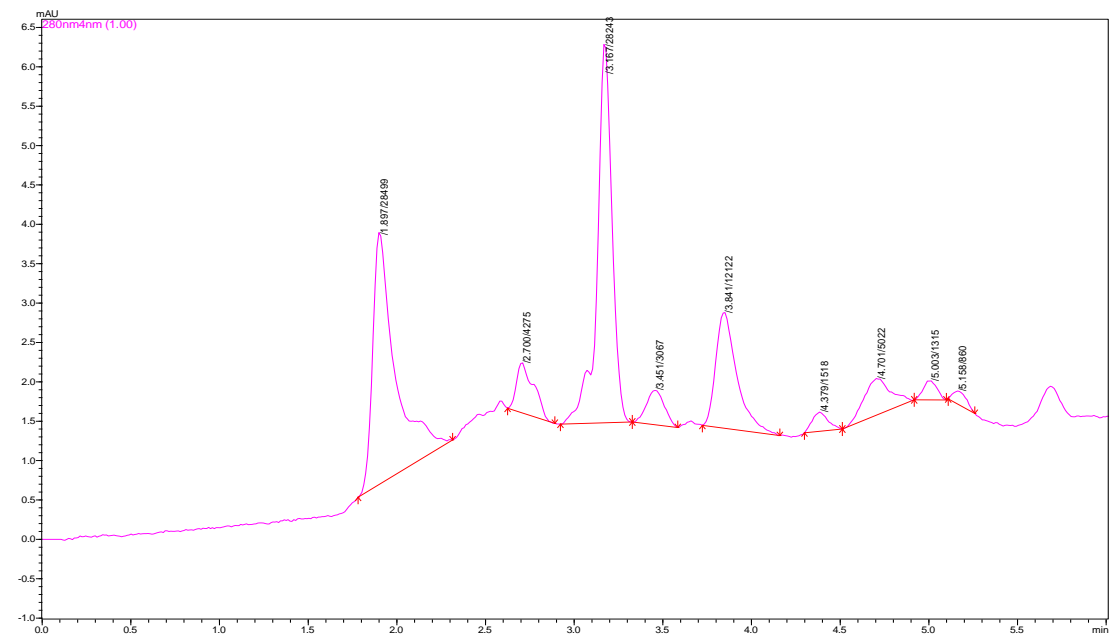
Appendix Figure 8. 5 The plot of the antioxidant activity of Ascorbic Acid determined using FRAP

APPENDIX IV

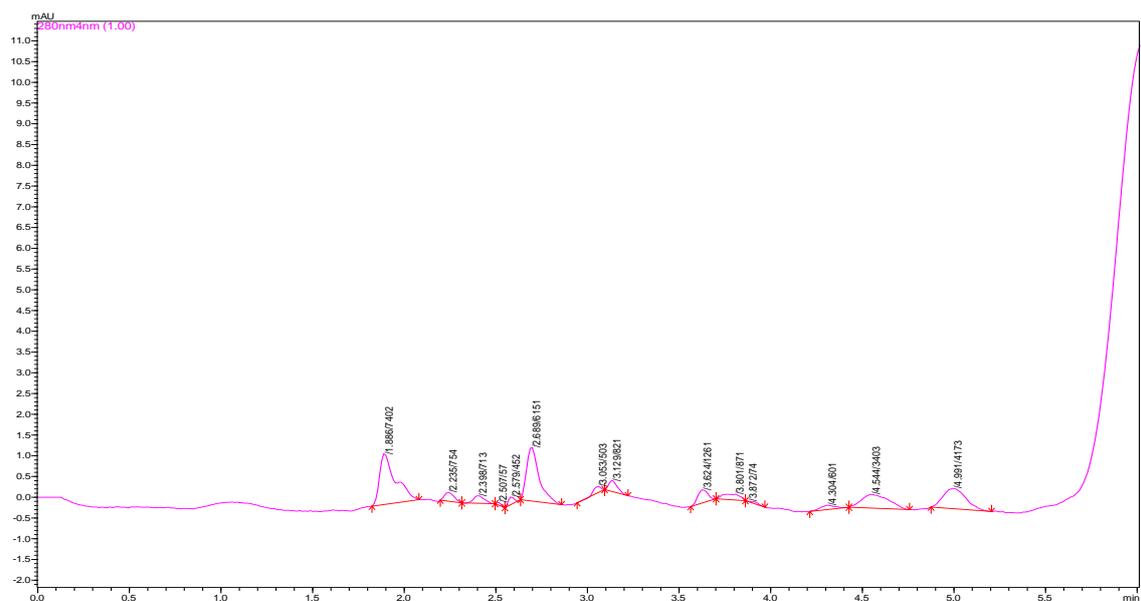
8.5 HPLC Confirmatory Test



Appendix Figure 8. 6. Chromatogram of Gallic acid standard at retention time 3.13 mins. Giving the time Gallic acid would be expected in a Red or White wine.



Appendix Figure 8. 7. Chromatogram of Red Wine showing the Gallic acid peak at retention 3.16 min.

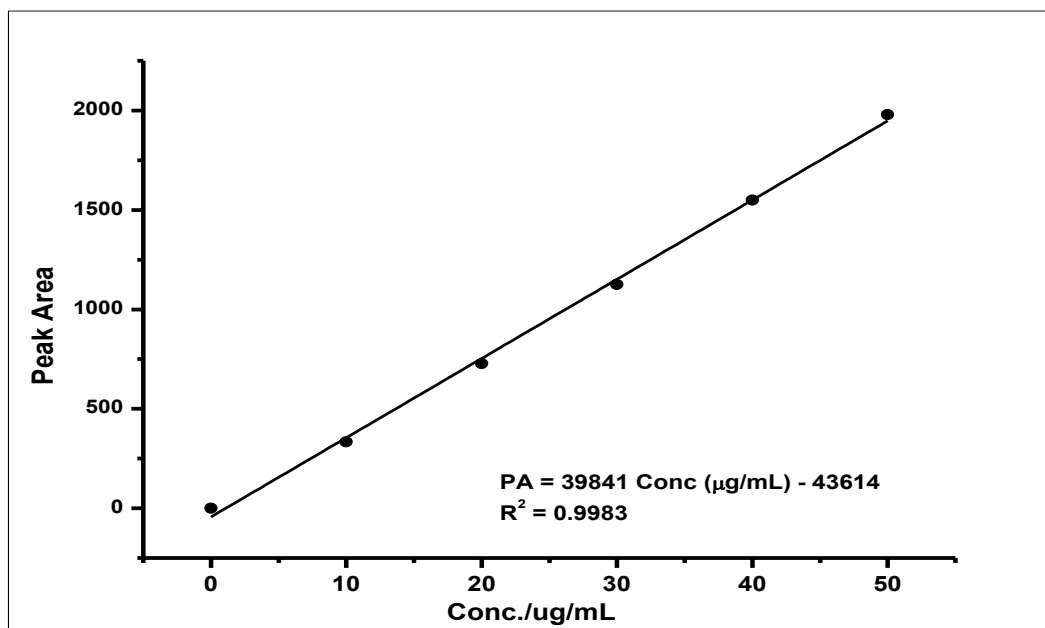


Appendix Figure 8. 8. Chromatogram of White Wine showing the Gallic acid peak at the retention time 3.12 min

The chromatograms for the increasing concentration of the standards were used to create a calibration graph. As can be seen in Appendix Figure 8.9 and Appendix Table 8.2; used for the determination of the concentration of GA in the wine samples.

Appendix Table 8.1. Calibration data showing an increasing concentration of Gallic acid Standard and their peak areas

Conc./ $\mu\text{g/mL}$	Peak Area
0	0
10	333587
20	726486
30	1125336
40	1549449
50	1979562



Appendix Figure 8. 9. Calibration graph of the gallic acid standard, from the HPLC chromatograms

APPENDIX V

8.6 Electrochemical Optimisation with Gallic Acid in Methanol

The voltammetric behaviour of some antioxidants was studied using CV. Glassy carbon electrode was used to determine Vanillin (VA), Ascorbic acid (AA) and Gallic acid (GA) dissolved in methanol and the solvent activated by an active electrolyte (Potassium chloride).

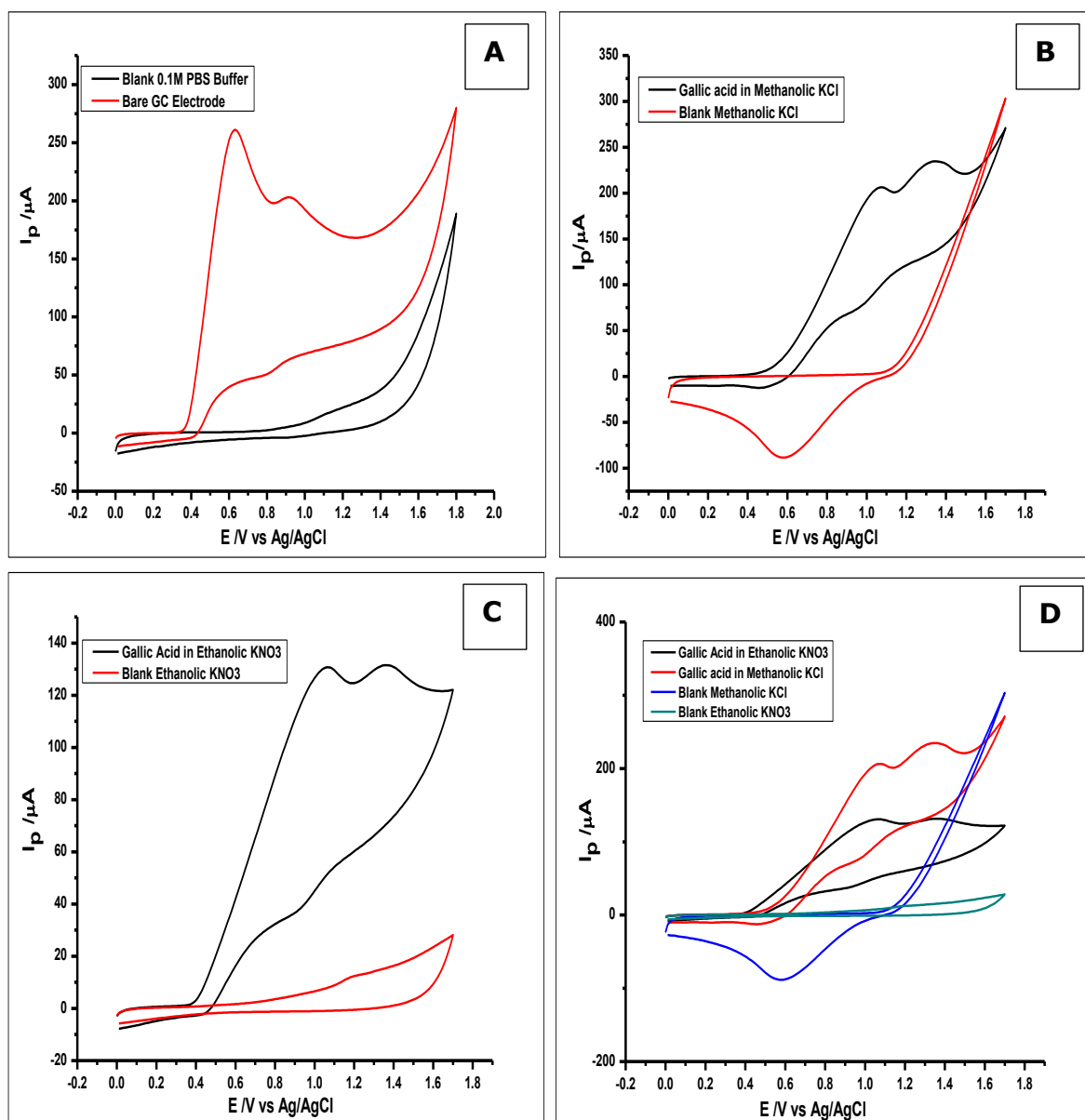
This was done to ascertain, the possibility of using electrochemical methods to analyse antioxidants in organic solvents as this is not common practice. The results recorded are described here below as an appendix to this thesis.

8.6.1 Effect of electrolyte in the Methanol solvent

The effect of the different electrolyte in methanol were studied, using CV in the determination of GA, AA and VA. The voltammograms show (Appendix Figure 8.10) the study of GA ($1 \times 10^{-2} \text{ mol L}^{-1}$) in phosphate buffer, methanolic KCl ($3.3 \times 10^{-2} \text{ mol L}^{-1}$) and ethanolic KNO_3 . With well-known buffers like, phosphate buffer, acetate buffer and Britton Robinson, the use of electrolyte activated organic solvents was a bit strange. However, the rationale was to examine the possibility of the electrochemical determination of antioxidants in organic solvents, like in DPPH and FRAP. This study gave some interesting insights.

The fact that, the antioxidants were dissolved in organic solvents (methanol) while being measured in using the spectrophotometric methods, these organic solvents were used in the electrochemical methods as buffers. However, these organic solvents were hardly electroactive, thus the need to make them electroactive by using KCl and KNO_3 to make the solvents electroactive.

The effect of the electrolytes was being investigated in this section of the work. Inasmuch as phosphate buffers are normally used for the analysis of antioxidants, the organic solvents were tried, and the results are shown in Figure 8.10. The results show that, GA in the following three medium (phosphate buffer, methanolic KCl and ethanolic KNO_3) produced peak currents of 254 μA , 206.68 μA and 130.18 μA respectively. Choosing from the organic solvents, the methanolic KCl was used for subsequent measurements.



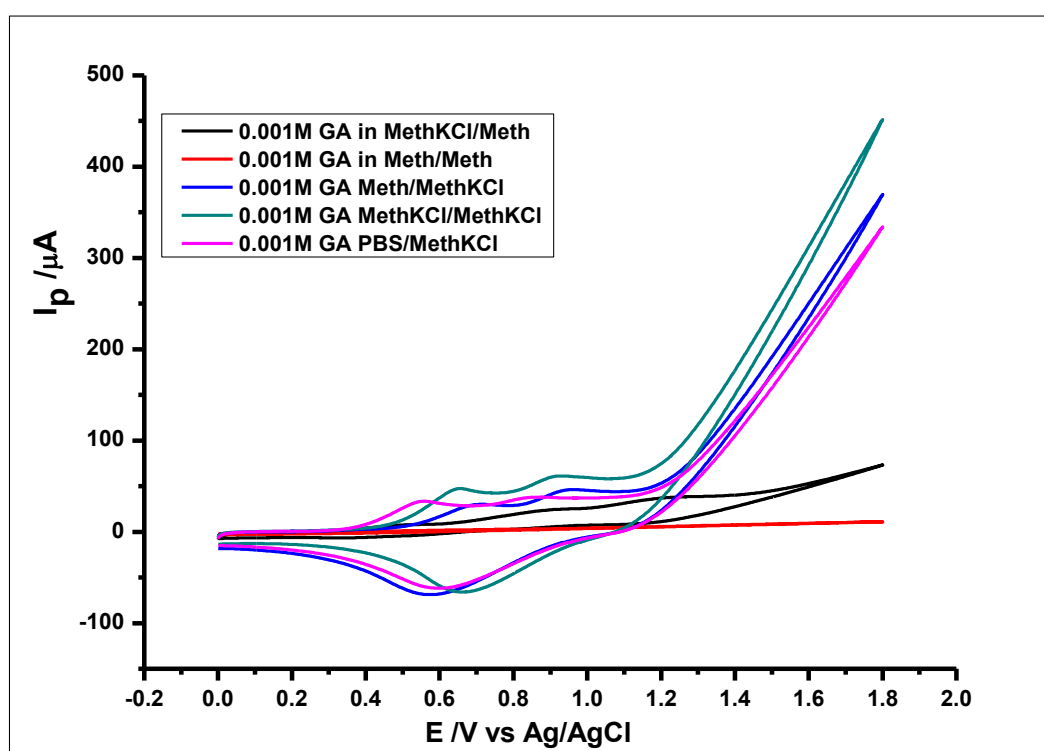
Appendix Figure 8. 10. Voltammograms of $1 \times 10^{-2} \text{ mol L}^{-1}$ Gallic acid in different buffers measured at a scan rate of 100 mVs^{-1} (A) 1×10^{-1} Phosphate buffer, (B) 0.33 mol L^{-1} methanolic KCl (C) Ethanolic KNO_3 (D) Combination of the voltammograms of $1 \times 10^{-2} \text{ mol L}^{-1}$ Gallic acid in methanolic KCl and that of ethanolic KNO_3

8.6.2 Determination of Gallic acid in Methanolic KCl

The electrochemical determination of GA in methanolic KCl was then studied. GA was then made up in methanolic KCl, methanol and phosphate buffer to a concentration of $1 \times 10^{-3} \text{ mol L}^{-1}$. As can be seen in Figure 8.11, GA dissolved in methanolic KCl was measured in an electrolyte of methanol, GA dissolved in methanol and measured in methanol, GA dissolved in methanol and measured in

methanolic KCl, GA in methanolic KCl and measured in methanolic KCl and finally GA in PBS and measured methanolic KCl.

From the results seen in Appendix Figure 8.11, it was found that the electrochemical measurements done with methanol alone as the solvent and electrolyte, showed no oxidation of GA. Meanwhile, when the electrochemical measurement was done using a methanolic KCl as the electrolyte, GA showed two oxidation peaks as can be seen in Appendix Figure 8.11. This is because of the fact that, the KCl dissolved in the methanol has made the methanol more electroactive, thus enhancing the movement of electrons between the GA and the electrode interface (Vasilescu *et al.* 2015).

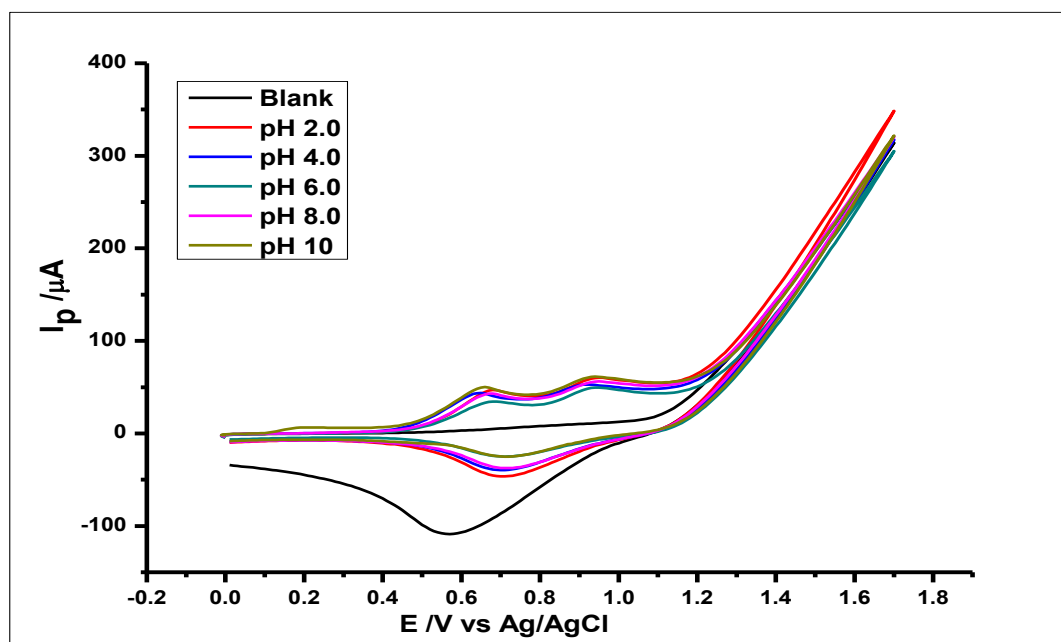


Appendix Figure 8. 11. Voltammograms of $1 \times 10^{-3} \text{ mol L}^{-1}$ GA in different solvents and electrolytes using cyclic voltammetry at a scan rate of 100 mVs^{-1} at room temperature.

8.6.3 Effect of pH Value

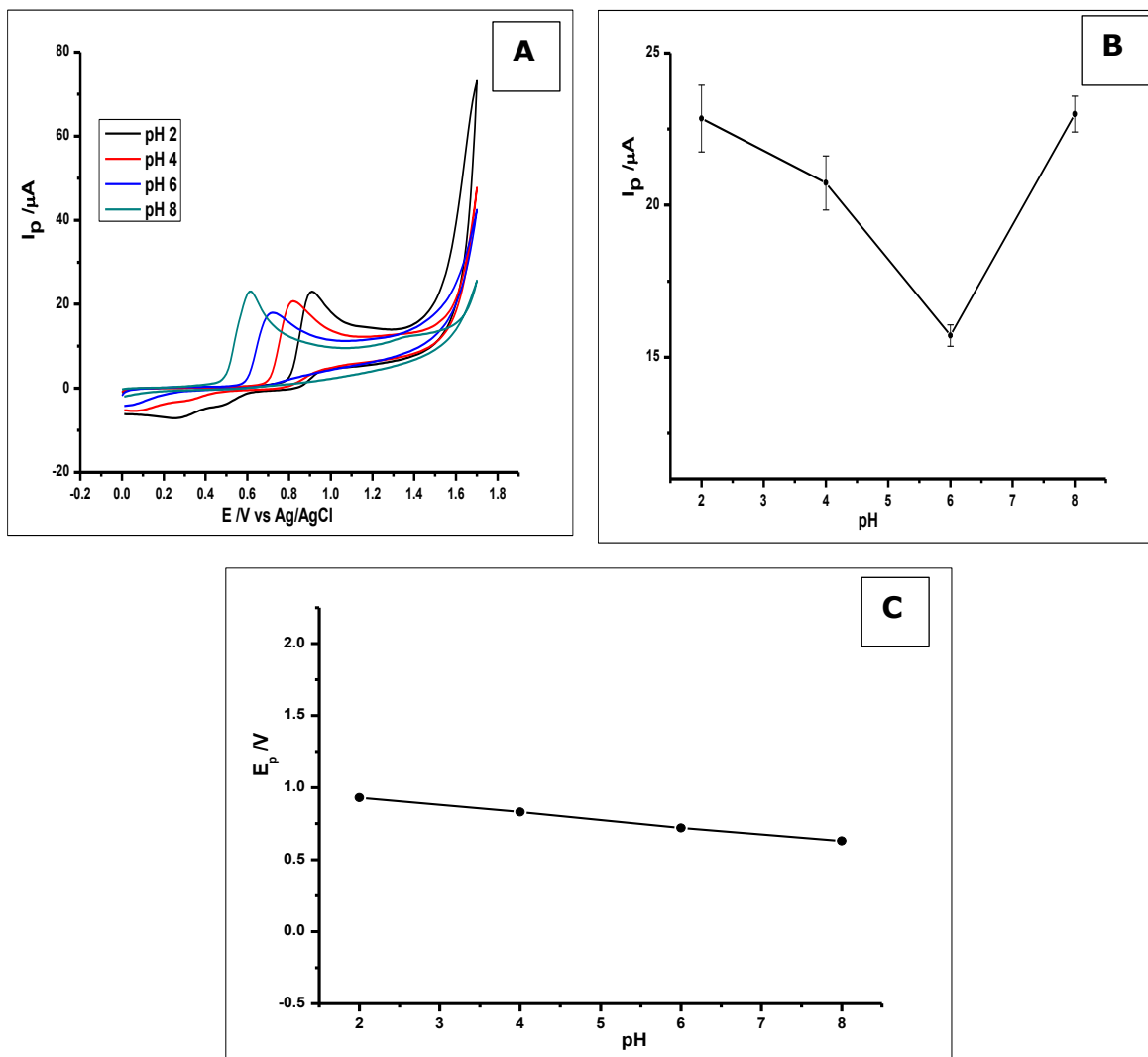
CV was also used to study if pH had any effect on the determination of the antioxidants in these organic solvents with the present of the ionic electrolytes

(KCl and KNO₃). The following antioxidants were studied individually Ascorbic acid, Vanillin and Gallic acid ($1 \times 10^{-3} \text{ mol L}^{-1}$) in pH values of 2.0 to 8.0. HCl ($1 \times 10^{-2} \text{ mol L}^{-1}$) and Potassium hydroxide (KOH) ($1 \times 10^{-2} \text{ mol L}^{-1}$) were used to make the pH changes to either directions. As can be seen in Appendix Figure 8.12, the pH did not influence the peak currents of GA oxidation, when methanolic KCl was used as an electrolyte. However, the reduction peak seen when the blank methanolic KCl was running at peak potential (E_p) of about 0.58 V during the reverse scan, reduces considerably. The visible reduction peaks, while GA is being measured, is seen at about 0.7 V. Just like in the case of GA, Vanillin (VA) and Ascorbic acid (AA) showed no change in the peak currents, with the changes in pH of the methanolic KCL electrolyte.



Appendix Figure 8. 12. Cyclic voltammograms showing the effect of the pH of the methanolic KCl electrolyte on the detection of 1 mmol L^{-1} Gallic acid at a scan rate of 100 mVs^{-1} room temperature

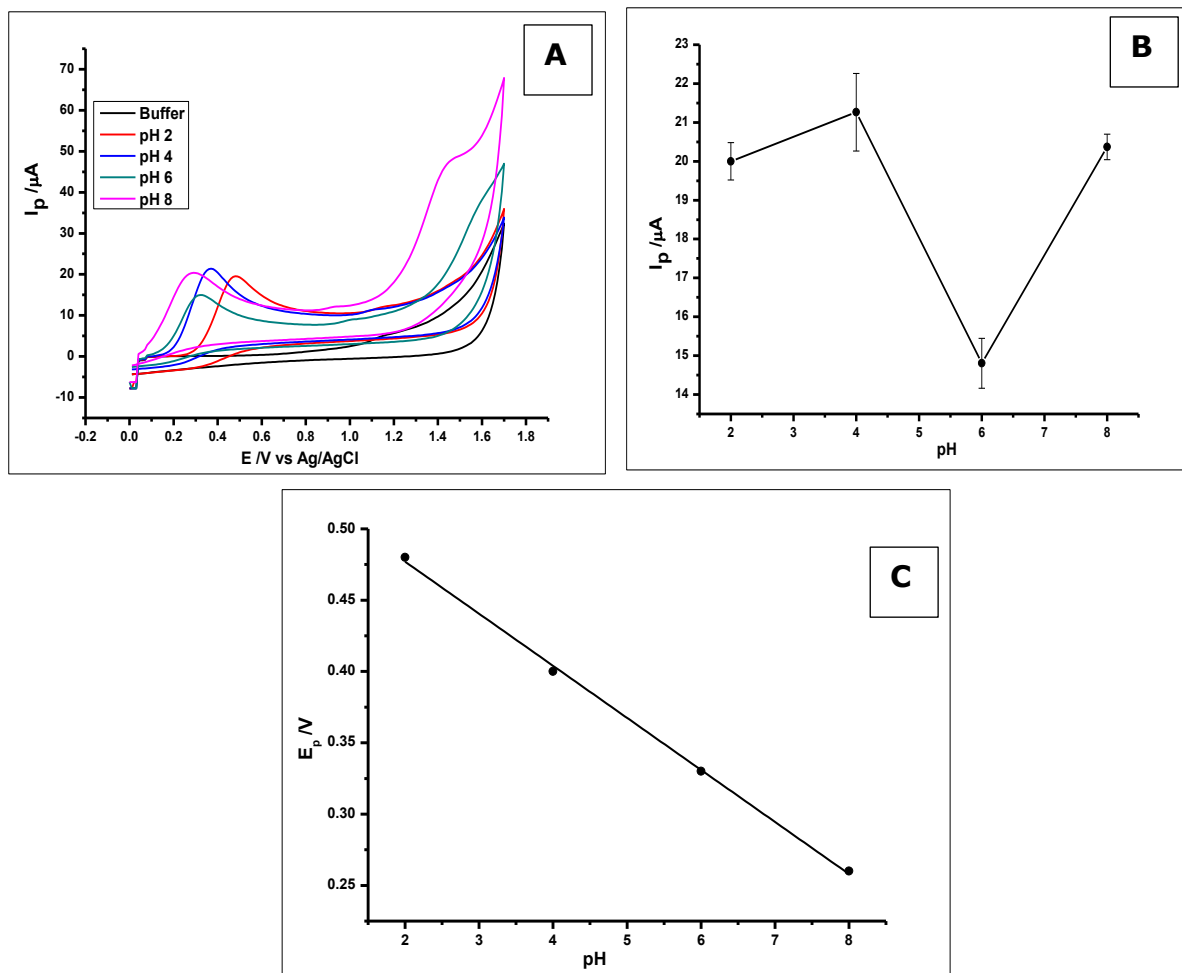
On the other, the effect of changes in the pH of $1 \times 10^{-1} \text{ mol L}^{-1}$ phosphate buffer within the range pH 2.0 to 8.0, whilst determining GA, VA and AA was also studied using cyclic voltammetry. Glassy carbon electrode was used for the determination of $1 \times 10^{-3} \text{ mol L}^{-1}$ of GA, VA and AA respectively as can be seen in Appendix Figure 8.13, 8.14 and 8.15.



Appendix Figure 8. 13. (A) Voltammograms of $1 \times 10^{-3} \text{ mol L}^{-1}$ VA in 0.1 mol L^{-1} phosphate buffer using Glassy Carbon Electrode at a scan rate of 100 mVs^{-1} at room temperature showing the effect of different pH (B) Plot of pH vs the peak currents (C) Plot of the effect of pH vs the peak potential

From the results and analysis in Figure 8.14, it was seen that, the oxidation of Vanillin was influenced by the pH of the solution. The pH of 2.0 and the pH of 8.0, produced the highest peak currents. However, the pH of 8.0 showed relatively minimal applied potential. Vanillin has a pKa value of 7.38 attributed to the deprotonation of the phenol group. The oxidation of VA at pH values below 6.0 happens when VA is present in their protonated form. Hence, VA was studied in this situation in an acidic pH of 2.0 as recorded in the literature (Yardim, Gulcan

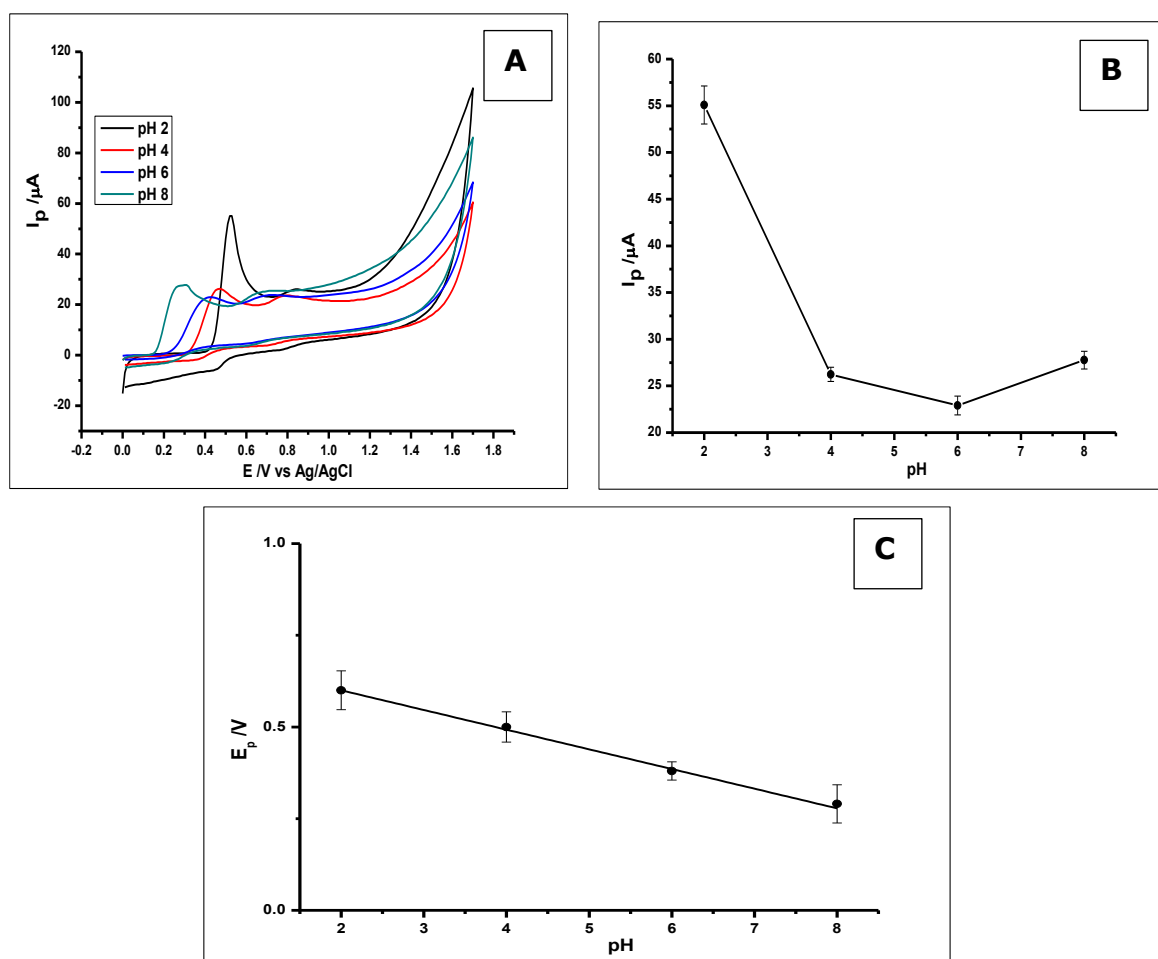
and Şenturk 2013). This is because they show high peak currents, better peak shape and the best background signal.



Appendix Figure 8. 14. (A) Voltammograms of 1×10^{-3} mol L^{-1} AA in 0.1 mol L^{-1} phosphate buffer using Glassy Carbon Electrode at a scan rate of 100 mVs^{-1} at room temperature showing the effect of different pH (B) Plot of pH vs the peak currents (C) Plot of the effect of pH vs the peak potential

From Appendix Figure 8.14 it could be seen that as the pH was increasing, there was an increase in the peak current produced. Ascorbic acid has a pK_a value of 4.10, the pH of the surrounding buffer should have an influence on the electrochemical determination of the compound. In an acidic environment as seen in Figure 8.14, there was a relatively poor electrochemical response, as the oxidation current increased with the increase in basicity. The pH also showed an effect on the peak potential as seen in Figure 8.14 (C) showing a negative shift of the peak potential as the pH increases; hence the use of in this case of a basic pH of 8 as evidenced in the literature (Özcan, Şahin and Şahin 2008; Li et al. 2011).

The plot of the peak potential vs the increasing pH, showed a linear relationship with a linear regression equation of $E_p = -0.365 \text{ pH} + 0.55$ and $R^2 = 0.9989$.



Appendix Figure 8. 15. (A) Voltammograms of $1 \times 10^{-3} \text{ mol L}^{-1}$ GA in 0.1 mol L^{-1} phosphate buffer using Glassy Carbon Electrode at a scan rate of 100 mVs^{-1} at room temperature showing the effect of different pH (B) Plot of pH vs the peak currents (C) Plot of the effect of pH vs the peak potential

GA at a concentration of $1 \times 10^{-3} \text{ mol L}^{-1}$ in a $1 \times 10^{-1} \text{ mol L}^{-1}$ phosphate buffer using CV at a scan rate of 100 mVs^{-1} was determined and the voltammograms recorded as seen in Appendix Figure 8.15. The electrochemical response of GA showed oxidation peaks and the peak potential show clear influence by the pH. From these voltammograms, one can easily see that the pH of 2.0 showed a clear oxidation peak, with the highest peak current of about 55 μA . The pH of 2.0, was subsequently used in further experiments where phosphate buffer was used. However, as the pH was increasing there was a decrease in the peak current towards the lowest peak current at pH 8.0. With this, there was also a negative shift of the

peak potential as the pH was increasing. Hence, in Figure 8.15 (C), one can see the development of a linear relationship between the pH and the peak potential within the pH range of 2.0 to 8.0. This relationship produced a linear regression equation of $E_p = -0.0525 \text{ pH} + 0.705$ and $R^2 = 0.9973$. Looking at the slope of the plot, which is $\sim 0.53 \text{ mV/pH}$ and being comparable to the Nernstian value of 0.59 mV/pH , GA shows an equal number of protons and electrons in the electrochemical reaction at the GCE surface. This is constituent with other works in the literature (Tashkhourian et al. 2013).

8.6.4 Effect of Scan Rate

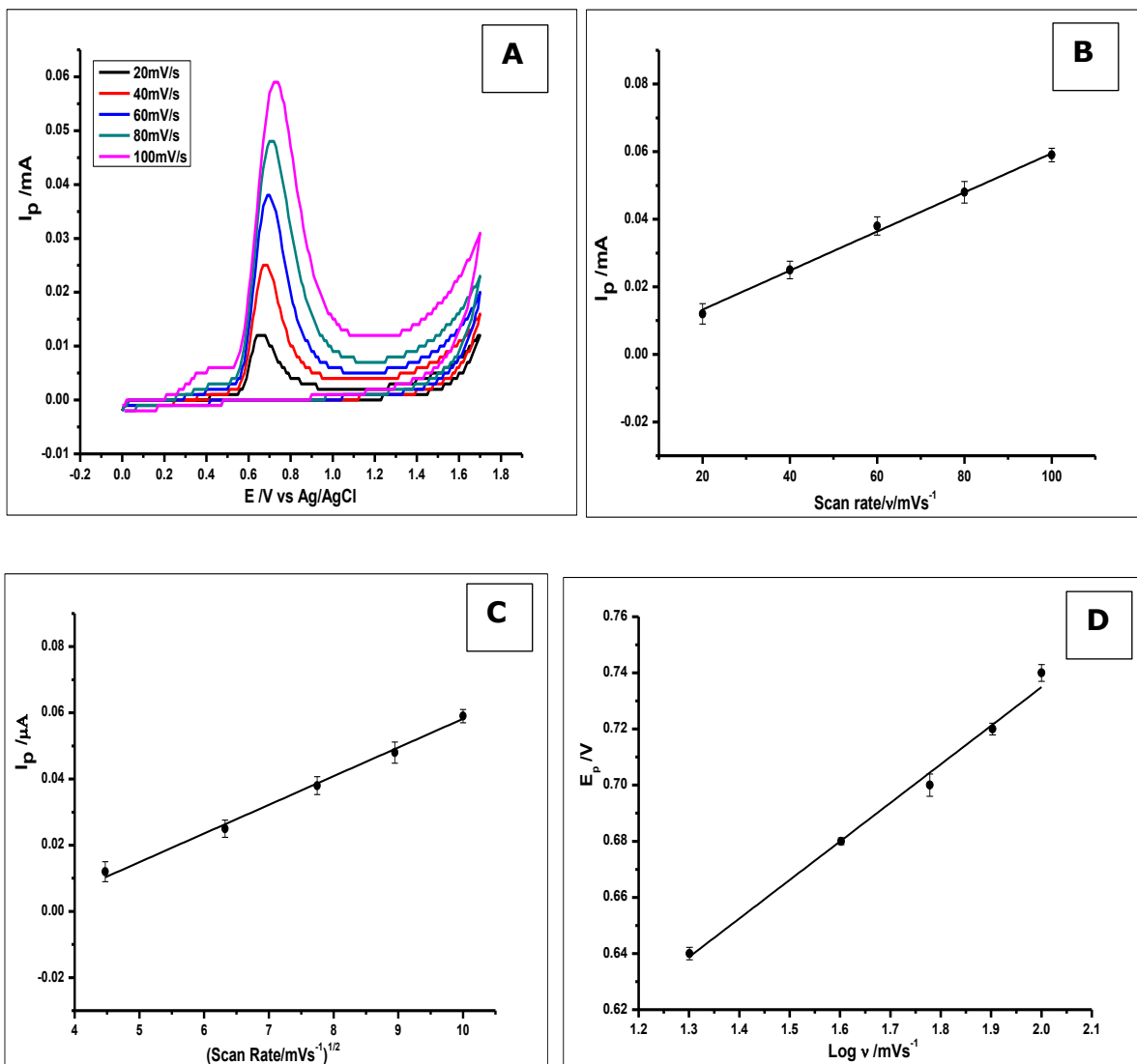
Cyclic voltammetry was further used to study the effect of the scan rate on the determination of antioxidants in these organic solvents. Useful information is normally deduced from the scan rate, as it gives us an idea of the sort of interaction the analyte has with the electrode. The scan rates were thus, studied for the following antioxidants Ascorbic acid, Vanillin and Gallic acid, using the glassy carbon electrode. Hence the electrochemical behaviours of the different antioxidants (GA, Vanillin, and Ascorbic acid) were investigated using the GCE.

Figures 8.16 and 8.17, shows that AA and GA showed a linear relationship between the peak current vs the scan rate, within a scan rate range of $20 \text{ mVs}^{-1} - 140 \text{ mVs}^{-1}$. They produced linear regression equations of $I_p = 12.744 (\text{mV/s})^{1/2} + 27.418$ and an R^2 value of 0.9908 for Ascorbic acid and $I_p = 2.167 (\text{mV/s})^{1/2} + 32.555$ and a correlation coefficient $R = 0.9972$ for GA. This reveals an adsorption-controlled reaction for the both antioxidants on the GCE.

For the vanillin, it can be observed in Figure 8.16 that, as the scan rate was increasing so too was the oxidation peak current. This can be seen in Figure 8.16 (b), where the linear relationship between the oxidation peak current (I_p) and scan rate produced a linear regression equation of $I_p (\text{mA}) = 0.0006 v (\text{mVs}^{-1}) + 0013$ and $R^2 = 0.9969$ within a range of $20 - 100 \text{ mVs}^{-1}$. This showed that, the oxidation of vanillin was an adsorption-controlled step. On the other hand, as the peak potential shifted to more positive values, with increasing scan rates; it created a linear relationship between the peak potential and logarithm of the scan rate. This was expressed in a linear regression equation as seen on the plot in Figure 8.16 (D); $E_p = 0.1388 \text{ Log } v + 0.4577$ and $R^2 = 0.9918$. Using Laviron's (1974) irreversible process experiment, as the oxidation of vanillin is an irreversible reaction (Equation 8.1).

$$E_p = E^{o'} + \frac{RT}{\alpha nF} \ln v \dots\dots\dots \text{Equation 8.1}$$

Where E_p is the peak potential, E° is the formal potential, R is the universal gas constant ($8.314 \text{ J K}^{-1} \text{ mol}^{-1}$), T is temperature (K), α (alpha) is the charge transfer coefficient and F is the Faraday constant ($96.485 \text{ C mol}^{-1}$). Meanwhile, n is the number of electrons involved in the rate-determining step of the reaction. Bard and Faulkner (2001) suggested that, for a totally irreversible wave, E_p is always a function of the scan rate, that shifts in a positive direction in an amount of $1.15 \text{ RT}/\alpha F$ for each ten-fold increase in scan rate. Using the Laviron equation and Bard Faulkner suggestions, the charge transfer coefficient was calculated, and the number of electrons n transferred was also calculated. For a totally irreversible process $\alpha = 0.5$, thus according to equation 8.1, the electron transfer n of vanillin on the GCE was approximately 2.114, thus two electrons were involved which is in line with (Zheng *et al.* 2010; Peng, Hou and Hu 2012).



Appendix Figure 8. 16. (A) Voltammograms of 1×10^{-2} mol L⁻¹ Vanillin in methanolic KCl at different scan rates showing changes in peak current as scan rate increases (B) Plot of the peak current against the scan rate from 20 mVs⁻¹ to 100 mVs⁻¹ (C) Plot of the peak current against the square root of scan rate (D) Plot of the peak potential against the log of the scan rate

For AA it is obvious from Appendix Figure 8.17 that, the oxidation peak current of AA was observed to increase with the increase in the scan rate from 10 to 140 mvs⁻¹. This suggests that, there is a kinetic limitation in the reaction between the redox surface of the GCE and the AA. Meanwhile, the anodic peak current as can be seen in Figure 8.17 (B), is proportional to the square root of the scan rate. This indicates a typical diffusion-controlled reaction.

On the other hand, getting the rate-determining step of the electrochemical oxidation of AA at the surface of the GCE, the plot of peak potential (E_p) against the log of the scan rate was done. As can be seen in Figure 8.17 (C) the plot

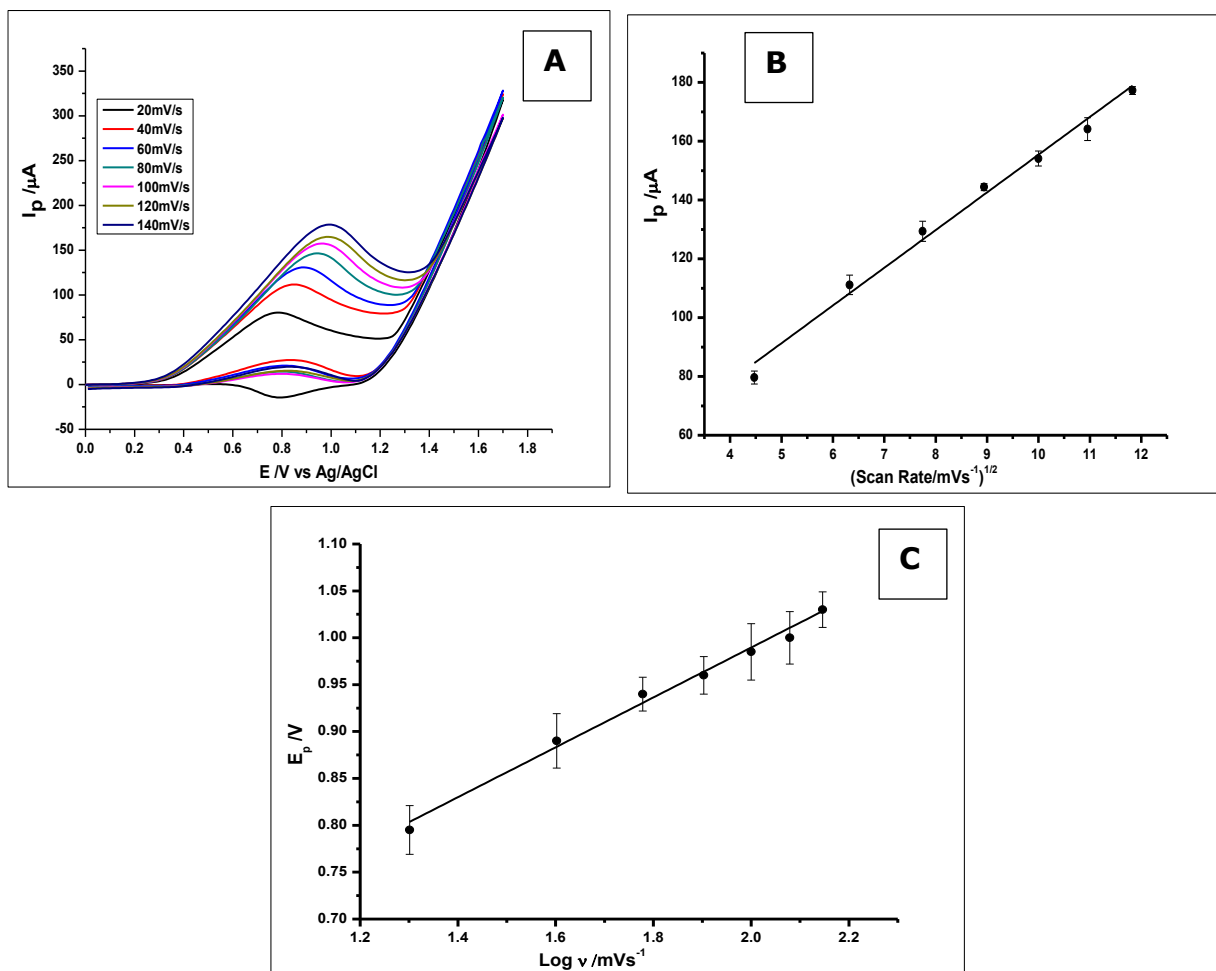
showed a linear relationship with a regression equation of $E_p = 0.2649 \text{ Log } v + 0.458$ and R^2 of 0.9910, showing an irreversible diffusion-controlled reaction (Zhang *et al.* 2014), that obeys the following reaction,

$$E_p = \frac{b}{2} \log v + \text{constant} \dots\dots\dots \text{Equation 8.2}$$

where E_p indicates the oxidation peak potential, and b is the Tafel slope as demonstrated in the following equation in Zare and Chatraei (2011).

$$b = \frac{2.303RT}{(1-\alpha)nF} \dots\dots\dots \text{Equation 8.3}$$

Where α is the anodic transfer coefficient, n is the number of electrons involved in the rate-determining step of the reaction and F is Faraday's constant = 96,500 C mol⁻¹. With a slope of 0.0529 V, the Tafel slope $b = 2 \times 0.0529$ V, showing that a one-electron process is a rate-determining step, when assuming the transfer coefficient is $\alpha = 0.43$ and $n=1$.



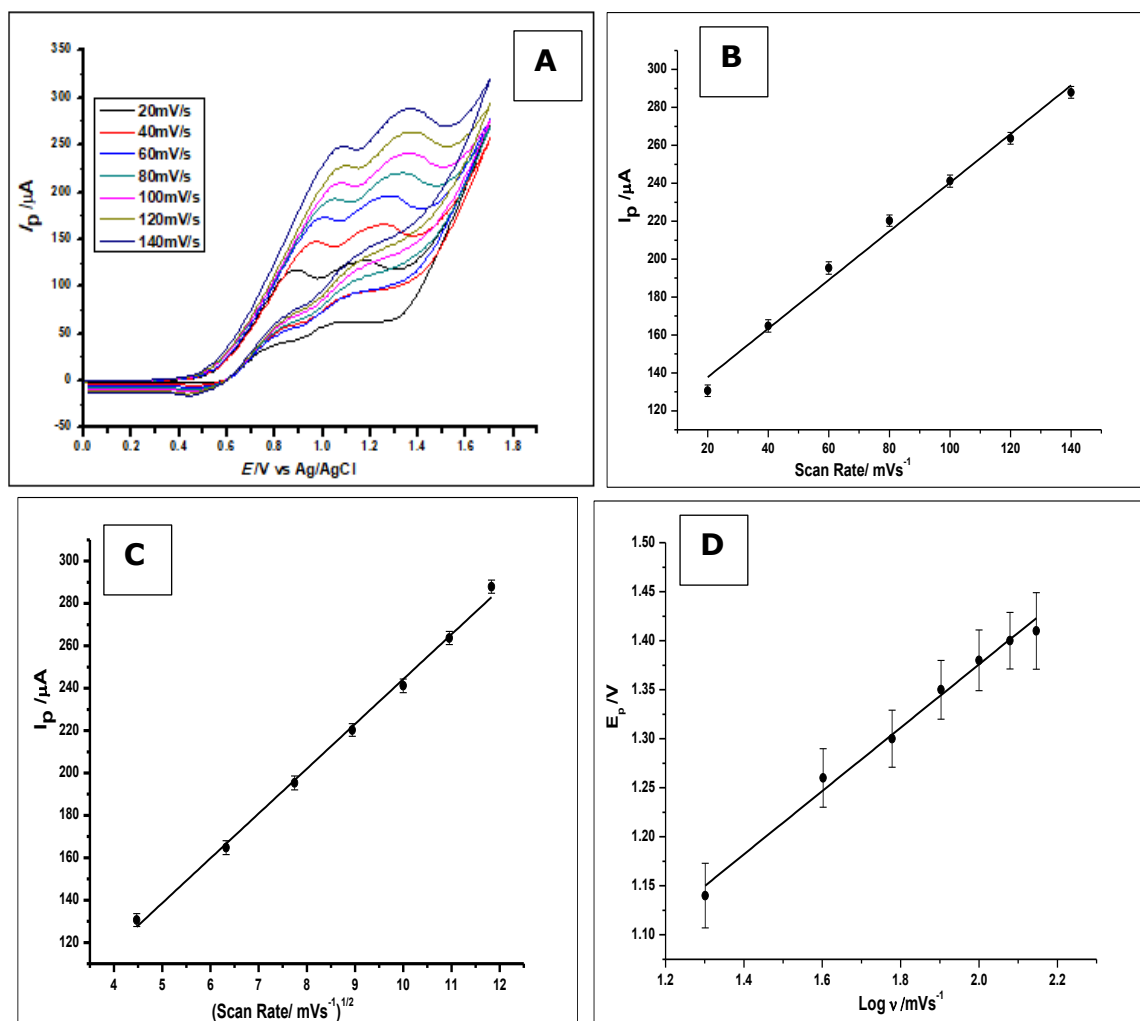
Appendix Figure 8. 17. (a) Voltammograms of 1×10^{-2} mol L⁻¹ Ascorbic Acid in methanolic KCl at different scan rates of range 20 mVs⁻¹ to 140 mVs⁻¹, showing changes in peak current as scan rate increases (b) Plot of the peak current against the square root of scan rate (c) Plot of the peak potential against the log of the scan rate

For GA as observed in Figure 8.18, just like in AA there is an increase in the oxidation peak current as of the scan rate increases. The increasing peak current that happens with the increase of the peak current, as seen in Figure 8.18 (B) demonstrates a linear relationship that gave a linear regression equation of I_p (μA) = $1.277 \sqrt{v}$ (mVs⁻¹) + 112.6 and $R^2 = 0.9922$, demonstrating adsorption-controlled interaction.

Looking at Figure 8.18 (C) it would be observed that the increasing anodic peak currents are proportional to the square root of the scan rate, within the scan rate ranges of 20-140 mVs⁻¹. This indicates a typical behaviour for a mass transfer-controlled reaction.

Figure 8.18 (D) on the other hand, shows a different linear relationship between the peak potential and the logarithm of scan rate, in GA determination. The relationship produced a linear regression equation of E_p (V) = $0.3216 \log v$ (mV/s) + 0.7314 and R^2 value of 0.9911. This shows that, there was a diffusion control process in the course of the GA determination and also an adsorption-controlled reaction.

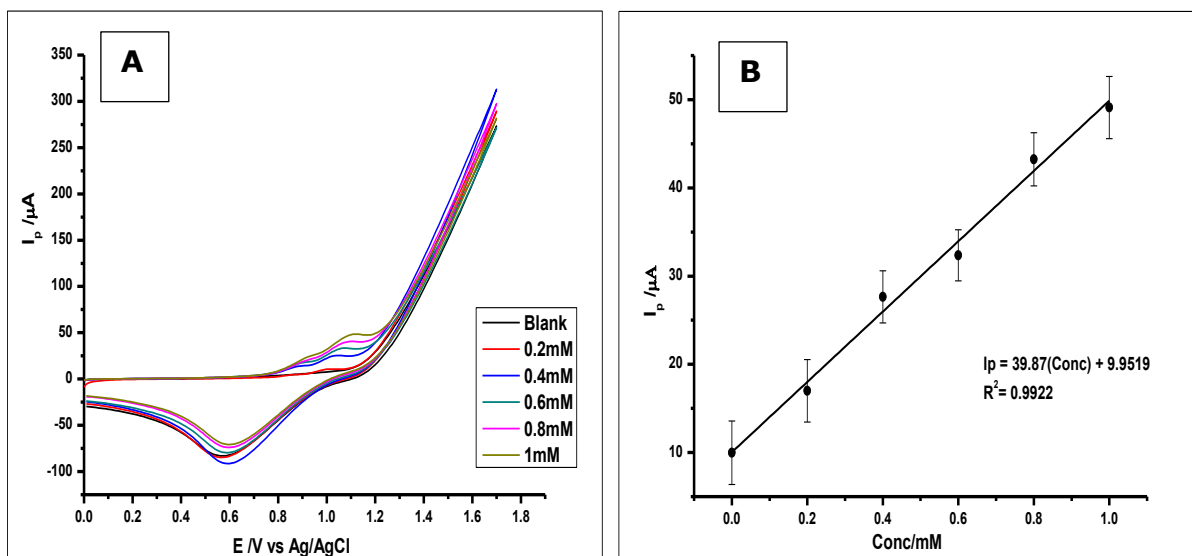
GA oxidation being an irreversible electrode oxidised process, the Laviron equation (Laviron 1974) (Equation 8.1, Page 232) can be used to describe the peak potential. Thus, in this reaction as shown by GA and the other antioxidants, the peak current (E_p) is a function of the scan rate, hence the positive shift in peak potential often seen when there is an increase in scan rate. This is easily depicted by $1.15RT/\alpha F$ (or $30/\alpha \text{mV}$ at 25°C) for each tenfold increase in scan rate (v). Using this, we calculate the number of electrons (n) transferred when the antioxidant is oxidised. For GA the number electrons was calculated to be 2.014 \sim 2.0.



Appendix Figure 8. 18. (a) Voltammograms of $1 \times 10^{-2} \text{ mol L}^{-1}$ Gallic acid in methanolic KCl at different scan rates showing changes in peak current as scan rate increases (b) Plot of the peak current against the scan rate from 20 mVs^{-1} to 140 mVs^{-1} (c) Plot of the peak current against the square root of scan rate (d) Plot of the peak potential against the log of the scan rate

8.6.5 Effect of Concentration

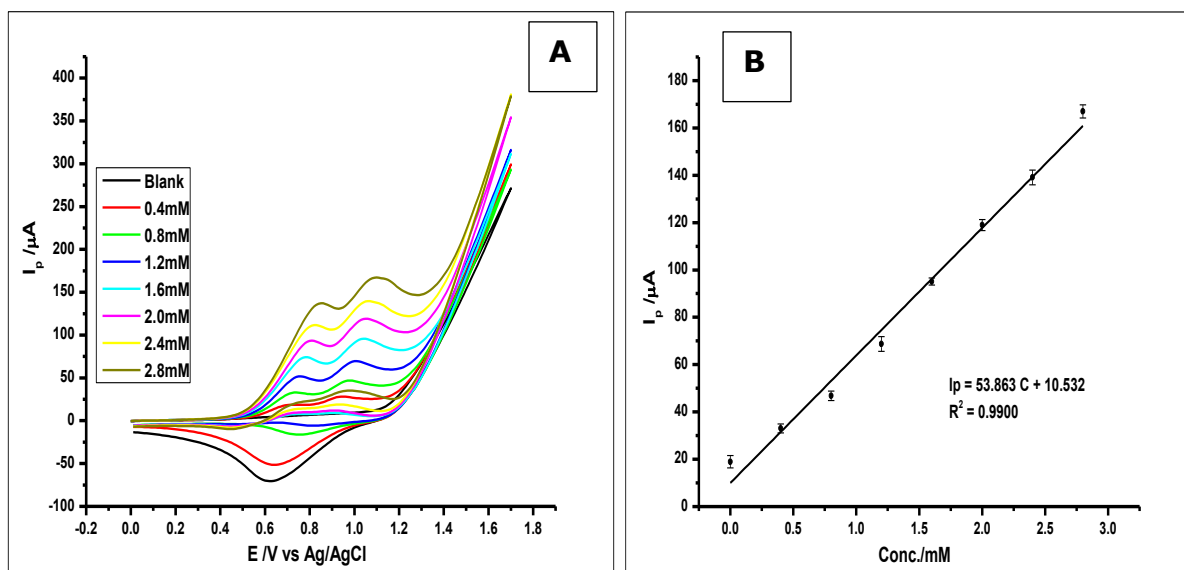
At the optimized condition, which includes a scan rate of 100 mVs^{-1} and the Methanolic KCl electrolyte, CV was then used for the study of the effect of increasing concentration towards antioxidant determination. Figure 8.19(A) and (B) shows an increase in peak current (I_p), as the VA concentration increased. Ascorbic acid and GA also showed the same trend (Figure 8.20).



Appendix Figure 8. 19. (a) Voltammograms of increasing concentration of Vanillin in Methanolic KCl buffer, at a scan rate of 100mV/s (b) Linear plot of Current against Potential; depicting the linear relationship between increase concentration of the Vanillin and the peak current; with linear regression equation of $I_p = 39.871 \text{ Conc.}(\text{mmol L}^{-1}) + 9.9519$ and $R^2= 0.9922$

Looking at the voltammograms in Figure 8.20 one can see increasing peak currents at a peak potential of about 1.1 V and a reduction peak at a potential of 0.59 V at the return scan. Vanillin was seen to be increasing linearly within a concentration range of 0.2 mmol L^{-1} and 1.0 mmol L^{-1} producing a linear regression equation of $I_p = 39.871 \text{ Conc.}(\text{mmol L}^{-1}) + 9.9519$ (I_p : μA , C : mmol L^{-1}) and correlation coefficient $R^2= 0.9922$. The limit of detection (LOD) was calculated using the equation $\text{LOD} = 3.3 (\text{STD of blank})/m$, where m is the slope of the calibration graph. Thus, producing an LOD of $3.05 \times 10^{-6} \text{ mol L}^{-1}$.

On the other hand, looking at Figure 8.20 CV was used to determine the increasing concentration of GA in a methanolic KCl electrolyte at a scan rate of 100 mVs^{-1} .



Appendix Figure 8. 20. (A) Voltammograms of increasing concentration of Gallic Acid in Methanolic KCl buffer, at a scan rate of 100mV/s (B) Linear plot of Current against Concentration; depicting the linear relationship between increase concentration of Gallic Acid and the peak current.

From the voltammograms shown in Figure 8.20, with the increasing concentration of GA, there was an increasing oxidation peak current. It can also be noted that, GA in the methanol KCL electrolyte shows two oxidation peaks at peak potential values of 0.76 V and 1.09 V, which is in line with GA electrochemical oxidation. Using the oxidation peak currents at the peak potential of 0.76 V, there was a linear relationship between the increasing concentration of GA and the peak current, within a concentration range of $4 \times 10^{-4} \text{ mol L}^{-1}$ to $28 \times 10^{-4} \text{ mol L}^{-1}$ creating a linear regression equation of $I_p = 53.863 C (\text{mmol L}^{-1}) + 10.532$ (I_p : μA , C: mmol L^{-1}) and correlation coefficient of $R = 0.9900$. The LOD was also calculated as $\text{LOD} = 3.3 (\text{STD of blank})/m$, where m is the slope of the calibration graph, thus LOD (S/N = 3) was $4.1 \times 10^{-6} \text{ mmol L}^{-1}$.

The results indicate the feasibility of this method for the quantitative detection of GA and hence could suggest a possible application of the method.